ISTANBUL TECHNICAL UNIVERSITY ★ GRADUATE SCHOOL OF SCIENCE ENGINEERING AND TECHNOLOGY

SEISMIC RETROFIT OF RC COLUMNS WITH BASALT MESH REINFORCED SPRAYED GRC: EFFECTS OF STIRRUP HOOK ANGLE AND HOOK LENGTH

M.Sc. THESIS

Saeid HAJIHOSSEINLOU

Department of Civil Engineering

Structural Engineering Program

Thesis Advisor: Prof. Dr. Alper İLKİ

JUNE 2014

ISTANBUL TECHNICAL UNIVERSITY ★ GRADUATE SCHOOL OF SCIENCE ENGINEERING AND TECHNOLOGY

SEISMIC RETROFIT OF RC COLUMNS WITH BASALT MESH REINFORCED SPRAYED GRC: EFFECTS OF STIRRUP HOOK ANGLE AND HOOK LENGTH

M.Sc. THESIS

Saeid HAJIHOSSEINLOU
501111050

Department of Civil Engineering

Structural Engineering Program

Thesis Advisor: Prof. Dr. Alper İLKİ

JUNE 2014

İSTANBUL TEKNİK ÜNİVERSİTESİ ★ FEN BİLİMLERİ ENSTİTÜSÜ

BETONARME KOLONLARIN BASALT HASIR DONATILI PÜSKÜRTME GRC İLE DEPREME KARŞI GÜÇLENDİRİLMESİ: ETRİYE KANCA AÇISI VE BOYUNUN ETKİSİ

YÜKSEK LİSANS TEZİ

Saeid HAJIHOSSEINLOU
501111050

İnşaat Mühendisliği Anabilim Dalı

Yapı Mühendisliği Programı

Tez Danışmanı: Prof. Dr. Alper İLKİ
Anabilim Dalı : Herhangi Mühendislik, Bilim
Programı : Herhangi Program

HAZİRAN 2014

Saeid HAJIHOSSEINLOU a M.Sc. student of ITU **Graduate School of Science Engineering and Technology** student ID **501111050**, successfully defended the thesis/dissertation entitled "**SEISMIC RETROFIT OF RC COLUMNS WITH BASALT MESH REINFORCED SPRAYED GRC: EFFECTS OF STIRRUP HOOK ANGLE AND HOOK LENGTH**", which he prepared after fulfilling the requirements specified in the associated legislations, before the jury whose signatures are below.

Thesis Advisor:	**Prof. Dr.Alper İLKİ** İstanbul Technical University	……..
Jury Members:	**Assoc. Prof. Dr. Beyza Taşkın** Istanbul Technical University	……..
	Assoc. Prof. Dr. Kutay Orakçal Boğaziçi University	……..

Date of Submission: 05 May 2014
Date of Defense: 30 June 2014

To my beloved parents

Who have forward me over themselves and given me all what they could.

To my sisters and my fiancée,

Whom always give their patience, support, encouragement, and extensive supports at important times of my life.

To Professor Alper İlki,

Who believed in me and gave me the opportunity to discover new things and challenge myself more than ever.

FOREWORD

I would like to express my deepest gratitude to my supervisor Prof. Dr. Alper İLKİ for his continuous support and persistent guidance during whole process. Working with him has been a great honor for me. I would like to thank Res.Assist.Dr. Medine İSPİR and Res.Assist.Dr. Cem DEMİR for their assistance, encouragement, and valuable suggestions throughout the course of this research. Special appreciations are extended to Eng. Muhammed MARAŞLI, member board of directors of FIBROBETON YAPI ELEMANLARI Corporation and his colleagues especially for supporting financially and providing all equipment, which we required for constructing specimens of the research program. In my rather short life, I have had the good fortune of being around many exemplary people, but none better than the graduate students here at the Istanbul Technical University. Although there are many of them, I would like to especially mention the following: Res.Assist. Mustafa CÖMERT (PhD candidate), Ali Osman ATEŞ (PhD candidate), Mehmet ŞENTÜRK (M.Sc. Student), Korhan Deniz DALGIÇ (PhD candidate), Yavuz ÇAVUNT (PhD candidate), Hamid FARROKH GHATTE (PhD candidate), for their assistance during the program, from Eng. Hakan SARUHAN, Mr. Mahmut ŞANLI, Mr. Ahmet ŞAHIN and Ms. Elif Deniz OĞUZ for their continuous support in Laboratory of Istanbul Technical University during the tests. I also would like to thank and celebrate my associate Amin NASRINPOUR for his efforts at every point of the work that inspired me during the entire process and aided me whenever I needed help as we have worked together at every stage of the process. They all have provided me with friendship, assistance, and enthusiastic support when I needed it most. Professor İlki's group is a very special group of people. If I am a better student now than when I arrived at ITU, the credit is all theirs; if not, the failure is all mine. Finally, my deepest thanks goes to my family: my parents Ali and Huriyye; my sisters: Akram, Elham, and Sahar and my fiancée Akmaral. Their constant support was a tremendous source of strength; they will always have my love.

JUNE 2014 Saeid HAJIHOSSEINLOU

TABLE OF CONTENTS

Page

DEDICATION ..... **vii**
FOREWORD ..... **ix**
TABLE OF CONTENTS ..... **xi**
ABBREVIATIONS ..... **xiii**
LIST OF TABLES ..... **xvii**
LIST OF FIGURES ..... **xvii**
SUMMARY ..... **xxvii**
ÖZET ..... **xxvii**
1. INTRODUCTION **1**
1.1 Research Significance 2
1.2 Purpose of Thesis 3
1.3 Literature Review 4
2. EXPERIMENTAL PROGRAM **19**
2.1 Design of Specimens 19
2.1.1 Test variables 19
2.1.2 Specimen details 20
2.1.3 Axial load strength 22
2.1.4 Shear strength 24
2.1.5 Material properties 27
2.1.5.1 Plain concrete 27
2.1.5.2 Reinforcing steel 28
2.1.5.3 Glass fiber reinforced polymer 29
2.1.5.4 Basalt textile reinforced polymer 30
2.1.6 Construction of specimens 31
2.1.6.1 Reinforcing cages 31
2.1.6.2 Formworks 31
2.1.6.3 Casting and curing 34
2.1.6.4 Column retrofitting 34
2.2 Test Setup 36
2.3 Instrumentation 38
2.3.1 Linear transducers 38
2.3.2 Strain-Gauges 40
2.4 Test Procedure and Loading Program 41
3. ANALYTICAL STUDY **43**
3.1 Internal Confinment 43
3.2 External Confinment 47
3.3 Proposed Confinement Model 47
4. TEST RESULTS **51**
4.1 General Behavior and Test Observations 51
4.2 Test Observation of Reference Columns 51

4.2.1 Specimen: Ref-S60-Ɵ90-L80 51
4.2.2 Specimen: Ref-S60-Ɵ112.5-L80 57
4.2.3 Specimen: Ref-S60-Ɵ135-L80 62
4.2.4 Specimen: Ref-S60-Ɵ135-L40 68
4.3 Test Observation of Retrofitted Columns 73
4.3.1 Specimen: Ret-S60-Ɵ90-L80-3TRM 73
4.3.2 Specimen: Ret-S60-Ɵ112.5-L80-3TRM 79
4.3.3 Specimen: Ret-S60-Ɵ135-L80-3TRM 85
4.3.4 Specimen: Ret-S60-Ɵ135-L40-3TRM 91
5. EVALUATION OF TEST RESULTS 97
5.1 Introduction 97
5.2 Moment-Curvature 97
5.3 Energy Dissipation 103
5.4 Failure Machanisms of the Specimens 105
5.5 Lateral load-Drift-Tip Displacement Relationships 108
5.6 Comparison of the all Reference Specimens 108
5.7 Comparison of the all Retrofitted Specimens 110
5.8 Reference Specimens versus Retrofitted Specimns 112
5.9 Theoretical Results versus Experimental Test Results 115
6. CONCLUSION AND RECOMMENDATIONS 123
6.1 Conclusions 123
6.2 Recommendation for Future Research 124
REFERENCES 127
APPENDICES 129
APPENDIX A: Test Observation's Summary 129
APPENDIX B: Thechnical Drawings of Specimens 195
APPENDIX C: Strain distribution in the Longitudinal Reinforcing Bars 209
CURRICULUM VITAE 213

ABBREVIATIONS

A_{sx}	: The total area of transverse bars running in the x directions
A_{sy}	: The total area of transverse bars running in the y directions
b_c	: Concrete core dimension to centerline of perimeter hoop in x-direction
d_c	: Concrete core dimension to centerline of perimeter hoop in y-direction
E_c	: The elasticity modulus of concrete
E_{sec}	: The elasticity modulus of concrete from the start of loading to the maximum strength
f_{je}	: Effective strength of jacket in lateral direction
f'_{co}	: Compressive strength (peak stress) of confined concrete
f'_{lx}	: Lateral confining stress on the concrete in *x* directions
f'_{ly}	: Lateral confining stress on the concrete in *y* directions
f_{lx}	: The effective lateral confining stress on the concrete in *x* directions
f_{ly}	: The effective lateral confining stress on the concrete in *y* directions
f'_{l1}	: Smaller confining stress
f'_{l2}	: Larger confining stress
f_{yh}	: Yield strength of the transverse reinforcement
H_{PL}	: The plastic hinge length of the column
H	: Height of the column
I	: Moment of inertia
K_a	: The efficiency factor
K_e	: Confinement effectiveness coefficient
K_1, K_2	: Empirical constants
m	: Empirical constants
M	: Moment
n	: Empirical constants
n_f	: The number of plies of wrapping material
p	: Lateral load
r	: Based on the modulus of elasticity for the concrete
S	: Center to center spacing or pitch of spiral or circular hoop
S'	: Clear spacing between spiral or hoop bars
t_f	: The effective thickness of plies of wrapping material
t_j	: Thickness of jacket
w'_i	: *i*th clear transverse spacing between adjacent longitudinal bars
x_p	: The average plastic curvature assumed to be uniformly distributed over the assumed plastic hinge length
ε_{cc}	: Strain at maximum concrete stress f'cc
ε_{co}	: Strain at maximum stress f'_{co} of unconfined concrete
ρ_{cc}	: Ratio of area of longitudinal steel to area of core of section

$\boldsymbol{\rho_s}$	**:** Ratio of volume to transverse confining steel to volume of confined concrete core
$\boldsymbol{\sigma_{lu}}$	**:** Ultimate lateral stress due to jacketing
$\boldsymbol{\theta_{pl}}$	**:** The plastic rotation of the assumed plastic hinge reinforcement
$\boldsymbol{\theta}$	**:** The arching angle
$\boldsymbol{\delta_{elastic}}$	**:** The elastic contribution to the total top displacement at ultimate lateral load
$\boldsymbol{\delta_{plastic}}$	**:** The plastic contribution to the total top displacement at ultimate lateral load

LIST OF TABLES

Page

Table 2.1 : Satisfaction of test parameters according to ABYYHY-1975..... 21
Table 2.2 : Specification of cross-sections. 23
Table 2.3 : Values of concrete compressive strength and reinforcement type..... 24
Table 2.4 : Specification of longitudinal and transverse reinforcement. 25
Table 2.5 : The mechanical characteristics of reinforcement bars.. 29
Table 4.1: General specification of Ref-S60-Ɵ90-L80 specimen..... 51
Table 4.2: General specification of Ref-S60-Ɵ112.5-L80 specimen..... 57
Table 4.3: General specification of Ref-S60-Ɵ135-L80 specimen..... 62
Table 4.4: General specification of Ref-S60-Ɵ135-L40 specimen..... 68
Table 4.5: General specification of Ret-S60-Ɵ90-L80-3TRM specimen..... 74
Table 4.6: General specification of Ret-S60-Ɵ112.5-L80-3TRM specimen. 80
Table 4.7: General specification of Ret-S60-Ɵ135-L80-3TRM specimen. 85
Table 4.8: General specification of Ret-S60-Ɵ135-L40-3TRM specimen. 91
Table 5.1: Failure mechanisms of specimens..... 106
Table A.1: Summary of the seismic behavior of the Ref-S60-Ɵ90-L80 129
Table A.2: Summary of the seismic behavior of the Ref-S60-Ɵ112.5-L80..... 137
Table A.3: Summary of the seismic behavior of the Ref-S60-Ɵ135-L80.. 144
Table A.4: Summary of the seismic behavior of the Ref-S60-Ɵ135-L40..... 151
Table A.5: Summary of the seismic behavior of the Ret-S60-Ɵ90-L80-3TRM..... 158
Table A.6: Summary of the seismic behavior of the Ret-S60-Ɵ112.5-L80-3TRM 167
Table A.7: Summary of the seismic behavior of the Ret-S60-Ɵ135-L80-3TRM... 176
Table A.8: Summary of the seismic behavior of Ret-S60-Ɵ135-L40-3TRM..... 185
Table D.1: Theoretical stress-strain distribution for Ref-S60-Ɵ90-L80..... 185
Table D.2: Theoretical stress-strain distribution for Ref-S90-Ɵ90-L80..... 186
Table D.3: Theoretical stress-strain distribution for Ref-S120-Ɵ90-L80..... 187
Table D.4: Theoretical stress-strain distribution for Ref-S180-Ɵ90-L80..... 188

LIST OF FIGURES

Page

Figure 1.1 : (a)Concrete cylinders Series A. (b)Concrete cylinders Series B. (c)Concrete prisms Series B. 14
Figure 1.2 : ypical failure of confined square specimen..... 15
Figure 2.1 : Concrete stress-strain diagram at the age of 180 days. 28
Figure 2.2 : Tensile test results of Φ14 bars..... 28
Figure 2.3 : Tensile test results of Φ8 bars..... 29
Figure 2.4 : Glass fiber reinforced concrete 30
Figure 2.5 : Basalt textile reinforced mesh..... 30
Figure 2.6 : Reinforcement of cages: (a)Stub cage. (b)Stub cage with column longitudinal bars. (c)Plan view of stub cage. (d)Stirrup with 135° hook angle. (e)Assembling of stirrups. (f)Plan view of column cages. 32
Figure 2.7 : Formwork of stubs and columns: (a)Placement of stub cages into form. (b)Attachment of PVCs to formwork for preventing movement. (c)Attachment of plastic spacers. (d)Plan view of inside of column. (e)Installation of threaded anchor rods. (f)Keeping columns vertically by installation of diagonal elements.. 33
Figure 2.8 : Casting and curing: (a)Casting of stub concrete. (b)Curing of stub concrete. (c)Equipment for column concrete casting. (d)Casting of column concrete (e)Taking cylinder and cube samples. (f)Curing of column concrete. 35
Figure 2.9 : Process of column retrofitting: (a)Saturation of retrofitting region by water before retrofitting process. (b)Leaving a gap between column and stub by wooden elements. (c)Spraying GRC. (d)Wrapping Basalt textile. (e)Wrapping Basalt and spraying GRC. (f)Retrofitted Columns..... 37
Figure 2.10 : Test Setup..... 39
Error! Reference source not found. The locations of the LVDTs 40
Figure 2.12 : Strain-gauge locations on longitudinal and transverse bars..... 41
Figure 2.13 : Loading history of the specimens during each test. 42
Figure 3.1 : Effectively Confined Core for Rectangular Hoop Reinforcement (Mander, Priestley & Park 1988)..... 44
Figure 3.2 : Confines strength determination from lateral confining stresses for rectangular sections (Mander, Priestley & Park 1988)……....45
Figure 3.3 : Proposed Stress-Strain Model (Mander, Priestley & Park 1988)..... 46
Figure 3.4: a)Section of confinement jacket. b)Approximate average confining stresses perpendicular to b-side. c)Approximate average confining stresses perpendicular to h side. d)Effectively confined area in columns with rectangular cross section (Thanasis C. Triantafillou 2006). 47
Figure 3.5 : Effectively confined cross-sectional area (Ilki et al, 2003). 48
Figure 3.6 : Stress-strain model for externally confined reinforced concrete 50

Figure 4.1 : Specimen Ref-S60-Ɵ90-L80 after the drift ratio of 0.4%. a)Face C. b)Definition of column optional faces. c)Face D 52
Figure 4.2 : a) Face C, and b) Face D of the specimen Ref-S60-Ɵ90-L80 after – 1.00% drift ratio 52
Figure 4.3 : Specimen Ref-S60-Ɵ90-L80 after the drift ratio of 1.50%. a)Face C. b)Definition of column optional faces. c)Face D. 53
Figure 4.4 : Specimen Ref-S60-Ɵ90-L80 after the drift ratio of 3.0%. a)Face A. b)Definition of column optional faces. c)Face D. 53
Figure 4.5 : Specimen Ref-S60-Ɵ90-L80 after the drift ratio of 6.0 % a) Face C, b) Definition of column optional faces, c) Face D 54
Figure 4.6 : Specimen Ref-S60-Ɵ90-L80 after the drift ratio of 6.0 %. a)Face C. b)Definition of column optional faces. c)Face D 54
Figure 4.7 : Crack pattern of Ref-S60-Ɵ90-L80 at different drift ratios 55
Figure 4.8 : Lateral Load-Drift-Tip Displacement curves for Ref-S60-Ɵ90-L80 56
Figure 4.9 : Lateral Load-Drift envelope curve of Ref-S60-Ɵ90-L80. 56
Figure 4.10 : Specimen Ref-S60-Ɵ112.5-L80 after the drift ratio of 0.1%. a)Face B.b)Definition of column optional faces. c)Face C 57
Figure 4.11 : Specimen Ref-S60-Ɵ112.5-L80 after the drift ratio of 0.6%. a)Face C.b)Definition of column optional faces. c)Face C 58
Figure 4.12 : Specimen Ref-S60-Ɵ112.5-L80 after the drift ratio of 1.0%. a)Face C.b)Definition of column optional faces. c)Face C 58
Figure 4.13 : Specimen Ref-S60-Ɵ112.5-L80 after the drift ratio of 2.5%. a)Face C.b)Definition of column optional faces. c)Face C 52
Figure 4.14 : Specimen Ref-S60-Ɵ112.5-L80 after the drift ratio of 4.0%. a)Face A.b)Definition of column optional faces. c)Face C 59
Figure 4.15 : Crack pattern of Ref-S60-Ɵ112.5-L80 at different drift ratios 59
Figure 4.16 : Specimen Ref-S60-Ɵ112.5-L80 after the drift ratio of 6.0 %. a)Face C. b)Definition of column optional faces. c)Face D.....60
Figure 4.17 : Lateral Load-Tip Displacement curves of Ref-S60-Ɵ112.5-L80 61
Figure 4.18 : Lateral Load-Drift envelope curve of Ref-S60-Ɵ112.5-L80 61
Figure 4.19 : Specimen Ref-S60-Ɵ135-L80 after the drift ratio of 0.2%. a)Face C.b)Definition of column optional faces. c)Face D 62
Figure 4.20 : Specimen Ref-S60-Ɵ135-L80 after the drift ratio of 0.6%. a)Face C.b)Definition of column optional faces. c)Face D 63
Figure 4.21 : Specimen Ref-S60-Ɵ135-L80 after the drift ratio of 2.0%. a)Face C.b)Definition of column optional faces. c)Face D 63
Figure 4.22 : Specimen Ref-S60-Ɵ135-L80 after the drift ratio of 3.0%. a)Face A.b)Definition of column optional faces. c)Face D 64

Figure 4.23 : Specimen Ref-S60-Ɵ135-L80 after the drift ratio of 5.0%. a)Face A.b)Definition of column optional faces. c)Face C..... 65
Figure 4.24 : Specimen Ref-S60-Ɵ135-L80 after the drift ratio of 5.0%. a)Face C.b)Definition of column optional faces. c)Face C..... 65
Figure 4.25 : Crack pattern of Ref-S60-Ɵ135-L80 at different drift ratios..... 66
Figure 4.26 : Lateral Load -Tip Displacement curves for Ref-S60-Ɵ135-L80. 67
Figure 4.27 : Lateral Load-Drift envelope curve of Ref-S60-Ɵ135-L80..... 67
Figure 4.28 : Specimen Ref-S60-Ɵ135-L40 after the drift ratio of 0.2%. a)Face C. b)Definition of column optional faces. c)Face D. 68
Figure 4.29 : Specimen Ref-S60-Ɵ135-L40 after the drift ratio of 0.6%. a)Face C. b)Definition of column optional faces. c)Face D 69
Figure 4.30 : Specimen Ref-S60-Ɵ135-L40 after the drift ratio of 1.5%. a)Face C. b)Definition of column optional faces. c)Face D 69
Figure 4.31 : Specimen Ref-S60-Ɵ135-L40 after the drift ratio of 2.5%. a)Face C. b)Definition of column optional faces. c)Face A. 70
Figure 4.32 : Specimen Ref-S60-Ɵ135-L40 after the drift ratio of 5.0%. a)Face C. b)Definition of column optional faces. c)Face D. 70
Figure 4.33 : Crack pattern of Ref-S60-Ɵ135-L40 at different drift ratios..... 71
Figure 4.34 : Specimen Ref-S60-Ɵ135-L40 after the drift ratio of 5.0 %. a)Face C. b)Definition of column optional faces. c)Face D 72
Figure 4.35 : Lateral Load -Tip Displacement curves of Ref-S60-Ɵ135-L40..... 72
Figure 4.36 : Lateral Load-Drift envelope curve of Ref-S60-Ɵ135-L40..... 73
Figure 4.37 : Specimen Ret-S60-Ɵ90-L80-3TRM after the drift ratio of 0.2%. a)Face C. b)Definition of column optional faces. c)Face D. 74
Figure 4.38 : Specimen Ret-S60-Ɵ90-L80-3TRM after the drift ratio of 0.6%. a)Face C. b)Definition of column optional faces. c)Face D. 75
Figure 4.39 : Specimen Ret-S60-Ɵ90-L80-3TRM after the drift ratio of 1.5%. a)Face C. b)Definition of column optional faces. c)Face A.. 75
Figure 4.40 : Specimen Ret-S60-Ɵ90-L80-3TRM after the drift ratio of 4.0%. a)Face A. b)Definition of column optional faces. c)Face D 76
Figure 4.41 : Specimen Ret-S60-Ɵ90-L80-3TRM after the drift ratio of 8.0 %. a)Face C. b)Definition of column optional faces. c)Face A.. 76
Figure 4.42 : The damaged jacket of Specimen Ret-S60-Ɵ90-L80-3TRM at the end of test. a)Face A. b)Definition of column optional faces. c)Face B.. 77
Figure 4.43 : Crack pattern of Ret-S60-Ɵ135-L80 at different drift ratios. 77
Figure 4.44 : Lateral Load-Drift- Tip Displacement curves for Ret-S60-Ɵ90-L80-3TRM 78
Figure 4.45 : Lateral Load-Drift envelope curve of Ret-S60-Ɵ90-L80-3TRM..... 79
Figure 4.46 : Specimen Ref-S60-Ɵ112.5-L80-3TRM after the drift ratio of 0.1%. a)Face C. b)Definition of column optional faces. c)Face B..... 80
Figure 4.47 : Specimen Ret-S60-Ɵ112.5-L80-3TRM after the drift ratio of 0.6%. a)Face C. b)Definition of column optional faces. c)Face D. 81

Figure 4.48 : Specimen Ref-S60-Ɵ112.5-L80-3TRM after the drift ratio of 1.5%. a)Face B. b)Definition of column optional faces. c)Face C..... 81
Figure 4.49 : Specimen Ret-S60-Ɵ112.5-L80-3TRM after the drift ratio of 8.0 %. a)Face C. b)Definition of column optional faces. c)Face B..... 82
Figure 4.50 : The damaged jacket of Specimen Ret-S60-112.5-L80-3TRM at the end of test. a)Face A. b)Definition of column optional faces. c)Face B. 82
Figure 4.51 : Crack pattern of Ret-S60-Ɵ112.5-L80 at different drift ratios..... 83
Figure 4.52 : Lateral Load-Drift-Tip Displacement curves for Ret-S60-Ɵ112.5-L80-3TRM. 84
Figure 4.53 : Lateral Load-Drift envelope curve of Ret-S60-Ɵ112.5-L80-3TRM... 84
Figure 4.54 : Specimen Ref-S60-Ɵ135-L80-3TRM after the drift ratio of 0.1%. a)Face B, b)Definition of column optional faces. c)Face D. 86
Figure 4.55 : Specimen Ret-S60-Ɵ135-L80-3TRM after the drift ratio of 0.4%. a)Face C. b)Definition of column optional faces. c)Face D 86
Figure 4.56 : Specimen Ref-S60-Ɵ135-L80-3TRM after the drift ratio of 1.5%. a)Face C. b)Definition of column optional faces. c)Face A 87
Figure 4.57 : Specimen Ret-S60-Ɵ135-L80-3TRM after the drift ratio of 8.0 %. a)Face C. b)Definition of column optional faces. c)Face A 88
Figure 4.58 : The damaged jacket of Specimen Ret-S60-135-L80-3TRM at the end of test. a)Face D. b)Definition of column optional faces. c)Face A..... 88
Figure 4.59 : Crack pattern of Ret-S60-Ɵ135-L80 at different drift ratios..... 89
Figure 4.60 : Lateral Load-Drift-Tip Displacement curves for Ret-S60-Ɵ135-L80-3TRM. 90
Figure 4.61 : Lateral Load-Drift envelope curve of Ret-S60-Ɵ135-L80-3TRM..... 90
Figure 4.62 : Specimen Ret-S60-Ɵ135-L40-3TRM after the drift ratio of 0.1%. a)Face C. b)Definition of column optional faces. c)Face D. 92
Figure 4.63 : Specimen Ret-S60-Ɵ135-L40-3TRM after the drift ratio of 0.8%. a)Face C. b)Definition of column optional faces. c)Face D. 92
Figure 4.64 : Specimen Ret-S60-Ɵ135-L40-3TRM after the drift ratio of 1.5%. a)Face C. b)Definition of column optional faces. c)Face D. 93
Figure 4.65 : Specimen Ret-S60-Ɵ135-L40-3TRM after the drift ratio of 8.0 %. a)Face C. b)Definition of column optional faces. c)Face A. 94
Figure 4.66 : The damaged jacket of Specimen Ref-S60-135-L40-3TRM at the end of test. a)Face C. b)Definition of column optional faces. c)Face A..... 94
Figure 4.67 : Crack pattern of Ret-S60-Ɵ135-L40-3TRM at different drift ratios... 95
Figure 4.68 : Lateral Load-Drift-Tip Displacement curves for Ret-S60-Ɵ135-L40-3TRM. 96
Figure 4.69 : Lateral Load-Drift envelope curve of Ret-S60-Ɵ135-L40-3TRM..... 96
Figure 5.1 : Location of the measurements system which are used for obtaining moment- curvature relationship..... 97

Figure 5.2 : Experimental Moment-Curvature diagrams for Ref-S60-Ɵ90-L80 and Ret-S60-Ɵ90-L80-3TRM. a)Elevation code of 150~310 mm. b)Elevation code of 30~155mm. c)Elevation code of 0~30 mm..... 99
Figure 5.3 : Experimental Moment-Curvature diagrams for Ref-S60-Ɵ112.5-L80 and Ret-S60-Ɵ112.5-L80-3TRM. a)Elevation code of 150~310 mm. b)Elevation code of 30~155mm. c)Elevation code of 0~30 mm..... 100
Figure 5.4 : Experimental Moment-Curvature diagrams for Ref-S60-Ɵ135-L80 and Ret-S60-Ɵ135-L80-3TRM. a)Elevation code of 150~310mm. b)Elevation code of 30~155mm. c)Elevation code of 0~30 mm..... 101
Figure 5.5 : Experimental Moment-Curvature diagrams for Ref-S60-Ɵ135-L40 and Ret-S60-Ɵ135-L40-3TRM. a)Elevation code of 150~310mm. b)Elevation code of 30~155mm. c)Elevation code of 0~30 mm..... 102
Figure 5.6 : Comparison of energy dissipation capacity of the reference specimens. 103
Figure 5.7 : Comparison of energy dissipation capacity of the retrofitted specimens. 104
Figure 5.8 : a)Energy dissipation capacity of the Ref-S60-Ɵ90-L80 versus Ret-S60-Ɵ90-L80-3TRM. b)Energy dissipation capacity of the Ref-S60-Ɵ112.5-L80 versus Ret-S60-Ɵ112.5-L80-3TRM. c)Energy dissipation capacity of the Ref-S60-Ɵ135-L80 versus Ret-S60-Ɵ135-L80-3TRM. d)Energy dissipation capacity of the Ref-S60-Ɵ135-L40 versus Ret-S60-Ɵ135-L40-3TRM. 104
Figure 5.9 : All specimens photographs at the end of tests. a)Ref-S60-Ɵ90-L80 at the end of 6% drift ratio. b)Ref-S60-Ɵ112.5-L80 at the end of 6% drift ratio. c)Ref-S60-Ɵ135-L80 at the end of 4% drift ratio. d)Ref-S60-Ɵ135-L40 at the end of drift ratio 5%. e)Ret-S60-Ɵ90-L80-3TRM at the end of 8% drift ratio. f)Ret-S60-Ɵ112.5-L80-3TRM at the end of 8% drift ratio. g)Ret-S60-Ɵ135-L80-3TRM at the end of 8% drift ratio. h)Ret-S60-Ɵ135-L40-3TRM at the end of 8% drift ratio 107
Figure 5.10 : The envelopes curves of the lateral load-drift for all reference specimens. 109
Figure 5.11 : Envelopes of the lateral load-drift curves for all retrofitted specimen. 111
Figure 5.12 : The envelope curves of test results. a)Ref-S60-Ɵ90-L80 versus Ret-S60-Ɵ90-L80-3TRM. b)Ref-S60-Ɵ112.5-L80 versus Ret-S60-Ɵ112.5-L80-3TRM. c)Ref-S60-Ɵ135-L80 versus Ret-S60-Ɵ135-L80-3TRM. d)Ref-S60-Ɵ135-L40 versus Ret-S60-Ɵ135-L40-3TRM. 113
Figure 5.13 : Envelopes of the lateral load-drift curves for all reference and retrofitted specimens. 114
Figure 5.14 : Moment, curvature and deflection relationship for a prismatic RC cantilever (M.J.N. Priestly, F.Seible and G.M. Calvi). 115
Figure 5.15 : Theoretical result versus test results Ref-S60-Ɵ90-L80. 116
Figure 5.16 : Theoretical result versus test results Ref-S60-Ɵ112.5-L80. 117

Figure 5.17 : Theoretical result versus test results Ref-S60-Ɵ135-L80 117
Figure 5.18 : Theoretical result versus test results Ref-S60-Ɵ135-L40. 118
Figure 5.19 : Theoretical result and experimental result of Ret-S60-Ɵ90-L80-3TRM.. 119
Figure 5.20 : Theoretical results and experimental results of Ret-S60-Ɵ112.5-L80-3TRM.. 119
Figure 5.21 : Theoretical results versus experimental results of Ret-S60-Ɵ135-L80-3TRM. 120
Figure 5.22 : Theoretical results versus experimental results of Ret-S60-Ɵ135-L40-3TRM. 120
Figure B.1 : Specimen detail for Ref-S60-Ɵ90-L80..... 195
Figure B.2 : Specimen detail for Ref-S60-Ɵ112.5-L80. 196
Figure B.3 : Specimen detail for Ref-S60-Ɵ135-L80..... 197
Figure B.4 : Specimen detail for Ref-S60-Ɵ135-L40..... 198
Figure B.5 : Specimen detail for Ret-S60-Ɵ90-L80-3TRM. 199
Figure B.6 : Specimen detail for Ret-S60-Ɵ112.5-L80-3TRM 200
Figure B.7 : Specimen detail for Ret-S60-Ɵ135-L80-3T..... 201
Figure B.8 : Specimen detail for Ret-S60-Ɵ135-L40-3TRM. 202
Figure B.9 : The arrangement of reinforcement and assembly of cages 203
Figure B.10 : The arrangement of reinforcement and assembly of cages 204
Figure B.11 : The arrangement of reinforcement and assembly of cages. 205
Figure B.12 : The arrangement of reinforcement and assembly of cages. 206
Figure B.13 : Specimens hook details.. 207
Figure C.1 : The strain distribution in the longitudinal reinforcing bars of specimen Ref-S60-Ɵ90-L80 and Ret-S60-Ɵ90-L80-3TRM. a)Bar which has 7 strain-gages at the pushing. b)Bar which has 7 strain-gages at the pulling. c)Bar which has 3 strain-gages at the pushing. d)Bar which has 3 strain-gages at the pulling. e)Bar which has 7 strain-gages at the pushing. f)Bar which has 7 strain-gages at the pulling. g)Bar which has 7 strain-gages at the pushing. h)Bar which has 7 strain-gages at the pulling..... 209
Figure C.2 : The strain distribution in the longitudinal reinforcing bars of s pecimen Ref-S60-Ɵ112.5-L80 and Ret-S60-Ɵ112.5-L80-3TRM. a)Bar which has 7 strain-gages at the pushing. b)Bar which has 7 strain-gages at the pulling. c)Bar which has 3 strain-gages at the pushing. d)Bar which has 3 strain-gages at the pulling. e)Bar which has 7 strain-gages at the pushing. f)Bar which has 7 strain-gages at the pulling. g)Bar which has 7 strain-gages at the pushing. h)Bar which has 7 strain-gages at the pulling. 210
Figure C.3 : The strain distribution in the longitudinal reinforcing bars of specimen Ref-S60-Ɵ135-L80 and Ret-S60-Ɵ135-L80-3TRM a) Bar which has 7 strain-gages at the pushing b) Bar which has 7 strain-gages at the pulling c) Bar which has 3 strain-gages at the pushing d) Bar which has 3 strain-gages at the pulling e) Bar which has 7 strain-gages at the pushing f) Bar which has 7 strain-gages at the pulling g)

Bar which has 7 strain-gages at the pushing h) Bar which has 7 strain-gages at the pulling. 211
Figure C.4 : The strain distribution in the longitudinal reinforcing bars of specimen Ref-S60-Ɵ135-L40 and Ret-S60-Ɵ135-L40-3TRM a) Bar which has 7 strain-gages at the pushing b) Bar which has 7 strain-gages at the pulling c) Bar which has 3 strain-gages at the pushing d) Bar which has 3 strain-gages at the pulling e) Bar which has 7 strain-gages at the pushing f) Bar which has 7 strain-gages at the pulling g) Bar which has 7 strain-gages at the pushing h) Bar which has 7 strain-gages at the pulling. 212

SEISMIC RETROFIT OF RC COLUMNS WITH SPRAYED BASALT MESH REINFORCED GRC:
EFFECTS OF STIRRUP HOOK ANGLE AND HOOK LENGTH

SUMMARY

Turkey is one of the most seismically active regions on the earth which is exposed to large magnitude earthquakes, resulting in substantial loss of life and property damage. Recent earthquakes in Turkey revealed that a remarkable number of existing buildings have poor seismic performance because of very low axial compressive strength of the concrete, inadequate lateral reinforcement in the columns, insufficient details in the stirrups or design/construction errors and change in the facility use. Most of the structures which were built by previous versions of Turkish codes (i.e. ABYYHY 1975 and TS500-1984) were expected to have a sufficient performance during the earthquakes but according to the New Turkish codes (i.e. DBYBHY 2007 and TS500-2000), strengthening is required to improve the performance of the same structures to prevent from another disaster. All of mentioned reasons were caused New Turkish Seismic Code introduced a section to improve the performance of old structures to prevent disastrous consequences.

Confinement of concrete by FRP is an efficient technique used to increase the load carrying capacity and/or ductility of a column and lateral pressure in the concrete case. There are several advantages of using FRP for rehabilitation of RC structures. However, some drawbacks require attention of FRP users. These drawbacks are (1) poor behavior of epoxy resins at temperature, (2) relatively high cost of epoxies, (3) hazards for the manual worker, (4) inability to apply FRP on wet surfaces or at low temperatures, (5) lack of vapor permeability, which may cause damage to the concrete structure, and (6) incompatibility of epoxy resins and substrate materials.

One possible solution to the previous problems would be use of textile with cement based mortars in place of fiber sheets. In the last decades, a large amount of research has indicated that textile reinforced mortar jacketing is promising solution for the confinement of RC columns, including poorly detailed ones in seismic regions. Using textile with special mortars (GRC) as a mix component and special applying system (spraying the mortar until covering all textile) is separate this study with other experimental studies. This composite material is known as Textile Reinforced Mortar (TRM) and the presence of glass fibers in the cement matrix instead of resin matrix offers the new way for the use of lower textile, which is less expensive. The use of Textile Reinforced Mortar (TRM) as an external reinforcement is currently being explored by the construction industry as a new material.

In this study, seismic performance of poor and well detailed RC columns and effectiveness of TRM for improving flexural behavior and energy dissipation capacity of the same characteristic reinforced concrete columns are experimentally investigated and compared with theoretical models which are used to estimate the hysteretic behavior of columns.

The test specimens were cantilever type columns, representing half a column in a real building frame. A total of eight rectangular columns of dimensions 300 x 200 x 1500 mm along with a stub of dimensions 700 x 700 x 450 mm were constructed. All columns are reinforced with four longitudinal bars Φ14 placed symmetrically. The transverse steel reinforcement was given by stirrups Φ8. All specimens were subjected to cyclic lateral and constant high-axial loads. At the stage of specimen designing, columns were expected to fail in flexural behavior before reaching their shear strength. In addition, four of the columns were designed as reference specimens and others, which had the same characteristics, were confined by three layers of Basalt mesh sprayed with Glass Fiber Reinforced Cement until covering all textile layers.

Characteristics of the specimens are low strength concrete with plain longitudinal reinforcement bar. Corners of all columns were rounded about 30 mm and clear cover thickness of columns were 15 mm. Transverse reinforcement bars with hook angles of 90°, 112.5°, 135° and hook lengths of 40 and 80 mm at both ends were examined. Stirrups were placed at a spacing of 60 mm.

For this purpose, primarily in the first chapter of the thesis, purpose and scope of the study was explained. In continuation of the work done in the past about the subject, a summarized literature review was mentioned and TRM composites as a significant retrofitting method in the future are emphasized. In the second chapter, properties of the test specimens, material properties, manufacturing steps of the test specimens and experimental setup are indicated. A summarized analytical study at the third chapter of thesis discusses about internal and external confinement in columns. The forth chapter describes the behavior of columns that was observed during the test. Into the fifth chapter, a variety of experimental and theoretical results are described in detail and are compared by using graphics. At the end, the sixth chapter discusses conclusions and recommendations related with thesis.

Experimental results indicated that Basalt mesh jacketing, especially with sprayed GRC is quite effective as a means of increasing drift ratio and cyclic deformation capacity of poor and well detailed RC columns which resulted from more energy dissipation.

BETONARME KOLONLARIN BASALT HASIR DONATILI PÜSKÜRTME GRC İLE DEPREME KARŞI GÜÇLENDİRİLMESİ : ETRİYE KANCA AÇISI VE BOYUNUN ETKİSİ

ÖZET

Türkiye dünyanın sismik yönden en aktif bölgelerinden birisidir ve can ve mal kaybına neden olan büyük magnitüdlü pek çok depreme maruz kalmıştır. Son depremler, Türkiye'deki mevcut yapı stokunun çok düşük beton basınç dayanımı, kolonlardaki yetersiz enine donatılar, etriyelerdeki detay zayıflıkları/yapım hataları ve bina kullanımının tasarımdaki amaca uygun olmaması gibi pek çok nedenlerle yetersiz deprem davranışına sahip olduğunu açığa çıkarmıştır. FRP kompozit malzemelerin bu eksikliklerin giderilmesi amacı ile yapı mühendisliğinde de kullanımı günden güne artmaktadır. Önceki yıllarda ABYYHY-1975 ve TS500-1984 yönetmeliklerine göre deprem esnasında yeterli davranışı göstermesi beklenen yapılar yeni tasarım yönetmelikleri olan DBYBHY-2007 ve TS500-2000 e göre yetersiz çıkmakta ve bu yapıların güçlendirilmesi gerekmektedir.Meydana gelen depremler sonrası betonarme yapılarda yapılan araştırmalar, yapının en fazla zarar görmesine neden olan yapısal elemanın kolonlar olduğunu ortaya koymuştur. Betonarme bir yapıda kolonlar eğer kendisinden beklenen performansı göstermiş ise yapı ayakta kalmış ve daha az hasarla depremi atlatmıştır. Betonarme yapıların deprem anında ayakta kalması büyük ölçüde kolonlar aracılığıyla olduğu için, yapılan çalışmalar bu yapı elemanı üzerinde yoğunlaşmakta ve yıllardan beri bu konu üzerinde sayısız bilimsel çalışma yapılmış ve yapılmaktadır.

Türkiye de güçlendirme ihtiyacı duyulan yapıların ortak kusurlarından bazıları, yetersiz ve düz yüzeyli donatı kullanımı, düşük beton dayanımı ve yetersiz süneklikteki kesitler olarak kabul edilebilir. Çeşitli güçlendirme yöntemleriyle bu eksikliklerin giderilme imkânı vardır. Özellikle de betonarme kolonları süneklik ve dayanım açısından belirli bir seviyeye getirmek için enine donatı(etriye) çok önemlidir. Çünkü betonarme kolonlarda enine donatı yerleşimi gerek dayanım gerekse süneklik açısından davranış üzerinde önemli etkilere sahiptir. Literatürdeki çalışmalarda genel olarak yönetmelik kurallarına uygun enine donatı yerleşimleri incelenmiş, sınırlı sayıda çalışmada ise yönetmelik kurallarına bütünü ile uymayan enine donatı yerleşimleri ve bu durumda davranışta ortaya çıkan zayıflıkların giderilmesine ağırlık verilmiştir. Bunlara karşılık yönetmelik şartlarını kısmen sağlayan, kısmen sağlamayan enine donatı yerleşimlerinin davranışa etkisi araştırılmamıştır. Bu konuya yönelik olarak İTÜ Yapı ve Deprem Mühendisliği Laboratuvarında çok kapsamlı bir çalışma sürmektedir. Bu tezde devam eden çalışmaların bir bölümüne ait sonuçlar sunulmaktadır.

Uzun yıllar uçak ve otomobil üretiminde kullanılan fiber takviyeli polimerler (FRP) son yıllarda yapı elemanlarının güçlendirilmesinde de kullanılmak üzere araştırma konusu olmuştur. Çeşitli geometrik özelliklerde bulunan FRP 'ler, deprem güçlendirilmesinde genellikle kullanıma hazır karbon fiber takviyeli polimer örtüler halinde kullanılır. Duvar kağıdını veya kumaşı andıran elyaflar genellikle 0,30-0,60 metre eninde rulolar halinde satılır. Yapı elemanları üzerine reçine sistemi ile

uygulanan FRP çok yüksek çekme dayanımına sahiptir. Yalnız bu dayanım, malzemenin uygulanış şekli ve işçilik kalitesi ile değişebilir. Bu nedenle çok dikkatli olmak gerekir. Sonuçta ortaya çıkan kompozit malzemenin özellikleri kullanılan elyaf miktarı ile yakından ilgilidir. Örneğin, bol reçineli bir uygulama, karbon elyafın elastisite modülü ve dayanımı ne denli yüksek olursa olsun, ortaya çıkan kompozit malzemenin elastisite modülünü ve dayanımını büyük ölçüde düşürür. Öte yandan, kullanılması öngörülen özel çelik rulolar ile reçine fazlası alınan uygulamalarda elastisite modülü ve çekme dayanımı önemli ölçülerde artar. Bu değişimlerden dolayı, her uygulama için çekme deneyi yapmak ve malzeme özelliklerini deneysel olarak belirlemek gerekebilir.

Hasar görmüş betonarme elemanlara başlangıçtaki orijinal mukavemetlerini kazandırmak veya güçlendirmek amacı ile karbon lifi – cam lifi takviyeli epoksi esaslı kompozit malzemeler çelik plakalarla yapılan geleneksel güçlendirme sistemlerine alternative olarak geliştirilmişlerdir. Çekme dayanımları çelikten fazla olan bu tür kompozit malzemelerin en büyük avantajları hafif olmaları, korozyona uğramamaları, ve rulolar halinde saklanabilmeleri ve kolaylıkla uygulanabilmeleridir. Polimer esaslı bu malzemelerin yüksek maliyetleri ve UV ışınlarına dayanıksız olmaları nedeniyle özel sıvalar veya kaplamalarla korunmalarının gerekmesi dezavantajlarıdır. Polimerlerin uzun süreli sabit yükler altında sünme deformasyonlarının yüksek oluşu da bir diğer problemdir. Frp'ler sadece lif eksenine paralel çekme kuvvetlerini karşılayabildikleri için uygulama yönü önemlidir. İki yönlü tabakalar halinde uygulandığında kirişlerde eğilme ve kesme dayanımının, kolonlarda eğilme ve sargılama etkisiyle basınç dayanımının arttırılması mümkündür.

Betonun sargılaması, yük taşıma kapasitesinin ve /veya sünekliğin arttırılması için kullanılan verimli bir yöntemdir. Son 10 yıllık sürede pek çok araştırma, betonarme kolonlarda -sismik açıdan zayıf detaylandırılmış olanlar da dahil olmak üzere- TRM ile sargılamanın gelecek vaat eden bir yöntem olduğunu göstermiştir. Bu çalışmayı diğer deneysel çalışmalardan ayıran yönü tekstilin karışım bileşeni olarak özel bir harçla (GRC) kullanımı ve özel uygulama (harcın tekstilin tamamını kaplayacak şekilde püskürtülmesi) tekniğidir. Bu kompozit malzeme Tekstille Güçlendirilmiş Harç (TRM) olarak bilinmekte ve çimento matrisinde reçine yerine cam liflerin bulunması daha yüksek modül sunmakta ve matris daha ucuz olan düşük modüllü tekstil kullanımına yol açmaktadır. Yeni bir malzeme ve dış donatı olarak TRM nin kullanımı yapı endüstrisi tarafından incelenmektedir.

Bu çalışmada; zayıf ve iyi donatılmış betonarme kolonların sismik performansları ve aynı karakteristiklere sahip betonarme kolonlarda TRM nin eğilme davranışında ve enerji tüketme kabiliyetindeki etkileri deneysel olarak incelenmiş ve sonuçlar kolonların histeretik davranışlarını tahmin için önerilen modellerle teorik olarak karşılaştırılmıştır. Deneyler; dikdörtgen kesitli, sabit yüksek eksenel kuvvete sahip ve çevrimsel yatay yüklemeye maruz 8 adet kolonda yürütülmüştür. Ek olarak 4 adet kolon kontrol numunesi olarak tasarlanmış ve diğerleri kontrol numuneleriyle aynı özelliklere sahip olmak üzere 3 kat Basalt Hasır Donatılı Püskürtme GRC (basalt textile reinforced mortar) ile sarılmış ve bütün tekstil katmanlarını kapatacak kadar cam lifli harç püskürtülmüştür. Numunelerde düşük dayanımlı beton ve düz donatı

kullanılmıştır. Bütün kolonlarda paspayı 15 mm dir ve kolonların köşeleri 30 mm yarıçapında dairesel hale getirilmiştir. Etriyerler 60 mm aralıklarla yerleştirilmiştir. Etriyelerin kanca açıları 90,112.5, 135 derece ve kanca boyları 40 ve 80 mm dir.
Bu amaç doğrultusunda çalışmanın ilk bölümünde öncelikle çalışmanın amacı ve kapsamı anlatılmıştır. Konunun devamında ilgili geçmişte yapılan çalışmalardan kronolojik sıraya göre bahsedilmiş, TRM malzeme ile güçlendirme yönteminin gelecekte çok sık kullanılacak bir yöntem olduğu vurgulanmıştır. İkinci bölümde, deney numunelerinin özellikleri, deney numunelerinin üretim aşamaları ve deney düzeneği açıklanmış, deneylerde kullanılan malzeme özellikleri belirtilmiştir. İç ve dıştan sargılanmış kolonların davranışı üçüncü bölümde analitik çalışma kapsamında sunulmuştur. Dördüncü bölümde, test sırasında gözlenmiş kolonların davranışı anlatılmıştır. Deney sonuçlarının detaylı şekilde anlatıldığı ve çeşitli grafikleri kullanarak sonuçları birbirile karşılaştırdığı beşinci bölümün sonrasında, altıncı bölümde deney sonuçları yorumlanmış ve değerlendirmeler anlatılmıştır. Teorik çalışmalar kapsamında elemanların yük kapasiteleri, yük-yerdeğiştirme (öteleme oranı) ilişkileri, hasar durumları ve deprem sırasında maruz kalacakları öteleme oranları tahmin edilmeye çalışılmıştır. Deney sonuçları dayanım, süneklik, enerji yutma kapasitesi, rijitlik, kalıcı deformasyonlar ve göçme modları bakımından değerlendirilmistir ve sonuçlar Basalt Hasır Donatılı Püskürtme GRC ile sargının ötelenme oranı ve çevrimsel deformasyon kapasitesi bakımından zayıf ve iyi detaylandırılmış kolonlarda çok etkili olduğunu göstermiştir.

1. INTRODUCTION

Earthquake is unexpected natural disaster and thousands of people were injured, lost their lives or were left homeless in the last years. Recent earthquakes in Turkey, revealed that a remarkable number of existing buildings have poor seismic performance because of very low axial compressive strength of the concrete, inadequate lateral reinforcement in the columns or insufficient details in the stirrups. In the past three decades, most of the structures, which were built by previous versions of Turkish Codes, were expected to have a sufficient performance during the earthquakes but after reviewing the New Turkish Codes, because of revisions of code requirements, retrofitting and strengthening are felt to improve the performance of the same structures to preventing from another catastrophe.

The use of Textile Reinforced Mortar (TRM) reinforcement is currently being explored by the construction industry as a new material. Nowadays, it is commonly seen the need of strengthening or rehabilitating RC columns which are resulted from higher load capacity demands because of design/construction errors, change in the facility use, or revisions of code requirements. Ductility enhancement is typically required in existing columns that are subjected to a combination of axial load and bending moment because of reasons similar to those listed for strengthening. Among these reasons, seismic upgrade and correction of detailing defects (lack of stirrups, 90° angle or length of stirrups at closed ends) are the most common. Confinement of concrete is an efficient technique used to increase the load carrying capacity and/or ductility of a column and lateral pressure in the concrete case to increase compressive strength and ultimate axial strain. A large amount of research in the last decade has been indicate that TRM jacketing is an extremely promising solution for the confinement of RC columns, including poorly detailed ones in seismic regions. Using Textile with special mortars (GRC) as a mix component and special applying system (spraying the mortar until covering all textile) is separate this study with other experimental studies. This composite material is known as Textile Reinforced Mortar

(TRM). The presence of glass fibers in the cement matrix instead of resin matrix offers the new technique for the use of lower modulus textile.

In this experimental study, eight full-scale rectangular columns with their foundations were built and these specimens with different variables will be test in a laboratory of the Istanbul Technical University. All the specimens are rectangular and dimension of the cross section is 200×300 mm and the height of the specimens is 1500 mm and the actuator were applied the lateral load at the point of 1300 mm.

The average compressive strength of concrete for the characteristic age of 180 days was 7.5 MPa by testing standard cylinders (the average equivalent compressive strength value for reference and retrofitted specimens was about 9.9 and 7.5 MPa by testing core samples, respectively). Two different type of vibration process were used during the casting of concrete, then two different concrete strength result for specimens were undesirable.The main differences of specimens are different hook angle and hook length of the stirrups. In a majority of the 1985s constructed reinforced concrete (RC) frame buildings, the longitudinal reinforcement bars are plain and the angle of the stirrups were 90 degree so by considering this, we used angle of the 90-112.5 and 135 degree in this specimens. Flexural behavior of the RC columns were investigated so failure of the columns by shear force was not desirable for this study which were subjected to high axial load. Meanwhile, for preventing the shear failure, the ribbed stirrups were used. For summarizing the test results, a number of behavior characteristics; such as displacement capacity, strength, moment-curvature relationship, ductility, strain distribution, and displacement components, which are among main indicators of seismic performance, are evaluated. Previous experimental evidence showed that the magnitude and loading pattern of axial force had a significant effect on the seismic response of the columns. As an important part of this research program, the effects of constant high axial load were seen in the column failure patterns, hysteresis loops, and load-carrying capacities.

1.1 Research Significance

The recent earthquakes in Turkey have caused extensive damage to many buildings. Investigation of these damages, based on onsite observations and available ground motion data, has demonstrated that concrete columns with inadequate confinement significantly contributed to the catastrophic collapse of these structures. Confinement

through stirrups and spirals, if properly detailed and anchored, can prevent sudden loss of bond and buckling of longitudinal bars. Therefore, to ensure ductile behavior of columns during earthquake type loading, it is imperative to provide adequate confinement. Recently, innovative techniques such as external wrapping and bonding of Fiber Reinforced Polymer (FRP) sheets or straps around potential plastic hinge regions in columns has become increasingly popular. Some of the advantages of FRPs over the conventional external confinement techniques (reinforced concrete jacketing and steel plate jacketing) are higher strength, greater contact area, increased resistance to corrosion, ease of installation, lighter weight, and maintenance of the original column stiffness.

1.2 Purpose of Thesis

The structures built in Turkey in early 70's and 80's were designed according to the codes prevalent at that time, which incorporated large spacing of lateral steel in the potential plastic hinge regions of columns as well as inadequate hook length with commonly 90 degree hook angle. The main objective of this research program was to study the seismic behavior of reinforcement low strength concrete rectangular columns with and without confining Basalt Mesh Sprayed GRC Reinforced under constant high axial load and simultaneously lateral load while relating the details of transversal reinforcement. To accomplish these objectives, the following methodology was developed:

- Design, construction, instrumentation, and testing of eight large-scale RC rectangular structural members that allows relating adequately the amount of transversal reinforcement with low strength concrete, inadequate angle and length of the end of the stirrups.
- Investigation of the behavior of Basalt Mesh Sprayed GRC Reinforced and concrete confined by such reinforcement.
- Investigation of analytical relationships of Basalt Mesh Sprayed GRC Reinforced, and concrete confined by such reinforcement.
- Verify the validity of the stirrup hook angle and hook length limits required by the Turkish Standard TS-500 for the structural design of concrete columns.

- Execution of cyclic flexural test under constant high axial load on each specimen. The main data acquired from these tests were: lateral force applied by the actuators, tip displacement, strain gages and LVDT's lectures;
- Data processing consisting mainly in: the elaboration of load-displacement relationships and moment-curvature relationships, the calculus of ductility and energy dissipation, and the normalization of the moment-curvature relationships to allow comparison between specimens of different strength;
- Comparisons of all parameters estimated in the previous stage between specimens with same transversal steel spacing but having different hook angle and length at the end of stirrups. These analyses allowed studying the influence of angle and length of transversal steel on the behavior of the columns in relation to the ductility, energy absorption, and resistance gains;
- Study of the influence of Basalt Mesh Sprayed GRC Reinforced on the failure mode of the cover and damage levels of the specimens, made from the tests observations and the final aspect of the specimens.

1.3 Literature Review

Even though extensive research has been conducted on the seismic behavior of concrete columns in the past several decades, the available information is still limited regarding their seismic behavior when different materials, such as FRP, are used for transverse confinement. In particular, only a limited number of experiments have been conducted on realistically sized concrete columns transversely confined by steel reinforcement and/or FRP jackets under high axial load and lateral displacement excursions. The influences of factors, such as the transverse confinement and the external retrofitting, on the ductility performance of columns have been gradually revealed by the test data and analytical studies.

This section presents a literature review of relevant work about seismic tests on steel-confined or FRP-confined concrete columns. Some selected experimental studies are discussed in detail, in which most of all specimens were tested under reversed cyclic lateral load while simultaneously subjected to constant axial load. The enhancement of compressive strength of concrete due to transverse confinement was originally reported by Considere (1903) and the first widely accepted relationship between

strength enhancement and transverse confinement was proposed by Richart et al. (1928, 1929) for normal strength concrete confined by spirals or hydraulic pressure. Since then many experimental and theoretical investigations have been conducted on this research topic.

A general conceptual model for confinement by circular and rectilinear confining reinforcement was developed at the University of Toronto (Sheikh, 1978; Sheikh and Uzumeri, 1982) which formed the basis for a full stress-strain relationship for steel-confined concrete in tied columns under concentric compression. This was further extended to include the effect of strain gradient by Sheikh and Yeh (1986) for columns under seismic loading. The concept and determination of the effectively confined concrete area proposed by Sheikh and Uzumeri (1982) have been widely used by researchers for confined concrete columns since then. Mander et al. (1988) used this concept and developed a general stress-strain model applicable to normal-strength concrete columns with either circular or rectangular sections, under static and dynamic loading, and taking into account the effect of cyclic loading.

As an alternative to conventional confinement technologies, fiber-reinforced polymer (FRP) composites show great potential in replacing traditional steel reinforcement to retrofit concrete columns with deficient transverse reinforcement and have attracted considerable research in the past two decades. Sheikh and Yau (2002) and Li (2003) have introduced the material properties of FRP and various factors that affect FRP performance in detail.

Mirmiran and Shahawy, (1997) resulted that the externally bonded FRP jackets with fibers aligned mainly in the circumferential direction can effectively provide confinement which leads to significant enhancement of compressive strength and deformability of concrete. In steel-confined columns, the transverse steel may yield at the early stage of concrete deformation and the confining pressure keeps approximately constant afterwards. Therefore, the confining pressure is evaluated based on the yield strength of steel. On the contrary, FRP behavior under tension is almost perfectly linearly elastic and the confining pressure applied by FRP wrapping does not remain constant with increased load. Due to this reason, the existing compressive stress-strain models for steel confined concrete are not applicable for the concrete with transverse FRP-confinement.

Sheikh and Bayrak (2004) were aiming to demonstrate a practical limit that the rectilinear ties can be strained to under moderate to high axial load levels and reversed cyclic lateral displacement excursions, mainly focusing on at the usage of high strength steel as the confining reinforcement. The columns used in the experiments were representing a column in a typical building frame between maximum moment and point of contraflexure zones. The core area of all test specimens were identically designed to be 74.4% of the gross area of the column section. The test procedure took place under axial load and reversed cyclic lateral displacement excursion until it cannot maintain the axial load any more. As a result, it is stated that mechanical properties of lateral reinforcement have a direct effect on the effectiveness of confinement. In spite of the fact that ductile behavior was the target behavior of the concrete section, confinement steel does not have to be ductile with a flat yield plateau. After the transverse steel reaches its yield strain, the core may continue its expansion until the transverse reinforcement goes under strain hardening, meanwhile significant damage taking place in the concrete core. Evaluating all it is concluded that for confinement reinforcement, high yield strength steel with short yield plateau is preferable to low yield strength steel with a long yield plateau.

Mirmiran et al (2006) summarized the test results of an extensive research program sponsored by the US Transportation Research Board of the National Research Council to examine the behavior of high-strength concrete rectangular columns subjected to concentric and eccentric loading conditions. The variables considered in this investigation were concrete strength ranging from 7.9 ksi (55 MPa) to 16.5 ksi (114 MPa), longitudinal and transverse reinforcement ratios. Test results were combined with reported data in the literature to examine the validity of the current AASHTO LRFD Bridge Design Specification for high-strength concrete up to 18 ksi (124 MPa). Research findings indicate that the current specification overestimate the load carrying capacity of columns with high-strength concrete under both concentric and eccentric loading conditions. This paper recommends several provisions to the current AASHTO LRFD Bridge Design Specifications to extend the use of high-strength concrete up to 18 ksi (124 MPa) for axially and eccentrically loaded short columns. A total of thirty rectangular columns with concrete strengths ranging from 7.9 ksi (55 MPa) to 16.5 ksi (114 MPa) were tested under monotonically increasing concentric and eccentric loading. The test parameters for concentric loading included concrete

strength, specimen size, longitudinal and transverse reinforcement ratios. For eccentric loading, the parameters were concrete strength, specimen size and eccentricity of the applied load. The concrete cover used was ½ in (13 mm) to the face of the tie for all the test specimens. All columns were reinforced with six longitudinal steel bars and confined with #4 (Φ13) bars as transverse reinforcements. The two ends of the test specimens were reinforced with closely spaced ties and confined with external steel tubes, as shown in Figure 1, to avoid premature failure at the two ends of the test specimens. All columns were cast vertically to simulate typical column construction practice.

Ilki et al (2008) tested 68 reinforced concrete columns with circular, square and rectangular cross sections under uniaxial compression after being jacketed externally with carbon fiber-reinforced polymer CFRP sheets. The test program included 21 cylinder columns with a diameter of 250 mm, 24 columns with the cross-sectional dimensions of 250 mm x 250 mm, and 24 columns with the cross sectional dimensions of 150 mm x 300 mm. The height of all specimens was 500 mm. Forty specimens were cast using low strength concrete and inadequate internal transverse reinforcement, while 28 specimens were cast with medium strength concrete and a varying amount of internal transverse reinforcement. Thickness of the CFRP jacket, cross-section shape, concrete strength, amount of internal transverse reinforcement, corner radius, existence of pre-damage, loading type monotonic or cyclic, and the bonding pattern orientation, spacing, anchorage details, additional corner supports of CFRP sheets were the main test parameters of this extensive experimental work. The 28-day standard cylinder strength fc was 10.94 and 23.86 MPa, respectively, for low and medium strength concrete. It should be noted that unconfined concrete strength of the member was assumed to be 85% of the standard cylinder strength at the time of testing, when the strength of the same size unconfined specimen was not obtained experimentally. Longitudinal reinforcement ratio was around 0.01 and the clear concrete cover was 25 mm for all specimens. For longitudinal reinforcement 6Φ10, 4Φ14, and 4Φ12 bars were used for specimens with circular, square, and rectangular cross sections, respectively. For low strength series (LSR), the spacing of the transverse reinforcement was chosen as approximately 14.5 times of the diameter of the longitudinal bars to allow buckling of longitudinal reinforcing bars under axial stresses, and for representing frequently met transverse bar spacing in relatively older

structures. Since the diameter of longitudinal bars were 10, 12, and 14 mm for circular, rectangular and square cross sections, respectively, the transverse reinforcement was Φ8/145 (8 mm diameter with 145 mm spacing) for circular specimens, Φ8/175 for rectangular specimens, and Φ8/200 for square specimens. For normal strength series (NSR), the volumetric ratio of transverse reinforcement was also a test variable. A clear cover of 20 mm was formed for longitudinal reinforcement at the bottom and top faces of the specimens for preventing direct loading of reinforcing bars. Only plain bars were used for both longitudinal and transverse reinforcement, for representing the columns of existing older structures in developing countries. Yield strength, yield strain and tensile strength were 367 MPa, 0.0018, and 523 MPa for 10 mm diam bars, 339 MPa, 0.0017, and 471 MPa for 12 mm diam bars, and 345 MPa, 0.0017, and 477 MPa for 14 mm diam bars, respectively. Yield strength and yield strain of 8 mm diam bars were 476 MPa and 0.0024, respectively. The specimens were tested after being jacketed with 1, 3, or 5 plies of CFRP sheets. The tensile strength, elasticity modulus, ultimate rupture strain, and nominal thickness tf of dry fiber-reinforced polymer fabric were 3430 MPa, 230 GPa, 1.5%, and 0.165 mm, respectively. These properties are taken from the specifications of the manufacturer. Test results showed that external confinement of columns with CFRP sheets resulted in an increase in ultimate strength and ductility. While the strength enhancement was more pronounced for specimens with circular cross section, specimens with square and rectangular cross sections exhibited larger ultimate axial deformations without a substantial loss in strength. The efficiency of retrofitting was much more pronounced in the case of relatively lower strength concrete. CFRP jackets increased the compressive strength and corresponding axial strain of the columns with circular, square, and rectangular cross sections. The enhancement in strength and deformability was significantly more remarkable in the case of low strength concrete. The high efficiency of CFRP jacketing in the case of low strength concrete may provide cost effective and occupant friendly solutions for existing structures built with low strength concrete. While the strength enhancement was more pronounced for circular cross sections, deformability enhancement was more for square and rectangular cross sections both for the cases of low and medium strength concrete. CFRP jackets prevented buckling of longitudinal bars and maintained the dual confinement effect provided together with internal transverse bars, as well as preventing spalling of cover concrete. Therefore, the contribution of cover concrete to axial strength and the contribution of longitudinal reinforcement to the

axial strength and ductility were maintained until very large axial deformations, making the specimens benefit from the strain hardening of longitudinal bars at the ultimate state. Independent of the jacket thickness, the measured maximum transverse strains of CFRP jackets for LSR and NSR specimens were between 0.007–0.018 and 0.012–0.015, respectively.

The average values of measured transverse strains were about 80–93% of the value given by the manufacturer. The average values of measured transverse strains for square, rectangular, and circular cross sections were about 88, 83, and 79% of the value given by the manufacturer, respectively.

New empirical equations are proposed for the compressive strength and corresponding axial deformation of FRP jacketed columns, considering the effects of internal transverse and longitudinal steel reinforcement as well. The predictions of the proposed model and two other available models were compared with experimental results of more than 400 specimens, reported in 55 different references. After this comparison, it was seen that the proposed model predicted the compressive strength and corresponding axial strains of the specimens with a reasonable accuracy, with a smaller scatter than the other considered models. The proposed model, together with two other available models, were used for predicting the strength and corresponding axial deformations of more than 300 specimens tested by other researchers, as well as more than 100 specimens tested by the writers during this study and before. It was shown that the predicted results by the proposed model were in reasonable agreement with this extensive database of experimental studies.

Issa et al (2011) explored the behavior of GFRP and steel reinforced concrete columns when subjected to eccentrically axial loads. Six columns of 150*150 mm cross section were tested. Four of them had GFRP reinforcement and two had steel reinforcement. The concrete strength of the GFRP reinforced columns was either 24.73 MPa or 38.35 MPa while for the steel reinforced columns it was 24.73 MPa. The eccentricity was either 50 mm or 25 mm and the tie spacing was either 80 mm or 130 mm. Large longitudinal deformations were recorded for columns with GFRP reinforcement and for columns with large tie spacing. However, tie spacing had no notable effect on the maximum lateral deflection and ductility of GFRP columns of this research. The average maximum stress was about 60% of the concrete compressive strength for columns with initial eccentricity of 50 mm. GFRP bars recorded higher strains than

steel bars and these strains were larger when the tie spacing was large. The increase in the strength of the concrete was associated with reduction in the GFRP bar strain. Two interaction diagrams were plotted for the columns and they present lower bound to the obtained experimental results. In general, all the specimens failed by sudden crushing of the most compressed concrete fibers on the compression face with the exception of one specimen which showed spalling of the cover before failure. Columns with greater tie spacing deform more than those with smaller tie spacing. The difference in deformations is clear for GFRP reinforced columns and is small for steel reinforced columns. In this research, tie spacing had no notable effect on the maximum lateral deflection. At high loads, the GFRP and steel bar strains are larger when the tie spacing is larger. Tie spacing had small effect on the ductility of the GFRP reinforced columns of this research. Smaller ductility is obtained for steel reinforced columns with larger tie spacing.

James Liu (2013) evaluated the seismic behavior of concrete columns transversely confined by steel spirals, ties or fiber reinforced polymer (FRP) wrapping. In the experimental program of that study, fifteen circular concrete columns of 356 mm diameter and 1473 mm length were tested under lateral cyclic displacement excursions while simultaneously subjected to constant axial load thus simulating earthquake loads. The main variables were axial load level, spacing of spirals, type of confinement (steel vs. FRP), and type and amount of FRP jackets. All fifteen specimens were cast in one batch of normal-weight concrete with a specified 28-day compressive strength of 30 MPa. There were at least three cylinders in each group which were tested at 7, 14, and 28 days after casting, and throughout the columns testing period. Testing of column specimens started at 91 days after casting of concrete and completed at 150 days, during which the compressive strength of concrete did not change much and was measured between 39.6 and 40.5 MPa. Hence, the compressive strength of concrete was taken as 40 MPa for all columns. Each column cast monolithically with a 508 x 762 x 813 mm reinforced concrete stub. Column part represented a portion of a bridge column or a building column between the section of maximum moment and the point of contraflexure, while the stub represented a discontinuity such as a beam-column joint or a footing. The specimens were classified into two categories according to the material used for transverse confinement. The first category of specimens were referred to as steel-confined columns and consisted of eight columns which were solely

reinforced by conventional steel cages of longitudinal and spiral reinforcement. The second category of specimens, referred to as FRP- confined or FRP-retrofitted columns, included seven columns which initially contained only minimal amount of spiral steel (US#3@300 mm) and were later retrofitted with transverse GFRP or CFRP wrapping. The longitudinal steel reinforcement in both types of columns was similar. The volumetric ratio of transverse steel reinforcement to concrete core, in the potential plastic-hinge region were 0.3 %, 06%, 0.9%, 1.2% and 1.63% for different columns, repectively. Sapacing of transverse steel reinforcement bars were 75 mm, 100 mm, 150 mm and 300 mm, respectively. Test results revealed that the increased transverse confinement can improve the energy dissipation capacity, ductility, deformability and flexural strength of concrete columns. The required transverse confinement should also be enhanced with the increase of axial load level to satisfy certain seismic design criterion.

Triantafillou and Papanicolaou (2006) studied the application of textile-reinforced mortars (TRMs) as a means of increasing the axial capacity of concrete through confinement is investigated experimentally in this study. TRM may be thought of as an alternative to fiber-reinforced polymers (FRPs), addressing many of the problems associated with application of the latter without compromising performance by a significant degree. Based on the response of confined cylinders and short rectangular columns, it is concluded that textile-mortar jacketing provides a substantial gain in compressive strength and deformability; this gain is higher as the number of confining layers increases and depends on the tensile strength of the mortar. Compared with their resin-impregnated counterparts, mortar-impregnated textiles may result in reduced effectiveness. This reduction was more pronounced in cylindrical specimens but rather insignificant in rectangular ones. Favorable confinement characteristics on rectangular columns were also obtained by using helically applied unbonded strips with end anchorages—an interesting concept that deserves further investigation. Modeling of concrete confined with jackets other than resin impregnated ones is presented by the authors as a rather straightforward procedure through the proper introduction of experimentally derived jacket effectiveness coefficients. From the results obtained in this study, it is believed that TRM jacketing is an extremely promising solution for the confinement of reinforced concrete.

Based on the response of confined cylinders, it is concluded that: 1) textile-mortar confining jackets provide substantial gain in compressive strength and deformability. This gain is higher as the number of confining layers increases and depends on the tensile strength of the mortar, which determines whether failure of the jacket will occur due to fiber fracture or debonding; 2) compared with their resin-impregnated counterparts, mortar-impregnated textiles may result in reduced effectiveness, in the order of approximately 80% for strength and 50% for ultimate strain, for the specific mortar used in this study. It is believed that these numbers depend very much on the type of mortar and could be increased with proper modification of mortar constituent materials, a task not addressed in this study; and 3) failure of mortar-impregnated textile jackets is less abrupt compared with that of their resin-impregnated counterparts, due to the slowly progressing fracture of individual fiber bundles. From the response of rectangular columns, it is concluded that mortar-impregnated textile jackets are quite effective in confining columns of rectangular cross sections for strength and axial deformability. In comparison with their epoxy-based counterparts, mortar-impregnated textile jackets gave approximately the same effectiveness in strength terms and a slightly inferior one in ultimate strain terms. The same conclusion applies in the case of spirally applied unbounded strips with end anchorages, except if the number of layers is quite low, which may adversely affect the deformability. This concept of spirally applied unbounded jacketing appears to be quite interesting and certainly deserves further investigation. Modeling of concrete confined with jackets other than resin-impregnated ones becomes a rather straightforward procedure through the introduction of experimentally derived jacket effectiveness coefficients, a concept developed in this study to compare the confining action of mortar-based jackets or spirally applied unbounded jackets to their resin based counterparts. From the results obtained in this study, the authors believe that TRM jacketing is an extremely promising solution for the confinement of reinforced concrete. Naturally, further investigation is needed (part of it is already underway) toward the optimization of mortar properties and the understanding of various other aspects, including long-term performance, response under cyclic loading, and jacket-steel reinforcement interactions. This notable difference in the failure mechanisms is attributed to the different mortar strengths. It is believed that the property determining which of the two failure mechanisms will be activated first is the inter laminar shear strength of the

textile mortar composite, which is proportional to the tensile (that is, the flexural) strength of mortar.

Bournas and Triantafillou (2009) experimentally investigated the effectiveness of a new structural material, namely, textile-reinforced mortar _TRM and gave results of the confining old type reinforced concrete _RC_ columns with limited capacity due to bar buckling or due to bond failure at lap splice regions. Comparisons with equal stiffness and strength fiber-reinforced polymer _FRP_ jackets allow for the evaluation of the effectiveness of TRM versus FRP. Tests were carried out on nearly full scale non-seismically detailed RC columns subjected to cyclic uniaxial flexure under constant axial load. Ten cantilever-type specimens with either continuous or lap-spliced deformed longitudinal reinforcement at the floor level were constructed and tested. Experimental results indicated that TRM jacketing is quite effective as a means of increasing the cyclic deformation capacity of old-type RC columns with poor detailing, by delaying bar buckling and by preventing splitting bond failures in columns with lap-spliced bars. Compared with their FRP counterparts, the TRM jackets used in this study were found to be equally effective in terms of increasing both the strength and deformation capacity of the retrofitted columns. From the response of specimens tested in this study, it can be concluded that TRM jacketing is an extremely promising solution for the confinement of reinforced concrete columns, including poorly detailed ones with or without lap splices in seismic regions. A total of 10 large scale reinforced concrete column specimens with the same geometry were constructed and tested under cyclic uniaxial flexure with constant axial load. Four of the columns were reinforced with continuous longitudinal reinforcement and six columns had lap-spliced rebar at the base. The specimens were flexure-dominated cantilevers with a height to the point of application of the load _shear span_ of 1.6 m _half a typical story height_ and a cross section of 250×250 mm2. The columns were fixed into a heavily reinforced 0.5-m-deep base block, 1.2×0.5 m2 in plan, within which the longitudinal bars were anchored with 90º hooks at the bottom. To represent old-type non-seismically designed and detailed columns, both series of continuous and spliced specimens were reinforced longitudinally with four 14-mm-diameter deformed bars with an effective depth of 225 mm and 8-mm diameter smooth stirrups at a spacing of 200 mm, closed with 90º hooks at both ends. The performance and failure mode of all tested specimens with continuous longitudinal reinforcement was controlled by

flexure. Buckling of longitudinal bars initiated thereupon their yielding _next loading cycle_ for each specimen. The failure mode of the un-retrofitted specimen was controlled by buckling of longitudinal rebar above the column base, which led to strength degradation. TRM jackets are quite effective as a means of increasing the cyclic deformation capacity and the energy dissipation of old-type RC columns with poor detailing, by delaying bar buckling. Compared with equal stiffness and strength FRP, TRM jacketing has a higher effectiveness by about 50%. TRM confining jackets provide substantial gain in lateral strength and deformation capacity of cyclically loaded reinforced concrete columns with lap splices at the columns base. Compared with equal stiffness and strength FRP jackets. For columns with deformed lap-spliced bars the Euro code 8 predicted drift ratios are in good agreement for FRP and TRM jacketed members with shorter lap lengths, while its predictions are quite conservative in the case of columns with longer lap splices. All test results presented in this study indicate that TRM jacketing is an extremely promising solution with great potential for the confinement of poorly detailed reinforced concrete columns in seismic regions.

Piero Colajanni et al (2014) investigated the structural behavior of concrete columns strengthened with a system made up of fiber nets embedded in an inorganic stabilized cementitious matrix under an uniaxial load. Medium size specimens with circular and square cross-section were cast and subjected to monotonic uniaxial compression, to investigate the efficiency of a Phenylene Benzobis Oxazole (PBO) Fiber Reinforced Cementitious Mortar (FRCM) system in increasing both strength and ductility. The experimental campaign was focused on investigating the effectiveness of various jacketing schemes (geometry, number of layers) based on the use of textile made of continuous fiber (PBO) in combination with inorganic matrix (cementbased mortars). Tests were carried out in two phases. In the first one, namely Series A, eight cylindrical specimens with diameter D = 154 mm and height H = 335 mm were cast; in the second one, namely Series B, seven cylindrical specimens with diameter D = 200 mm and height H = 335 mm and seven specimens with square cross-section having side l = 200 mm and height H = 425 mm were cast (Figure 1.1). All the four corners of square specimens were cast rounded with a curvature radius r_c = 20 mm.

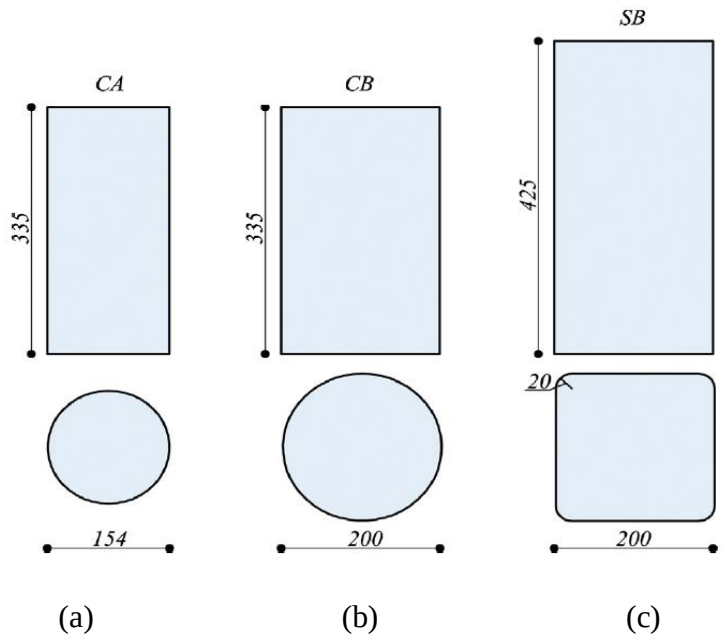

Figure 1.1 : (a)Concrete cylinders Series A. (b)Concrete cylinders Series B. (c)Concrete prisms Series B.

For the cylindrical specimens of Series A, two unconfined specimens, three specimens wrapped with two layers of textile, and three specimens with three layers of textile were tested. Referring to the seven cylindrical specimens in Series B, two specimens were unconfined, three specimens were confined with three layers of textile, and two with two layers of textile.

Lastly, for the square specimens of series B with side L = 200 mm, one was tested unconfined, and three with two layers of textile and three with three layers of textile were tested. As a result, a total of 22 tests were carried out. The choice of these parameters aimed at the following: investigating the effect of PBO-FRCM as a confinement system, with regard to the interaction between fiber and mortar; investigating the role of number of layers of confinement system and the influence of the shape cross-section of specimen on the confinement effect. Specimens were designed to obtain a cylindrical compressive strength equal to 25 MPa.

The cementitious matrix was prepared so as to obtain, after 28 days curing, a minimum compressive strength equal to 15 MPa and a flexural strength of minimum 2 MPa. As showed by the experimental results obtained, the PBO-FRCM confinement system provides substantial gain in compressive strength and ductility.

The efficiency of the confinement system is strictly related to the stiffness of the package of mortar and textile utilized depending on the following parameters: the thickness and stiffness of fiber; the number of layers used; and the bond between fiber

and mortar related to their mechanical properties and the mortar layer thickness. For all square specimens, the failure was due to textile rupture at the corners, as shown in Figure 1.2.

Figure 1.2 : Typical failure of confined square specimen.

Modelling of concrete confined with FRCM is presented as a rather straightforward procedure through the sum of stress contributions of the confined concrete and the mortar of the confinement system, separately. Thus, the effective confining pressure for FRCM specimens in the adapted Spoelstra and Monti model can be evaluated as follows (the proposed formulation is accurate and consistent with experimental results):

$$f_{l,e} = \frac{1}{2}\rho \cdot E_f \cdot \varepsilon_f \cdot k_e \cdot k_{fl,FRCM} \tag{1.1}$$

Where ρ=confinement volumetric ratio, E_f = elasticity modulus of fiber, k_e=shape efficiency factor, $k_{fl,FRCM}$ =confining pressure reduction coefficient for FRCM. The ultimate compressive strain (ε_{ccu}) was evaluated as empirically found by Spoelstra and Monti for RC members confined with FRP:

$$\frac{\varepsilon_{ccu}}{\varepsilon_{co}} = 2 + 1.25 \cdot \frac{Ec}{f_{co}} \cdot \varepsilon_{fu} \cdot \sqrt{\frac{f_{l,eu}}{f_{co}}} \tag{1.2}$$

Where ε_{ccu}=strain at failure of confined concrete, ε_{co}= strain corresponding to cylindrical compressive strength of unconfined concrete, E_c =elasticity modulus of concrete, f_{co}=cylindrical compressive strength of unconfined concrete,

ε_{fu}=experimental fibre strain at failure, $f_{l.eu}$=ultimate effectiveness confining pressure and $k_e\varepsilon_{fuo}$ and $f_{l,eu}$ is obtained assuming $\varepsilon_f = \varepsilon_{fu}$.

On the basis of the response of RC cylindrical and square specimens confined with PBO-FRCM, it was concluded that: (1) a PBOFRCM confining system provides substantial gain in compressive strength and ductility. This gain is related to the number of confining layers and overlapping length, which influences deformability at failure; (2) as unexpected, the PBO-FRCM is quite effective in confining columns of square cross-sections both for strength and axial deformability; (3) the use of a cementitiuos mortar in place of the resin-impregnated system determines a ‘‘delay’’ in activating the confinement system, and a post-peak stiffness degradation was observed, immediately retrieved by the specimen due to the effectiveness of the PBO-FRCM. A theoretical model for PBO-FRCM confined concrete elements was proposed. It is based on the iterative formula of Spoelstra and Monti for FRP confined concrete elements, taking into account the interaction of cementitious matrix and PBO-FRCM by a simple stress sum. First, the effectiveness of the PBO-FRCM confinement system was evaluated analyzing the results of experimental tests, then a suitable algebraic law to analytically reproduce the confining pressure reduction coefficient was evaluated as a function of the current axial compression strain and introduced in the formulation. The proposed model was verified by the laboratory tests presented and the results of this study indicated that the analytical formulation can effectively predict the behaviour of cylindrical and square specimens confined by FRCM, in terms of both strength and ductility.

2. EXPERIMENTAL PROGRAM

2.1 Design of Specimens

2.1.1 Test variables

As mentioned earlier in summary section, recent earthquakes in Turkey, revealed that a remarkable number of existing buildings have poor seismic performance because of very low axial compressive strength of the concrete, inadequate lateral reinforcement in the columns or insufficient details in the stirrups. Most of the structures which were built by previous or some recent versions of Turkish Codes were expected to have an insufficient performance during the earthquakes, so retrofitting was felt to improve the performance of the same structures to preventing from another catastrophe. Transverse reinforcements in columns in the form of hoops, stirrups, or spirals play an important role in safeguarding the columns, especially when they are subjected to strong earthquakes or accidental lateral loads. It is well known that one of the functions of external transverse confinement with FRP in concrete columns is to provide lateral confinement to the core concrete so that the axial compressive strength of the concrete is enhanced and the ductility improved. The main variables of this research is to study how hook angle/length of stirrups could influence confining behavior of the RC columns.

Another objective is to investigate effects of the application of Sprayed Basalt Mesh by Glass reinforced concrete (GRC) for RC columns retrofitted by this method. Therefore, three main parameters is studied experimentally:

- hook angle of stirrups (90° , 112.5° and 135°)
- hook length of stirrups (40 mm and 80 mm)
- effects of the application of sprayed three plies Basalt mesh reinforced GRC in RC columns

2.1.2 Specimen details

At the stage of specimen designing, columns were expected to fail in flexural behavior before reaching their shear strength. So at the pre-calculation stage, shear strength of the weakest specimen was controlled by recent Turkish Code (TS500-2000).

The test specimens were cantilever type columns, representing half a column in a real building frame. A total of eight rectangular columns of dimensions 300 x 200 x 1500 mm along with a stub of dimensions 700 x 700 x 450 mm were constructed.

The average compressive strength of concrete for the characteristic age of 180 days was 7.5 MPa by testing standard cylinders (the average equivalent compressive strength value for reference and retrofitted specimens was about 9.9 and 7.5 MPa by testing core samples, respectively). Two different type of vibration process were used during the casting of concrete, then two different concrete strength result for specimens were undesirable. The average concrete compressive strength for stubs was 15 MPa. All columns are reinforced with four longitudinal bars Φ14 (615.44 mm2) placed symmetrically. The transverse steel reinforcement was given by stirrups Φ8 (50.24 mm2), having a distance center-to-center of 60 mm.

Two different types of reinforcing bars were used. S420 deformed bars with a diameter of 14 mm, which had an average yield strength of 300 MPa, were used as longitudinal bars and S420 deformed bars with a diameter of 8 mm, which had an average yield strength of 517 MPa, were used as transverse bars.

To prevent premature failure of the specimens at the upper part of the columns, closely spaced steel transverse reinforcement was placed at these locations with a spacing of 100 mm. Stirrups of two columns were provided with 90 degree hooks, as typically found in older buildings. The rest six columns were provided with 112.5 and 135 degree hooks, respectively. Length of hooks were 40 mm and 80 mm which were closed at both ends.

According to results of ABYYHY-1975 provisions (Previous Turkish Seismic Code), satisfaction of two main test parameters are studied in Table 2.1 at the following.

Table 2.1 : Satisfaction of test parameters according to ABYYHY-1975.

Test Parameters	Turkish Code	Specimens							
		Ref-S60-Θ90-L80	Ref-S60-Θ112.5-L80	Ref-S60-Θ135-L80	Ref-S60-Θ135-L40	Ret-S60-Θ90-L80-3TRM	Ret-S60-Θ112.5-L80-3TRM	Ret-S60-Θ135-L80-3TRM	Ret-S60-Θ135-L40-3TRM
Hook Angle (Degree)	ABYYHY-1975	135	135	135	135	135	135	135	135
	Existing Sample	**90**	**112.5**	135	135	**90**	**112.5**	135	135
Hook Length (mm)	ABYYHY-1975	80	80	80	80	80	80	80	80
	Existing Sample	80	80	80	**40**	80	80	80	**40**

The arrangement of reinforcement and assembly of cages were given in appendix B. At the stage of retrofitting, four specimens wrapped with three layers of Basalt Textile bonded with mortar (Fibrobeton GRC Mortar). Three layers of basalt fiber mesh as column's jacket was provided using by a single strip for every specimen. The strip was wrapped around the column in a spiral configuration. Comprehensive information on the strengthening of the specimens can be found in "Column Retrofitting" Section 2.1.6.4.

Table 2.2 was designed considering different variables for showing, namely: the name of all the specimens, side-aspect ratio (h/b), height-to-side aspect ratio (H/h), side dimensions of the rectangular specimens(b x h), side-aspect ratio (h/b), height of the specimen (H), height-to-side aspect ratio (H/h), cross-section gross area (Ag), ratio of the area of longitudinal steel reinforcement to the cross-sectional area of the specimen (ρ_g), volumetric ratio of transverse steel reinforcement to concrete core (ρ_t), and volumetric ratio of TRM Jacket (ρ_{TRM}).

The alphanumeric characters present in the names of all the specimens in Table 2.2 have the following meaning, which is composed by five terms: The first term can be written, Ref_ or Ret_, indicates the reference specimens or retrofitted specimens, respectively. The second term, S_, indicates the longitudinal spacing of transverse reinforcement in mm, the third one, Θ_, indicates the hook angle in degree, the fourth one, L_, indicates the hook length in mm, and the fifth one, indicates the number of

Basalt textile layers used in the test region of the specimens. For example, Ret-S60-Ө90-L80-3TRM signifies that it is a retrofitted column, having a stirrup with a spacing of 60 mm, a hook angle of 90 degree, a hook length of 80 mm and 3 Basalt textile layers used in the test region.

Table 2.3 and Table 2.4 give useful information about axial loads, compressive strength of concrete, steel reinforcement details used for longitudinal and transverse reinforcement.

The stub represented the discontinuity similar to a footing or a beam-column joint and was heavily reinforced with a top and bottom mesh in both directions to avoid any failure. The specimens were tested under high axial compression and cyclic lateral loading. All columns were loaded in the strong direction. Columns were all approximately 1290 mm high from the top of the stub to the point of lateral load application. A clear concrete cover of 15 mm and 20 mm was provided for all column ties and stub meshes, respectively. All of the rectangular specimens were designed with the radius of the chamfered corner of 30 mm. There were no lap-splices in longitudinal rebars of specimens. Four PVC pipes with 75 mm diameter and 500 mm height were placed at the corners of stubs before casting concrete. The stubs of the specimens were fixed to the laboratory strong floor by using high-strength prestressed bars of 32-mm diameter during tests.

2.1.3 Axial load strength

This load represented gravity loads of the buildings. The axial load, based on percentages of the gross compressive strength of the concrete section, was maintained at a constant level through the test. Amount of axial load capacity which was applied to the columns is calculated by Eq. (2.1) and Eq. (2.2) which is seventy percent of column axial load capacity. The weight of the setup steel-beam, which was used to apply axial load to the column spacemen, is 8000 N.

$$N_{axial} = 0.7 \times f_c^{'} \times b \times h + \textit{The weight of the setup steel-beam} \qquad \textbf{(2.1)}$$

The amount of axial load that should be applied by jack at the top of the column specimen is 323 kN.

Table 2.2 : Specification of cross-sections.

Type	Alphanumeric Name	Cross section Dimension h × b (mm)	Side aspect Ratio $\frac{h}{b}$	Height of Columns H_{column} (mm)	$\frac{H_{colum}}{h}$	$\frac{H_{column}}{b}$	Cross Section Gross Area A_g (mm$^{2)}$	Cross Section Core Area A_c (mm$^{2)}$	$\frac{A_g}{A_c}$
Reference	Ref-S60-Θ90-L80	300 x 200	1.5	1290	4.3	6.5	60000	42444	71 %
	Ref-S60-Θ112.5-L80	300 x 200	1.5	1269	4.2	6.4	60000	42444	71 %
	Ref-S60-Θ135-L80	300 x 200	1.5	1285	4.3	6.4	60000	42444	71 %
	Ref-S60-Θ135-L40	300 x 200	1.5	1290	4.3	6.5	60000	42444	71 %
Retrofitted	Ret-S60-Θ90-L80-3TRM	300 x 200	1.5	1293	4.3	6.5	60000	42444	71 %
	Ret-S60-Θ112.5-L80-3TRM	300 x 200	1.5	1283	4.3	6.4	60000	42444	71 %
	Ret-S60-Θ135-L80-3TRM	300 x 200	1.5	1286	4.3	6.4	60000	42444	71 %
	Ret-S60-Θ135-L40-3TRM	300 x 200	1.5	1290	4.3	6.5	60000	42444	71 %

Table 2.3 : Values of concrete compressive strength and reinforcement type.

Type	Alphanumeric Name	Compressive strength of cylinder samples for columns (MPa)	Equivalent Compressive strength of core samples for columns (MPa)	Compressive strength of cylinder samples for Stubs (MPa)	Plain bar for Longitudinal reinforcement	Ribbed bar for Transverse reinforcement
Reference	Ref-S60-Ɵ90-L80	7.5	9.9	15	S-220	S-420
	Ref-S60-Ɵ112.5-L80	7.5	9.9	15	S-220	S-420
	Ref-S60-Ɵ135-L80	7.5	9.9	15	S-220	S-420
	Ref-S60-Ɵ135-L40	7.5	9.9	15	S-220	S-420
Retrofitted	Ret-S60-Ɵ90-L80-3TRM	7.5	7.5	15	S-220	S-420
	Ret-S60-Ɵ112.5-L80-3TRM	7.5	7.5	15	S-220	S-420
	Ret-S60-Ɵ135-L80-3TRM	7.5	7.5	15	S-220	S-420
	Ret-S60-Ɵ135-L40-3TRM	7.5	7.5	15	S-220	S-420

Table 2.4 : Specification of longitudinal and transverse reinforcement.

Type	Alphanumeric Name	Equivalent Compressive strength of core samples for columns (MPa)	Axial Load N_{axial} (kN)	Hook Length of Stirrup L	Hook Angle of Stirrup ϴ°	$\frac{N_{axial}}{A_g f_c'}$ %	Transverse Reinforcement Size @ Spacing (mm)	Transverse Reinforcement ρ_t %	Longitudinal Reinforcement Number and Size of Bars (mm)	Longitudinal Reinforcement ρ_l %	Basalt Textile Layers	Basalt Textile ρ_{TRM} %
Reference	Ref-S60-ϴ90-L80	9.9	323	80	90	54.4	Φ8 @60	1.41	4Φ14	1.03	-	-
	Ref-S60-ϴ112.5-L80	9.9	323	80	112.5	54.4	Φ8 @60	1.41	4Φ14	1.03	-	-
	Ref-S60-ϴ135-L80	9.9	323	80	135	54.4	Φ8 @60	1.41	4Φ14	1.03	-	-
	Ref-S60-ϴ135-L40	9.9	323	40	135	54.4	Φ8 @60	1.30	4Φ14	1.03	-	-
Retrofitted	Ret-S60-ϴ90-L80-3TRM	7.5	323	80	90	71.8	Φ8 @60	1.41	4Φ14	1.03	3	4.25
	Ret-S60-ϴ112.5-L80-3TRM	7.5	323	80	112.5	71.8	Φ8 @60	1.41	4Φ14	1.03	3	4.25
	Ret-S60-ϴ135-L80-3TRM	7.5	323	80	135	71.8	Φ8 @60	1.41	4Φ14	1.03	3	4.25
	Ret-S60-ϴ135-L40-3TRM	7.5	323	40	135	71.8	Φ8 @60	1.30	4Φ14	1.03	3	4.25

2.1.4 Shear strength

TS500-2000 Provisions is selected for shear strength determination of the weakest specimen. The concrete contribution to shear strength is given by Eq. (2.2).

Before specimen testing material specification assumed as below:

f_c = 7.5 MPa; *h*= 300 mm; *b*= 200 mm; *d'*=30 mm; longitudinal bars 4Φ14; transverse bars Φ8@60 mm; f_w=517 MPa; H_{column}= 1300 mm and concrete cover 30 mm.

$$V_c = 0.8V_{cr} \tag{2.2}$$

$$V_{cr} = 0.65 \cdot f_{ct} \cdot b \cdot (h - d') \cdot (1 + \gamma \cdot \frac{N_{axial}}{b \cdot h}) \tag{2.2a}$$

$$f_{ct}=0.35 \cdot \sqrt{f_c} \tag{2.2b}$$

In case of axial compression, γ is taken as 0.07 (TS 500- 2000).

Therefore, V_c is equal to V_c=0.8·46322=37058 N

Total shear strength is calculated by Eq. (2.3).

$$V_r=V_w+V_c \tag{2.3}$$

The contribution of transverse reinforcement is calculated as follows:

$$V_w=\frac{A_{sw}}{s}. f_w.d \tag{2.3a}$$

Therefore, V_w and V_r are equal to 233.8 kN and 270.8 kN, respectively. On the other hand, the average moment capacities of the column, which was calculated by XTRACT computer program, was 44.84 kNm. In the moment-curvature analysis, for unconfined and confined concrete stress-strain behavior, the models proposed by Mander et al. (1988) are used. Steel reinforcing bars are assumed to behave in an elastic-plastic manner with strain hardening. The maximum shear force that was applied to the column during the test, was calculated by Eq. (2.4).

$$V_{XTRACT} = \frac{M_{XTRACT}}{H_{COLUMN}} \tag{2.4}$$

Therefore, because of $(V_r = 270.8\ kN) > (V_{XTRACT} = 34.5\ kN)$ the specimens are expected to fail in flexure before they reach shear strength.

2.1.5 Material properties

2.1.5.1 Plain concrete

Normal weight concrete with a slump of 185 mm was used for all the specimens. All of the specimens were built up from one single batch of ready-mix concrete having constituents and mix proportions at FIBROBETON Co. as follows: Portland cement 215 kg/rn3, stone chips no1; 923 kg/rn3 crusher dust 1104 kg/rn3, super plasticizer 2.75 kg/rn3, water 232 kg/rn3.

Standard concrete cylinders 150 x 300 mm were prepared and cured under the same conditions of the specimens. These cylinders were tested according to ASTM C39 (2004) at 28 and 180days, and at the corresponding age at which the related specimens were tested. The average compressive strength of concrete for the characteristic age of 180 days was 7.5 MPa by testing standard cylinders (the average equivalent compressive strength value for reference and retrofitted specimens was about 9.9 and 7.5 MPa by testing core samples, respectively). Two different type of vibration process were used during the casting of concrete, then two different concrete strength result for specimens were undesirable. The average concrete compressive strength for stubs was 15 MPa.

A 2200 kN-capacity Foumey Hydraulic Testing Machine was used to test cylinders in accordance with ASTM method C39, since this machine could be connected to the data acquisition system. A compressometer with three-point contacts was used with two Linear Variable Displacement Transducers (LVDTs) to measure concrete compressive strains. Stress-strain relationships from compression test at 180 days was shown in Figure 2.1.

Also, equivalent compressive concrete strength were obtained at the same day of the test by taking core samples in order to determine the exact mechanical properties of every specimen. The compressive strength of concrete are reported for each specimen were mentioned in Tables 2.3 at section 2.1.2.

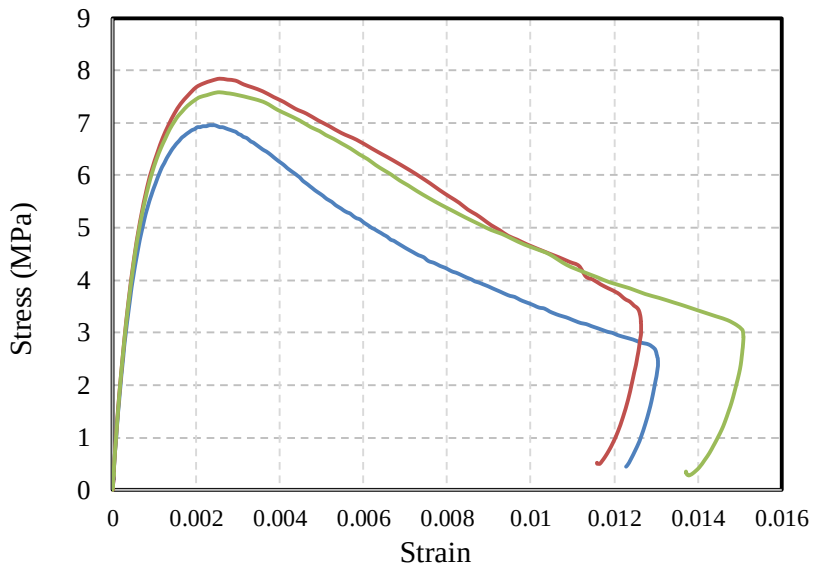

Figure 2.1: Concrete stress-strain diagram at the age of 180 days.

2.1.5.2 Reinforcing steel

Plain 14 mm diameter longitudinal reinforcement bar and 8 mm diameter ribbed reinforcement bar as a stirrup was used in columns and mechanical properties were estimated using the averages of tensile test results performed on three steel coupons for each type. Yield strength is f_y and yield strain is ε_y. Strain corresponding to the beginning of steel hardening ε_{sh}, the ultimate strain ε_{su} that corresponds to ultimate stress f_{su} and the modulus of elasticity Es calculated from stress strain diagram. Only those parts of the curves that were used for the analytical work for most columns are shown. Tensile test results of bars are shown in Figure 2.2 and 2.3. Numerical values of mentioned diagrams was presented in Table 2.5.

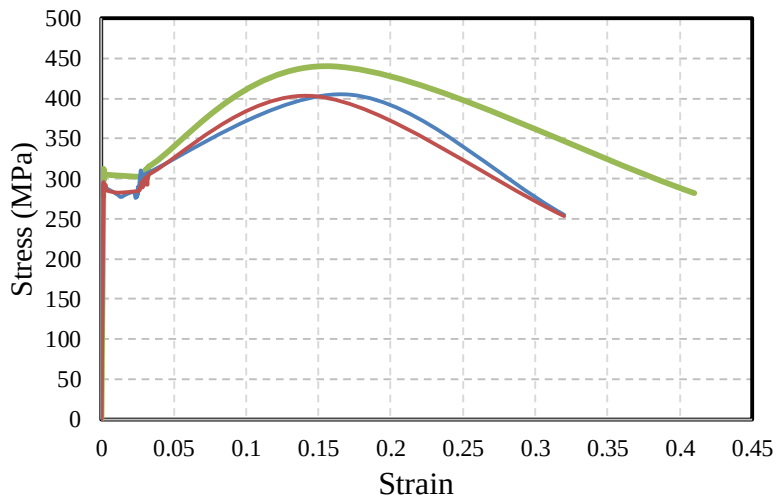

Figure 2.2: Tensile test results of Φ14 bars.

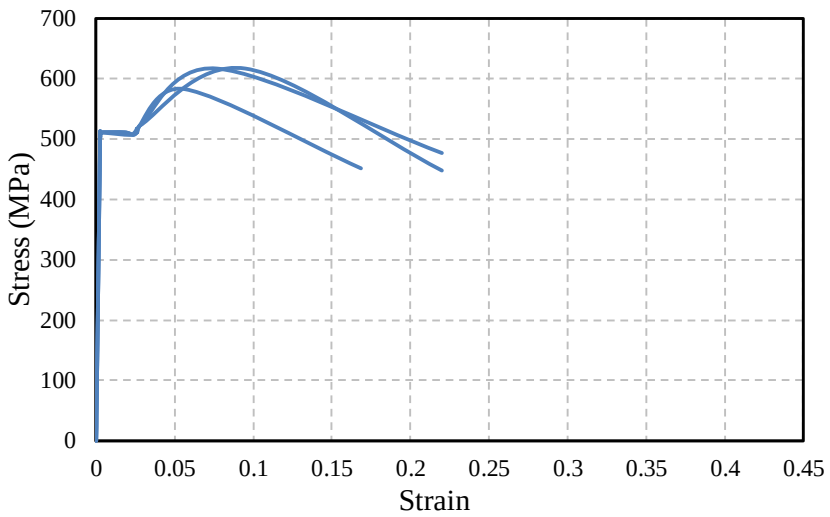

Figure 2.3: Tensile test results of Φ8 bars.

Table 2.5 : The mechanical characteristics of reinforcement bars.

Reinforcing Bars	f_y (MPa)	ε_y	f_{max} (MPa)	ε_{max}	f_u (MPa)	ε_u
ϕ14	289	0.0014	404	0.172	254	0.32
ϕ14	295	0.0014	402	0.148	254	0.32
ϕ14	300	0.0014	440	0.168	282	0.41
ϕ8	517	0.0025	582	0.057	452	0.17
ϕ8	519	0.0025	617	0.077	477	0.22
ϕ8	517	0.0025	617	0.095	448	0.22

2.1.5.3 Glass fiber reinforced concrete

Glass Fiber Reinforced Concrete, also known as GFRC or GRC, is a type of fiber reinforced concrete. Glass fiber concretes are mainly used in exterior building façade panels and as architectural precast concrete. In this research program, Fibrobeton GRC Commercial Mortar was used as an important part of external confinement system. Fibrobeton Commercial GRC Mortar consists of high strength Glass fiber (with 24 mm fiber length, 72 GPA Elastic modulus and 1700 MPa Tensile Strength) embedded

in a cementitious matrix (Fig.2.4). The average flexural and compressive strength values at 28 days for Fibrobeton Commercial GRC Mortar was 13.7 Mpa and 44.5 MPa, respectively. Flexural and Compression test was carried out in 40 x 40 x 160 mm and 50 x 50 x 50 mm hardened mortar prisms, respectively.

Figure 2.4: Glass fiber reinforced concrete.

2.1.5.4 Basalt textile reinforced mortar

Three layers of Basalt fiber mesh were sprayed with GRC as column's jacket for every specimen. The strips were wrapped around the columns in a spiral configuration and wrapping were started from one of the longer sides and was stopped at the same side by 300 mm overlap length. The technical details of the Basalt Textile, which was used in this experimental study as a strengthening material using Spinteks Corporation technical details (manufacturer corporation) is 1600 MPa for Basalt textile tensile stress, 0.05 for ultimate strain and 32 GPa for elastic modulus. Retrofitting system in this research program was manufactured either from basalt fibers, impregnated with Glass reinforced concrete (GRC). The grids had a square configuration with 250 mm out-to-out dimension (Figure 2.5)

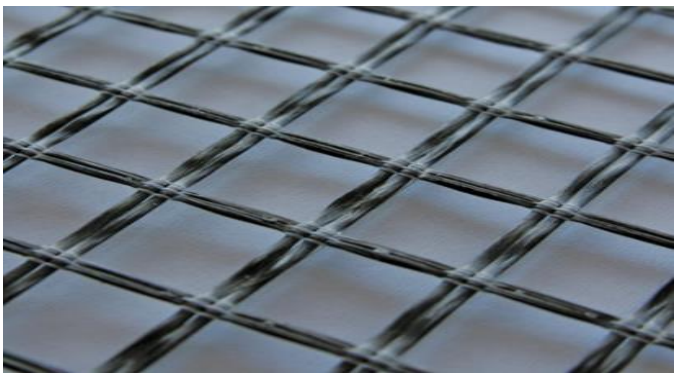

Figure 2.5: Basalt textile reinforced mesh.

2.1.6 Construction of specimens

2.1.6.1 Reinforcing cages

Each reinforcing cage was composed of two parts: the cages for columns and the cages for foundations. They were assembled separately and connected to each other before being placed in the form. The reinforcement for the foundation contained ϕ10 for horizontal and ϕ 14 for vertical stirrups at 150 mm spacing. In addition, ϕ 14 bars with 135° hooks were placed at bottom sides of the foundation in opposite direction. The longitudinal bars in columns were completely extended into the foundation whereas the stirrups were extended into the bottom of foundation at a spacing of 100 mm. The design of the specimens aimed at forcing the failure in the potential plastic hinge region, within 1000 mm from the face of foundation. Figure 2.6.a-b-c show some stages of reinforcing cages for stubs and Figure 2.6.d-e-f show reinforcing cages for columns. As mentioned in section "2.1.2, Specimen details" figures related with details of reinforcing cages of al1 specimens are given in appendix B.

2.1.6.2 Formworks

Plywood formwork was prepared separately for casting the columns and footings in two stages. The stubs formwork was constructed with 19 mm plywood and 700 x 700 x 450 mm (Figure 2.7.a). Before placing the reinforcing cages inside the column and stub formworks, the inner surfaces of them were lightly coated with a thin layer of oil to avoid bond between the concrete and formwork. Four PVC pipes, 70 mm in diameter, was placed in stubs reinforcement cage in order to anchor the specimen to strong floor at the laboratory. Another wooden frame was then attached to the top sides of the PVCs to place them vertically (Figure 2.7.b). Plastic spacers were attached to the cages to provide a constant clear cover thickness of 15 mm in columns and 20 mm in foundations (Figure 2.7.c). Each specimen had six threaded anchor rods to the column frame which would be used to install the LVDTs at testing phase. After column formwork placement, columns were kept by diagonal wooden elements to make sure the columns were straight and the center of the columns lined up with the center of the stub (Figure 2.7.d-e-f). From inside of the column formwork the corners was rounded in 30 mm radius and using silicone to prevent leakage of concrete grout. The internal instrumentation in all specimens consisted of electrical strain-gauges was located on the longitudinal and transverse steel reinforcement.

(a)

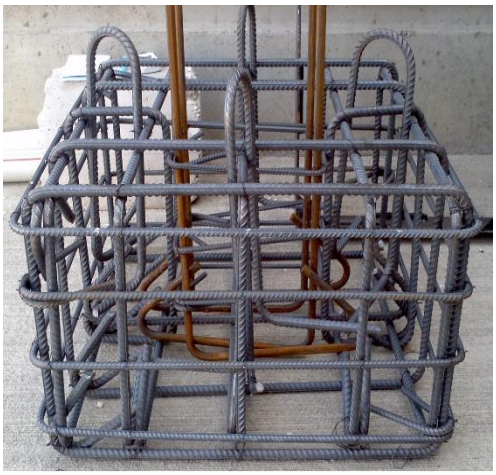

(b)

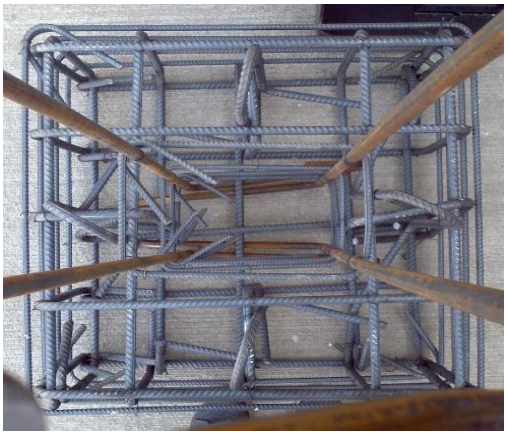

(c)

(d)

(e)

(f)

Figure 2.6 : Reinforcement of cages: (a)Stub cage. (b)Stub cage with column longitudinal bars. (c)Plan view of stub cage. (d)Stirrup with 135° hook angle. (e)Assembling of stirrups. (f)Plan view of column cages.

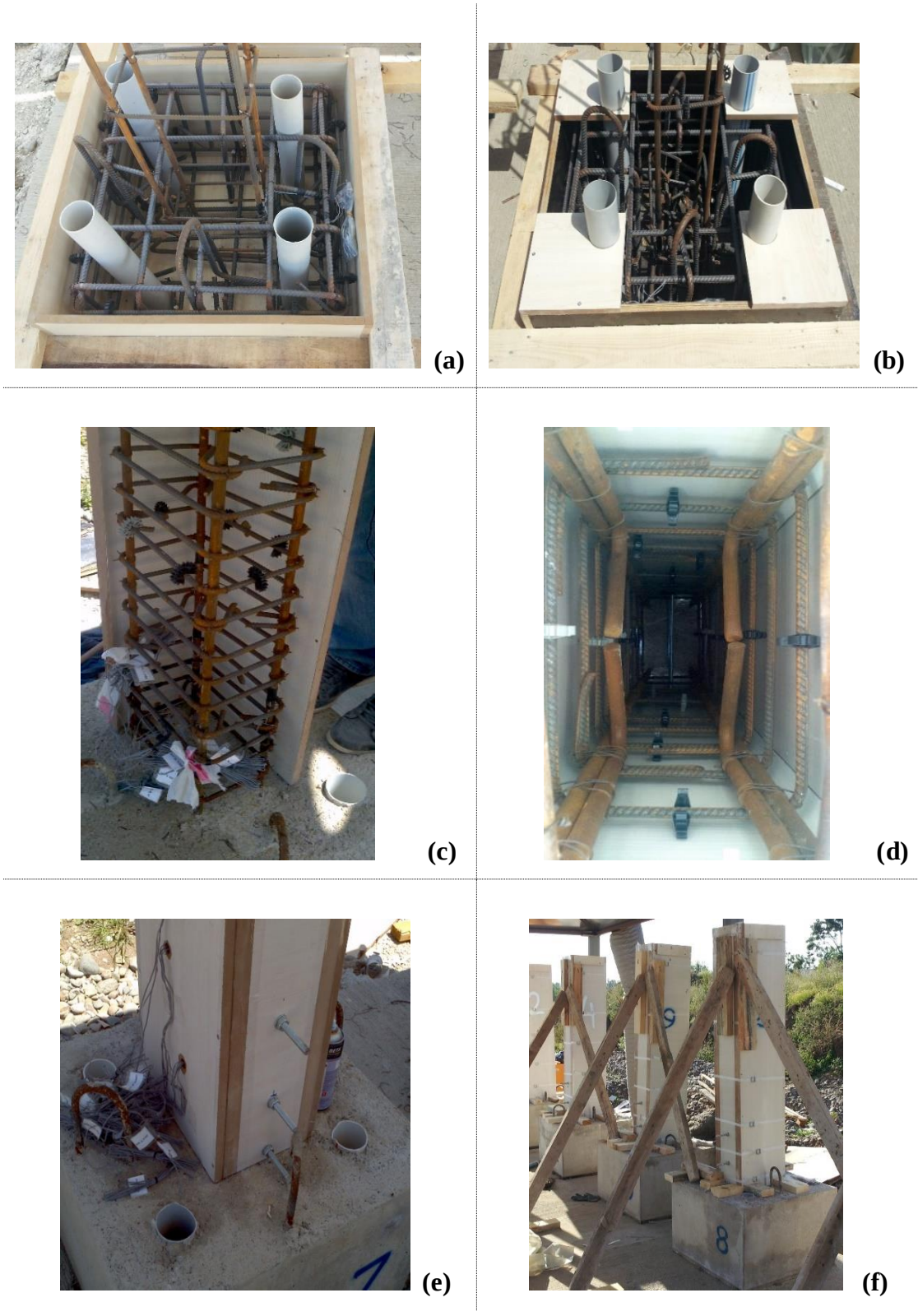

Figure 2.7: Formwork of stubs and columns: (a)Placement of stub cages into form. (b)Attachment of PVCs to formwork for preventing movement. (c)Attachment of plastic spacers. (d)Plan view of inside of column. (e)Installation of threaded anchor rods. (f)Keeping columns vertically by installation of diagonal elements.

2.1.6.3 Casting and curing

Plywood formwork was prepared separately for casting the columns and stubs in two stages. Ready-mix concrete was used to cast the stubs first and then after one month the columns concrete were cast. The stub-column interface (construction joint) was intentionally left rough. At the end of casting, wet burlaps were used to cover the top surface of the base formwork (Figure 2.8.a-b). All eight columns were cast vertically from one batch of concrete. The columns were cast vertically to simulate the actual construction practice a few weeks after the casting of footings (Figure 2.8.c-d). The initial slump of the ready mix concrete was 185 mm. Al1 the specimens were thoroughly vibrated using rod vibrators. At the same time, twenty-five 150 x 300 mm cylinders and eighteen 200 x 200 mm cube specimen were also cast to monitor concrete strength (Figure 2.8-e). Al1 the cylinders were kept with the specimens until the seventh day when the formwork was removed and the cylinders were demolded. The cylinders were air cured with the columns until they were tested. Wet burlap and plastic sheets cured the columns for at least two weeks (Figure 2.8-f).

2.1.6.4 Column retrofitting

Textile Reinforced Mortar (TRM) is a composite material consisting of a finely grained reinforced cement-based matrix and high performance, continuous multifilament-yarns made from basalt. The major advantages of mentioned material is its high tensile strength and pseudo-ductile behavior, which is characterized by large deformations due to its tolerance of multiple cracking. With its excellent mechanical properties this material can be highly appropriate to many applications both for new structures and for the strengthening or repair of old structural elements made of reinforced concrete or other traditional materials.

Retrofitting system in this research program was manufactured either from Basalt mesh, spraying with Glass Reinforced Concrete (GRC). The Basalt grids had a square configuration with 250 mm out-to-out dimension. Before wrapping of all the specimens, test regions were saturated by water to prevent suction of mortar's water by column concrete (Figure 2.9.a) and a gap of about 15~20 mm was left at the bottom ends of the columns to avoid direct axial compressive loading of the confinement

(a)

(b)

(c)

(d)

(e)

(f)

Figure 2.8 : Casting and curing: (a)Casting of stub concrete. (b)Curing of stub concrete. (c)Equipment for column concrete casting. (d)Casting of column concrete (e)Taking cylinder and cube samples. (f)Curing of column concrete.

jacket (Figure 2.9.b). Application of the mortar layers were made with spraying glass reinforced concrete in three step due to applying three layers of basalt fiber mesh (Figure 2.9.c). Thickness of the mortar were approximately 28~32 mm in middle of both surface of columns and 18~22 mm at the corners. The jackets extended from the base of each column (a gap of about 15~20 mm was left) to a height of 510 mm. After application of the first mortar layer on the concrete surface, the textile was applied and pressed slightly into the mortar, which comes out through all the opening between fiber rovings (Figure 2.9.d-e). The next mortar layer covered the textile completely and the operation was repeated until all textile layers were applied and covered by FIBROBETON mortar (Figure 2.9.f). The AutoCAD drawings related with retrofitting process was given in appendix B.

2.2 Test Setup

All specimens were constructed at the FIBROBETON YAPI ELEMANLARI SAN. INŞ. TIC. LTD.ŞTI. Corporation and were tested at Istanbul Technical University, Structural and Earthquake Engineering Laboratory. The specimens were tested under constant high axial load and reversed cyclic lateral load. A 250 KN capacity MTS hydraulic actuator was used to apply the transverse load which was controlled by the software Visual LOG TDS-7130. The maximum stroke of the actuator was 600 mm, which allowed horizontal displacement of up to ± 300 mm relative to the neutral position. The actual stroke and load during testing were monitored and recorded by data acquisition systems. This actuator is fixed to the reaction wall by high strength special bolts and was capable to apply pushing and pulling loading with displacement and force control capabilities. The horizontal actuator applied a reversed cyclic loading in displacement control mode on the tip of the specimen to simulate seismic loading by markers. At the beginning of each test, the first step was the application of the axial load. This load represented gravity loads of the buildings. The axial load, based on percentages of the gross compressive strength of the concrete section, was maintained at a constant level through the test. The axial load was applied to the specimen via two special high strength threaded rods. The rods passed through steel T-shape beam between the two sides of the column. At the top of the column, the rods were attached to another steel beam which allowed the rods to be loaded by a centrally located jack.

(a)

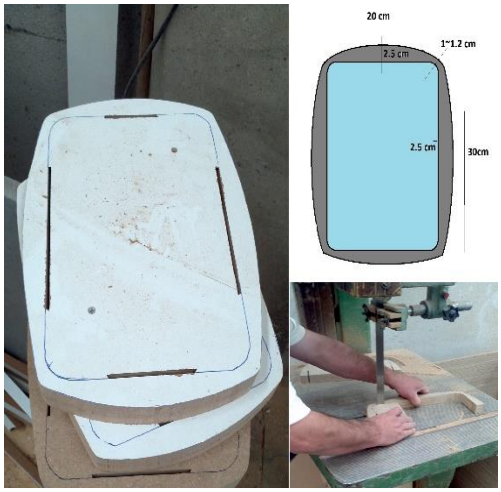

(b)

(c)

(d)

(e)

(f)

Figure 2.9 : Process of column retrofitting: (a)Saturation of retrofitting region by water before retrofitting process. (b)Leaving a gap between column and stub by wooden elements. (c)Spraying GRC. (d)Wrapping Basalt textile. (e)Wrapping Basalt and spraying GRC. (f)Retrofitted Columns.

A hand-operated screw-gear jack was used to apply the constant axial compression load. The maximum load capacity of the jack was 1000 kN and the maximum stroke was 100 mm.The stubs of specimens were fixed to the reaction laboratory floor by means of 800 MPa, 63 mm steel threaded bolts. The stubs had four holes, two on each side of the stub that accommodated 63 mm diameter bolts to secure column samples. A 1000 kN capacity load cell was placed between the jack and the top steel beam for measuring amount of axial load. Figure 2.10 shows the typical column installation and test setup in the laboratory. At the test during, the overall behavior of columns was manually recorded and the crack patterns were observed. For this purpose, horizontal and vertical lines were drawn every 100 mm on the surface of the test region. Ten mm diameter threaded rods were placed into the specimens before concrete casting at h and h/2 distances away from the column-stub interface, where h is the cross-sectional dimension of columns for recording flexural rotations. All the instrumentation, including the load cells, strain-gauges and LVDTs were connected to data acquisition systems and MTS controller for data collection. There was a rigid steel frame was fixed to the strong floor of the laboratory and three ones of the LVDTs were mounted on mentioned frame for measuring of mid-tip and tip displacement as well as column out of plane. Typical test duration lasted between four to five hours for reference specimens and seven to nine hours for retrofitted columns. The entire setup was symmetrical to avoid eccentric loading as much as possible.

2.3 Instrumentation

2.3.1 Linear transducers

Displacements, rotations, and curvatures at the plastic hinge region were monitored using six Linear Variable Displacement Transducers (LVDTs), which fixed vertically parallel to the column measuring approximately in (22~32) mm, (140~160) mm and (300~330) mm gauge lengths from the column base. All of six LVDTs were CDP50. Two LVDTs were placed horizontally at the mid (CDP100) and tip (SDP200) of the column length to measure the lateral displacement of the column. Two LVDTs (CDP10) were placed on the footing for measuring the possible rotations and one LVDT (CDP10) was placed horizontally at the mid of the footing. The locations of the LVDTs are shown in Figure 2.11. The data of these instruments reached TML TDS 303 data logger through TML ASW-50C switch box and gathered as Excel document.

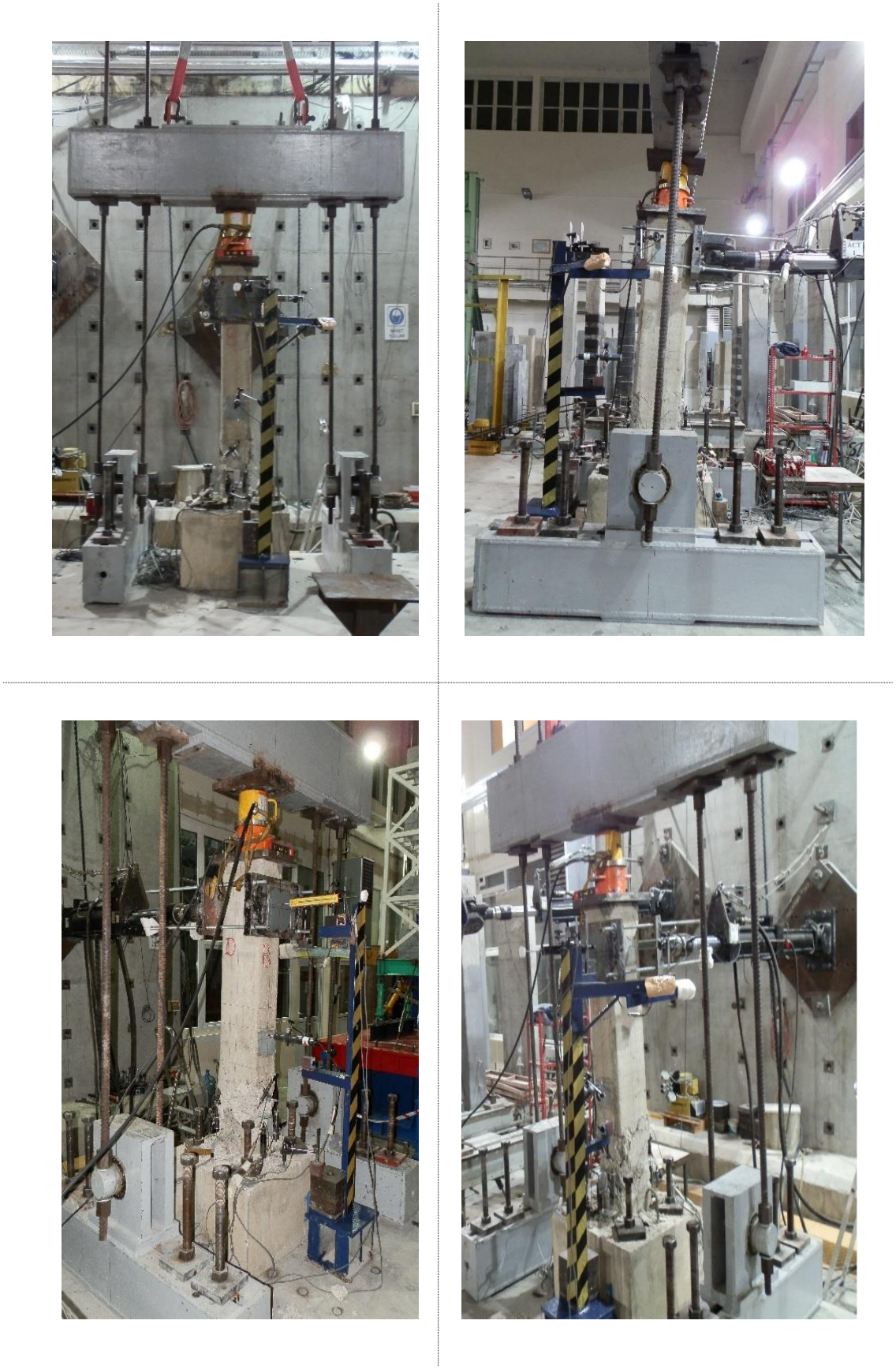

Figure 2.10 : Test Setup.

2.3.2 Strain-Gauges

The instrumentation also comprised a total of 16 strain gauges for each column, as shown in Fig. 2.12. The electrical strain gages used in this research were YFLA-2-3L and YFLA-5-3L made by Tokyo Sokki Kenkyujo Co, Ltd. Measured gauge length in longitudinal bars and stirrups were 5mm and 2mm, respectively. Stirrup strains were also measured by six strain gages that were laid on two legs of three stirrup from the column base. The strain gauges were adhered on the reinforcing cage of the specimens before casting. The surfaces of the reinforcing bars were cleaned from rust with mechanical grindstone and sandpapers, and then with acetone. Strain gauges were adhered to these surfaces with strong adhesive. Before the strain gauges were wrapped with an VM-tape isolation strap and one ply of insulated band, N-1 (water resistant material) was applied on the strain gauges. The data of these instruments reached TML TDS 303 data logger through TML ASW-50C switch box and gathered as Excel document.

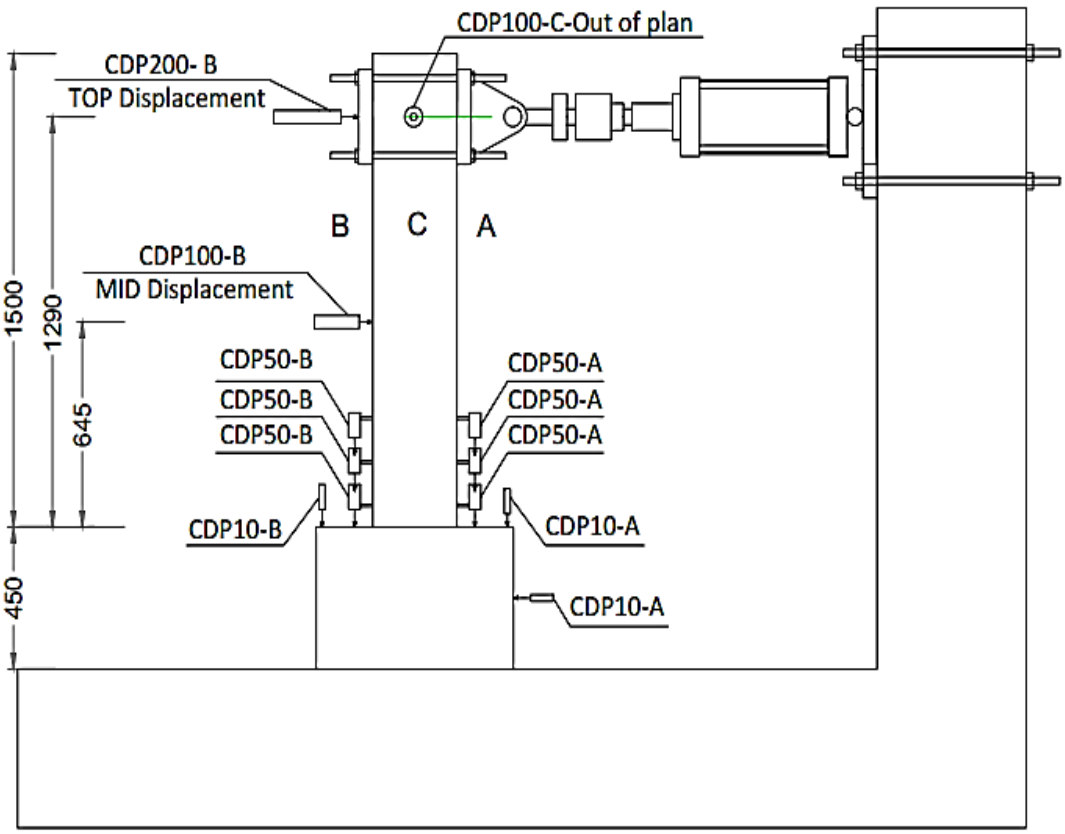

Figure 2.11 : The locations of the LVDTs.

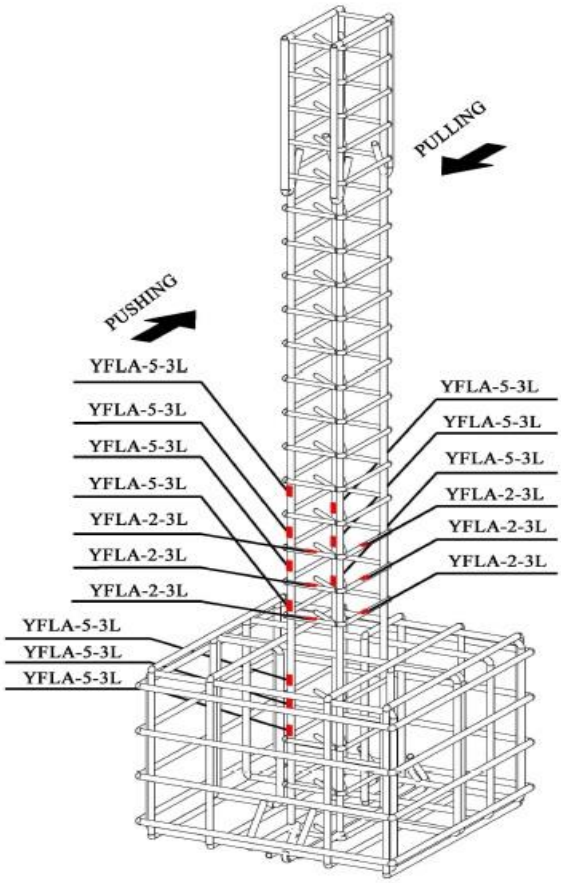

Figure 2.12 : Strain-gauge locations on longitudinal and transverse bars.

2.4 Test Procedure and Loading Program

At the beginning of each test, the first step is the application of the axial load. This load represented gravity loads of the buildings. The axial load, based on percentages of the gross compressive strength of the concrete section, was maintained at a constant level through the test. Recording of data began when the axial load was first applied. When the target level of axial load was achieved, the horizontal actuator applied a reversed cyclic loading in displacement control mode on the tip of the column to simulate seismic loading. This lateral load was applied approximately at 1290 mm height from the column-stub interface and the column was cycled through both tensile and compressive loads. Loading history of the specimens are shown in Figure 2.13. At this diagram, drift ratios (Δ / L) for all specimens were calculated where Δ is the lateral displacement of the tip of the column and L is the column length. The loading history was composed of excursions at certain drift ratios of 0.001, 0.002, 0.004, 0.006, 0.008, 0.010, 0.015, 0.020, 0.025, 0.030, 0.035, 0.04, .05, 0.06, 0.07 and 0.08 for pulling and pushing cycles.

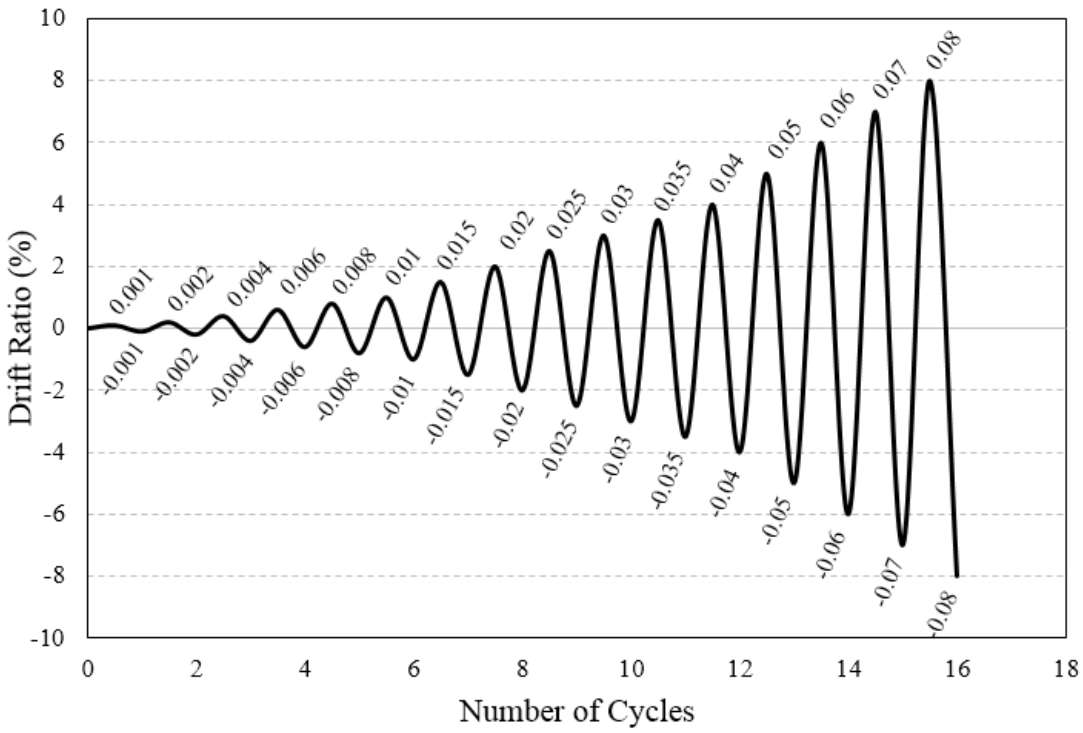

Figure 2.13: Loading history of the specimens during each test.

At the test during, the overall behavior of columns was manually recorded and the crack patterns were observed. The test ended when at least one of the following events occurred: 1) Drop of more than 20% of the maximum flexural capacity at the reference specimens; 2) After achieving to target drift ratios (commonly 3% for Reference specimens and 8% for Retrofitted specimens); 3) Rupture of the stirrups, inducing a large drop of flexural capacity.

3. ANALYTICAL STUDY

3.1 Internal Confinement

Concrete under uniaxial compression tends to expand laterally and the longitudinal strains generated by such loading give rise to transverse tensile strains. Which cause vertical cracking and failure in concrete. Lateral pressure that confines the concrete counteracts the lateral expansion, and results in a significant increase in ductility along with the strength. At low level of longitudinal strains in concrete. The lateral expansion of concrete will be small; hence, the lateral confinement provided by the transverse reinforcement will be negligible. As the longitudinal mains increase, the lateral strains of concrete also increase.

The expansion of core concrete is restrained by the transverse reinforcement; result in the confinement of core and separation of the cover from the core. The cover concrete behaves as unconfined concrete and becomes ineffective after the compressive strength is anained while the core concrete continue to more stress at high strains. After the cover spalls, the load carrying capacity of the concrete core depends on the nature of confinement. Therefore, the compressive stress distributions for the core and cover concrete follow the confined and unconfined concrete stress-strain relations, respectively.

The theoretical stress-strain model for confined concrete developed by Mander, Priestley and Park in 1988 is applicable to members with either circular or rectangular sections under static or dynamic axial loading, either monotonically or cyclically applied load. The concrete section may contain any kind of confinement with spirals, circular hoops or rectangular hoops with or without cross ties. The influence of various types of confinement is taken into consideration by defining an effective lateral confining pressure, which depends on the area of effectively confined concrete core that proposed by Sheikh and Unimen (1982). For obtaining, the theoretical stress-strain relationship of confined concrete the model of Mander et al was used as presented in following.

In Figure 3.1, the arching action is again assumed to act in the form of second-degree parabolas with an initial tangent slope of 45°. Arching occurs vertically between layers of transverse hoop bars and horizontally between longitudinal bars. The effectively confined area of concrete at hoop level is found by subtracting the area of the parabolas containing the ineffectively confined concrete. For one parabola, the ineffectual area is $(w_{i'})^2/6$, where $w_{i'}$ is the i'th clear distance between adjacent longitudinal bars as seen in Figure 3.1.

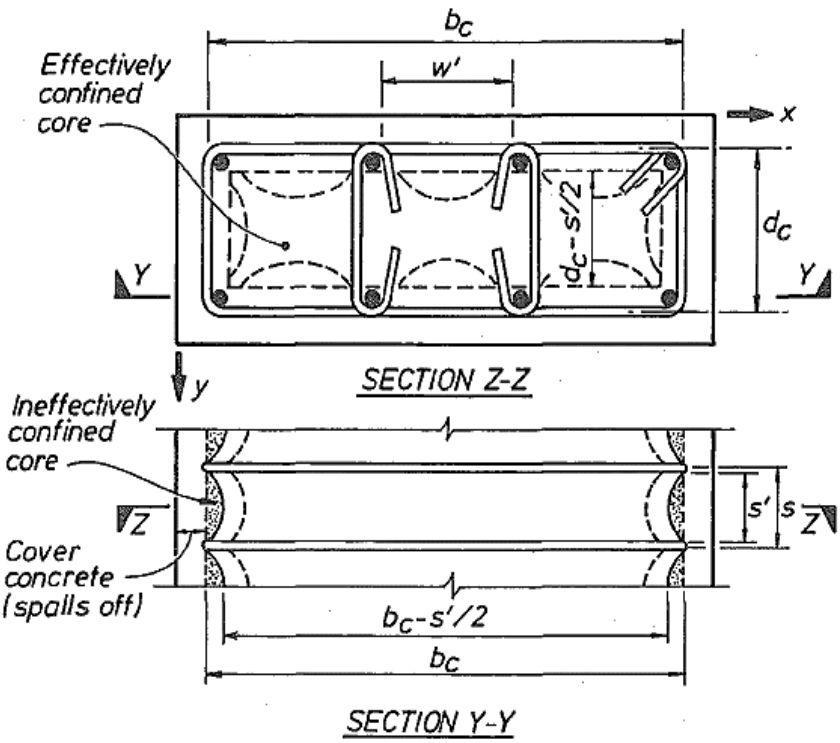

Figure 3.1: Effectively Confined Core for Rectangular Hoop Reinforcement (Mander, Priestley & Park 1988).

Incorporating the influence of the ineffective areas in the elevation (Figure 3.1), the area of effectively confined concrete core at midway between the levels of transverse hoop reinforcement is

$$A_e = \left(b_c d_c - (\sum_{i=1}^{n} \frac{(w_{i'})^2}{6}) \right) \left(1 - \frac{s'}{2b_c} \right) \left(1 - \frac{s'}{2d_c} \right) \quad \textbf{(3.1)}$$

Where b_c and d_c = core dimensions to centerlines of perimeter hoop in x and y directions, respectively, where $b_c > d_c$. In addition, Eq. (3.1) gives the area of concrete core enclosed by the perimeter hoops. Hence, from Eq. (3.2) the confinement effectiveness coefficient is for rectangular hoops

$$k_e = \frac{\left(1-(\sum_{i=1}^{n}\frac{(w_{i'})^2}{6b_c d_c})\right)\left(1-\frac{s'}{2b_c}\right)\left(1-\frac{s'}{2d_c}\right)}{(1-\rho_{cc})} \quad \textbf{(3.2)}$$

It is possible for rectangular reinforced concrete members to have different quantities of transverse confining steel in the x and y directions so from Eq. (3.3) and Eq. (3.4) the effective lateral confining stresses in the x and y directions are

$$f'_{lx} = k_e \frac{A_{sx}}{Sd_c} f_{yh} \quad \textbf{(3.3)}$$

And in the y direction as

$$f'_{ly} = k_e \frac{A_{sy}}{Sb_c} f_{yh} \quad \textbf{(3.4)}$$

Where A_{sx} and A_{sy} are the total area of transverse bars running in the x and y directions, respectively (Figure 3.1) and K_e is given in Eq. (3.2). The general solution of the multi-axial failure criterion in terms of the two lateral confining stresses for obtaining the ultimate confined concrete strength, f'_{cc}, is presented in Figure 3.2.

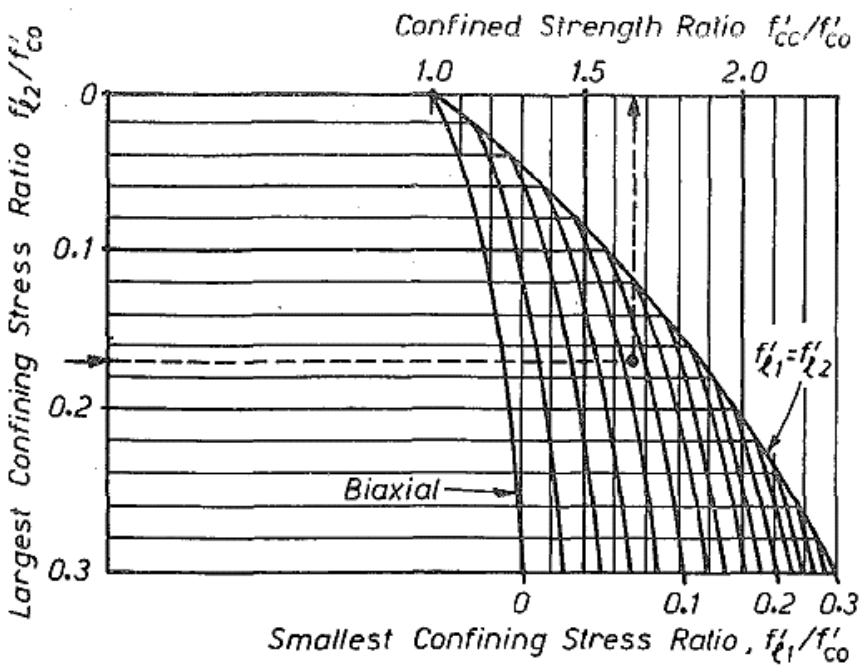

Figure3.2 : Confines strength determination from lateral confining stresses for rectangular sections (Mander, Priestley & Park 1988).

Behavioral graph developed by Mander et al. for comparing the behavior of unconfined and confined concrete is presented in Figure 3.3. For Mander et al., the concrete stress at any point is calculated using Equation (3.5).

$$f'_c = \frac{f'_{cc} r x}{r - 1 + x^r} \tag{3.5}$$

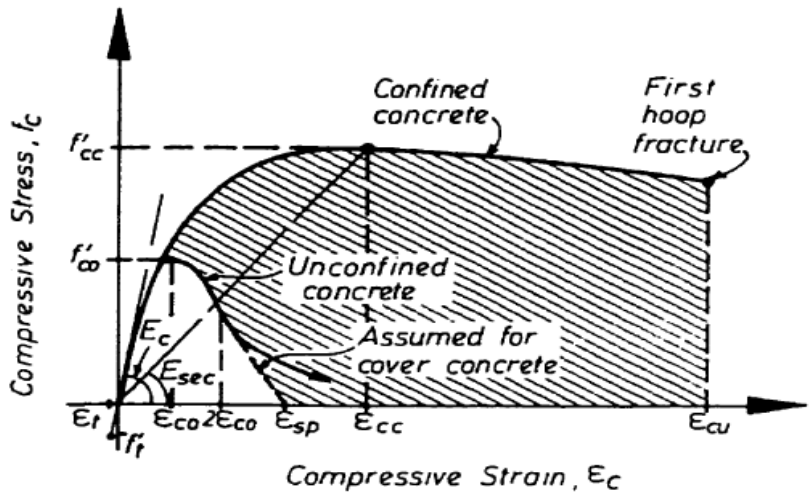

Figure 3.3 : Proposed Stress-Strain Model (Mander, Priestley & Park 1988).

In this case, f'_c is the measured strength of the concrete while $x = \varepsilon_c / \varepsilon_{cc}$, and r is calculated using Eq. (3.6). The factor, r, is based on the modulus of elasticity for the concrete, E_c, as well as the slope, $E_{\sec}$, from the start of loading to the maximum strength are calculated using Equations (3.7) and (3.8), respectively.

$$r = \frac{E_c}{E_c - E_{\sec}} \tag{3.6}$$

$$E_c = 5000\sqrt{f'_c} \tag{3.7}$$

$$E_{\sec} = \frac{f'_{cc}}{\varepsilon_{cc}} \tag{3.8}$$

Difference between Mander et al. model and the models that were discovered before it is that it is not suitable to assume the value of ε_{cc} to be equal to 0.002. A formula was developed that calculates this maximum strain value using the ultimate stress value of confined concrete as well as the ultimate stress, f'_{co}, and strain, ε_{co}, of unconfined concrete. The value of ε_{cc} is much greater than the value of ε_{co} because the confining reinforcement allows the member to sustain larger axial deformations and is calculated by following Equation.

$$\varepsilon_{cc} = \varepsilon_{co}\left[1 + 5\times\left(\frac{f'_{cc}}{f'_{co}} - 1\right)\right] \quad \textbf{(3.9)}$$

The theoretical and experimental load displacement relationships for reference specimens are compared in Figures 5.10.

3.2 External Confinement with BTRM

Studies on the use of textiles in the upgrading of concrete structures have been limited in literature and most of these studies have focused on flexural or shear strengthening of beams and on aspects of bond between concrete and cement-based textile composites. Simple confinement model for concrete confinement with Textile-Reinforced Mortar Jackets is presented by Thanasis C. Triantafillou (2006) and experimentally investigated the use of TRM jackets as a means of confining poorly detailed RC columns, which suffer from limited deformation capacity under seismic loads due to buckling of the longitudinal bars (Figure 3.4). A typical approach toward modeling confinement is to assume that the confined strength f_{cc} and ultimate strain ε_{ccu} depend on the confining stress at failure, σ_{lu}, as follows:

$$\frac{f_{cc}}{f_{co}} = 1 + K_1\left(\frac{\sigma_{lu}}{f_{co}}\right)^m \quad \textbf{(3.10)}$$

$$\varepsilon_{ccu} = \varepsilon_{co} + K_2\left(\frac{\sigma_{lu}}{f_{co}}\right)^n \quad \textbf{(3.11)}$$

Where K_1, K_2, m, and n are empirical constants.

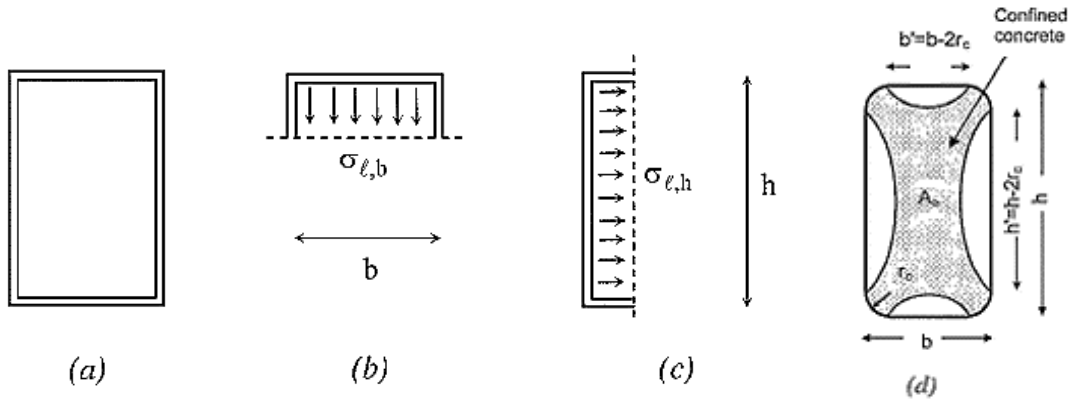

Figure 3.4: a)Section of confinement jacket. b)Approximate average confining stresses perpendicular to b-side. c)Approximate average confining stresses perpendicular to h side. d)Effectively confined area in columns with rectangular cross section (Thanasis C. Triantafillou 2006).

Confined area (A_e in Figure 3.4-d) to the total cross-sectional area A_g as follows

$$K_e = 1 - \frac{b'^2 + h'^2}{3A_g} \quad \textbf{(3.12)}$$

$$\sigma_{lu} = K_e \frac{(b+h)}{bh} t_j f_{je} \quad \textbf{(3.13)}$$

Hence, the confining stress at failure σ_{lu} is given by Eq. (3.13) where, f_{je} is the effective jacket strength in the lateral direction.

3.3 Proposed Confinement Model

In detail, the stress-strain of reinforced concrete column confined with Basalt textile mesh is evaluated as the sum of two portion (Figure 3.5): the stress-strain of internal confined concrete calculated using the Mander et al (1988) model ($f'cc_{ITR}$) and the stress-strain of external confined concrete calculated using the Ilki et al (2003) model ($f'cc_{TRM}$). As shown in the theoretical model proposed by Mander et al (2008), noticeable increments in strength and ductility provided by the stirrups. In the following section, expected capacity of externally confined specimen with basalt textile mesh will be explained.

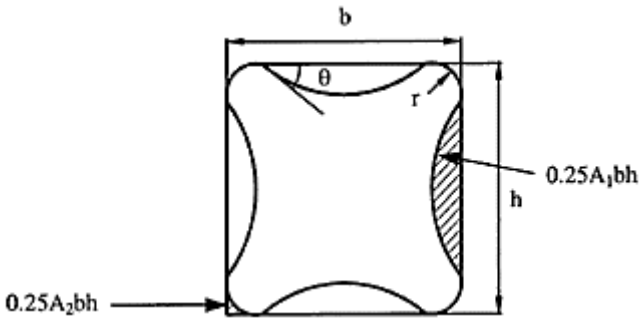

Figure 3.5 : Effectively confined cross-sectional area (Ilki et al, 2003).

$$f'_{cc(TRM)} = f'_{co}\left[1 + 2.4\left(\frac{f'_{l\max}}{f'_{co}}\right)^{1.2}\right] \quad (3.17)$$

$$f'_{l(\max)} = \frac{k_a \rho_f \varepsilon_{h,rup} E_{TRM}}{2} \quad (3.18)$$

In Eq. (6), κ_a is the efficiency factor that is to be determined based on the section geometry as the ratio of effectively confined cross-sectional area to the gross cross-

sectional area, Figure 3.6. The efficiency factor ,κ_a , can be assumed as 1 for circular cross-sections. For rectangular cross-sections, κ_a can be determined by Eqs. (3.19), (3.20) and (3.21), as also proposed by Wang and Restrepo (2001). In Eq. (3.18), E_{TRM} and ρ_f are the tensile elasticity modulus and ratio of wrapping material to the concrete cross-section, respectively. The ratio of the wrapping material to the concrete cross-section can be determined by Eq. (3.22) for rectangular cross-sections.

$$k_a = 1 - A_1 - A_2 - \rho \tag{3.19}$$

$$A_1 = \frac{(b-2r)^2 + (h-2r)^2}{3bh} \times \tan\theta \tag{3.20}$$

$$A_2 = \frac{4r^2 - \pi r^2}{bh} \tag{3.21}$$

$$\rho_f = \frac{t_f \times n_f \times (b+h) \times 2}{bh \times w'} \tag{3.22}$$

In above equations, ρ is the ratio of cross-sectional area of the longitudinal reinforcement to the cross-sectional area of wrapped member, θ is the arching angle and r is the radius of the member corner. Wang and Restrepo (2001) reported that θ varied between 42 and 47 degrees. In this study, based on the observations on the damaged specimens, θ is assumed as 45 degrees. In Eq. (3.22), t_f and n_f are the effective thickness and the number of plies of wrapping material, b and h are the width and depth of the rectangular member to be wrapped. After statistical evaluation of the experimental data, the equation given below is proposed for the ultimate axial strain of FRP composite jacketed low strength concrete, Eq. (3.23).

$$\varepsilon_{cc(TRM)} = \varepsilon_{co}\left[1 + 20\left(\frac{h}{b}\right)\left(\frac{f'_{l\max}}{f'_{co}}\right)^{0.5}\right] \tag{3.23}$$

The effect of confinement with Glass Fiber Reinforced Concrete (GFRC) is neglected in this study but experimental results indicated that there is a noticeable increment in strength and ductility provided by the GFRC. For obtaining this aim there is a large amount of specimens were built to understand the behavior of mortar during the compression test for further studies.

For obtaining ultimate compressive stress ($f'_{cc\,TOTAL}$) and strain ($\varepsilon_{ccuTOTAL}$) of external and internal confined of low strength concrete, Ilki et al (2006) model was used as presented in following:

$$\left[\frac{f'_{cc}-f'_{co}}{f'_{co}}\right]_{TOTAL}=\left[\frac{f'_{cc}}{f'_{co}}-1\right]_{ITR}+\left[\frac{f'_{cc(TRM)}}{f'_{co}}-1\right]_{TRM} \qquad \textbf{(3.14)}$$

$$\left[\frac{\varepsilon_{cc}-\varepsilon_{co}}{\varepsilon_{co}}\right]_{TOTAL}=\left[\frac{\varepsilon_{cc}}{\varepsilon_{co}}-1\right]_{ITR}+\left[\frac{\varepsilon_{cc(TRM)}}{\varepsilon_{co}}-1\right]_{TRM} \qquad \textbf{(3.15)}$$

The concrete stress at any point is calculated by using Equation (3.5) proposed by Mander et al and use $f'_{cc\,TOTAL}$ and $\varepsilon_{cc\,TOTAL}$ in this equation.

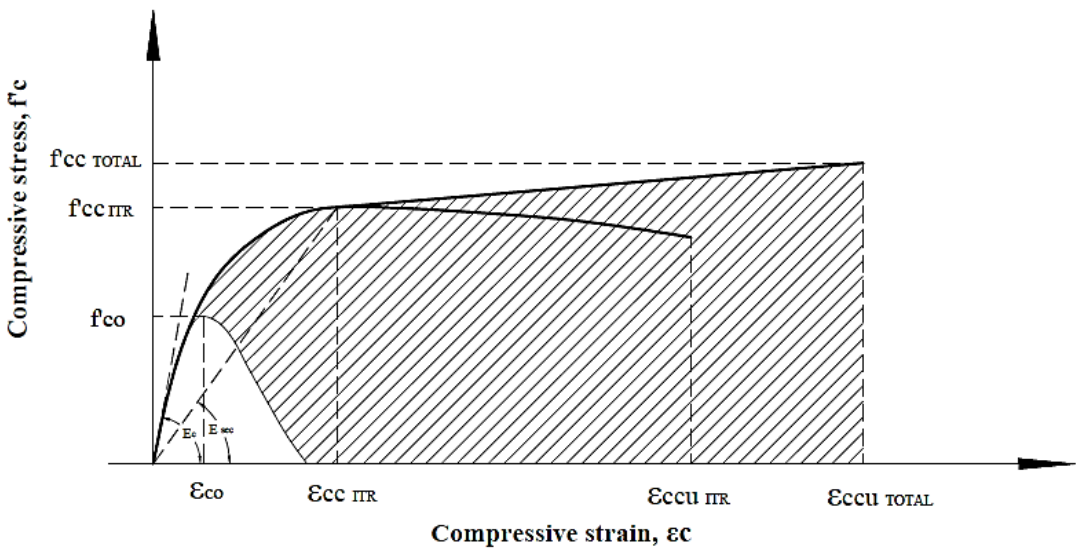

Figure 3.6 : Stress-strain model for externally confined reinforced concrete.

4. TEST RESULTS

4.1 General Behavior and Test Observations

Experimental observations made during full-scale model column tests are presented in this chapter. The failure process was documented by observing the overall response of the columns including cracking patterns and hysteretic Lateral load-Drift relationships. These observations and the data recorded are used in Chapter 5 to determine the effects of test parameters on the behavior of the specimens.

4.2 Test Observation of Reference Columns

4.2.1 Specimen: Ref-S60-Ɵ90-L80

Before describing test observation, some information about specification of specimen can be found at Table 4.1 at the below.

Table 4.1: General specification of Ref-S60-Ɵ90-L80 specimen.

Specimen: Ref-S60-Ɵ90-L80				
Cross section Dimension h × b (mm)	300 x 200	Hook Length L (mm)		80
Height of Columns H_{column} (mm)	1290	Hook Angle Ɵ (°)		90°
Compressive strength of standard cylinder samples for columns (MPa)	7.5	$\frac{N_{axial}}{A_g f_c'}$		54.4 %
Equivalent Compressive strength of core samples for columns (MPa)	9.9	Transverse Reinforcement (S-220 Type)	Size @Spacing (mm)	Φ8 @ 60
			ρ_t %	1.67
Axial Load N_{axial} (kN)	323	Longitudinal Reinforcement (S-420 Type)	Number and Size of Bars (mm)	4Φ14
			ρ_l %	1.03

All experimental observations, which were made during the test of Ref-S60-Ɵ90-L80, are presented at the appendix A. In this subsection, only the important events were pointed out. No cracks were observed while loading to target displacements of ± 5.16 mm (drift ratio of 0.4%) as illustrated in Figure 4.1.

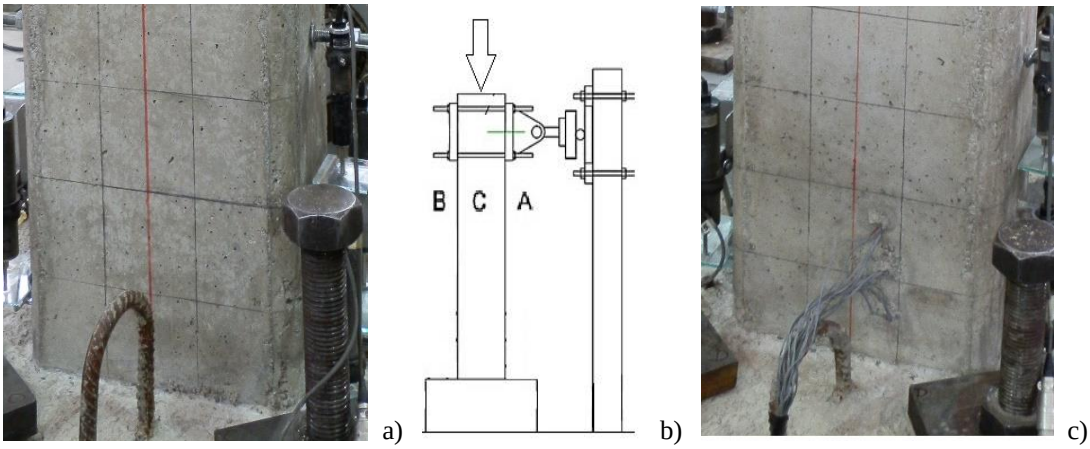

Figure 4.1 : Specimen Ref-S60-Ɵ90-L80 after the drift ratio of 0.4%. a)Face C. b)Definition of column optional faces. c)Face D.

At the column-foundation interface, during loading to target displacement of ±7.74 mm (drift ratio of 0.60%) first flexural crack was observed. During loading to target displacements of ±10.32 mm (drift ratio of 0.80%) new flexural cracks were observed as illustrated in Figure 4.2. While loading to target displacements of ±19.35 mm (drift ratio of 1.50%) no new cracks were observed only the previous flexural cracks became inclined and extended into the web zone of the column due to the influence of increased shear force as shown in Figure 4.3.

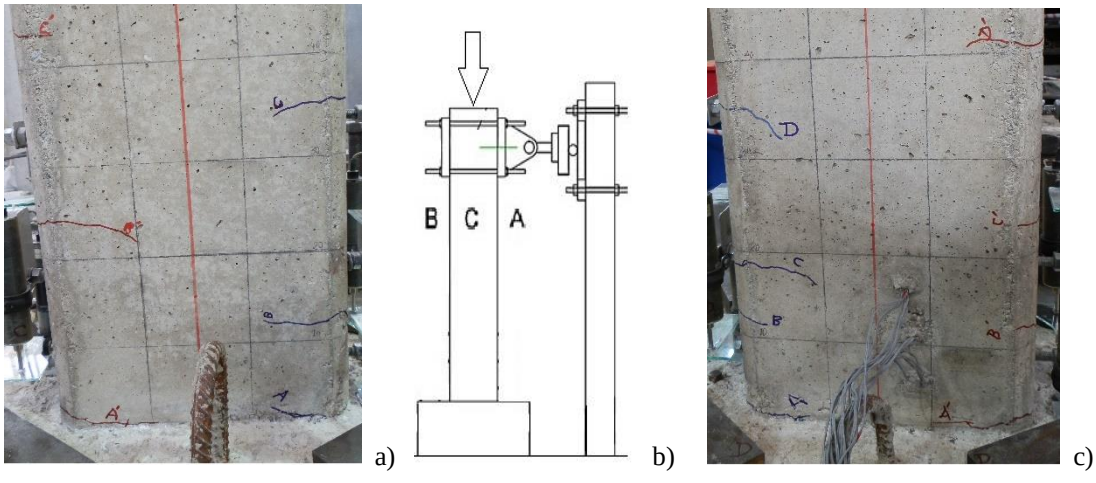

Figure 4.2 : Specimen Ref-S60-Ɵ90-L80 after the drift ratio of 0.8%. a)Face C. b)Definition of column optional faces. c)Face D.

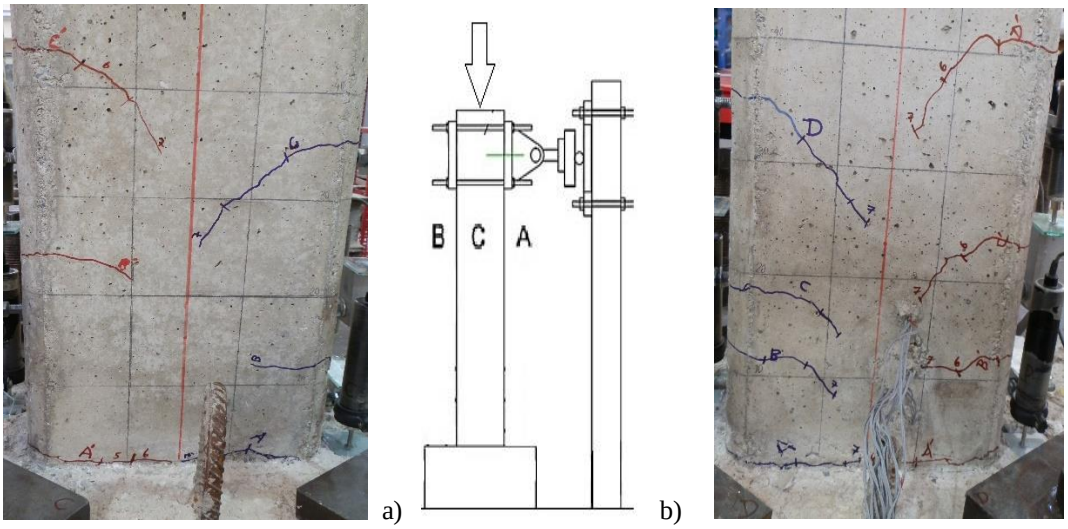

Figure 4.3 : Specimen Ref-S60-Ɵ90-L80 after the drift ratio of 1.50%. a)Face C. b)Definition of column optional faces. c)Face D.

During loading to target displacement of 19.35 mm (drift ratio 1.50%), concrete crushing was formed at the A-face of the column. After mentioned target drift ratio some new flexural cracks were observed on column surfaces. During loading to target displacement of 37.89 mm (drift ratio 3.0%), concrete cover started to spall off at the column surfaces in compression zone as shown in Figure 4.4.

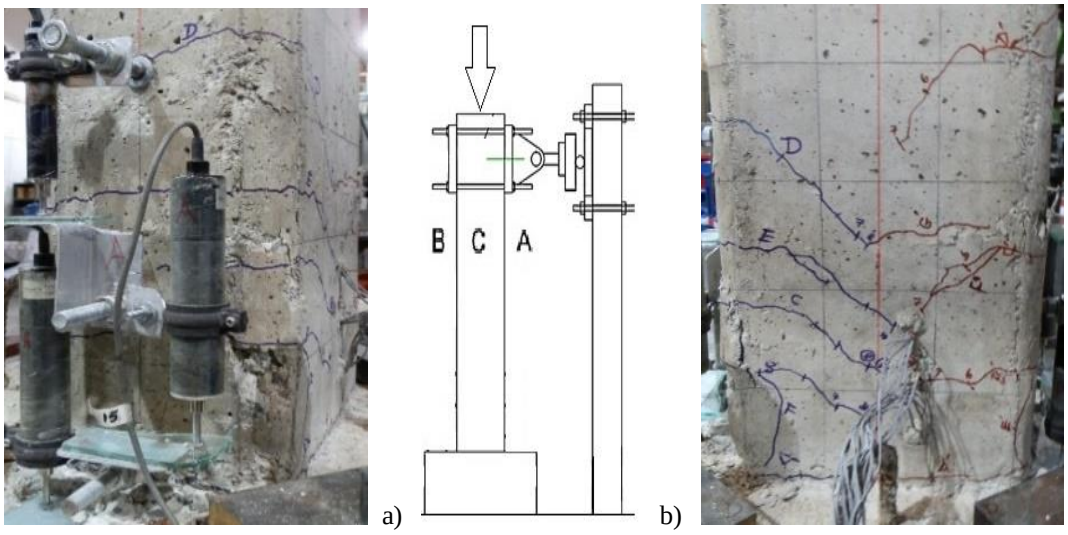

Figure 4.4 : Specimen Ref-S60-Ɵ90-L80 after the drift ratio of 3.0%. a)Face A. b)Definition of column optional faces. c)Face D.

After loading to target displacement of 77.4 mm (drift ratio of 6%), test was ended due to buckling of the longitudinal bars and 33% loss of strength. Figure 4.5 illustrated the damaged Ref-S60-Ɵ90-L80 specimen at the end of the test.

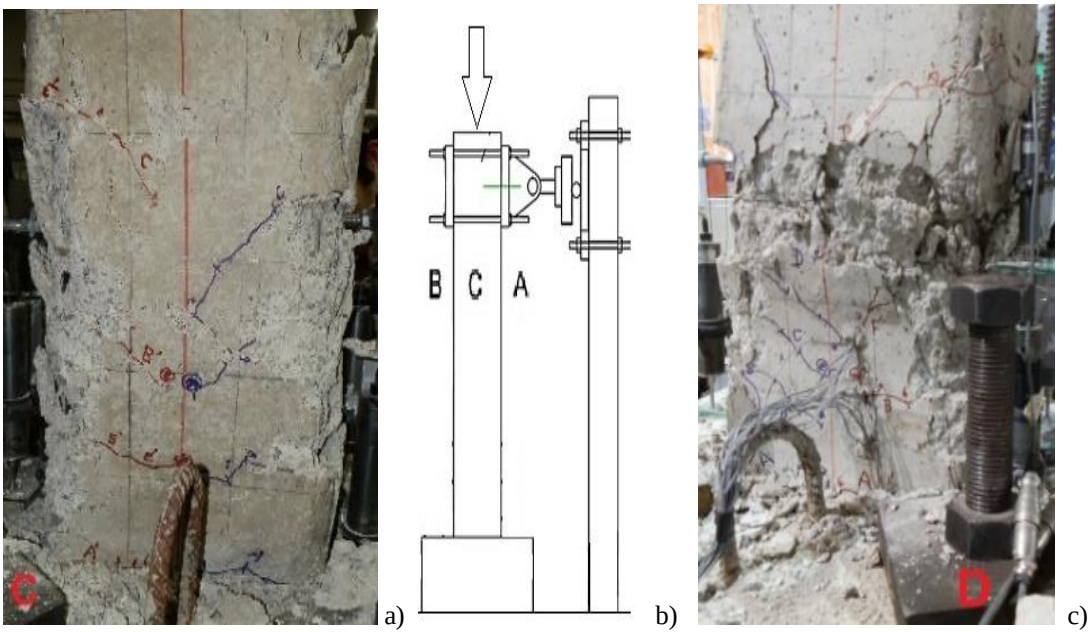

Figure 4.5: Specimen Ref-S60-Ɵ90-L80 after the drift ratio of 6.0 % a) Face C, b) Definition of column optional faces, c) Face D.

The plastic hinge length of specimen at the end of test was measured between 250 to 300 mm as was shown in the Figure 4.6.

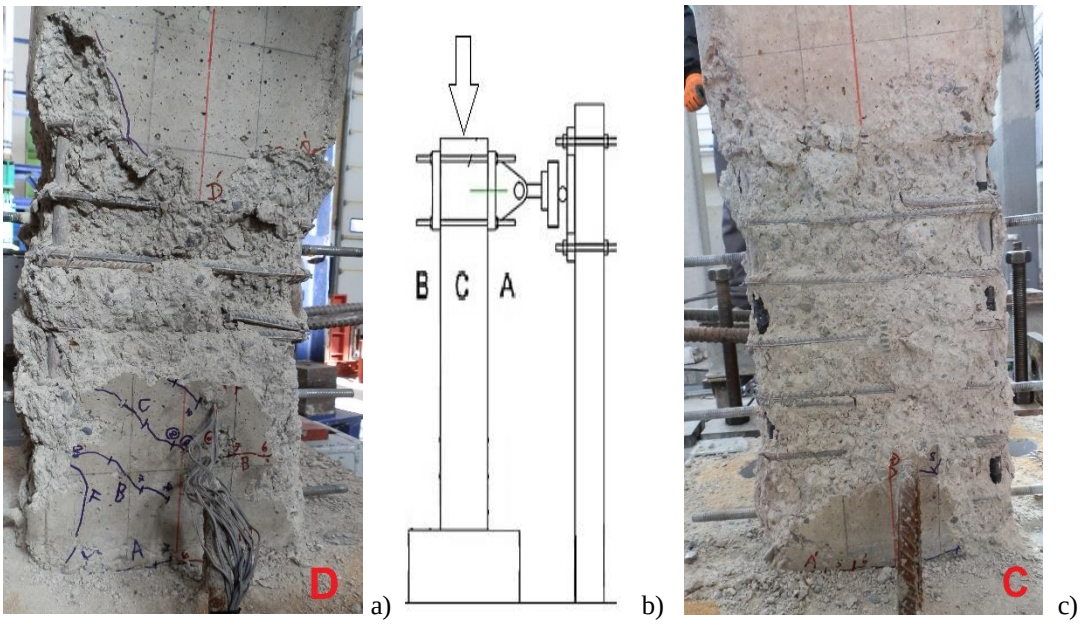

Figure 4.6 : Specimen Ref-S60-Ɵ90-L80 after the drift ratio of 6.0 %. a)Face C. b)Definition of column optional faces. c)Face D.

The extent of damage at progressive stages of testing can be seen in the Figure 4.7. All pictures were taken after the first cycle of each load stage.

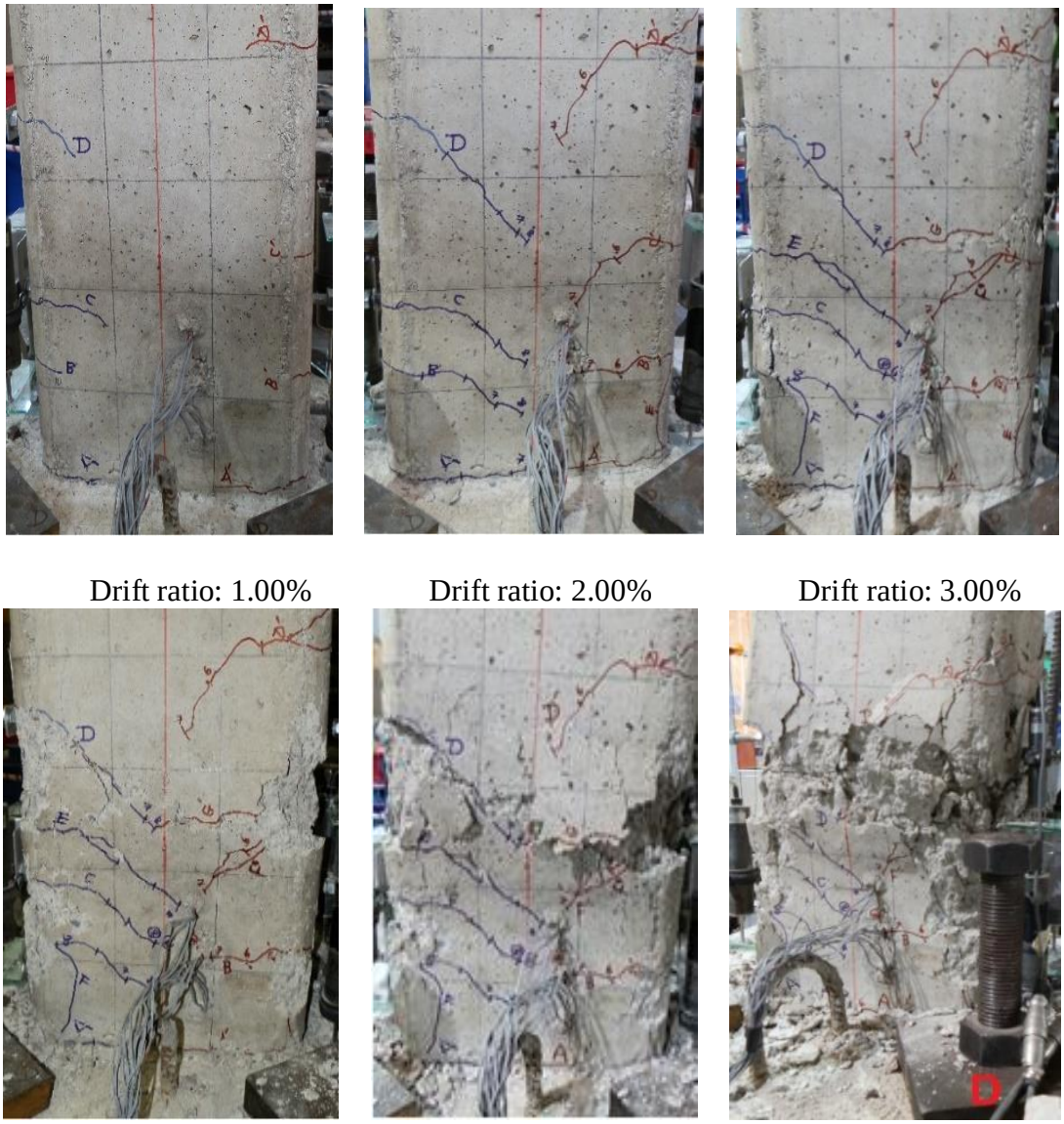

Drift ratio: 1.00% Drift ratio: 2.00% Drift ratio: 3.00%

Drift ratio: 4.00% Drift ratio: 5.00% Drift ratio: 6.00%

Figure 4.7 : Crack pattern of Ref-S60-Ɵ90-L80 at different drift ratios.

The lateral load-drift-displacement hysteresis curve of the Ref-S60-Ɵ90-L80 is shown in Figures 4.8. It is clear there is no difference between values of the lateral loads while pulling and pushing and almost damage shape was symmetric. The amount of plastic deformation at the point of lateral load application was around 44 mm after loading to target displacement of 77.4 mm (drift ratio +6.0%) and the measurement of out-of-plane at the level of lateral load application was +10.2 mm when lateral load was zero at the end of the test. Test was ended by losing 33% of lateral load capacity during pushing or pulling. Envelope curves for Ref-S60-Ɵ90-L80 specimen is drawn in Figures 4.9.

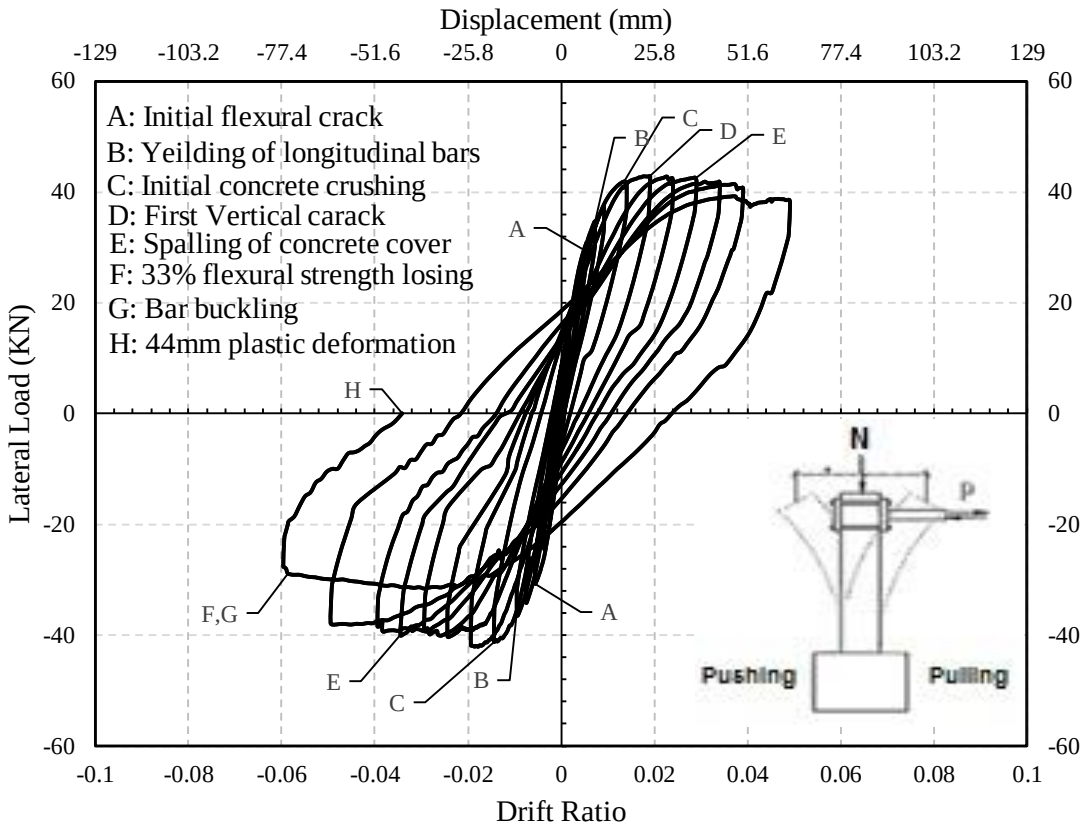

Figures 4.8 : Lateral Load-Drift-Tip Displacement curves for Ref-S60-Θ90-L80.

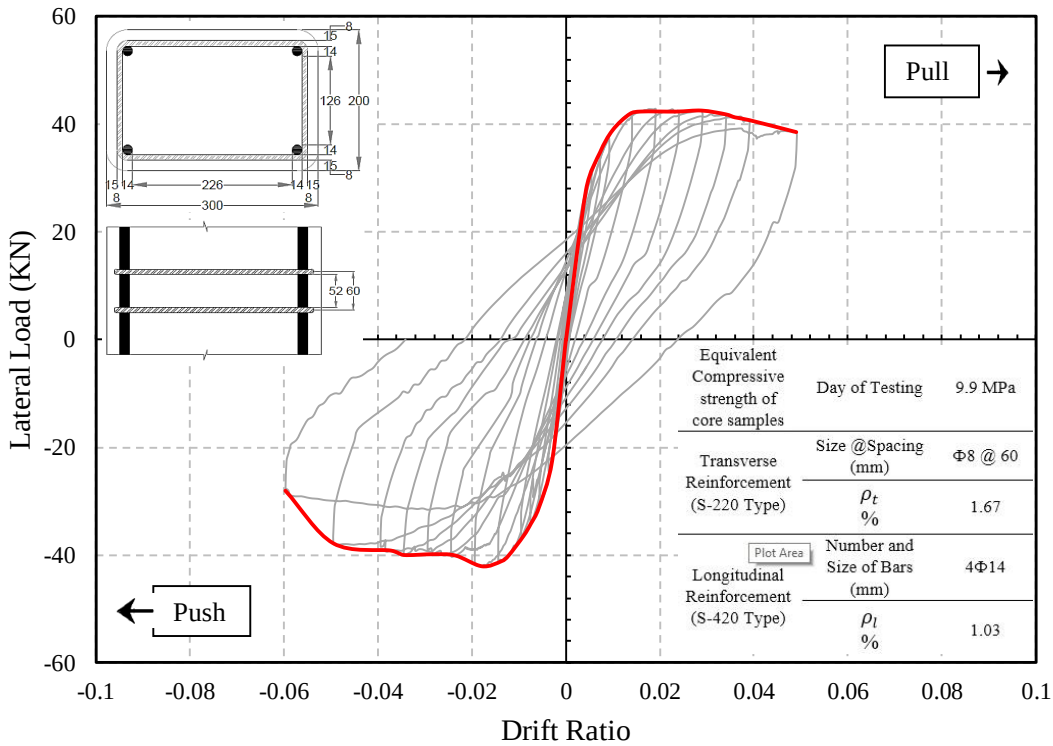

Figures 4.9 : Lateral Load-Drift envelope curve of Ref-S60-Θ90-L80.

4.2.2 Specimen: Ref-S60-Ɵ112.5-L80

Before describing test observation, some information about specification of specimen can be found at Table 4.2 at the below.

Table 4.2: General specification of Ref-S60-Ɵ112.5-L80 specimen.

Specimen: Ref-S60-Ɵ112.5-L80				
Cross section Dimension h × b (mm)	300 x 200	Hook Length L (mm)		80
Height of Columns H_{column} (mm)	1269	Hook Angle Ɵ (°)		112.5°
Compressive strength of standard cylinder samples for columns (MPa)	7.5	$\frac{N_{axial}}{A_g f_c'}$		54.4 %
Equivalent Compressive strength of core samples for columns (MPa)	9.9	Transverse Reinforcement (S-220 Type)	Size @Spacing (mm)	Φ8 @ 60
			ρ_t %	1.67
Axial Load N_{axial} (kN)	323	Longitudinal Reinforcement (S-420 Type)	Number and Size of Bars (mm)	4Φ14
			ρ_l %	1.03

All experimental observations, which were made during the test of Ref-S60-Ɵ112.5-L80, are presented at the appendix A. In this subsection, only the important events were pointed out. No cracks were observed while loading to target displacements of ±1.27 mm (drift ratio of 0.1%) as illustrated in Figure 4.10.

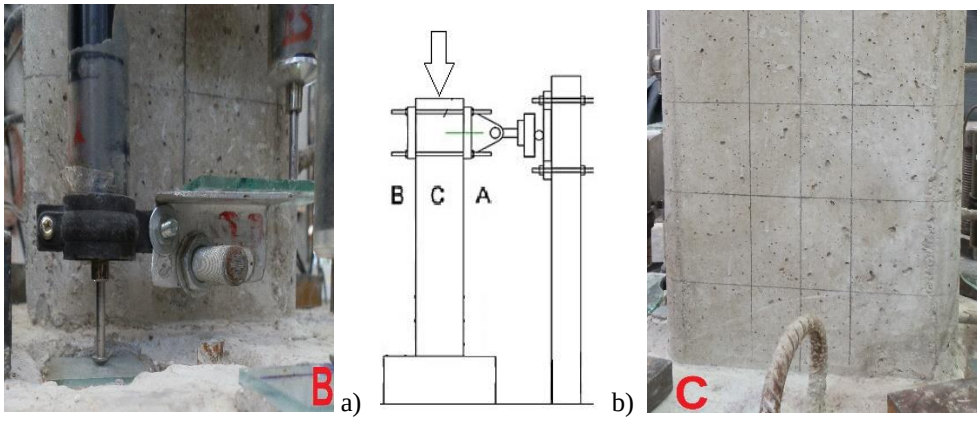

Figure 4.10 : Specimen Ref-S60-Ɵ112.5-L80 after the drift ratio of 0.1%. a)Face B. b)Definition of column optional faces. c)Face C.

At the column-foundation interface, during loading to target displacement of ±2.54 mm (drift ratio of 0.20%) first flexural crack was observed. During loading to target displacements of ±7.61 mm (drift ratio of 0.60%) new flexural cracks were observed as illustrated in Figure 4.11. While loading to target displacements of ±12.69 mm (drift ratio of 1.00%) no new cracks were observed only the previous flexural cracks became inclined and extended into the web zone of the column due to the influence of increased shear force as shown in Figure 4.12

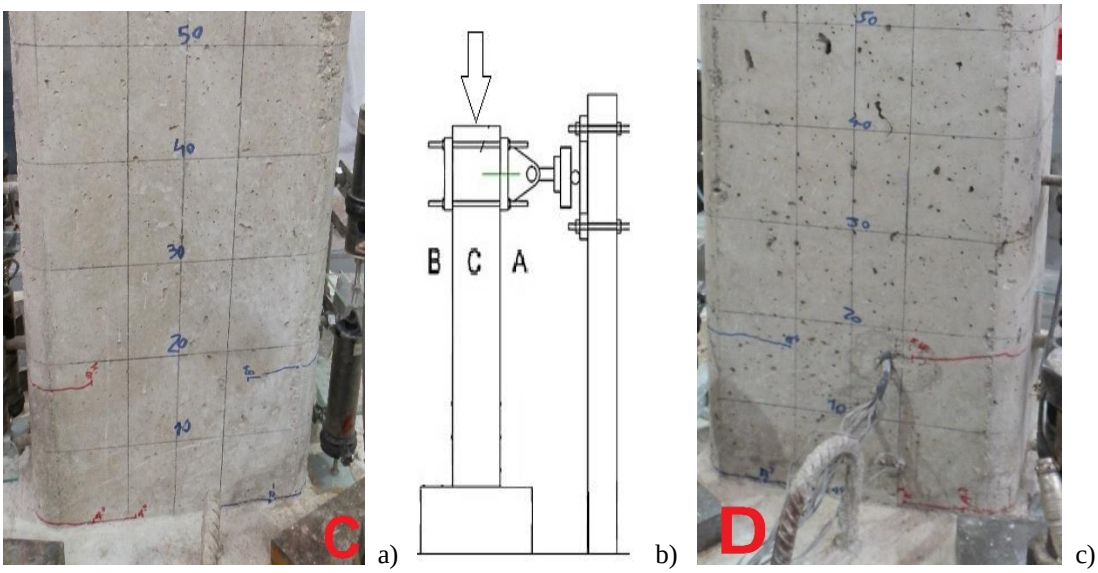

Figure 4.11 : Specimen Ref-S60-Ɵ112.5-L80 after the drift ratio of 0.6%. a)Face C. b)Definition of column optional faces. c)Face D.

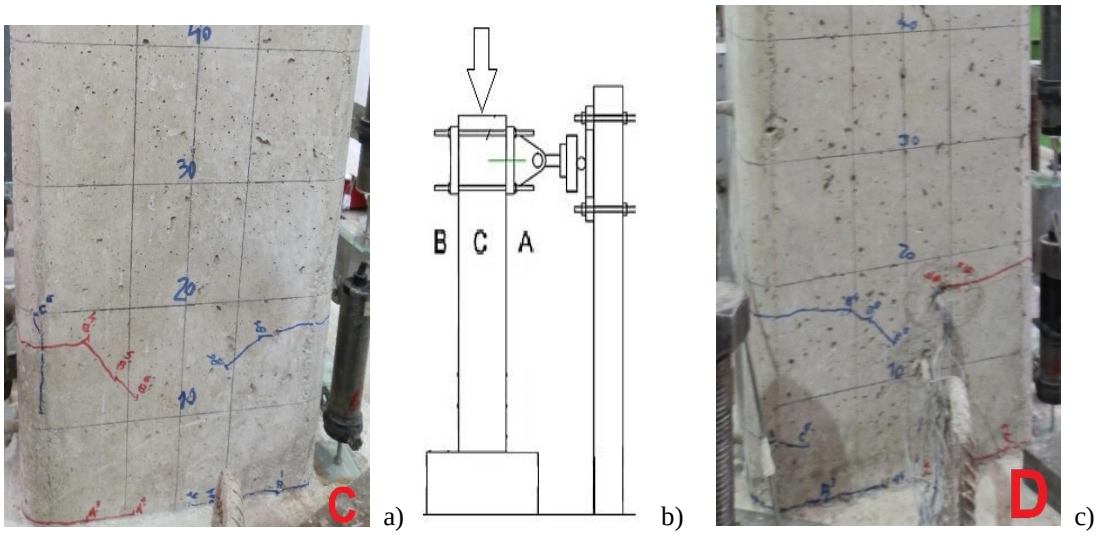

Figure 4.12 : Specimen Ref-S60-Ɵ112.5-L80 after the drift ratio of 1.00%. a)Face C. b)Definition of column optional faces. c)Face D.

During loading to target displacement of 19.04 mm (drift ratio of 1.50%), concrete crushing was formed at the A-face of the column. After mentioned target drift ratio some new flexural cracks were observed on column surfaces. During loading to target displacement of 31.73 mm (drift ratio 2.50%), concrete cover started to spall off at the column surfaces in compression zone as shown in Figure 4.13.

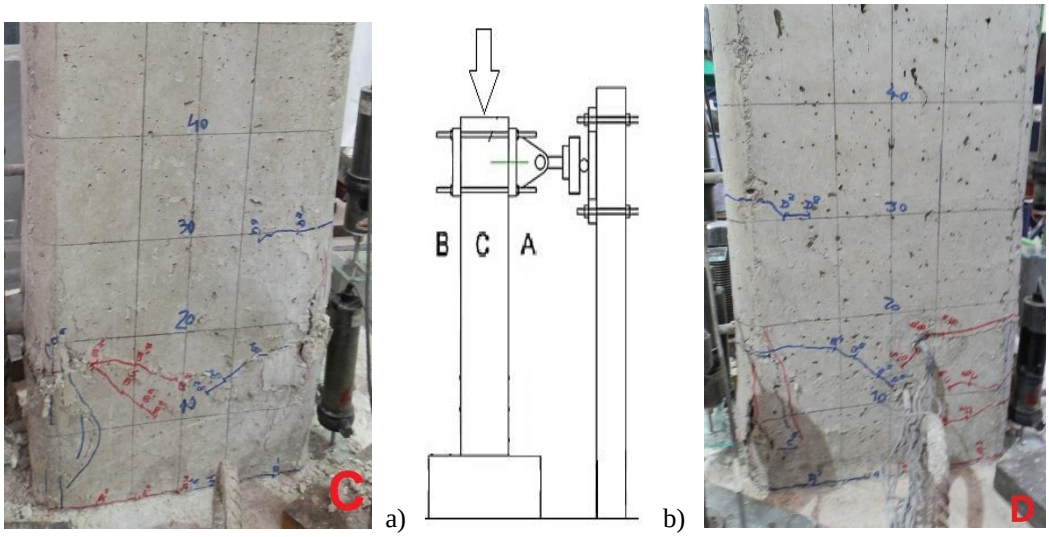

Figure 4.13 : Specimen Ref-S60-Ɵ112.5-L80 after the drift ratio of 2.50 %. a)Face C. b)Definition of column optional faces. c) Face D.

After loading to target displacement of 50.76 mm (drift ratio of 4%), test was ended by losing 15% of lateral load capacity. Figure 4.14 illustrated the damaged Ref-S60-Ɵ112.5-L80 specimen at the end of the test.

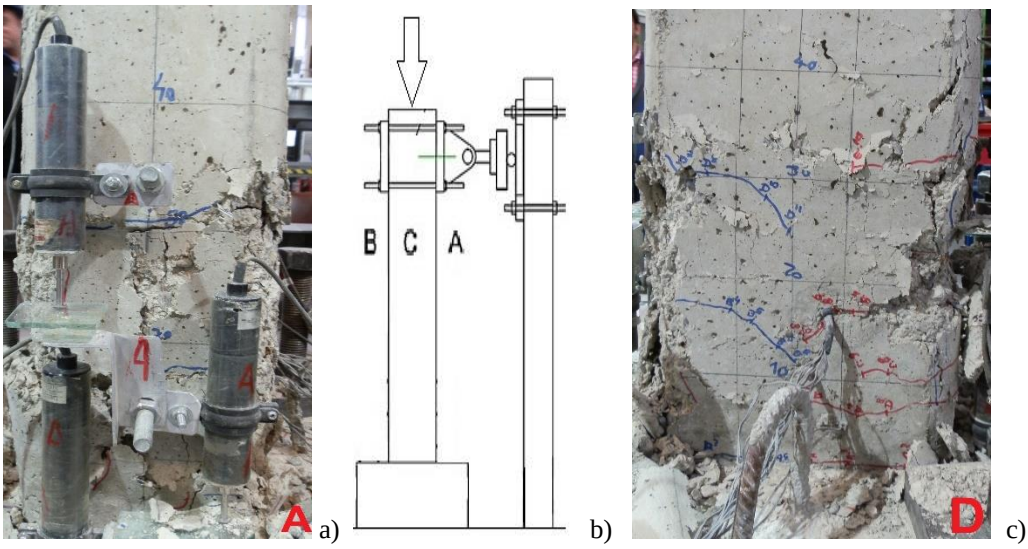

Figure 4.14 : Specimen Ref-S60-Ɵ90-L80 after the drift ratio of 4.0 %. a)Face A. b)Definition of column optional faces. c)Face D.

The extent of damage at progressive stages of testing can be seen in the Figure 4.15. All pictures were taken after the first cycle of each load stage.

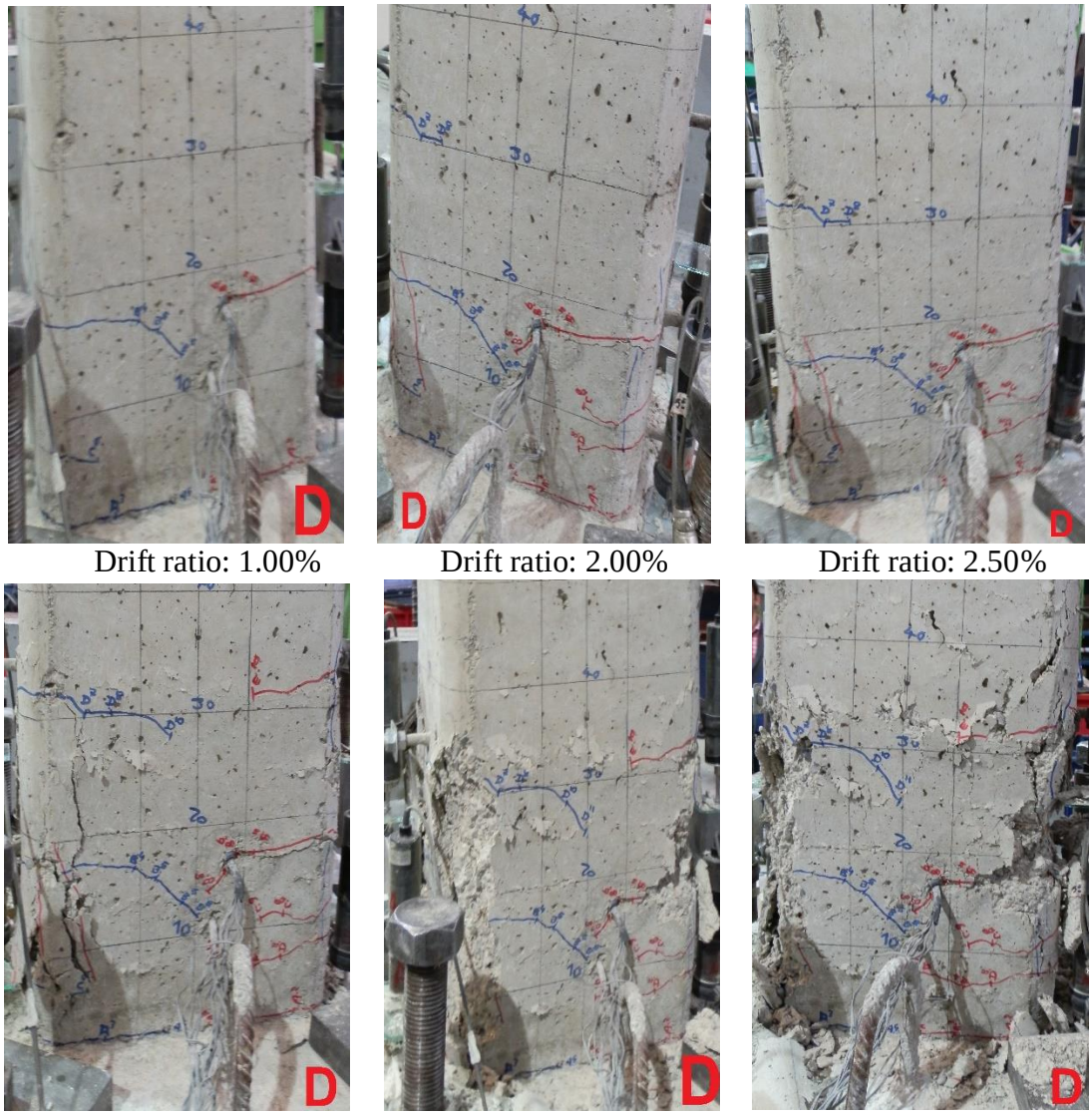

Figure 4.15 : Crack pattern of Ref-S60-Ɵ112.5-L80 at different drift ratios.

The plastic hinge length of specimen at the end of test was measured between 150 to 250 mm as was shown in the Figure 4.16.

The lateral load-drift-displacement hysteresis curve of the Ref-S60-Ɵ112.5-L80 is shown in Figures 4.17. It is clear there is no significant difference between values of the lateral loads while pulling and pushing and almost damage shape was symmetric. The amount of plastic deformation at the point of lateral load application was around 23.46 mm after loading to target displacement of 50.76 mm (drift ratio of +4.0%) and the measurement of out-of-plane at the level of lateral load application was +16.79

mm when lateral load was zero at the end of the test. Test was ended by losing 15% of lateral load capacity during pushing load at last cycle. Envelope curves for Ref-S60-Ɵ112.5-L80 specimen is drawn in Figures 4.18.

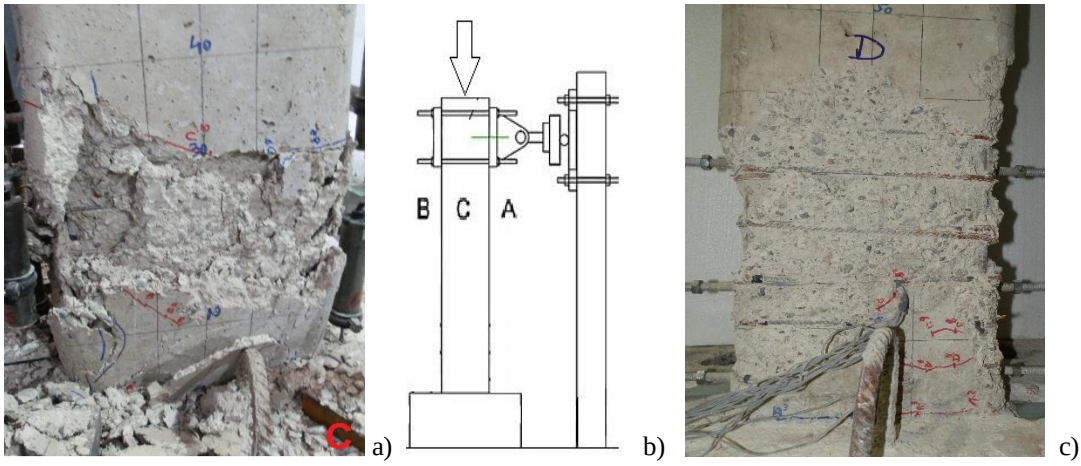

Figure 4.16 : Specimen Ref-S60-Ɵ112.5-L80 after the drift ratio of 6.0 %. a)Face C. b)Definition of column optional faces. c)Face D.

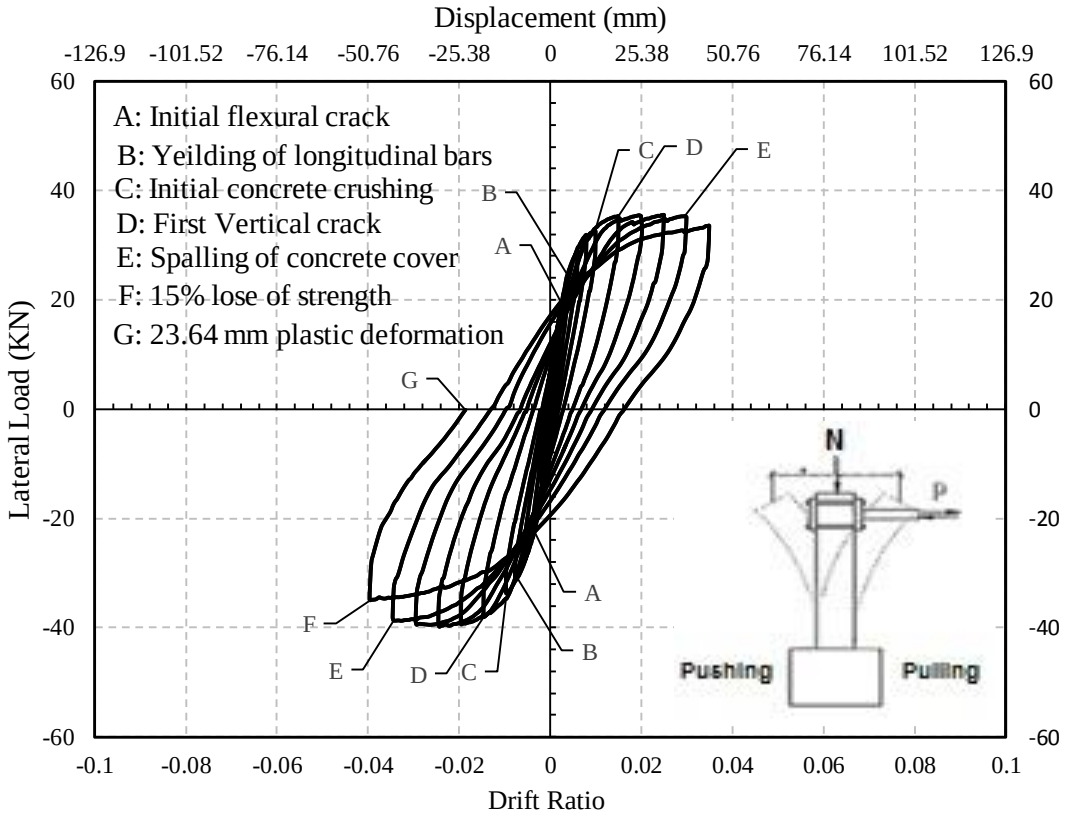

Figures 4.17 : Lateral Load-Drift-Tip Displacement curves of Ref-S60-Ɵ112.5-L80.

Equivalent

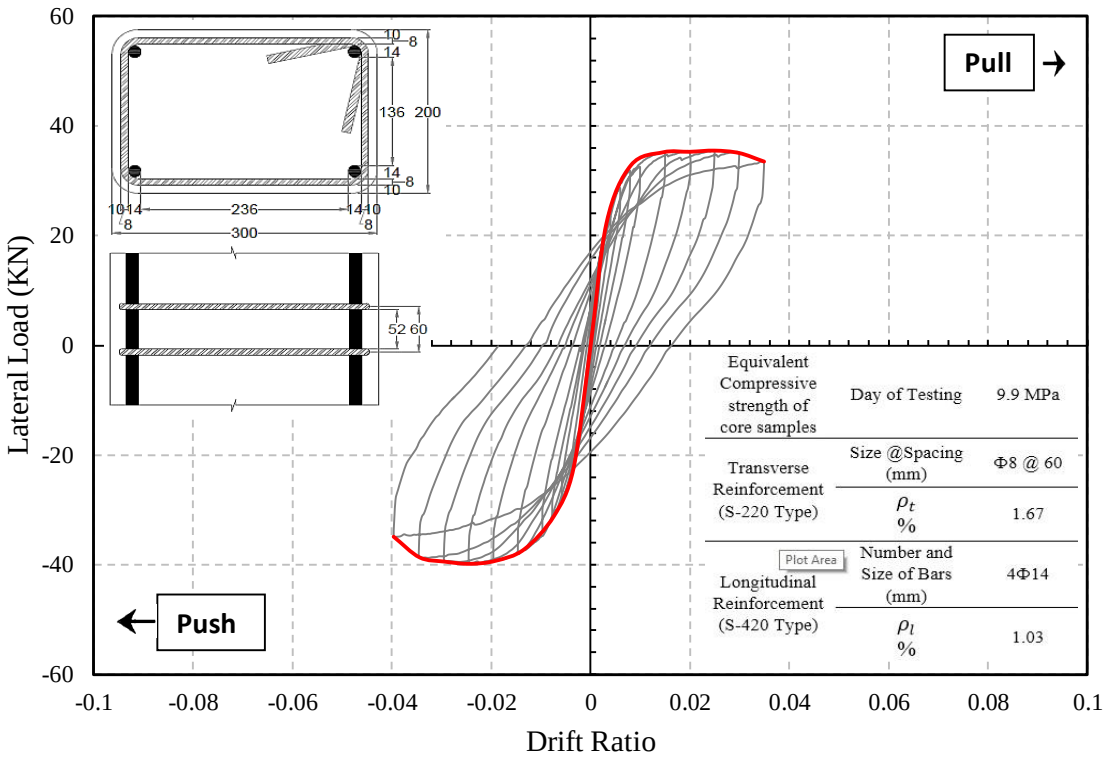

Figures 4.18 : Lateral Load-Drift envelope curve of Ref-S60-Θ112.5-L80.

4.2.3 Specimen: Ref-S60-Θ135-L80

Befor describing test observation, some information about specification of specimen can be found at Table 4.3 at the below.

Table 4.3: General specification of Ref-S60-Θ135-L80 specimen.

Specimen: Ref-S60-Θ135-L80				
Cross section Dimension h × b	300 x 200 mm	Hook Length L (mm)		80
Height of Columns H_{column}	1285 mm	Hook Angle Θ (°)		135°
Compressive strength of standard cylinder samples for columns	7.5 (MPa)	$\frac{N_{axial}}{A_g f_c'}$		54.4 %
Equivalent Compressive strength of core samples for columns	9.9 (MPa)	Transverse Reinforcement (S-220 Type)	Size @Spacing (mm)	Φ8 @ 60
			ρ_t (%)	1.67
Axial Load N_{axial} (kN)	323	Longitudinal Reinforcement (S-420 Type)	Number and Size of Bars (mm)	4Φ14
			ρ_l (%)	1.03

All experimental observations, which were made during the test of Ref-S60-Ɵ135-L80, are presented at the Appendix A. In this subsection, only the important events were pointed out. No cracks were observed while loading to target displacements of ±2.57 mm (drift ratio of 0.2%) as illustrated in Figure 4.19.

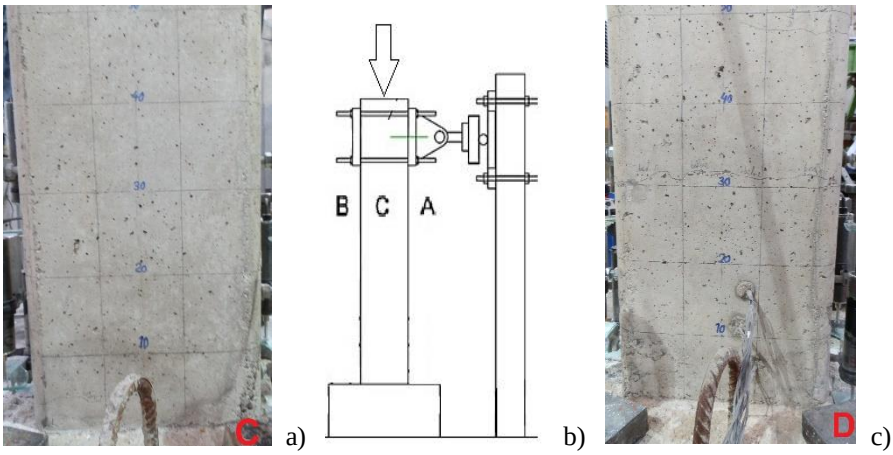

Figure 4.19 : Specimen Ref-S60-Ɵ135-L80 after the drift ratio of 0.2%. a)Face C. b)Definition of column optional faces. c)Face D.

At the column-foundation interface, during loading to target displacement of ±5.14 mm (drift ratio of 0.40%) first flexural crack was observed. During loading to target displacements of ±7.71 mm (drift ratio of 0.60%) new flexural cracks were observed as illustrated in Figure 4.20.

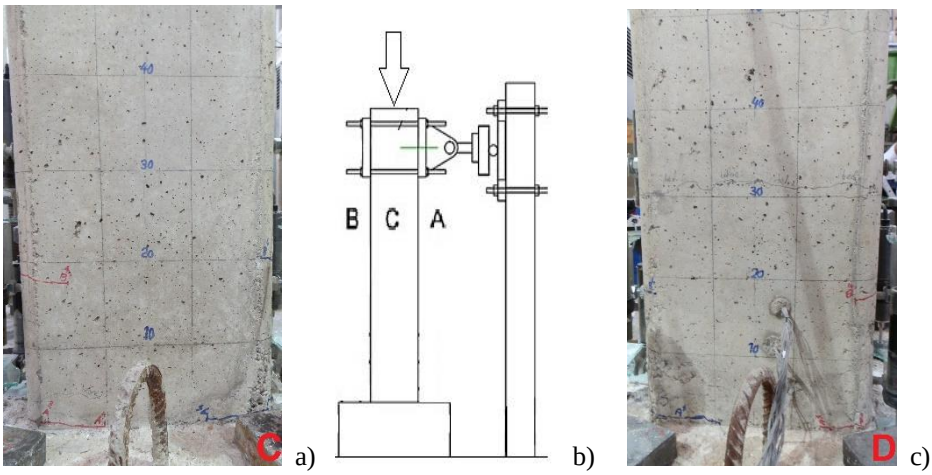

Figure 4.20 : Specimen Ref-S60-Ɵ135-L80 after the drift ratio of 0.6%. a)Face C. b)Definition of column optional faces. c)Face D.

During loading to target displacement of 10.28 mm (drift ratio 0.8%), concrete crushing was formed at the A-face of the column. While loading to target displacements of ±25.7 mm (drift ratio of 2.0%) some new cracks were observed and

the previous flexural cracks became inclined and extended into the web zone of the column due to the influence of increased shear force as shown in Figure 4.21.

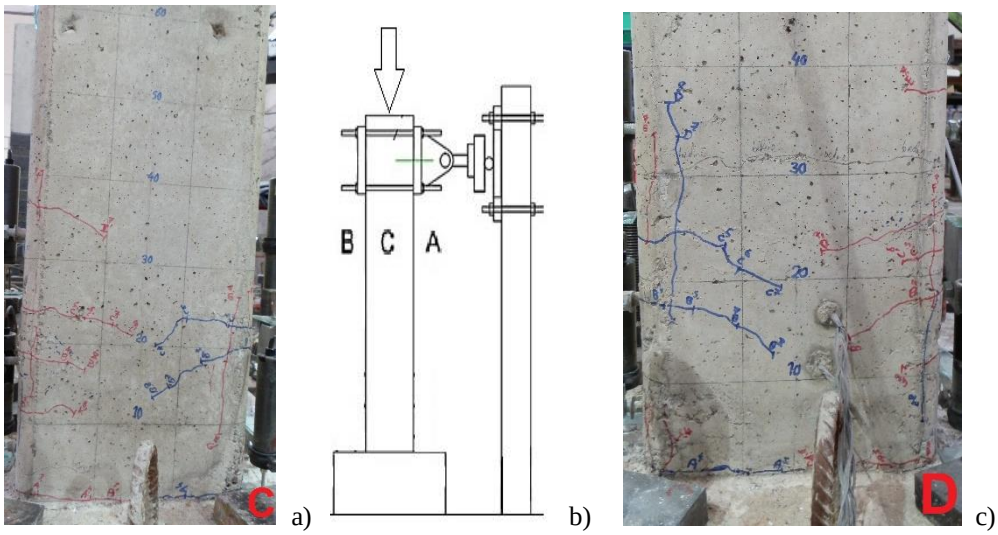

Figure 4.21 : Specimen Ref-S60-Ɵ135-L80 after the drift ratio of 2.0%. a)Face C. b)Definition of column optional faces. c)Face D.

During loading to target displacement of 38.55 mm (drift ratio 3.00%), concrete cover started to spall off at the column surfaces in compression zone as shown in Figure 4.22.

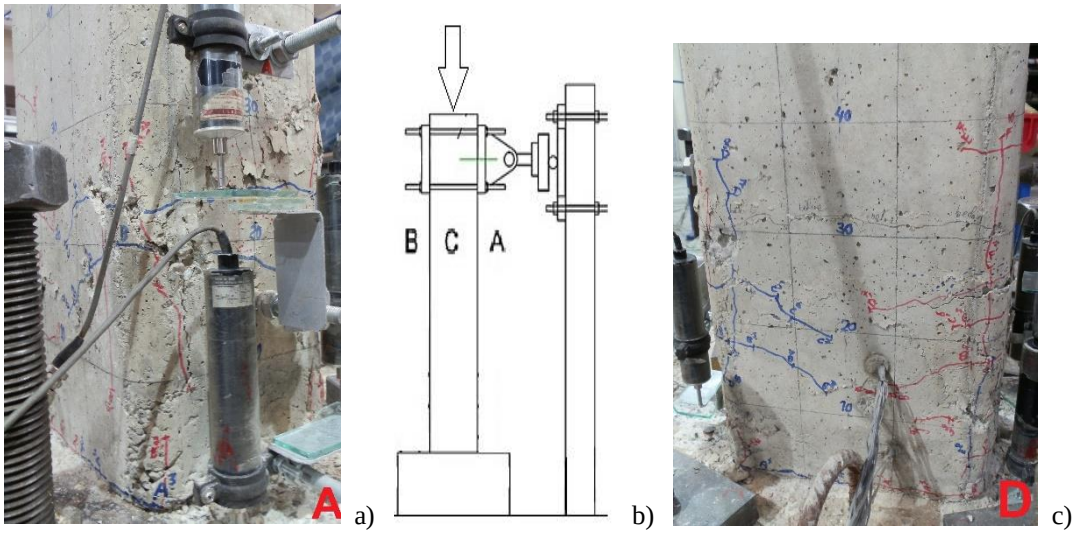

Figure 4.22: Specimen Ref-S60-Ɵ135-L80 after the drift ratio of 3.0%. a)Face A. b)Definition of column optional faces. c)Face D.

After loading to target displacement of 64.25 (drift ratio of 5%), test was ended due to 18% loss of lateral load capacity. Figure 4.23 illustrated the damaged Ref-S60-Ɵ135-L80 specimen at the end of the test.

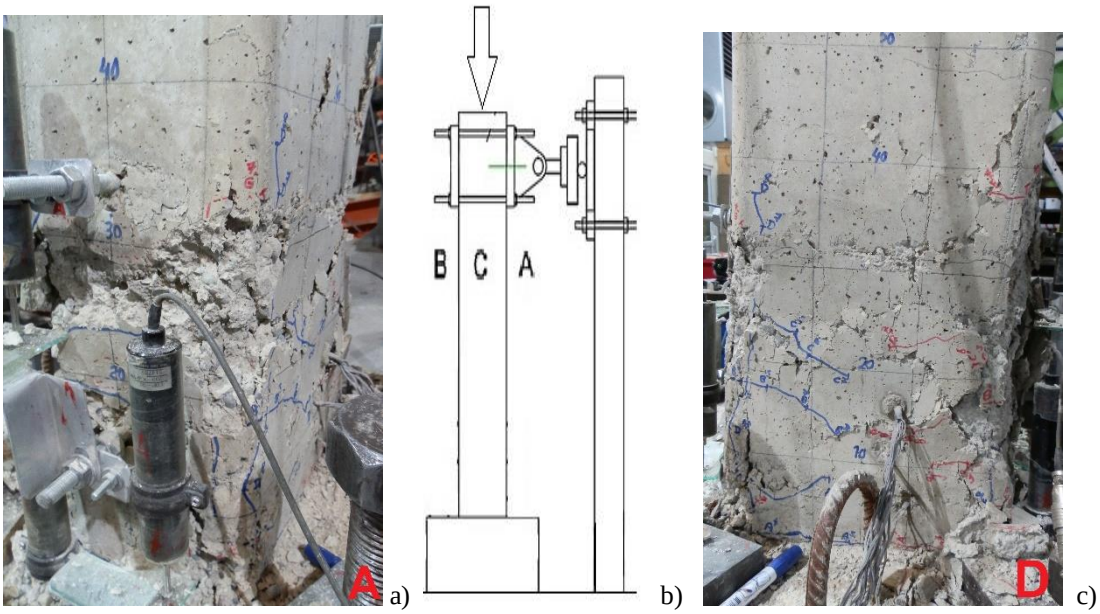

Figure 4.23 : Specimen Ref-S60-Ɵ135-L80 after the drift ratio of 5.0 %. a)Face A. b)Definition of column optional faces. c)Face C.

The plastic hinge length of specimen at the end of test was measured between 150 to 250 mm as was shown in the Figure 4.24.

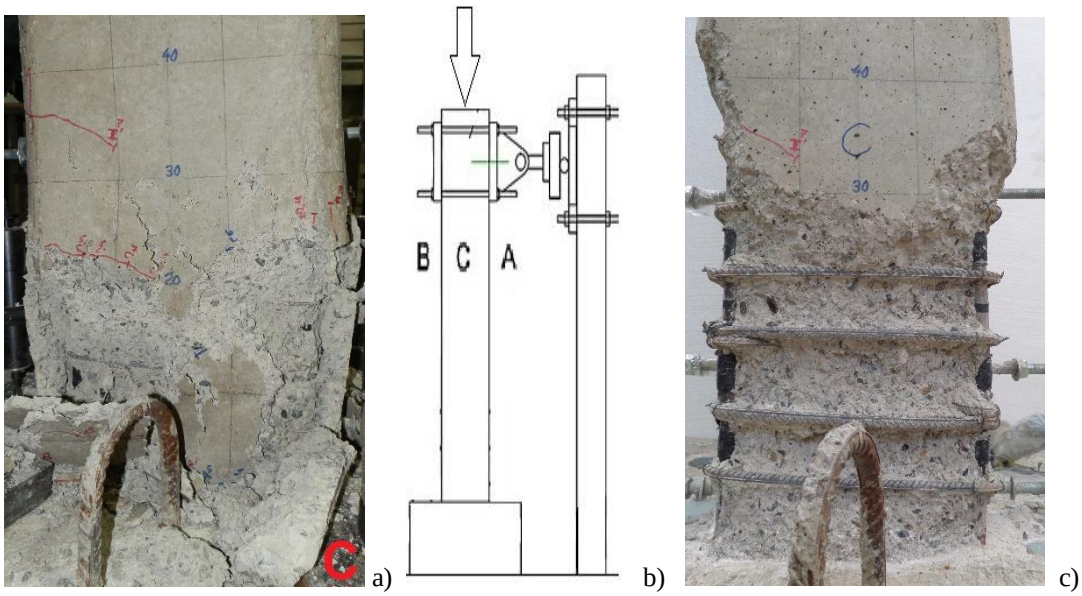

Figure 4.24 : Specimen Ref-S60-Ɵ90-L80 after the drift ratio of 5.0 %. a)Face C. b)Definition of column optional faces. c)Face C.

The extent of damage at progressive stages of testing can be seen in the Figure 4.25. All pictures were taken after the first cycle of each load stage.

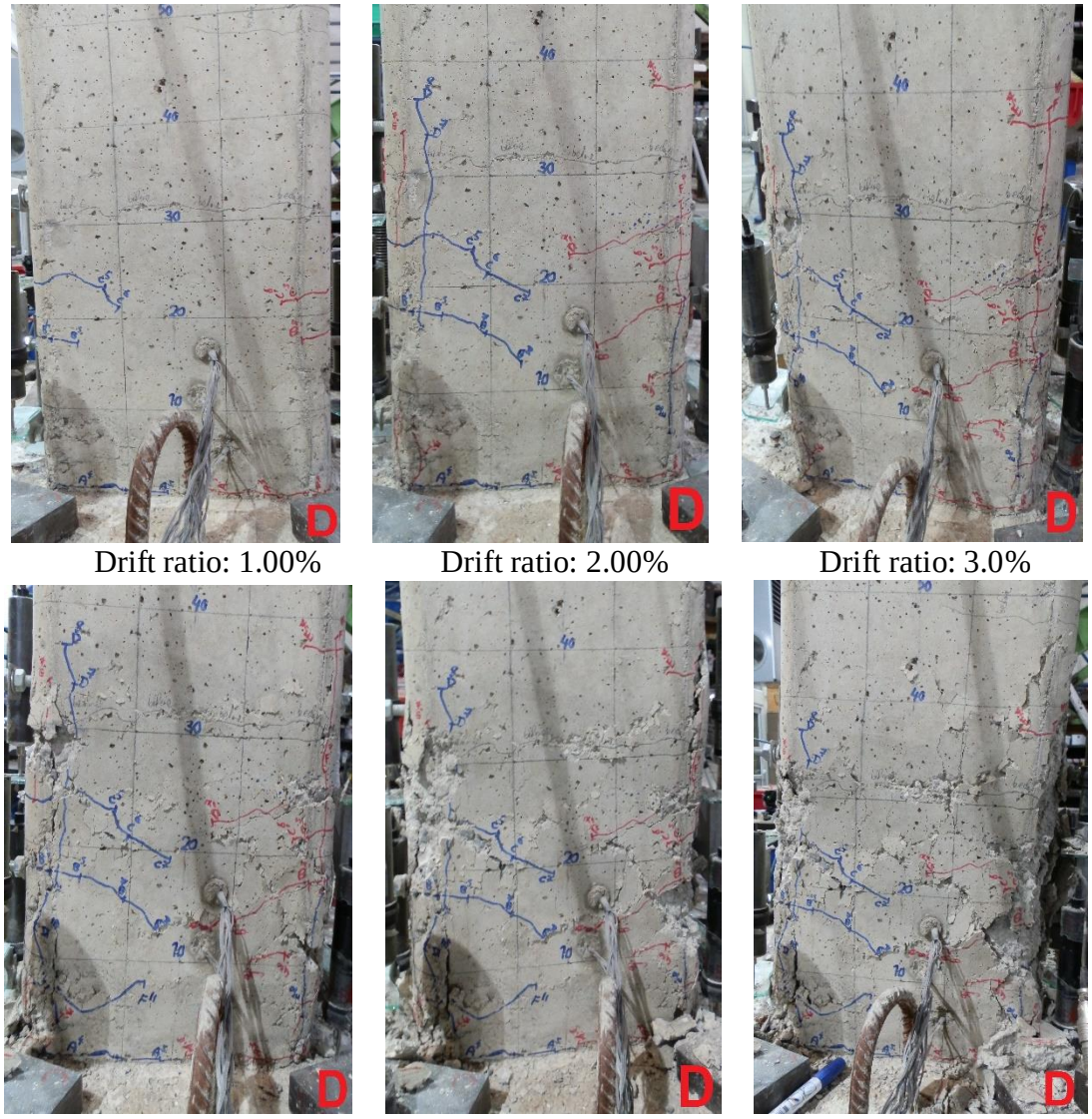

Figure 4.25 : Crack pattern of Ref-S60-Ɵ135-L80 at different drift ratios.

The lateral load-drift-displacement hysteresis curve of the Ref-S60-Ɵ135-L80 is shown in Figures 4.26. It is clear there is no difference between values of the lateral loads while pulling and pushing and almost damage shape was symmetric. The amount of plastic deformation at the point of lateral load application was around 40.48 mm after loading to target displacement of 64.25 mm (drift ratio of +5.0%) and the measurement of out-of-plane at the level of lateral load application was +1.60 mm when lateral load was zero at the end of the test. Test was ended by losing 18% of lateral load capacity during pushing. Envelope curves for Ref-S60-Ɵ135-L80 specimen is drawn in Figures 4.27.

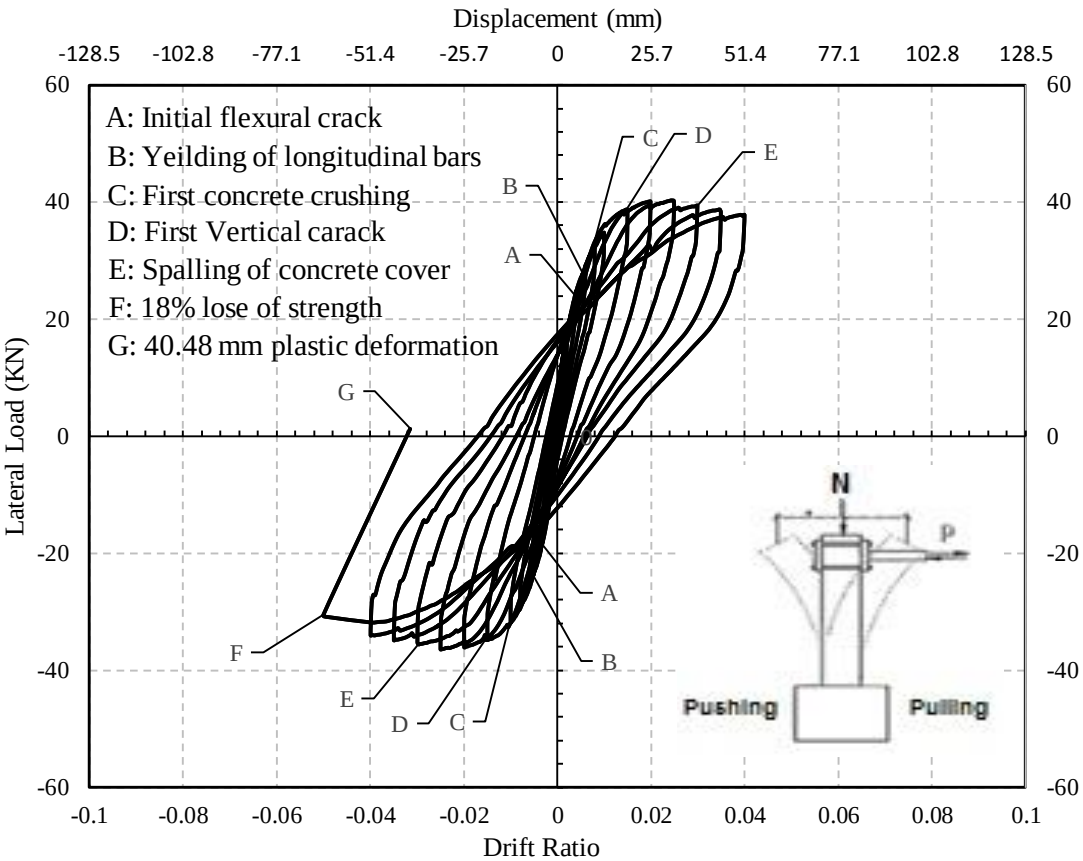

Figures 4.26 : Lateral Load-Drift-Tip Displacement curves for Ref-S60-Θ135-L80.

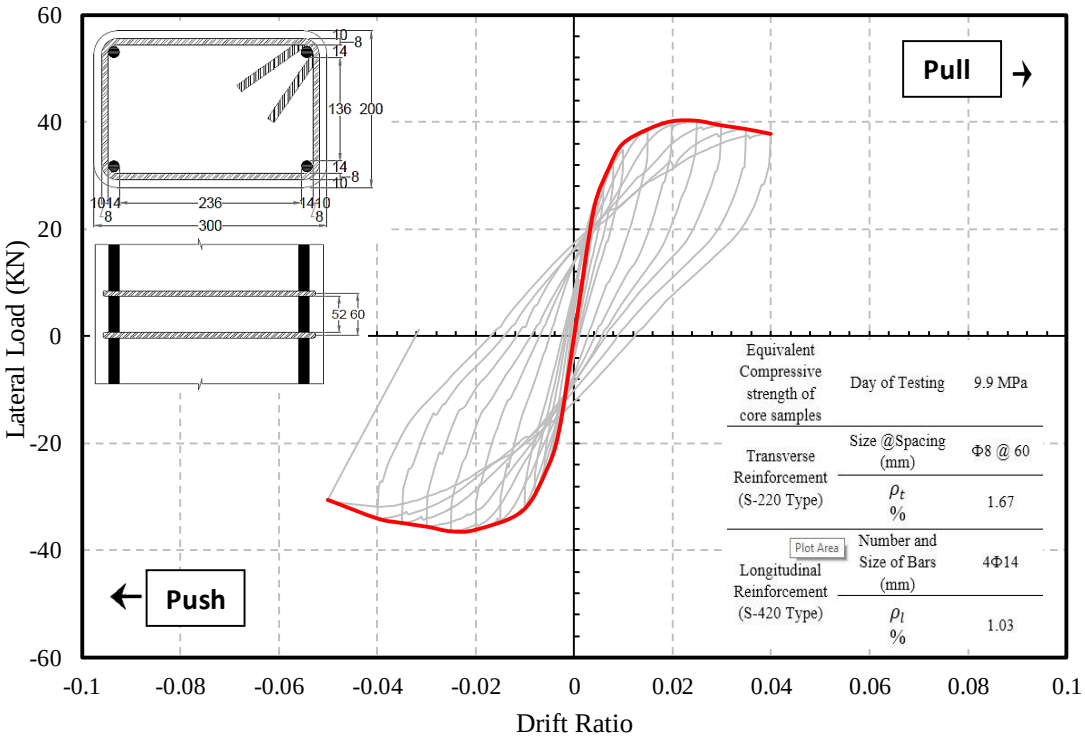

Figures 4.27 : Lateral Load-Drift envelope curve of Ref-S60-Θ135-L80.

4.2.4 Ref-S60-Ɵ135-L40

Before describing test observation, some information about specification of specimen can be found at Table 4.4 at the below.

Table 4.4: General specification of Ref-S60-Ɵ135-L40 specimen.

Specimen: Ref-S60-Ɵ135-L40				
Cross section Dimension h × b (mm)	300 x 200	Hook Length L (mm)		40
Height of Columns H_{column} (mm)	1290	Hook Angle Ɵ (°)		135°
Compressive strength of standard cylinder samples for columns (MPa)	7.5	$\frac{N_{axial}}{A_g f_c'}$		54.4 %
Equivalent Compressive strength of core samples for columns (MPa)	9.9	Transverse Reinforcement (S-220 Type)	Size @Spacing (mm)	Φ8 @ 60
			ρ_t %	1.67
Axial Load N_{axial} (kN)	323	Longitudinal Reinforcement (S-420 Type)	Number and Size of Bars (mm)	4Φ14
			ρ_l %	1.03

All experimental observations, which were made during the test of Ref-S60-Ɵ135-L40, are presented at the Appendix A. In this subsection, only the important events were pointed out. No cracks were observed while loading to target displacements of ±2.58 mm (drift ratio of 0.2%) as illustrated in Figure 4.28.

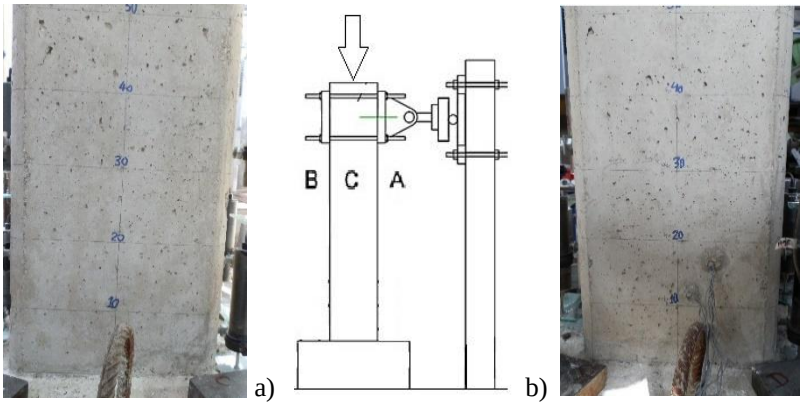

a) b) c)

Figure 4.28 : Specimen Ref-S60-Ɵ135-L40 after the drift ratio of 0.2%. a)Face C. b)Definition of column optional faces. c)Face D.

At the column-foundation interface and column surfaces, during loading to target displacement of ±5.16 mm (drift ratio of 0.40%) first flexural cracks were observed. During loading to target displacements of ±7.74 mm (drift ratio of 0.60%) new flexural cracks were observed as illustrated in Figure 4.29 but crack pattern was not totally symmetric until achieving mentioned drift ratio. While loading to target displacements of ±19.35 mm (drift ratio of 1.50%) some new cracks were observed and the previous flexural cracks became inclined and extended into the web zone of the column due to the influence of increased shear force as shown in Figure 4.30.

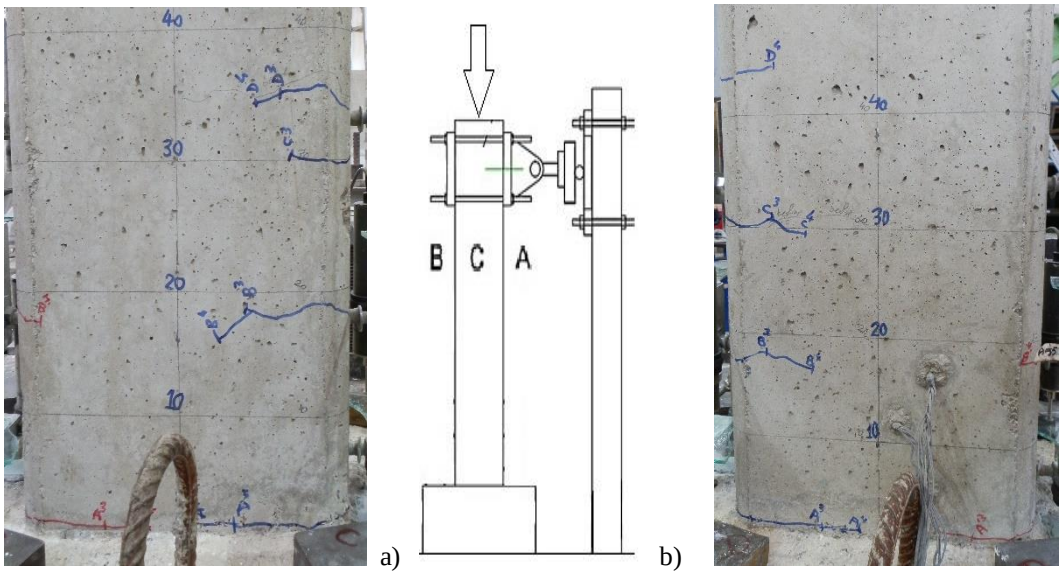

Figure 4.29 : Specimen Ref-S60-Ɵ135-L40 after the drift ratio of 0.6%. a)Face C. b)Definition of column optional faces. c)Face D.

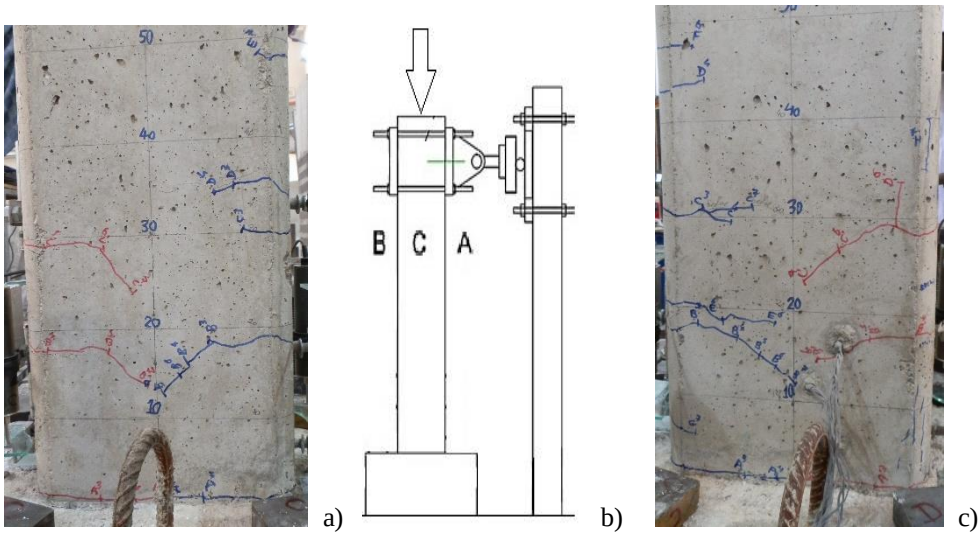

Figure 4.30 : Specimen Ref-S60-Ɵ135-L40 after the drift ratio of 1.50%. a)Face C. b)Definition of column optional faces. c)Face D.

During loading to target displacement of 19.35 mm (drift ratio of 1.50%), concrete crushing was formed at the A and B faces of the column. After mentioned target drift ratio some new flexural cracks were observed on column surfaces. During loading to target displacement of 32.25 mm (drift ratio 2.50%), concrete cover started to spall off at the column surfaces in compression zone as shown in Figure 4.31.

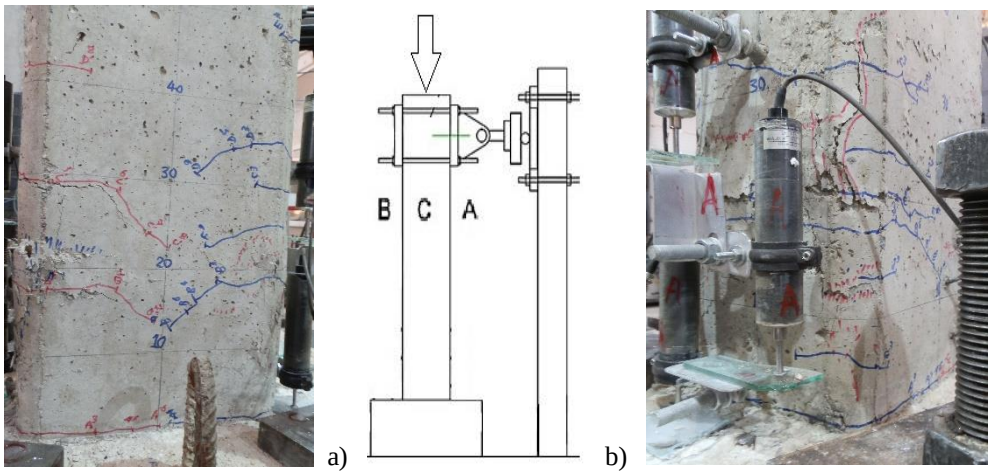

Figure 4.31 : Specimen Ref-S60-Θ135-L40 after the drift ratio of 2.50 %. a)Face C. b)Definition of column optional faces. c)Face A.

After loading to target displacement of 64.50 mm (drift ratio of 5%), test was ended due to buckling of longitudinal bars at the B-Face (250mm above the stub code) by losing 45% of lateral load capacity. Figure 4.32 illustrated the damaged Ref-S60-Θ135-L40 specimen at the end of the test.

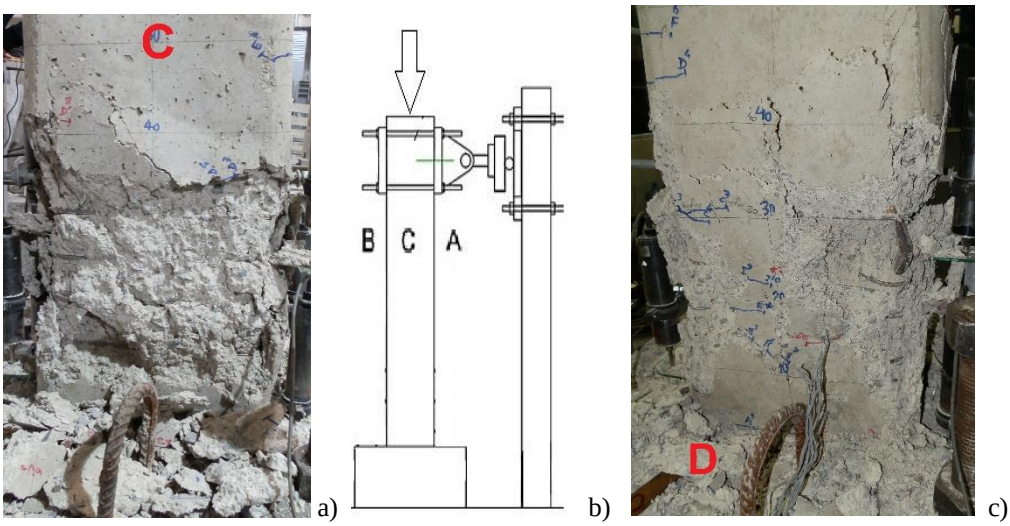

Figure 4.32 : Specimen Ref-S60-Θ135-L40 after the drift ratio of 5.0 %. a)Face C. b)Definition of column optional faces. c)Face D.

The extent of damage at progressive stages of testing can be seen in the Figure 4.33. All pictures were taken after the first cycle of each load stage.

Drift ratio: 1.00% Drift ratio: 2.00% Drift ratio: 3.00%

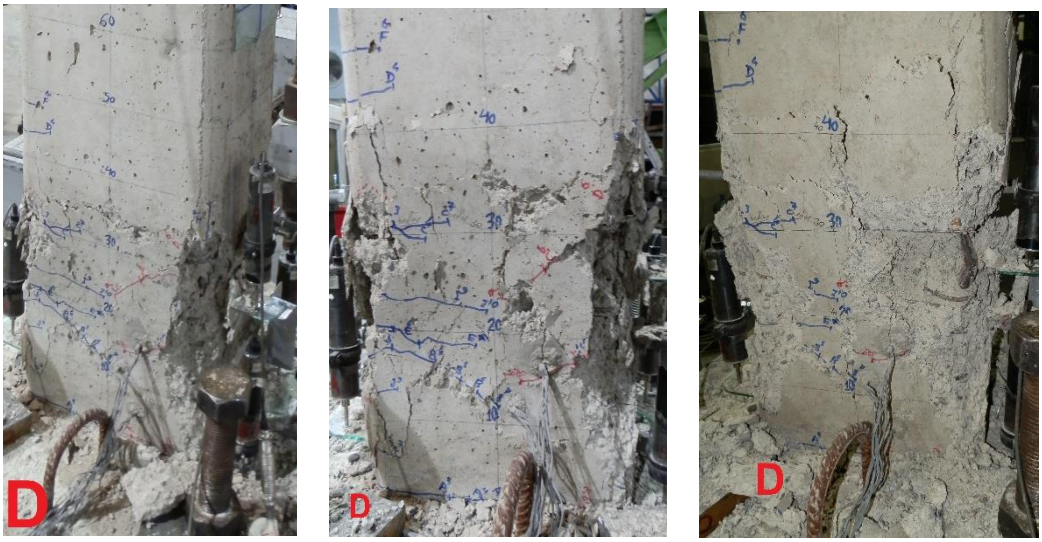

Drift ratio: 3.50% Drift ratio: 4.00% Drift ratio: 5.00%

Figure 4.33 : Crack pattern of Ref-S60-Ɵ135-L40 at different drift ratios.

The plastic hinge length of specimen at the end of test was measured between 200 to 300 mm as was shown in the Figure 4.34. The lateral load-drift-displacement hysteresis curve of the Ref-S60-Ɵ135-L40 is shown in Figures 4.35. It is clear there is no significant difference between values of the lateral loads while pulling and pushing and almost damage shape was symmetric at the end of test. The amount of plastic deformation at the point of lateral load application was around 50.84 mm after loading to target displacement of 64.5 mm (drift ratio of +5.0%) and the measurement of out-of-plane at the level of lateral load application was +2.4 mm when lateral load was

zero at the end of the test. Test was ended by losing 45% of lateral load capacity during pushing load at last cycle.. It should be note that, due to some problems which were occurred in MTS actuator and setup equipment, test were stopped for three times during to loading to target drift ratios -0.1%, -0.4% ,-0.6 % and teat was re-started again every time. Envelope curves for Ref-S60-Θ135-L40 specimen is shown in Figures 4.36.

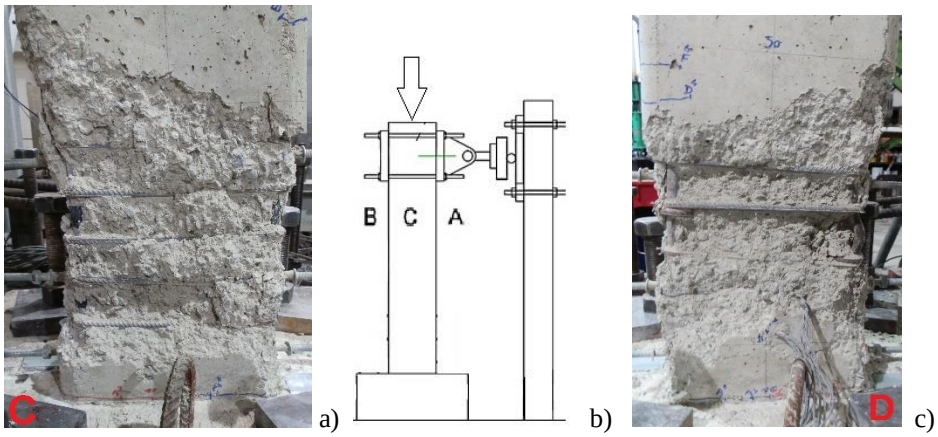

Figure 4.34 : Specimen Ref-S60-Θ135-L40 after the drift ratio of 5.0 %. a)Face C. b)Definition of column optional faces. c)Face D.

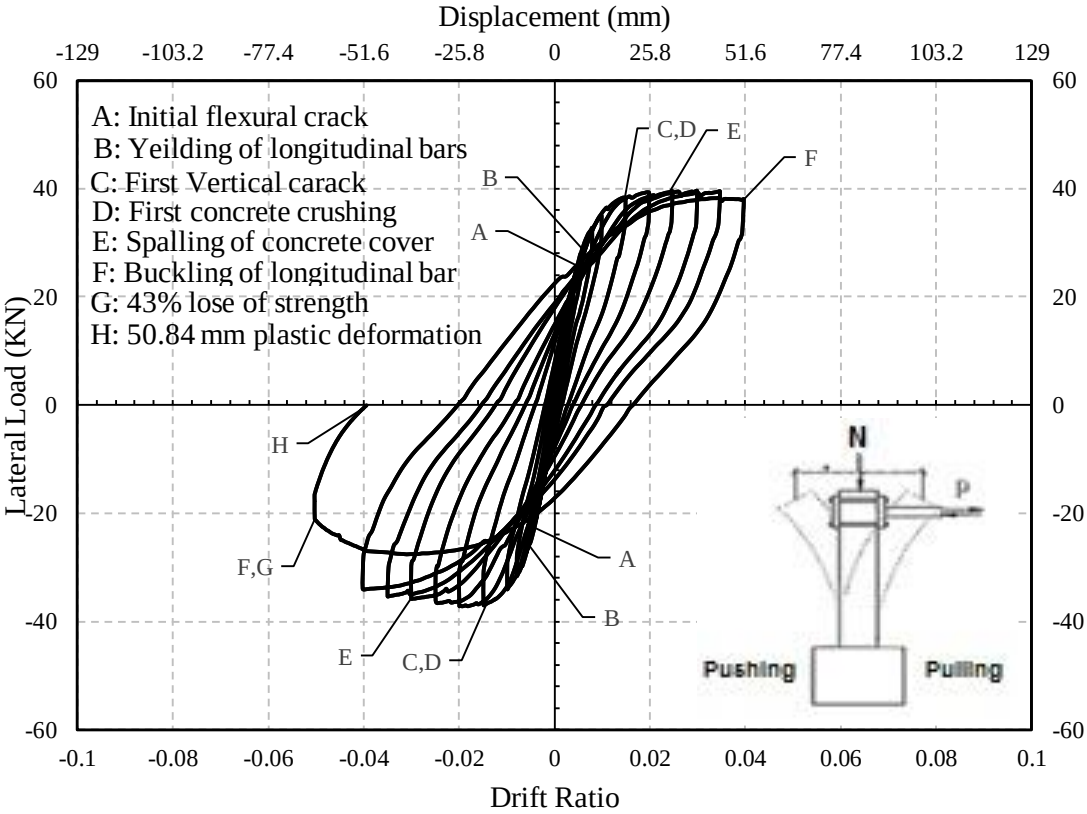

Figures 4.35 : Lateral Load-Drift-Tip Displacement curves of Ref-S60-Θ135-L40.

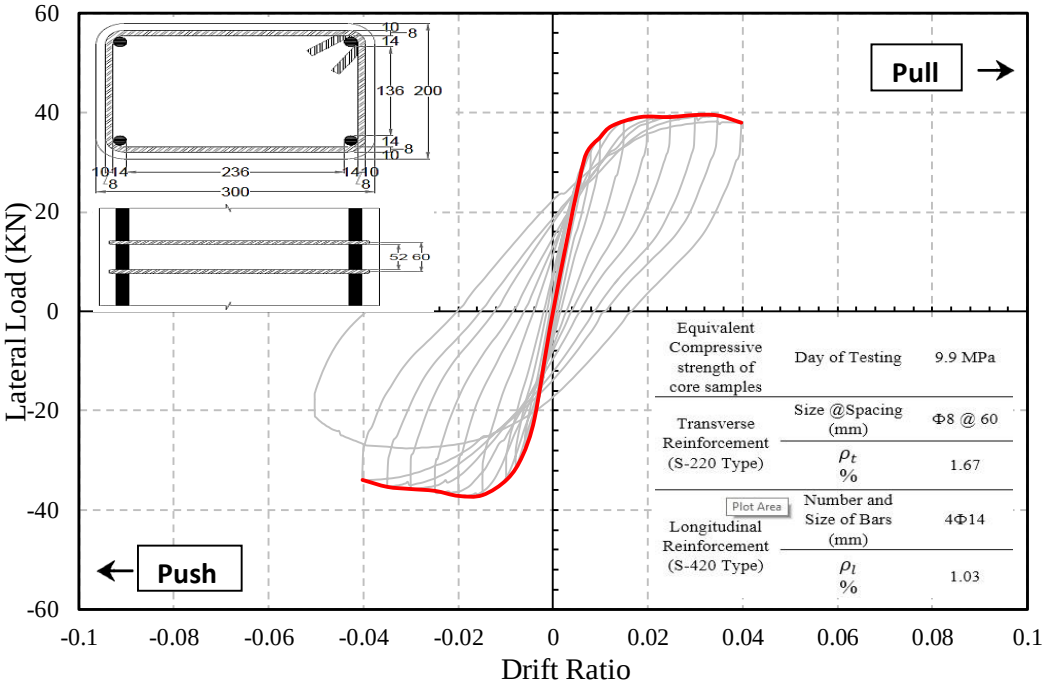

Figures 4.36 : Lateral Load-Drift envelope curve of Ref-S60-Ɵ135-L40.

4.3 Test Observation of Retrofitted Columns

4.3.1 Specimen: Ret-S60-Ɵ90-L80-3TRM

Before describing test observation, some information about specification of specimen can be found at Table 4.5. Retrofitting system in this research program was manufactured either from Basalt mesh, spraying with Glass Reinforced Concrete (GRC). The Basalt grids had a square configuration with 250 mm out-to-out dimension. Before wrapping of all the specimens, a gap of about 15~20 mm was left at the bottom ends of the columns to avoid direct axial compressive loading of the confinement jacket. Application of the mortar layers were made with spraying glass reinforced concrete in three step due to applying three layers of basalt fiber mesh. Thickness of the mortar were approximately 28~32 mm in middle of both surface of columns and 18~22 mm at the corners. The jackets extended from the base of each column (a gap of about 15~20 mm was left) to a height of 510 mm. After application of the first mortar layer on the concrete surface, the textile was applied and pressed slightly into the mortar, which comes out through all the opening between fiber rovings. The next mortar layer covered the textile completely and the operation was repeated until all textile layers were applied and covered by FIBROBETON mortar

Table 4.5 : General specification of Ret-S60-Ɵ90-L80-3TRM specimen.

Specimen: Ret-S60-Ɵ90-L80-3TRM				
Cross section Dimension h × b	300 x 200 mm	Hook Length L (mm)		80
Height of Columns H_{column}	1293 mm	Hook Angle Ɵ (°)		90°
Compressive strength of standard cylinder samples for columns	7.5 (MPa)	$\frac{N_{axial}}{A_g f_c'}$		71.8 %
Equivalent Compressive strength of core samples for columns	7.5 (MPa)	Transverse Reinforcement (S-220 Type)	Size @Spacing (mm)	Φ8 @ 60
			ρ_t (%)	1.67
Axial Load N_{axial} (kN)	323	Longitudinal Reinforcement (S-420 Type)	Number and Size of Bars (mm)	4Φ14
			ρ_l (%)	1.03

All experimental observations, which were made during the test of Ret-S60-Ɵ90-L80-3TRM, are presented at the Appendix A. In this subsection, only the important events were pointed out. No cracks were observed while loading to target displacements of ±2.59 mm (drift ratio of 0.2%) as illustrated in Figure 4.37.

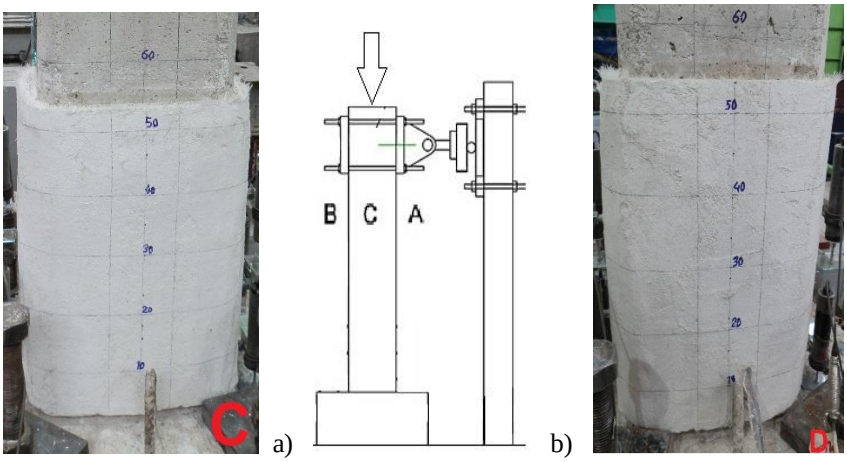

Figure 4.37 : Specimen Ret-S60-Ɵ90-L80-3TRM after the drift ratio of 0.2%. a)Face C. b)Definition of column optional faces. c)Face D.

At the column-foundation interface, during loading to target displacement of ±5.17 mm (drift ratio of 0.40%) first flexural crack was observed. During loading to target displacements of ±7.76 mm (drift ratio of 0.60%) new flexural cracks were observed on the column surface (unretrofitted faces) as illustrated in Figure 4.38.

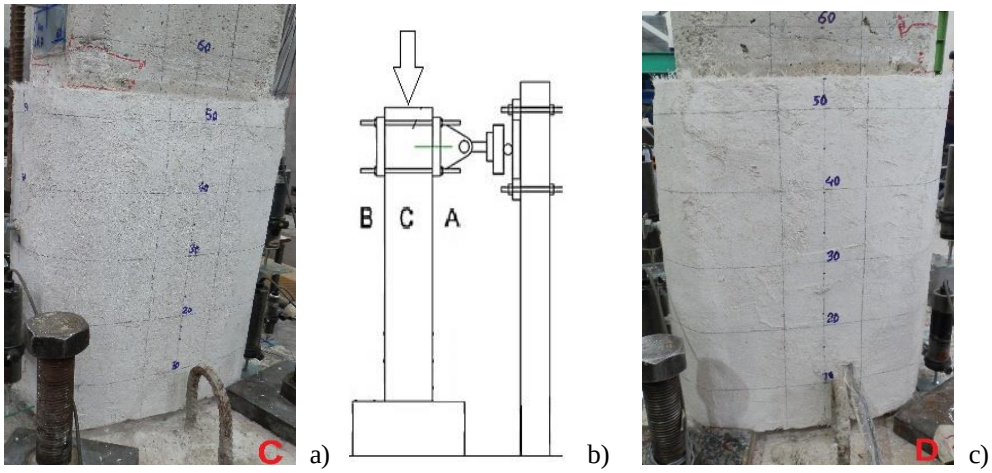

Figure 4.38 : Specimen Ret-S60-Ɵ90-L80-3TRM after the drift ratio of 0.6%. a)Face C. b)Definition of column optional faces. c)Face D.

During loading to target displacement of 12.9 mm (drift ratio 1.0%), concrete crushing was formed at the A-face of the column. While loading to target displacements of ±19.4 mm (drift ratio of 1.5%) some new flexural cracks were observed on the unretrofitted zone and the previous flexural cracks became inclined and extended into the web zone of the unretrofitted zone due to the influence of increased shear force as shown in Figure 4.39. Initial vertical crack on the jacket were observed at mentioned drift ratio.

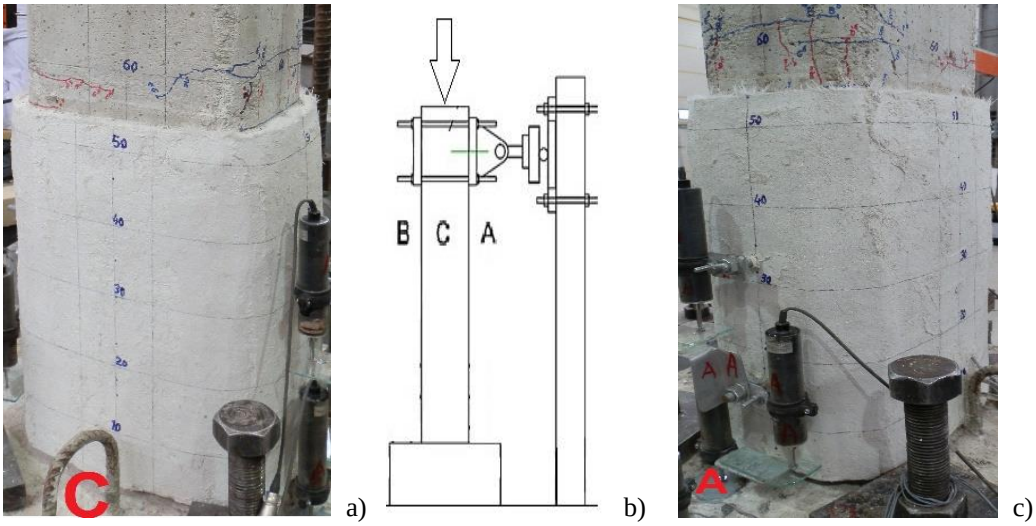

Figure 4.39 : Specimen Ret-S60-Ɵ90-L80-3TRM after the drift ratio of 1.5%. a)Face C. b)Definition of column optional faces. c)Face A.

During loading to target displacement of 51.72 mm (drift ratio 4.00%), concrete cover started to spall off at the column surfaces in compression zone as shown in Figure 4.40.

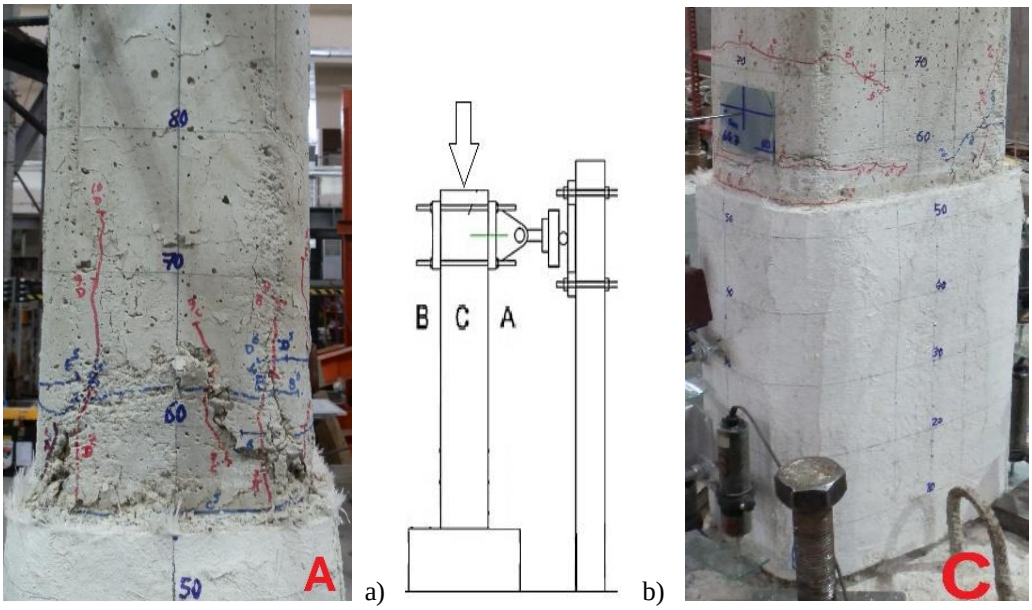

Figure 4.40 : Specimen Ret-S60-Ɵ90-L80-3TRM after the drift ratio of 4.0%. a)Face A. b)Definition of column optional faces. c)Face D.

After loading to target displacement of 103.44 (drift ratio of 8%), test was ended due to 33 % loss of lateral load capacity. Figure 4.41 illustrated the damaged Ret-S60-Ɵ90-L80-3TRM specimen at the end of the test. The damaged jacket of specimen at the end of test was shown in the Figure 4.42.

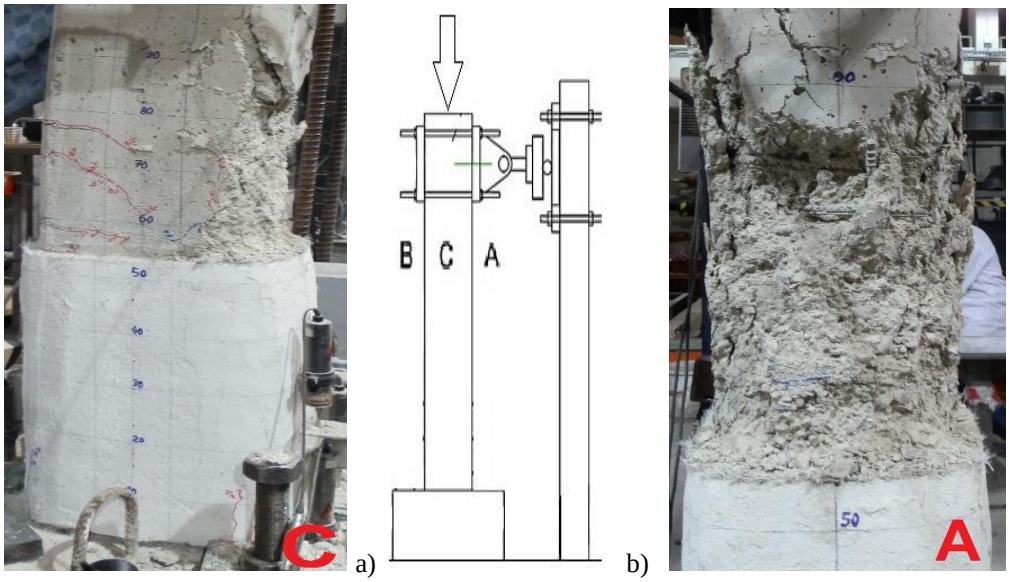

Figure 4.41 : Specimen Ret-S60-Ɵ90-L80-3TRM after the drift ratio of 8.0 %. a)Face C. b)Definition of column optional faces. c)Face A.

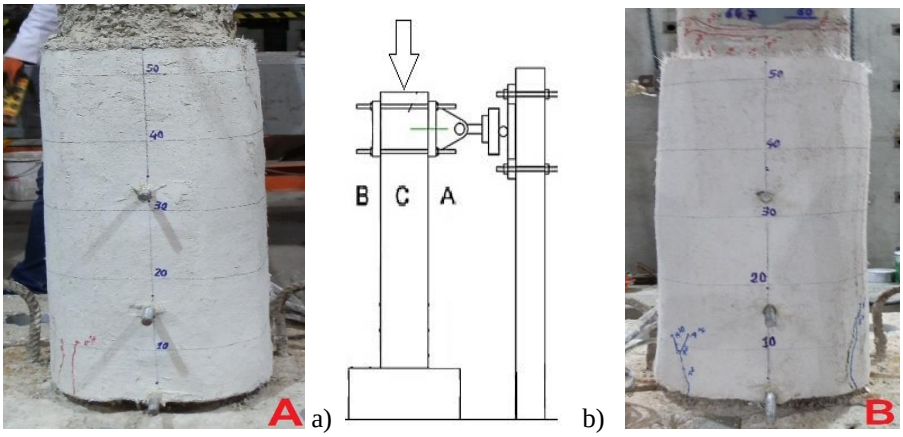

Figure 4.42 : The damaged jacket of Specimen Ret-S60-Ɵ90-L80-3TRM at the end of test. a)Face A. b)Definition of column optional faces. c)Face B.

The extent of damage at progressive stages of testing can be seen in the Figure 4.43. All pictures were taken after the first cycle of each load stage.

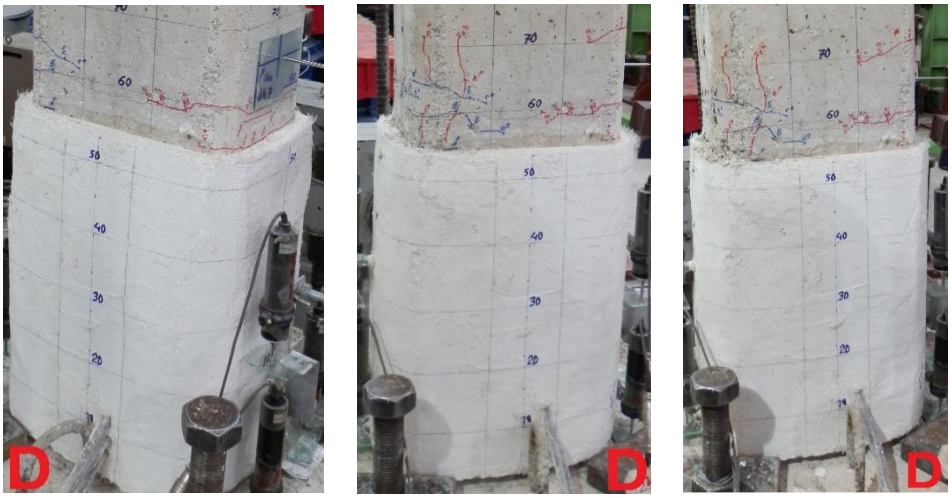

Drift ratio: 1.00% Drift ratio: 3.00% Drift ratio: 5.0%

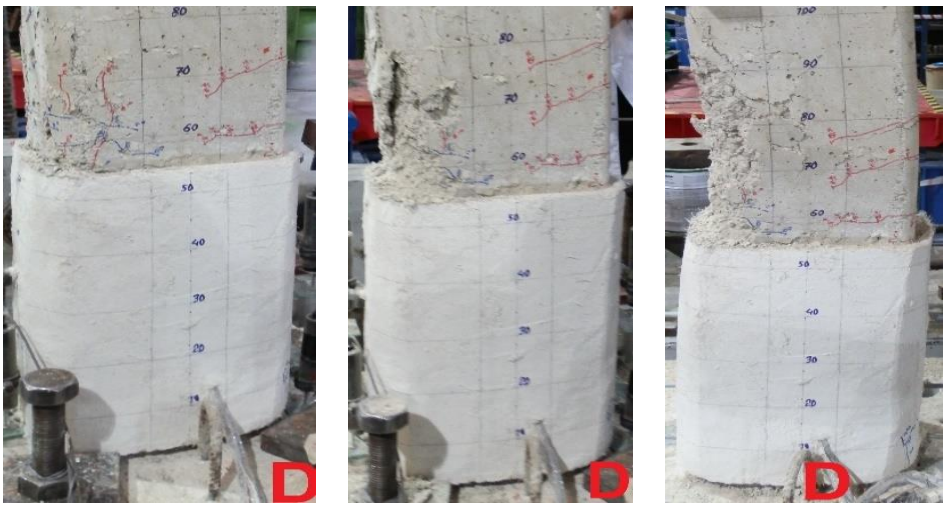

Drift ratio: 6.0% Drift ratio: 7.0% Drift ratio: 8.0%

Figure 4.43 : Crack pattern of Ret-S60-Ɵ135-L80 at different drift ratios.

The lateral load-drift-displacement hysteresis curve of the Ret-S60-Ɵ90-L80-3TRM is shown in Figures 4.44. It is clear there is no difference between values of the lateral loads while pulling and pushing, but almost damage shape was asymmetric.

The amount of plastic deformation at the point of lateral load application was around 45.66 mm after loading to target displacement of 103.44 mm (drift ratio of 8.0%) and the measurement of out-of-plane at the level of lateral load application was 4.96 mm when lateral load was zero at the end of the test.

Test was ended by losing 33% of lateral load capacity during pulling. Envelope curves for Ret-S60-Ɵ90-L80-3TRM specimen was drawn in Figures 4.45.

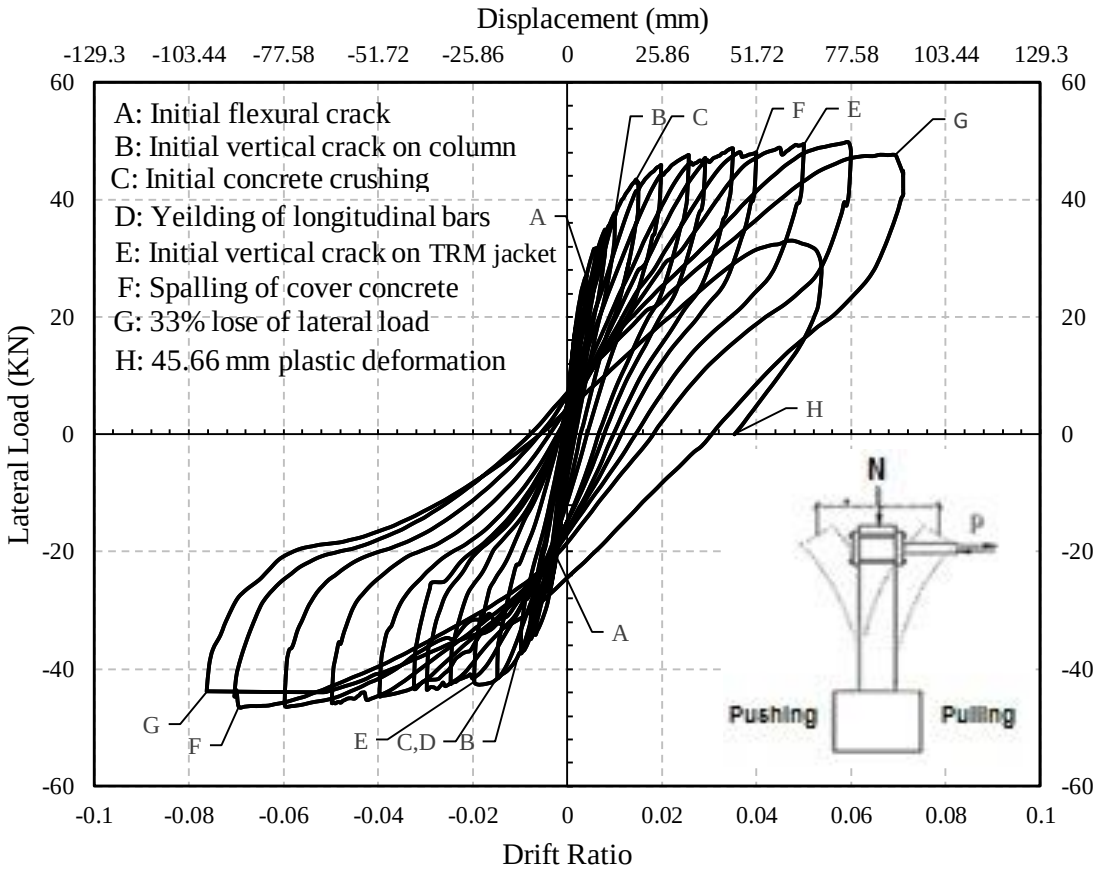

Figures 4.44 : Lateral Load-Drift-Tip Displacement curves for Ret-S60-Ɵ90-L80-3TRM.

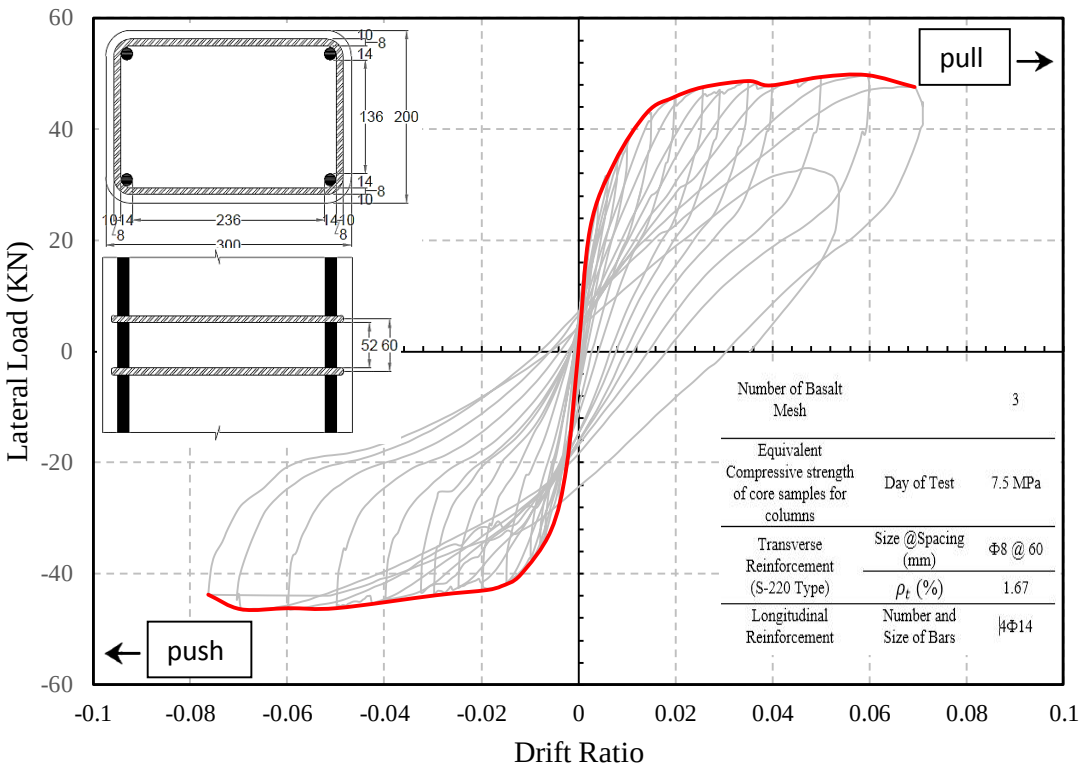

Figures 4.45 : Lateral Load-Drift envelope curve of Ret-S60-Ɵ90-L80-3TRM.

4.3.2 Specimen: Ret-S60-Ɵ112.5-L80-3TRM

Before describing test observation, some information about specification of specimen can be found at Table 4.6. Retrofitting system in this research program was manufactured either from Basalt mesh, spraying with Glass Reinforced Concrete (GRC). The Basalt grids had a square configuration with 250 mm out-to-out dimension. Before wrapping of all the specimens, a gap of about 15~20 mm was left at the bottom ends of the columns to avoid direct axial compressive loading of the confinement jacket. Application of the mortar layers were made with spraying glass reinforced concrete in three step due to applying three layers of basalt fiber mesh. Thickness of the mortar were approximately 28~32 mm in middle of both surface of columns and 18~22 mm at the corners. The jackets extended from the base of each column (a gap of about 15~20 mm was left) to a height of 510 mm. After application of the first mortar layer on the concrete surface, the textile was applied and pressed slightly into the mortar, which comes out through all the opening between fiber rovings. The next mortar layer covered the textile completely and the operation was repeated until all textile layers were applied and covered by FIBROBETON mortar

Table 4.6 : General specification of Ret-S60-Θ112.5-L80-3TRM specimen.

Specimen: Ret-S60-Θ112.5-L80-3TRM				
Cross section Dimension h × b	300 x 200 mm	Hook Length L (mm)		80
Height of Columns H_{column}	1283 mm	Hook Angle Θ (°)		112.5°
Compressive strength of standard cylinder samples for columns	7.5 (MPa)	$\frac{N_{axial}}{A_g f_c'}$		71.8 %
Equivalent Compressive strength of core samples for columns	7.5 (MPa)	Transverse Reinforcement (S-220 Type)	Size @Spacing (mm)	Φ8 @ 60
			ρ_t (%)	1.67
Axial Load N_{axial} (kN)	323	Longitudinal Reinforcement (S-420 Type)	Number and Size of Bars (mm)	4Φ14
			ρ_l (%)	1.03

All experimental observations, which were made during the test of Ret-S60-Θ112.5-L80-3TRM, are presented at the Appendix A. In this subsection, only the important events were pointed out. No cracks were observed while loading to target displacements of ±1.28 mm (drift ratio of 0.1%) as illustrated in Figure 4.46.

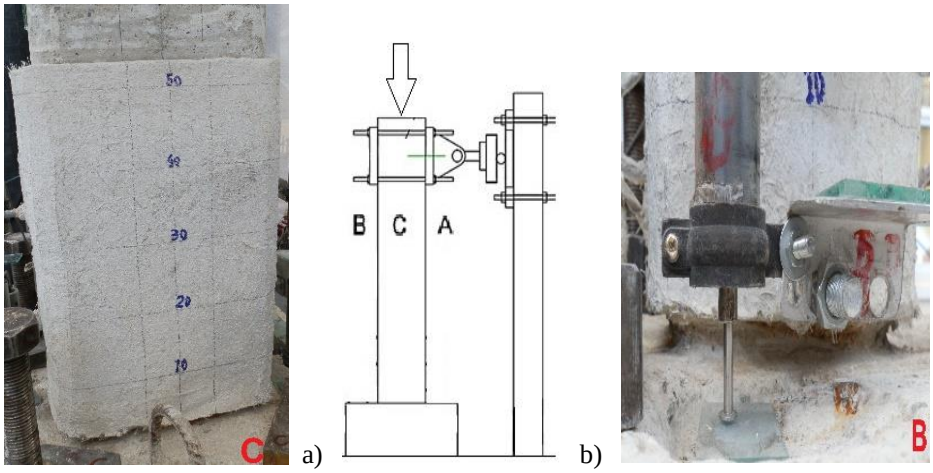

Figure 4.46 : Specimen Ref-S60-Θ112.5-L80-3TRM after the drift ratio of 0.1%. a)Face C. b)Definition of column optional faces. c)Face B.

At the column-foundation interface, during loading to target displacement of ±2.57 mm (drift ratio of 0.20%) first flexural crack was observed. During loading to target displacements of ±7.70 mm (drift ratio of 0.60%) new flexural cracks were observed on the column surface (unretrofitted faces) as illustrated in Figure 4.47.

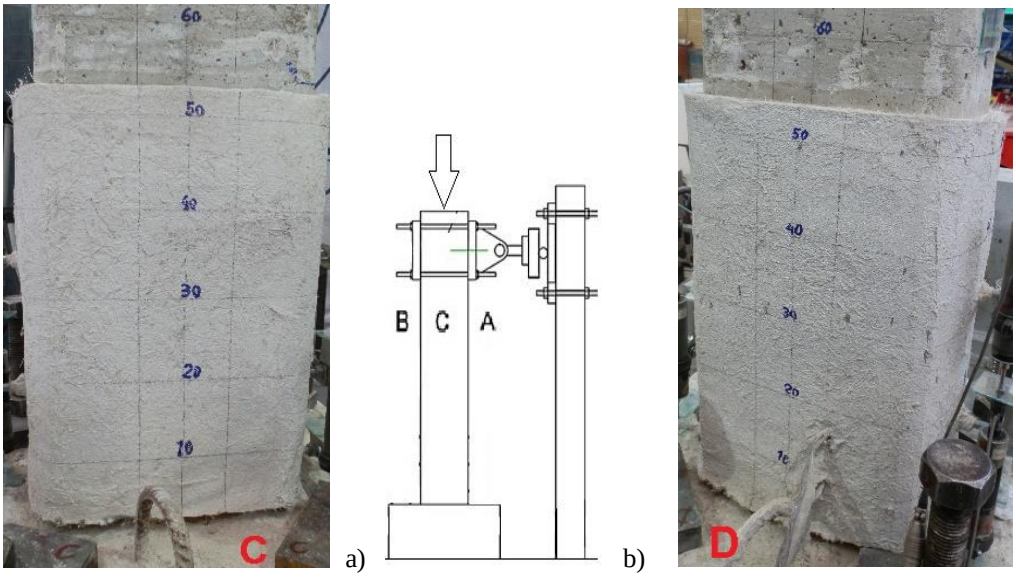

Figure 4.47 : Specimen Ret-S60-Ɵ112.5-L80-3TRM after the drift ratio of 0.6%. a)Face C. b)Definition of column optional faces. c)Face D.

During loading to target displacement of 12.83 mm (drift ratio 1.0%), initial vertical crack was formed on the jacket of the column. While loading to target displacements of ±19.25 mm (drift ratio of 1.5%) some new flexural cracks were observed on the unretrofitted zone and the previous flexural cracks became inclined and extended into the web zone of the unretrofitted zone due to the influence of increased shear force as shown in Figure 4.48. Initial concrete crushing was formed at the B-face of the column. at mentioned drift ratio.

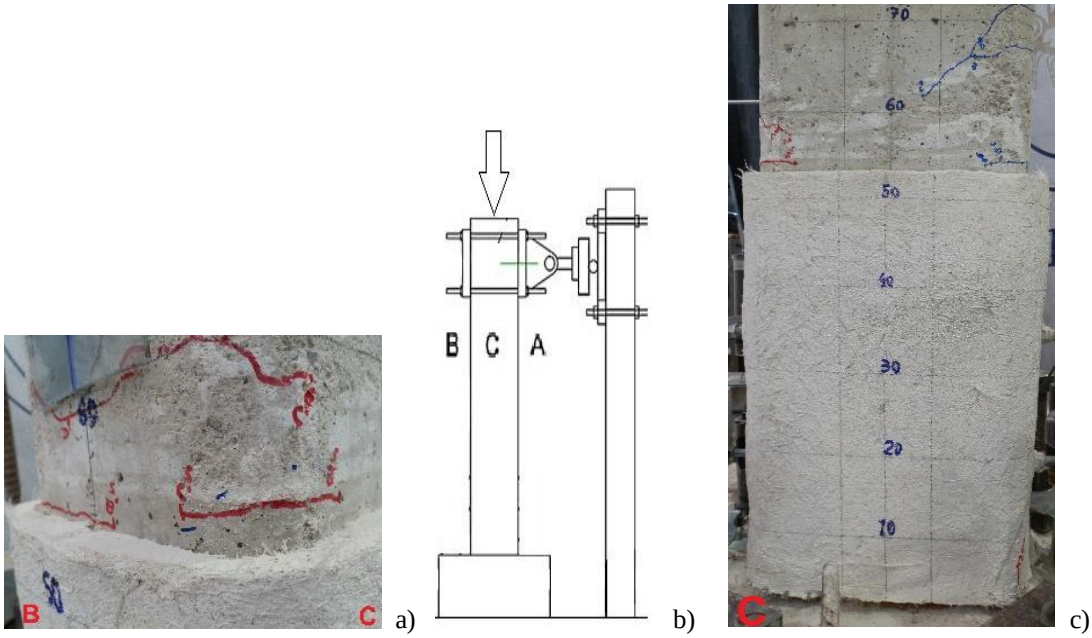

Figure 4.48 : Specimen Ref-S60-Ɵ112.5-L80-3TRM after the drift ratio of 1.5%. a)Face B. b)Definition of column optional faces. c)Face C.

During loading to various target displacements, concrete cover did not start to spall off at the column surfaces in compression zones.

After loading to target displacement of 102.26 (drift ratio of 8%), Test was ended due to use maximum capacity of top LVDT. There was a 9 % lose of lateral load capacity after loading to target drift ratio of 8% . Figure 4.49 illustrated the damaged Ret-S60-Ɵ112.5-L80-3TRM specimen at the end of the test. The damaged jacket of specimen at the end of test was shown in the Figure 4.50.

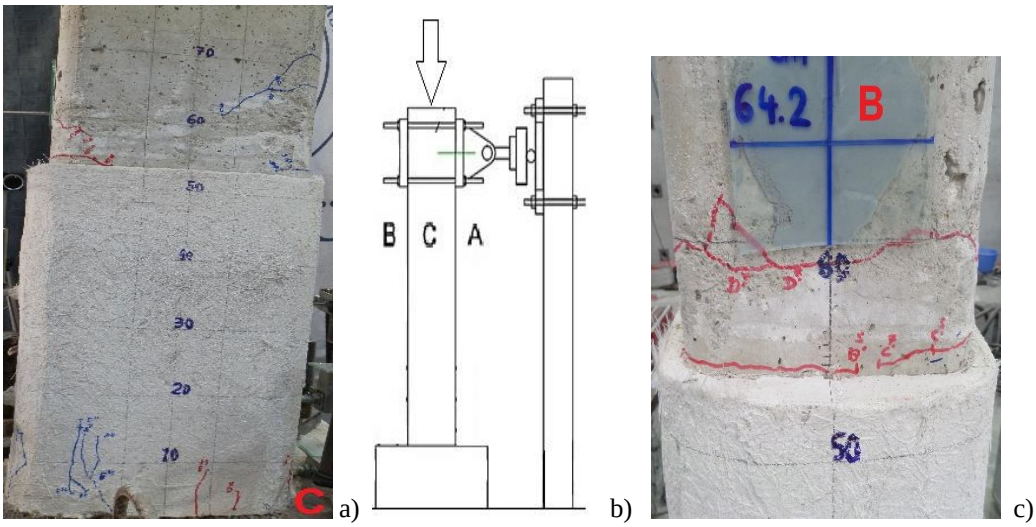

Figure 4.49 : Specimen Ret-S60-Ɵ112.5-L80-3TRM after the drift ratio of 8.0 %. a)Face C. b)Definition of column optional faces. c)Face B.

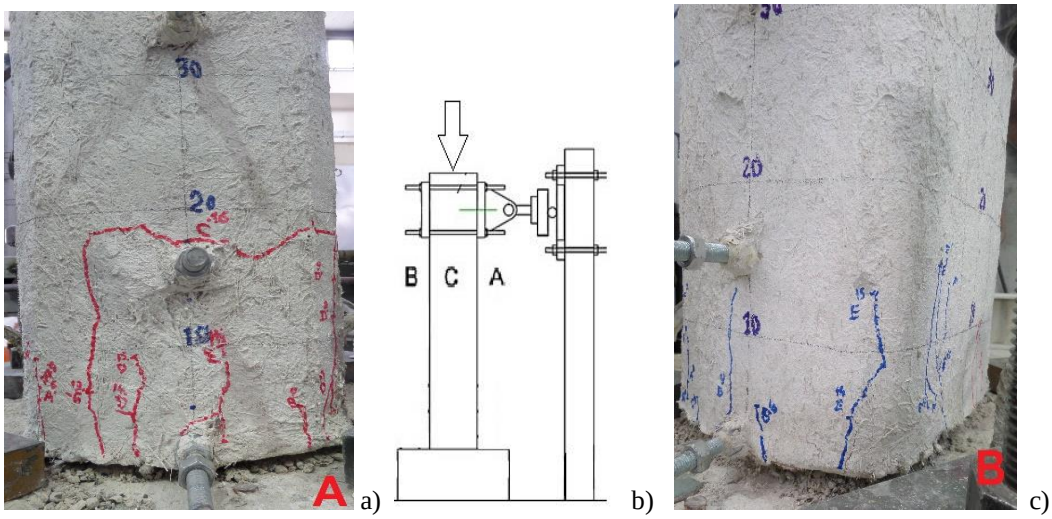

Figure 4.50 : The damaged jacket of Specimen Ret-S60-112.5-L80-3TRM at the end of test. a)Face A. b)Definition of column optional faces. c)Face B.

The extent of damage at progressive stages of testing can be seen in the Figure 4.51. All pictures were taken after the first cycle of each load stage.

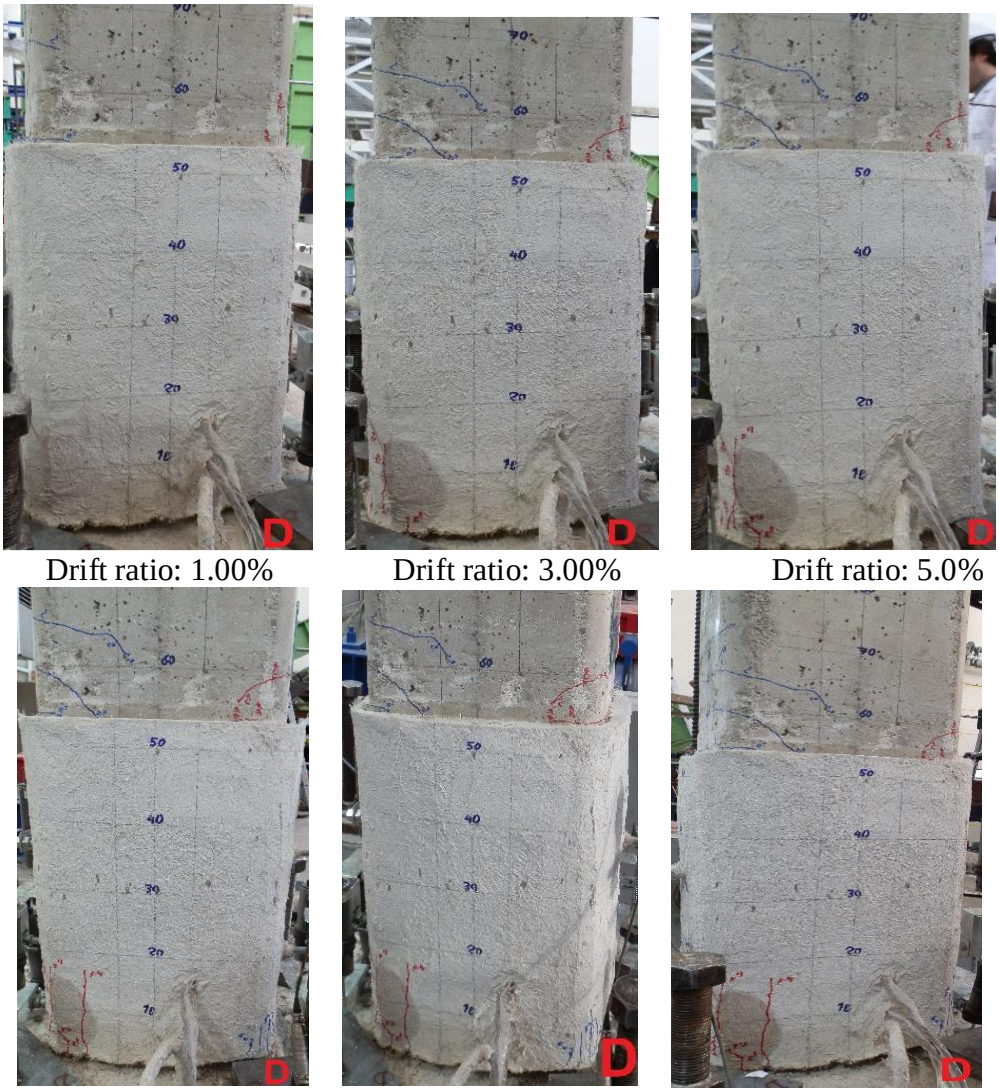

Figure 4.51: Crack pattern of Ret-S60-Ɵ112.5-L80 at different drift ratios.

The lateral load-drift-displacement hysteresis curve of the Ret-S60-Ɵ112.5-L80-3TRM is shown in Figures 4.52. It is clear there is a little difference between values of the lateral loads while pulling and pushing, but almost damage shape was symmetric. The amount of plastic deformation at the point of lateral load application was around 15.65 mm after loading to target displacement of 102.64 mm (drift ratio of 8.0%) and the measurement of out-of-plane at the level of lateral load application was 8.31 mm when lateral load was zero at the end of the test. Test was ended after 9 % losing of lateral load capacity during last applied drift ratio. Envelope curves for Ret-S60-Ɵ112.5-L80-3TRM specimen was drawn in Figures 4.53.

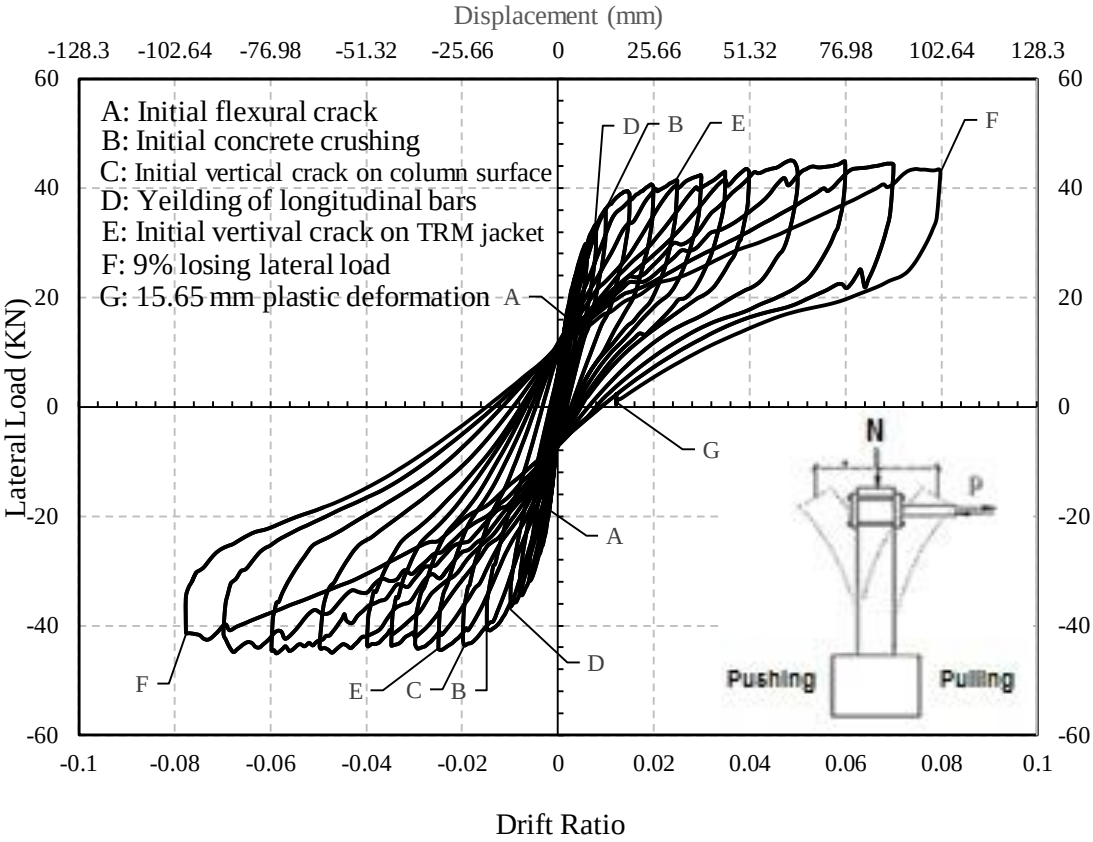

Figures 4.52 : Lateral Load-Drift-Tip Displacement curves for Ret-S60-Ɵ112.5-L80-3TRM.

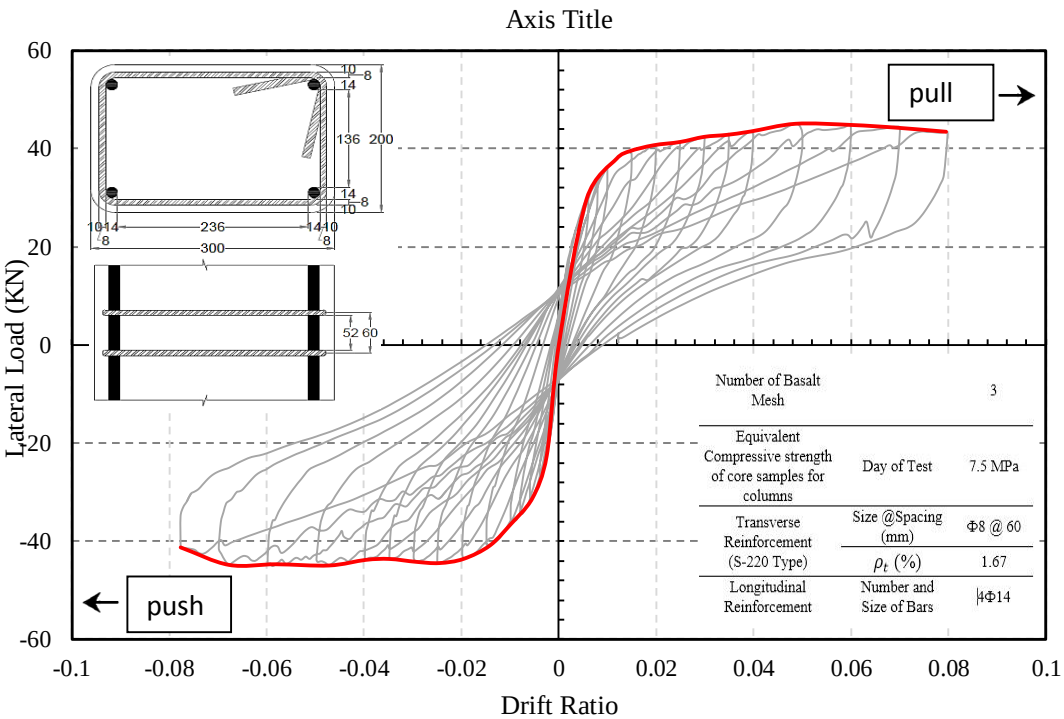

Figures 4.53 : Lateral Load-Drift envelope curve of Ret-S60-Ɵ112.5-L80-3TRM.

4.3.3 Specimen: Ret-S60-Θ135-L80-3TRM

Before describing test observation, some information about specification of specimen can be found at Table 4.7. Retrofitting system in this research program was manufactured either from Basalt mesh, spraying with Glass Reinforced Concrete (GRC). The Basalt grids had a square configuration with 250 mm out-to-out dimension. Before wrapping of all the specimens, a gap of about 15~20 mm was left at the bottom ends of the columns to avoid direct axial compressive loading of the confinement jacket. Application of the mortar layers were made with spraying glass reinforced concrete in three step due to applying three layers of basalt fiber mesh. Thickness of the mortar were approximately 28~32 mm in middle of both surface of columns and 18~22 mm at the corners. The jackets extended from the base of each column (a gap of about 15~20 mm was left) to a height of 510 mm. After application of the first mortar layer on the concrete surface, the textile was applied and pressed slightly into the mortar, which comes out through all the opening between fiber rovings. The next mortar layer covered the textile completely and the operation was repeated until all textile layers were applied and covered by FIBROBETON mortar.

Table 4.7: General specification of Ret-S60-Θ135-L80-3TRM specimen.

Specimen: Ret-S60-Θ135-L80-3TRM				
Cross section Dimension h × b	300 x 200 mm	Hook Length L (mm)		80
Height of Columns H_{column}	1286 mm	Hook Angle Θ (°)		135°
Compressive strength of standard cylinder samples for columns	7.5 (MPa)	$\frac{N_{axial}}{A_g f_c'}$		71.8 %
Equivalent Compressive strength of core samples for columns	7.5 (MPa)	Transverse Reinforcement (S-220 Type)	Size @Spacing (mm)	Φ8 @ 60
			ρ_t (%)	1.67
Axial Load N_{axial} (kN)	323	Longitudinal Reinforcement (S-420 Type)	Number and Size of Bars (mm)	4Φ14
			ρ_l (%)	1.03

All experimental observations, which were made during the test of Ref-S60-Ɵ135-L80-3TRM, are presented at the Appendix A. In this subsection, only the important events were pointed out. No cracks were observed while loading to target displacements of ±1.29 mm (drift ratio of 0.1%) as illustrated in Figure 4.54.

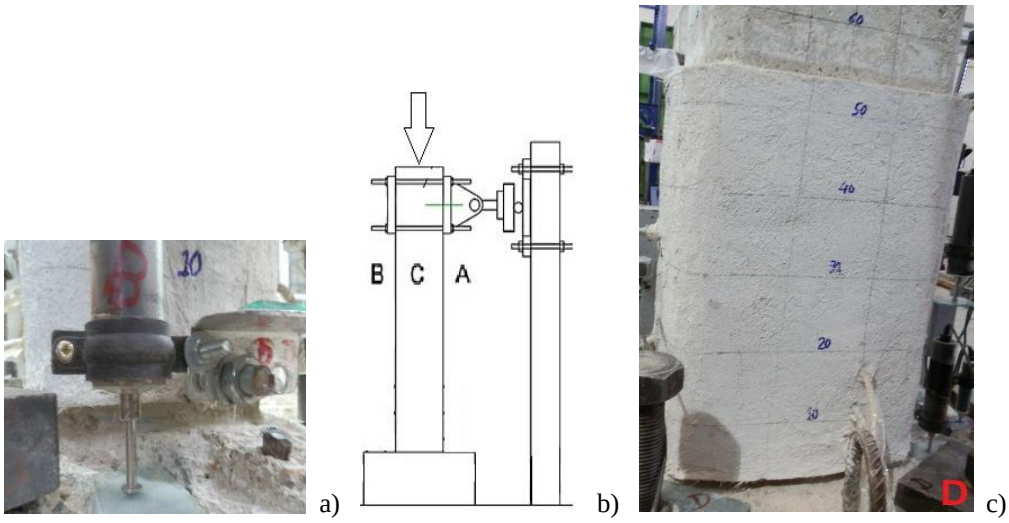

Figure 4.54 : Specimen Ref-S60-Ɵ135-L80-3TRM after the drift ratio of 0.1%. a)Face B, b)Definition of column optional faces. c)Face D.

At the column-foundation interface, during loading to target displacement of ±2.57 mm (drift ratio of 0.20%) first flexural crack was observed. During loading to target displacements of ±5.14 mm (drift ratio of 0.40%) new flexural cracks were observed on the column surface (unretrofitted faces) as illustrated in Figure 4.55.

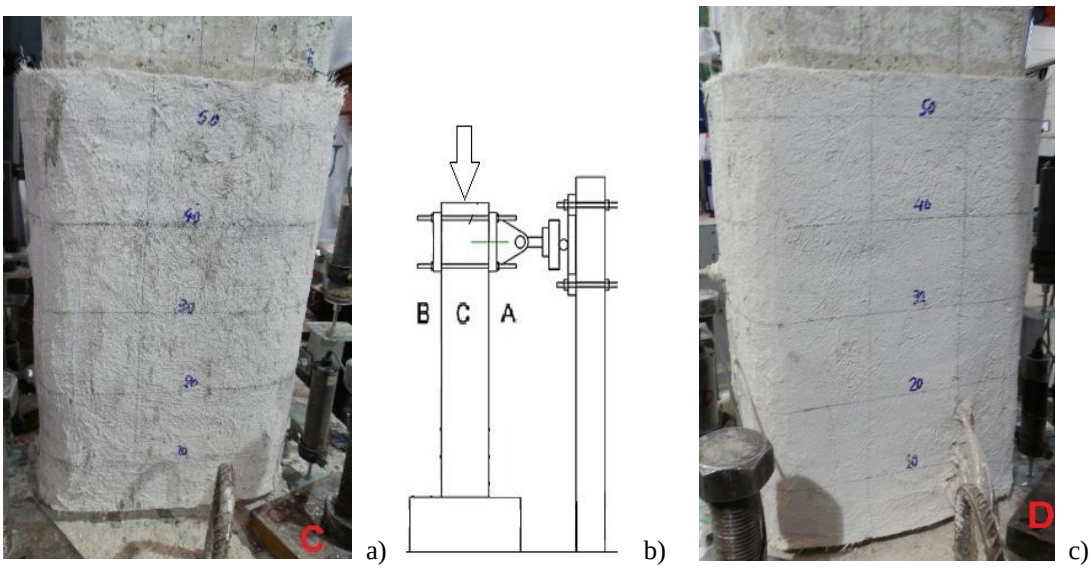

Figure 4.55 : Specimen Ret-S60-Ɵ135-L80-3TRM after the drift ratio of 0.4%. a)Face C. b)Definition of column optional faces. c)Face D.

During loading to target displacement of 10.29 mm (drift ratio 0.8%), concrete crushing was formed at the A-face of the column. While loading to target displacements of ±19.29 mm (drift ratio of 1.5%) some new flexural cracks were observed on the unretrofitted zone and the previous flexural cracks became inclined and extended into the web zone of the unretrofitted zone due to the influence of increased shear force as shown in Figure 4.56. Initial vertical crack on the jacket were observed at mentioned drift ratio.

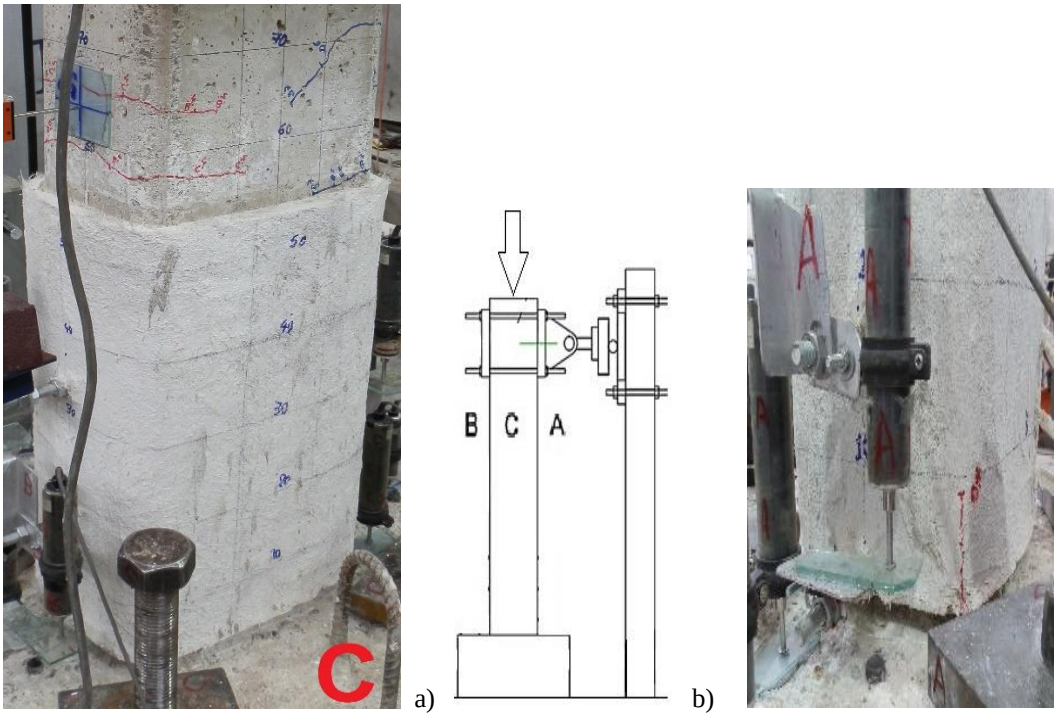

Figure 4.56 : Specimen Ref-S60-Ɵ135-L80-3TRM after the drift ratio of 1.5%. a)Face C. b)Definition of column optional faces. c)Face A.

During loading to various target displacements, concrete cover did not start to spall off at the column surfaces in compression zone.

After loading to target displacement of 103.44 (drift ratio of 8%), test was ended 6 % losing of lateral load capacity. Figure 4.57 illustrated the damaged Ret-S60-Ɵ135-L80-3TRM specimen at the end of the test. The damaged jacket of specimen at the end of test was shown in the Figure 4.58.

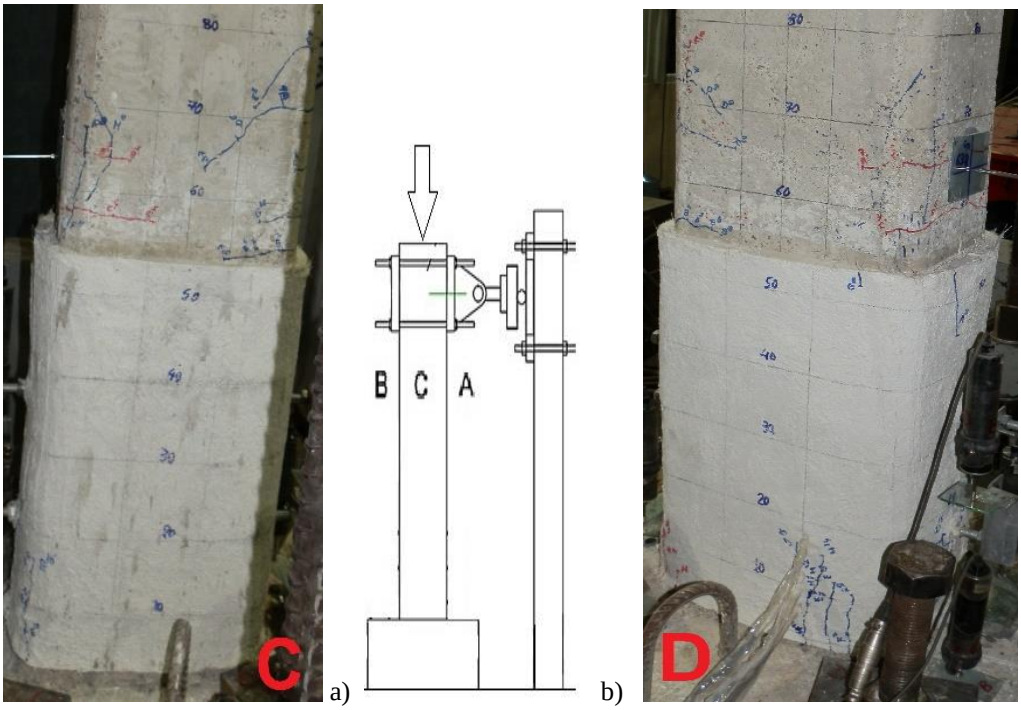

Figure 4.57 : Specimen Ret-S60-Θ135-L80-3TRM after the drift ratio of 8.0 %. a)Face C. b)Definition of column optional faces. c)Face A.

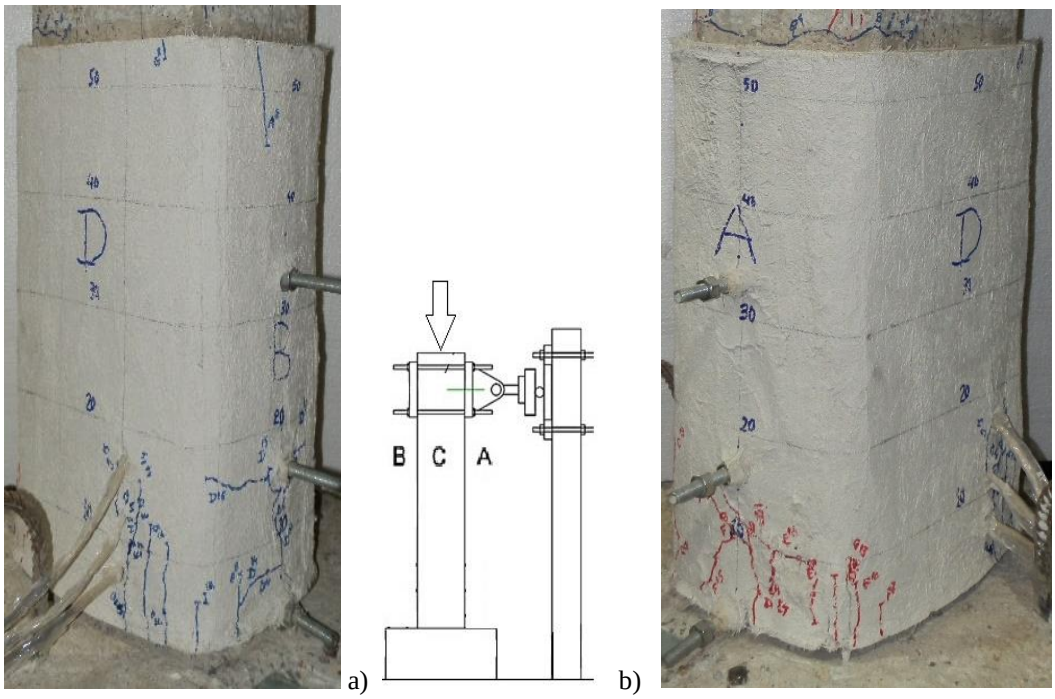

Figure 4.58 : The damaged jacket of Specimen Ret-S60-135-L80-3TRM at the end of test. a)Face D. b)Definition of column optional faces. c)Face A.

The extent of damage at progressive stages of testing can be seen in the Figure 4.59. All pictures were taken after the first cycle of each load stage.

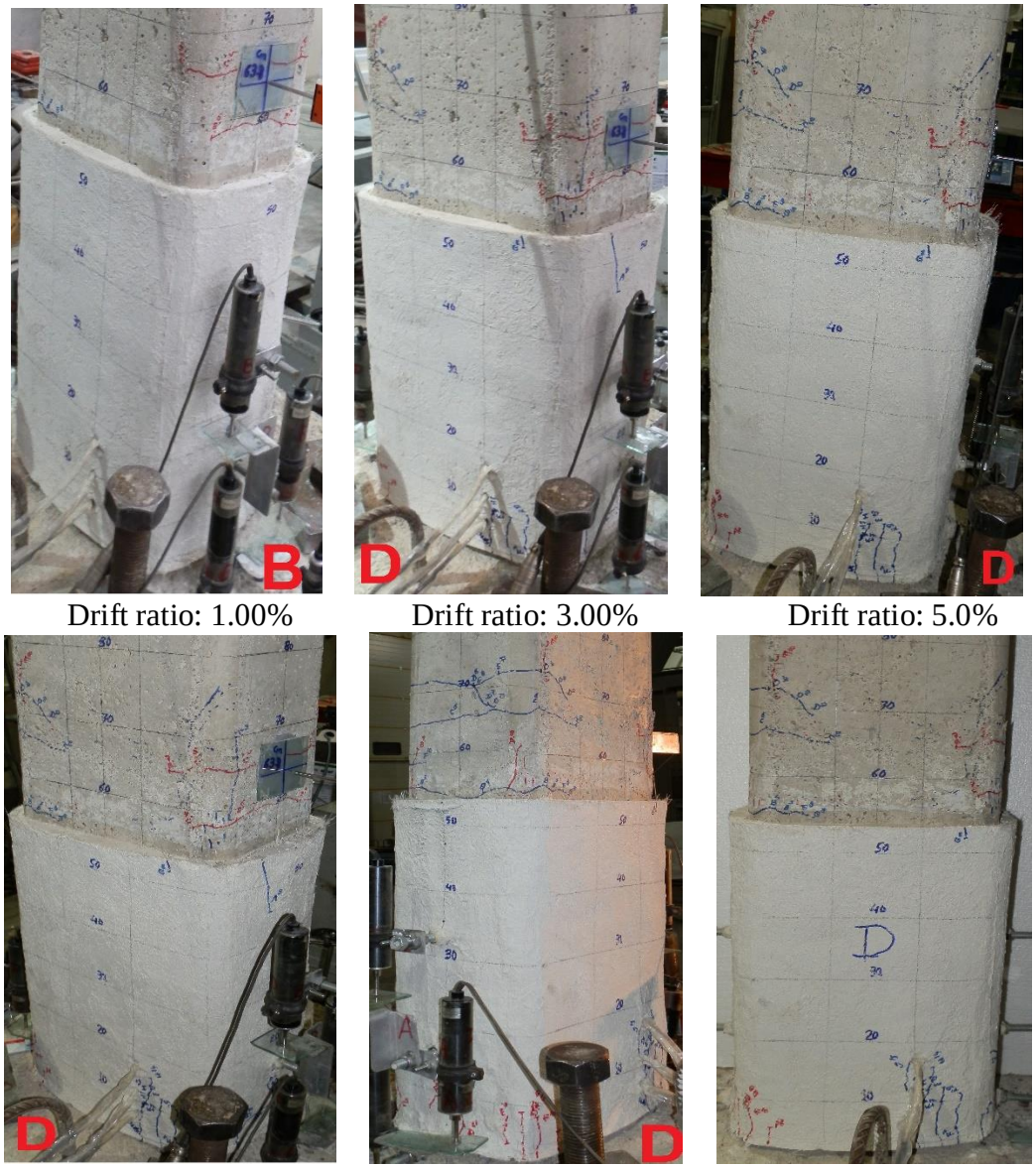

Figure 4.59 : Crack pattern of Ret-S60-Ɵ135-L80 at different drift ratios.

The lateral load-drift-displacement hysteresis curve of the Ret-S60-Ɵ135-L80-3TRM is shown in Figures 4.60. It is clear there is a little difference between values of the lateral loads while pulling and pushing, but almost damage shape was symmetric. The amount of plastic deformation at the point of lateral load application was around 19.16 mm after loading to target displacement of 102.88 mm (drift ratio of 8.0%) and the measurement of out-of-plane at the level of lateral load application was 25.34 mm when lateral load was zero at the end of the test. Test was ended 6 % losing of lateral load capacity during last pushing. Envelope curves for Ret-S60-Ɵ135-L80-3TRM specimen was drawn in Figures 4.61.

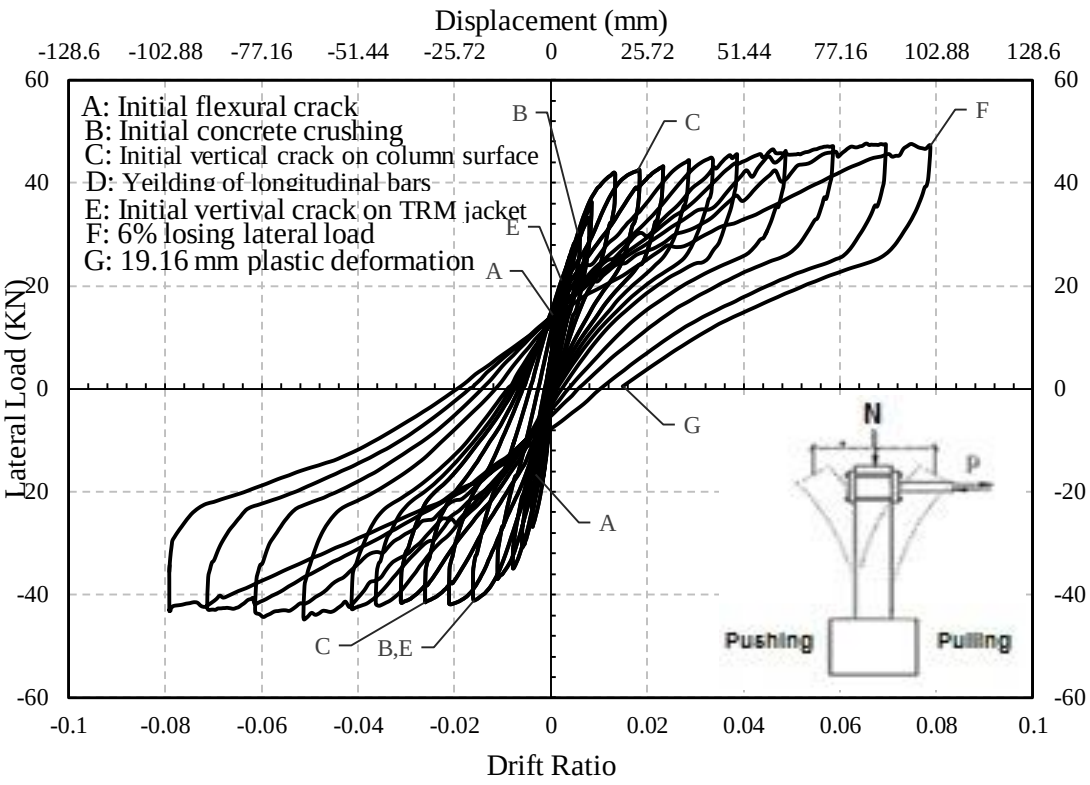

Figures 4.60 : Lateral Load-Drift-Tip Displacement curves for Ret-S60-Θ135-L80-3TRM.

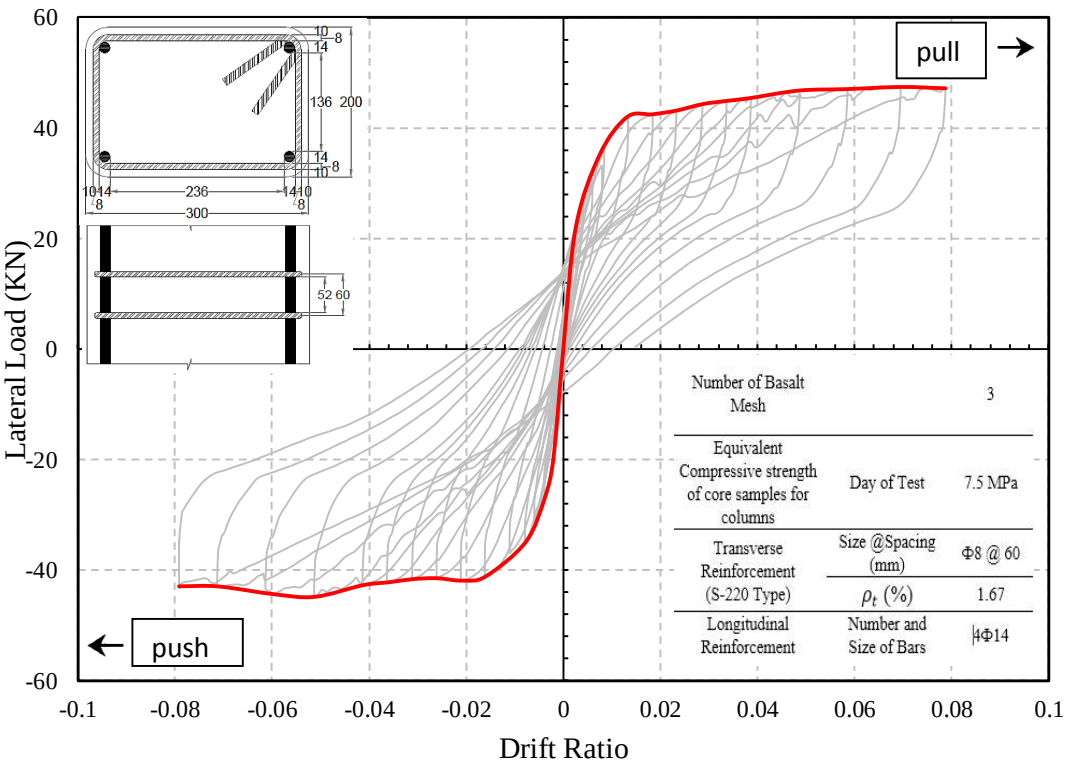

Figures 4.61 : Lateral Load-Drift envelope curve of Ret-S60-Θ135-L80-3TRM.

4.3.4 Specimen: Ret-S60-Ɵ135-L40-3TRM

Before describing test observation, some information about specification of specimen can be found at Table 4.8. Retrofitting system in this research program was manufactured either from Basalt mesh, spraying with Glass Reinforced Concrete (GRC). The Basalt grids had a square configuration with 250 mm out-to-out dimension. Before wrapping of all the specimens, a gap of about 15~20 mm was left at the bottom ends of the columns to avoid direct axial compressive loading of the confinement jacket. Application of the mortar layers were made with spraying glass reinforced concrete in three step due to applying three layers of basalt fiber mesh. Thickness of the mortar were approximately 28~32 mm in middle of both surface of columns and 18~22 mm at the corners. The jackets extended from the base of each column (a gap of about 15~20 mm was left) to a height of 510 mm. After application of the first mortar layer on the concrete surface, the textile was applied and pressed slightly into the mortar, which comes out through all the opening between fiber rovings. The next mortar layer covered the textile completely and the operation was repeated until all textile layers were applied and covered by FIBROBETON mortar.

Table 4.8 : General specification of Ret-S60-Ɵ135-L40-3TRM specimen.

Specimen: Ret-S60-Ɵ135-L40-3TRM				
Cross section Dimension $h \times b$	300 x 200 mm	Hook Length L (mm)		40
Height of Columns H_{column}	1290 mm	Hook Angle Ɵ (°)		135°
Compressive strength of standard cylinder samples for columns	7.5 (MPa)	$\frac{N_{axial}}{A_g f_c'}$		71.8 %
Equivalent Compressive strength of core samples for columns	7.5 (MPa)	Transverse Reinforcement (S-220 Type)	Size @Spacing (mm)	Φ8 @ 60
			ρ_t (%)	1.67
Axial Load N_{axial} (kN)	323	Longitudinal Reinforcement (S-420 Type)	Number and Size of Bars (mm)	4Φ14
			ρ_l (%)	1.03

All experimental observations, which were made during the test of Ret-S60-Ɵ135-L40-3TRM, are presented at the Appendix A. In this subsection, only the important events were pointed out. No cracks were observed while loading to target displacements of ±1.29 mm (drift ratio of 0.1%) as illustrated in Figure 4.62.

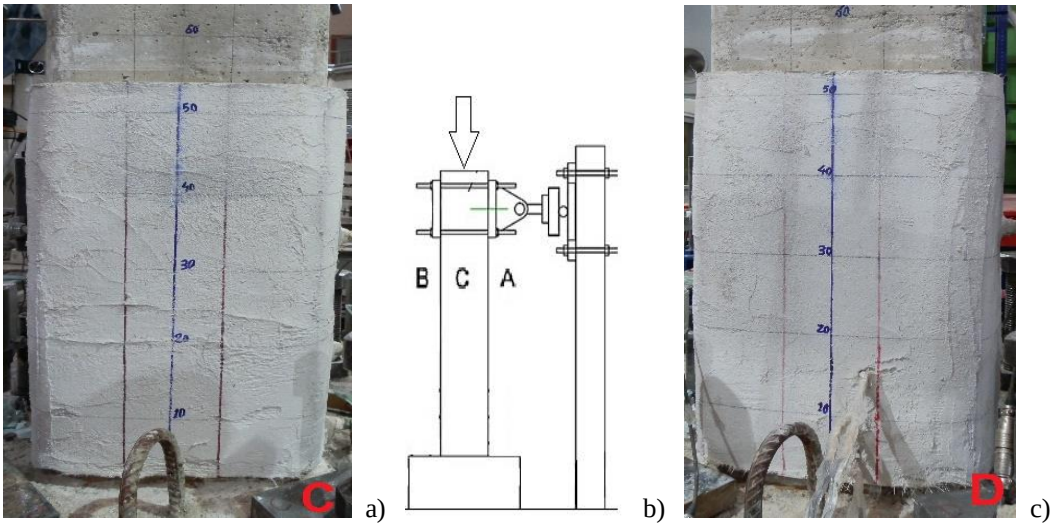

Figure 4.62: Specimen Ret-S60-Ɵ135-L40-3TRM after the drift ratio of 0.1%. a)Face C. b)Definition of column optional faces. c)Face D.

At the column-foundation interface, during loading to target displacement of ±2.58 mm (drift ratio of 0.20%) first flexural crack was observed. During loading to target displacements of ±10.32 mm (drift ratio of 0.80%) new flexural cracks were observed on the column surface (unretrofitted faces) as illustrated in Figure 4.63.

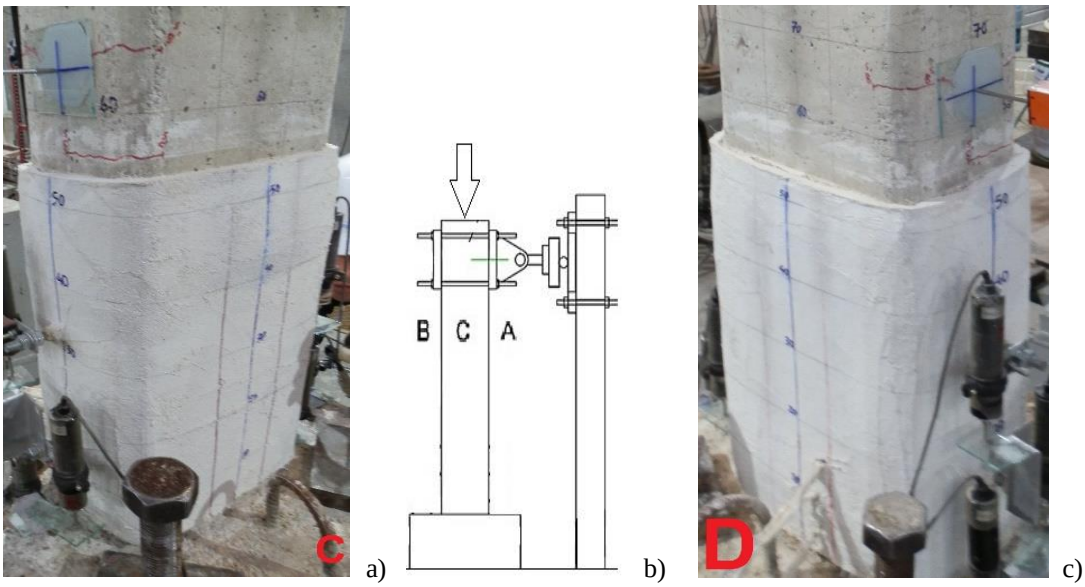

Figure 4.63 : Specimen Ret-S60-Ɵ135-L40-3TRM after the drift ratio of 0.8%. a)Face C. b)Definition of column optional faces. c)Face D.

Meanwhile, initial concrete crushing was formed at the B-face of the column at the mentioned drift ratio. While loading to target displacements of ±19.29 mm (drift ratio of 1.5%) some new flexural cracks were observed on the unretrofitted zone and the previous flexural cracks became inclined and extended into the web zone of the unretrofitted zone due to the influence of increased shear force as shown in Figure 4.64. Initial vertical crack on the jacket were observed at mentioned drift ratio.

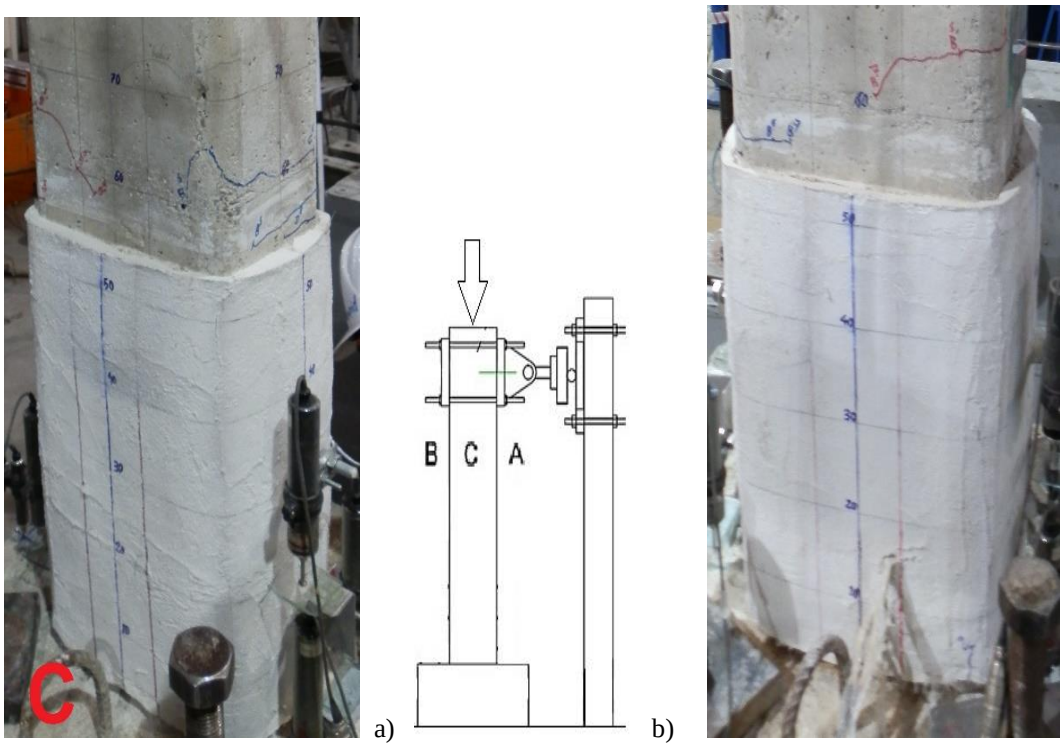

Figure 4.64 : Specimen Ret-S60-Ɵ135-L40-3TRM after the drift ratio of 1.5%. a)Face C. b)Definition of column optional faces. c)Face D.

During loading to various target displacements, concrete cover did not start to spall off at the column surfaces in compression zone.

After loading to target displacement of 103.44 (drift ratio of 8%), test was ended due to use maximum capacity of tip point LVDT which was measured top displacement of column. Specimen didn't lose its lateral load capacity during loading to target drift ratio of -8 %. Figure 4.65 illustrated the damaged Ret-S60-Ɵ135-L40-3TRM specimen at the end of the test. The damaged jacket of specimen at the end of test was shown in the Figure 4.66.

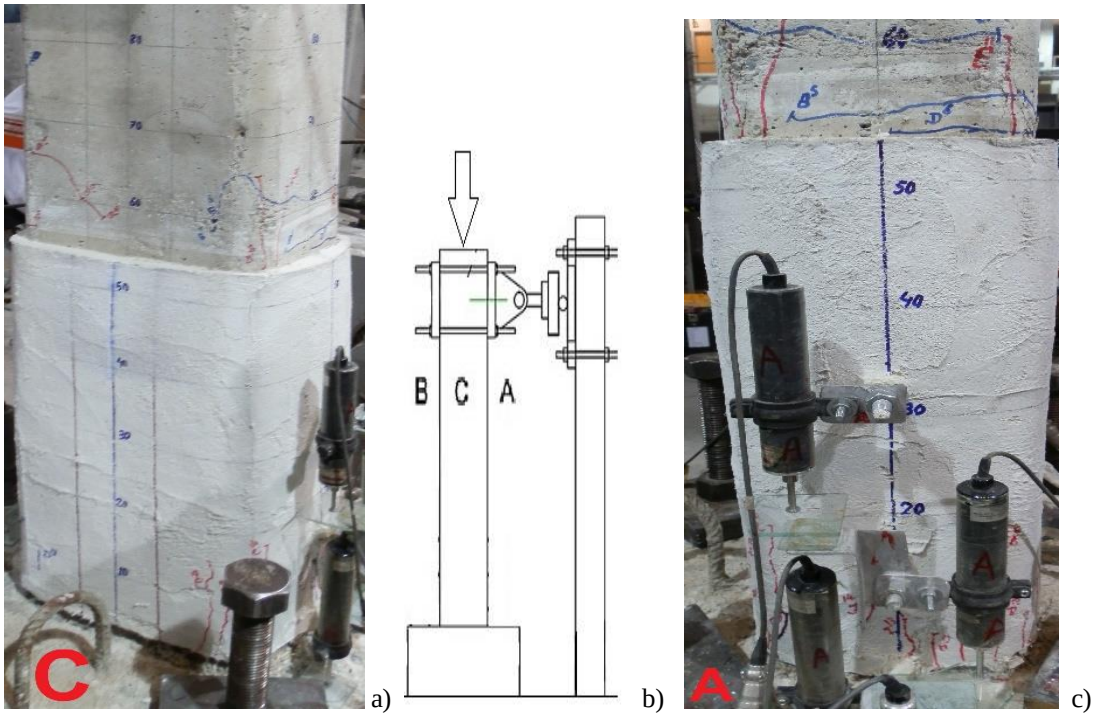

Figure 4.65 : Specimen Ret-S60-Θ135-L40-3TRM after the drift ratio of 8.0 %. a)Face C. b)Definition of column optional faces. c)Face A.

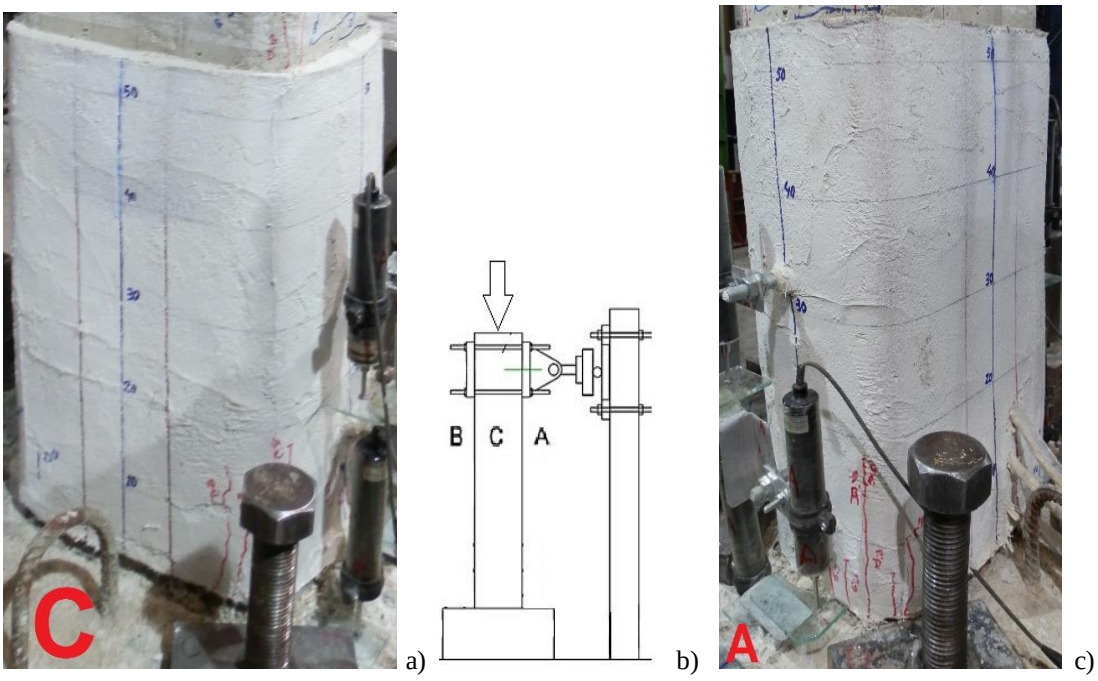

Figure 4.66 : The damaged jacket of Specimen Ref-S60-135-L40-3TRM at the end of test. a)Face C. b)Definition of column optional faces. c)Face A.

The extent of damage at progressive stages of testing can be seen in the Figure 4.67. All pictures were taken after the first cycle of each load stage.

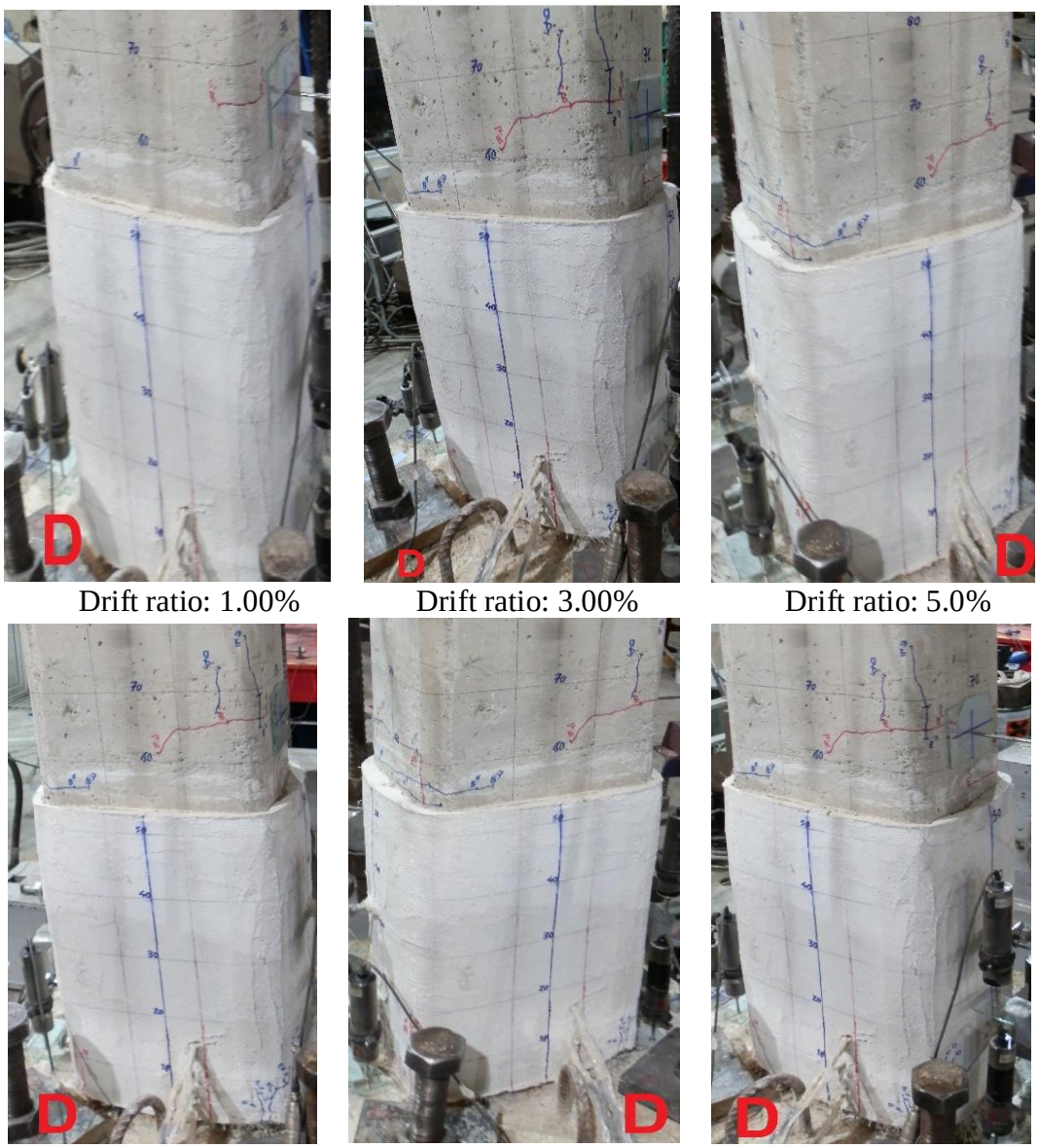

Drift ratio: 1.00% Drift ratio: 3.00% Drift ratio: 5.0%

Drift ratio: 6.0% Drift ratio: 7.0% Drift ratio: 8.0%

Figure 4.67 : Crack pattern of Ret-S60-Ɵ135-L40-3TRM at different drift ratios.

The lateral load-drift-displacement hysteresis curve of the Ret-S60-Ɵ135-L40-3TRM is shown in Figures 4.68. It is clear there is no difference between values of the lateral loads while pulling and pushing, almost damage shape was symmetric. The amount of plastic deformation at the point of lateral load application was around 24.62 mm after loading to target displacement of 102.36 mm (drift ratio of 8.0%) and the measurement of out-of-plane at the level of lateral load application was 21.42 mm when lateral load was zero at the end of the test. Test was ended without losing of lateral load capacity during last pulling. Envelope curves for Ret-S60-Ɵ135-L40-3TRM specimen was drawn in Figures 4.69.

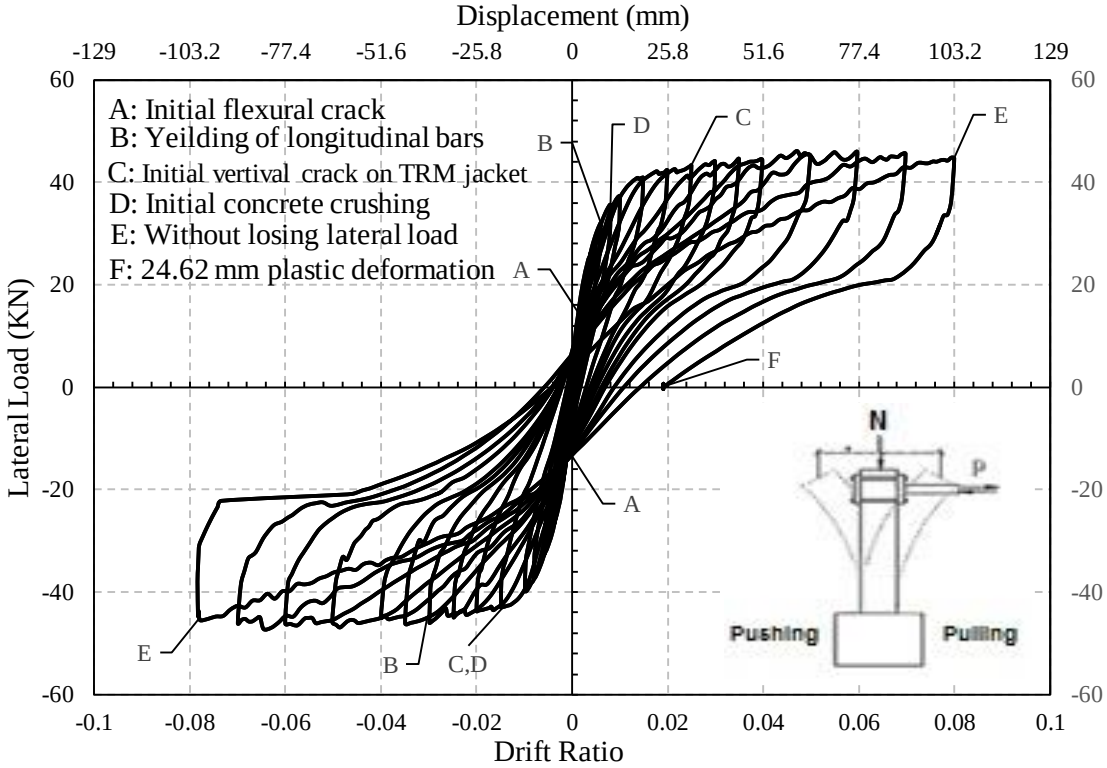

Figures 4.68 : Lateral Load-Drift-Tip Displacement curves for Ret-S60-Θ135-L40-3TRM.

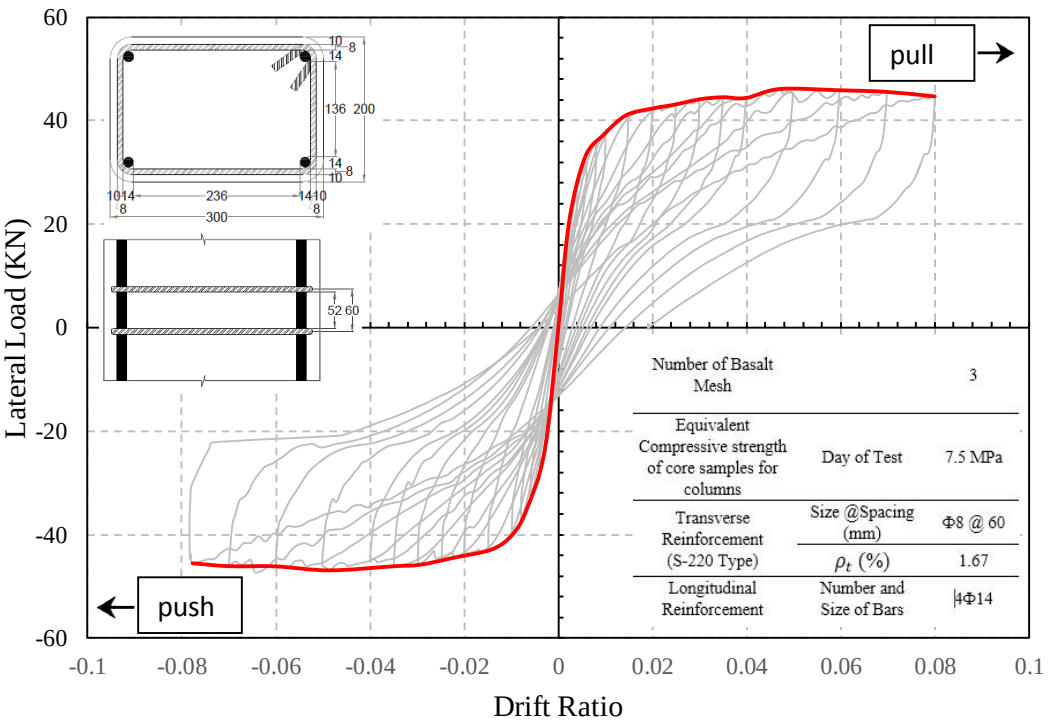

Figures 4.69 : Lateral Load-Drift envelope curve of Ret-S60-Θ135-L40-3TRM.

5. EVALUATION OF TEST RESULTS

5.1 Introduction

In this chapter, experimental and analytical test results of all specimens are evaluated by using moment curvature, energy dissipation and comparisons of reference specimens versus retrofitted specimens.

5.2 Moment-Curvature

For observing of damage distribution, moment-curvature relationship was obtained at different gauge lengths at the potential plastic hinge zones (Figure 5.1).

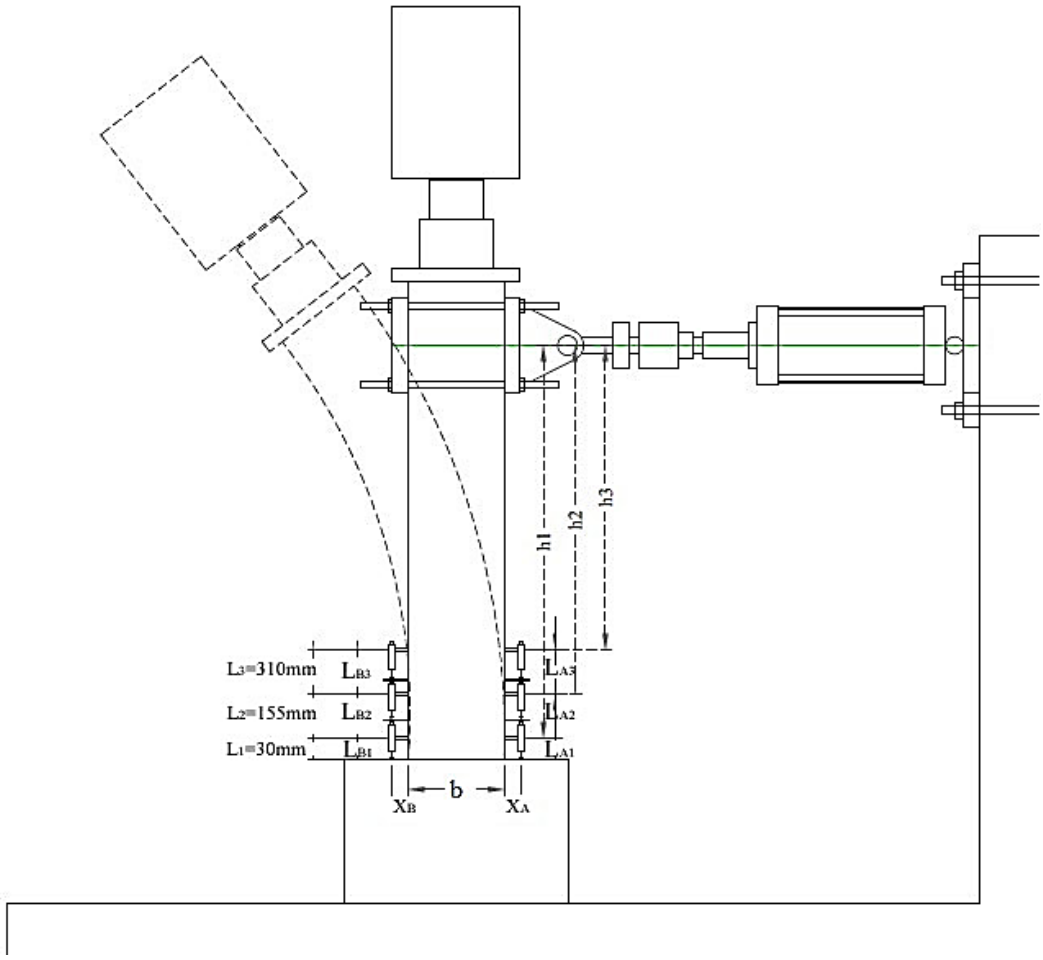

Figure 5.1 : Location of the measurements system which are used for obtaining moment- curvature relationship.

Plane sections remain plain, according to this assumption, the moment-curvature relationships can be obtained. Experimental curvatures were obtained based on the LVDT readings. For the calculation of moment-curvature relationships, the average curvature values were obtained in 30 mm, 155 mm and 330 mm above the column-foundation interface. Moments were calculated by using Eq. (5.1). In this equation, P is the lateral load at the tip point of column, h_i is the column height from column-foundation interface to applied lateral load point, as illustrated in Figure 5.1. Curvatures were calculated by dividing the obtained strains from the two LVDTs at the same level to the distance between the mentioned LVDTs by using Eq.(5.2). K_i is the curvature of the i'th level above the column-foundation interface.

$$M_i = P \times h_i \tag{5.1}$$

$$K_i = \frac{\varepsilon_{Bi} + \varepsilon_{Ai}}{X_{Bi} + b + X_{Ai}} \tag{5.2}$$

Experimental moment-curvature diagrams for the ranges of 0-30 mm, 30-155 mm and 155-310 mm heights above the footing are presented for all reference and retrofitted specimens in Fig. 5.2 through Fig. 5.5.

As seen from mentioned Figures, in all reference specimens the curvature values of the member measured in 0- 30 mm and 155-310 mm height above the column-stub interface are much bigger than the curvatures measured in 30-155 mm height and it can be noted that the damage is accumulated especially in 0-30 and 155-310 mm height above the column-stub interface.

On the other hand, in all retrofitted specimens, it seems large amount of curvatures gathered in 30-155 mm height especially in column-foundation interface expect of Ret-S60-Ɵ90-L80-3TRM because of strongly concrete spalling around the confined and unconfined zone in 510-830 mm height above the column-stub interface. Confinement jackets stayed without significant damages and it was observed the place of plastic hinge was changed by effect of composite jacket.

Experimental moment-curvature diagrams for the ranges of 0-30 mm, 30-155 mm and 155-310 mm heights above the footing are presented for the Ref-S60-Ɵ90-L80 and Ret-S60-Ɵ90-L80-3TRM in Fig. 5.2.

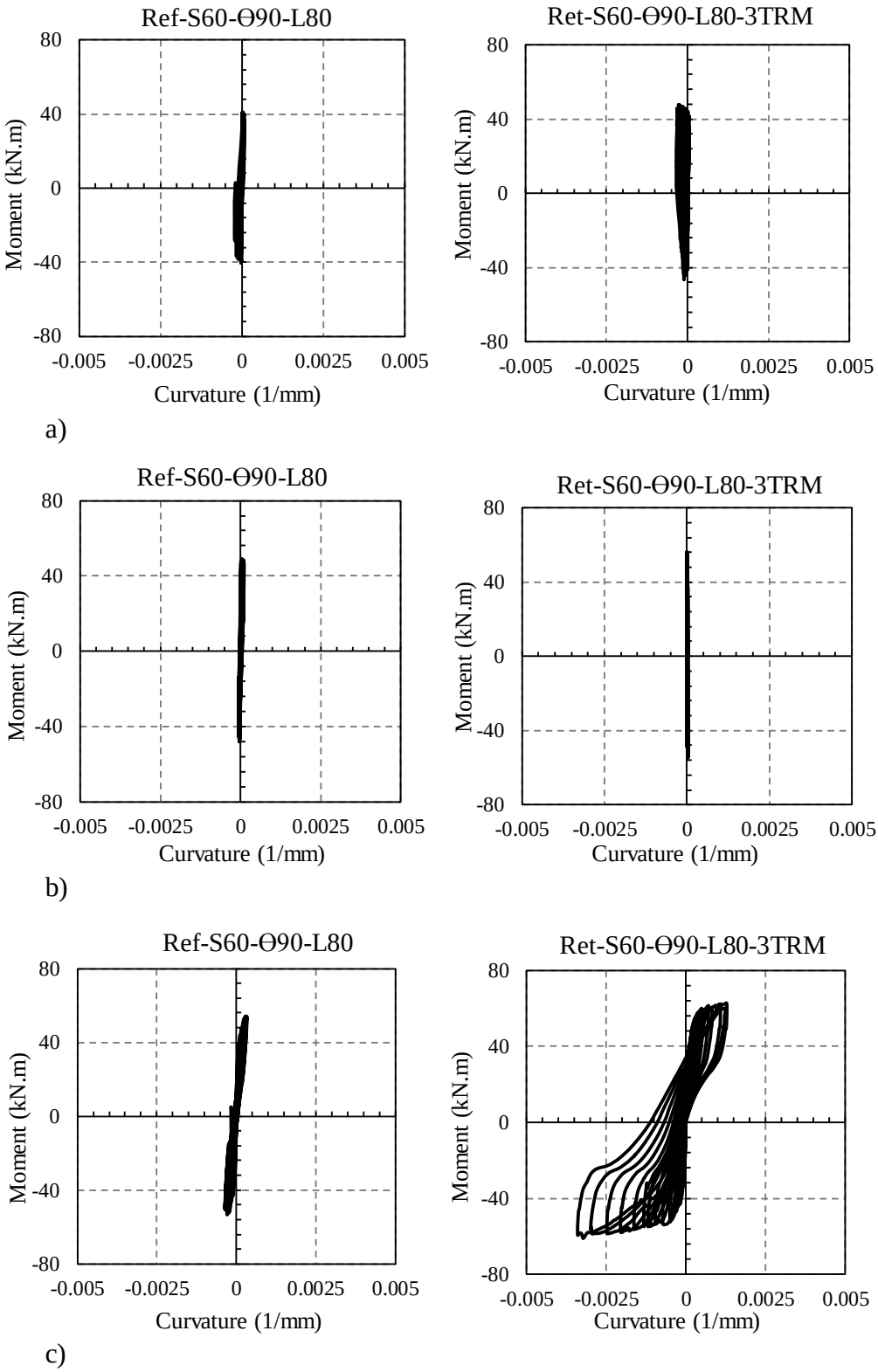

Figure 5.2 : Experimental Moment-Curvature diagrams for Ref-S60-Ɵ90-L80 and Ret-S60-Ɵ90-L80-3TRM. a)Elevation code of 150~310 mm. b)Elevation code of 30~155mm. c)Elevation code of 0~30 mm.

Experimental moment-curvature diagrams for the ranges of 0-30 mm, 30-155 mm and 155-310 mm heights above the footing are presented for the Ref-S60-Θ112.5-L80 and Ret-S60-Θ112.5-L80-3TRM in Fig. 5.3.

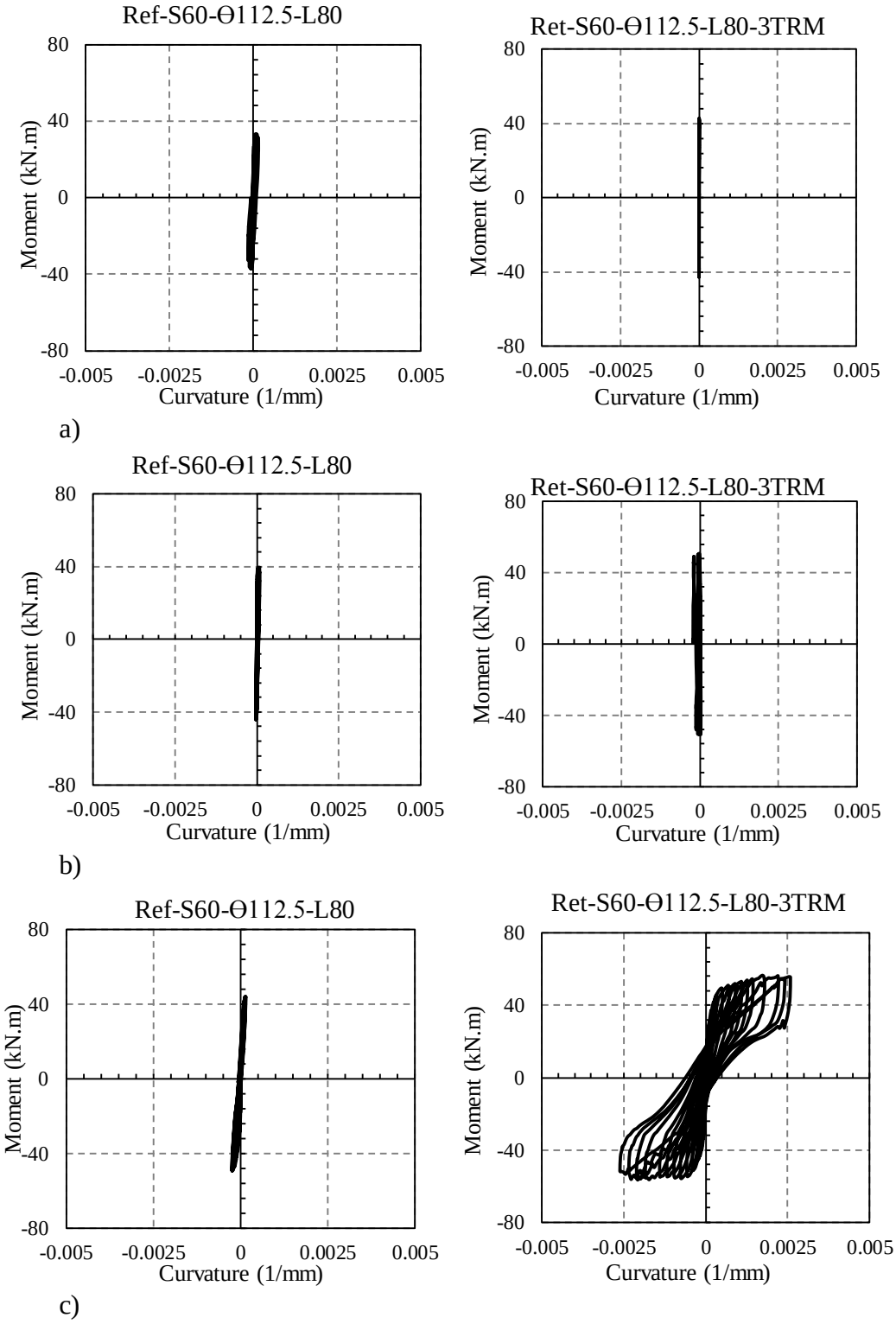

Figure 5.3 : Experimental Moment-Curvature diagrams for Ref-S60-Θ112.5-L80 and Ret-S60-Θ112.5-L80-3TRM. a)Elevation code of 150~310 mm. b)Elevation code of 30~155mm. c)Elevation code of 0~30 mm.

Experimental moment-curvature diagrams for the ranges of 0-30 mm, 30-155 mm and 155-310 mm heights above the footing are presented for the Ref-S60-Θ135-L80 and Ret-S60-Θ135-L80-3TRM in Fig. 5.4.

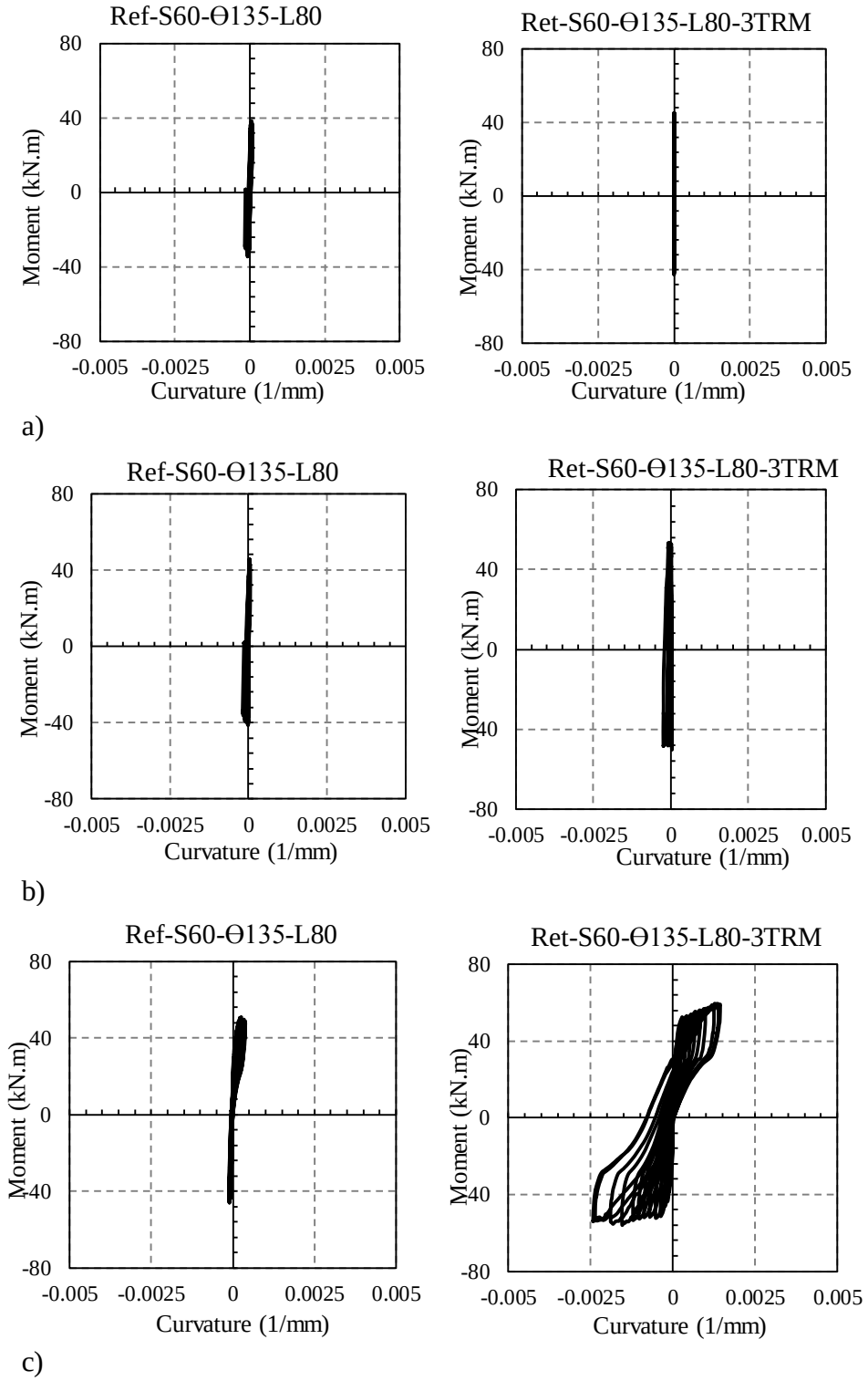

Figure 5.4 : Experimental Moment-Curvature diagrams for Ref-S60-Θ135-L80 and Ret-S60-Θ135-L80-3TRM. a)Elevation code of 150~310mm. b)Elevation code of 30~155mm. c)Elevation code of 0~30 mm.

Experimental moment-curvature diagrams for the ranges of 0-30 mm, 30-155 mm and 155-310 mm heights above the footing are presented for the Ref-S60-Θ135-L40 and Ret-S60-Θ135-L40-3TRM in Fig. 5.5.

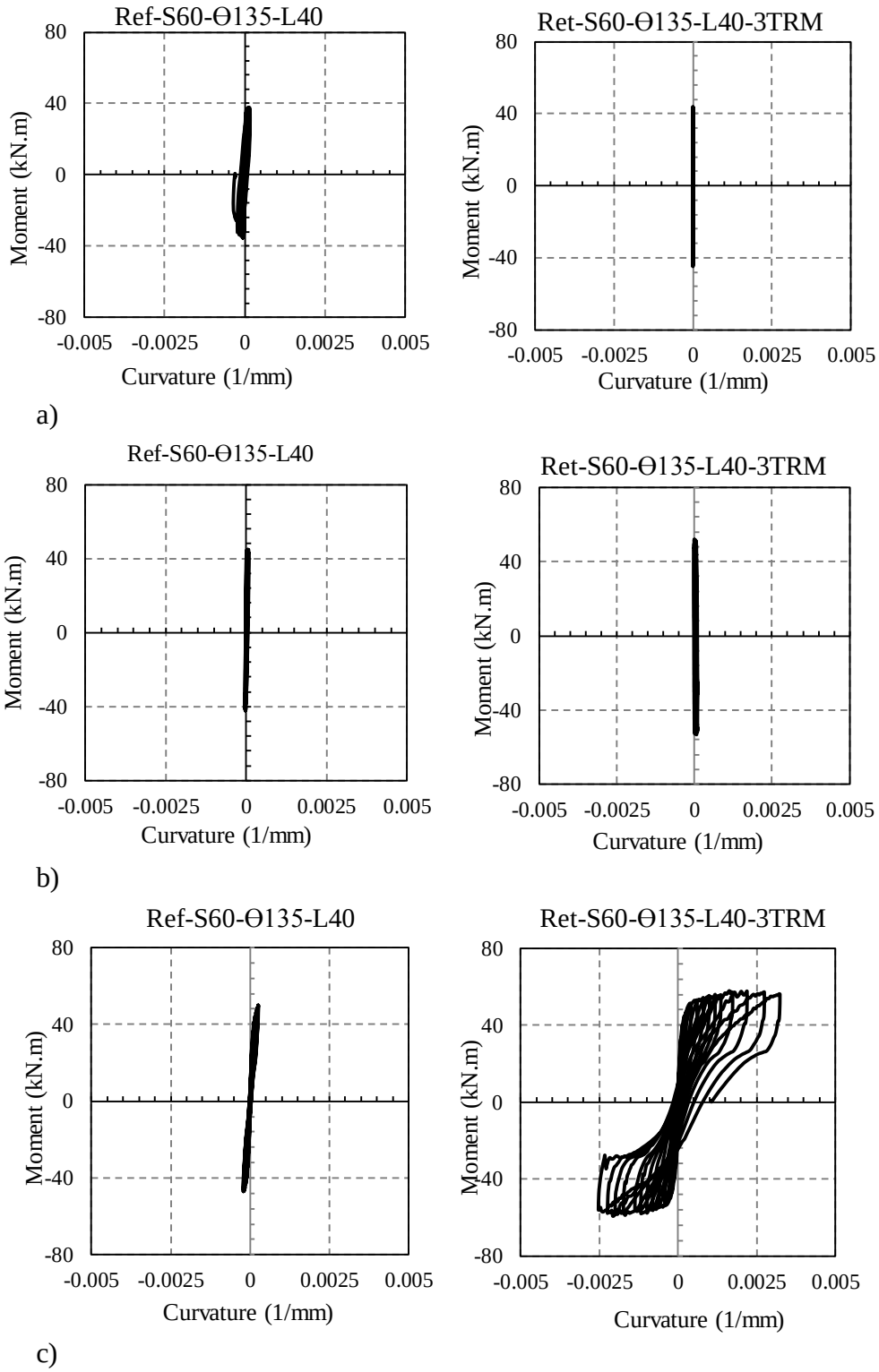

Figure 5.5 : Experimental Moment-Curvature diagrams for Ref-S60-Θ135-L40 and Ret-S60-Θ135-L40-3TRM. a)Elevation code of 150~310mm. b)Elevation code of 30~155mm. c)Elevation code of 0~30 mm.

5.3 Energy Dissipation

Energy dissipation is an important property of columns when being part of a structure placed in moderate/high seismic regions like Turkey. This property is directly related to the seismic performance of a structure. In order to survive major earthquakes, structures should be capable of absorbing and dissipating energy greater than that input to the structure by the earthquake. In this section, the cumulative energy dissipation by the columns during the tests is presented and discussed. For flexure cyclic loadings, the energy dissipated during one cycle is calculated as the area inscribed within the hysteresis loop. The energy dissipation of all reference and retrofitted specimens are presented in Figures 5.6 and 5.7, respectively.

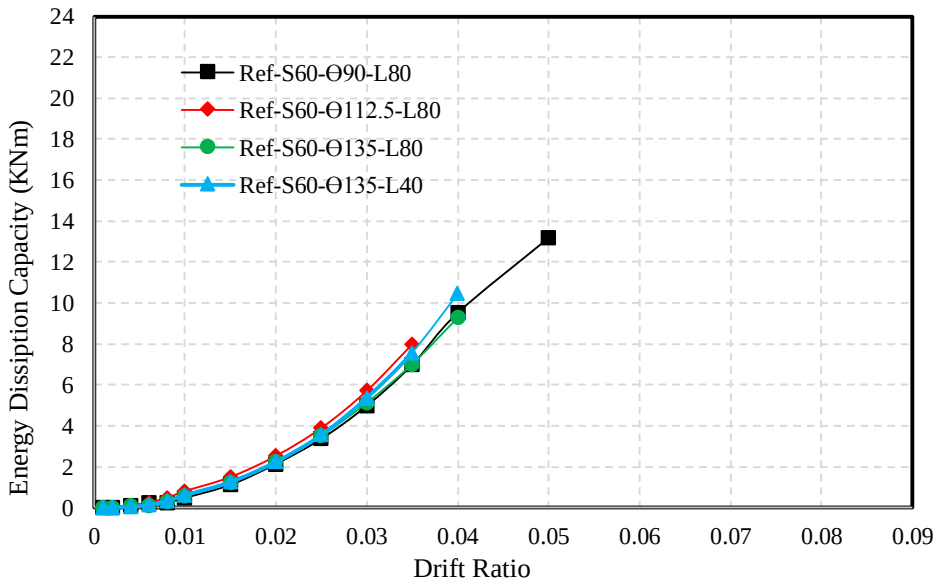

Figure 5.6 : Comparison of energy dissipation capacity of the reference specimens.

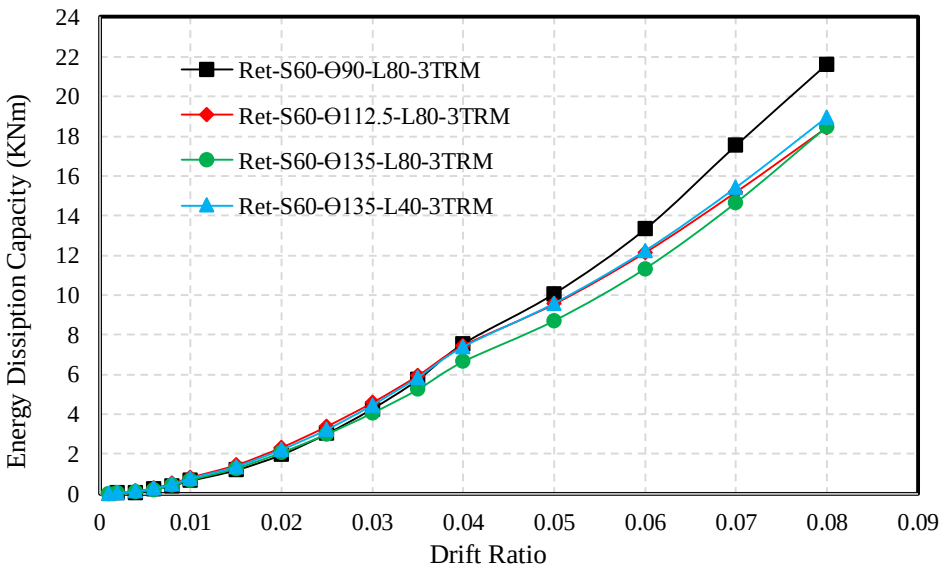

Figure 5.7 : Comparison of energy dissipation capacity of the retrofitted specimens.

As seen in Figure 5.6, the total energy dissipation capacity as obtained from the lateral load-drift response of reference specimens with different hook length/angle are approximately equal, at the same time, it is obvious that the total energy dissipation of Ref-S60-Θ112.5-L80 and Ref-S60-Θ135-L40 are slightly more than other reference specimens, respectively. It appears this behavior is influenced by angle/length of hooks. The results of retrofitted specimens show that the energy dissipation capacities at same drift (8 %) are approximately similar instead of Ret-S60-Θ90-L80-3TRM specimen. This specimen resulted more energy dissipation than the other retrofitted specimens after 4 % of drift ratio. It appears this behavior is influenced by large amount of plastic deformation due to concrete spalling that occurred after mentioned drift ratio. Figures 5.8-a through 5.8-d show the curves of the cumulative energy dissipated by every reference specimen versus its retrofitted sample.

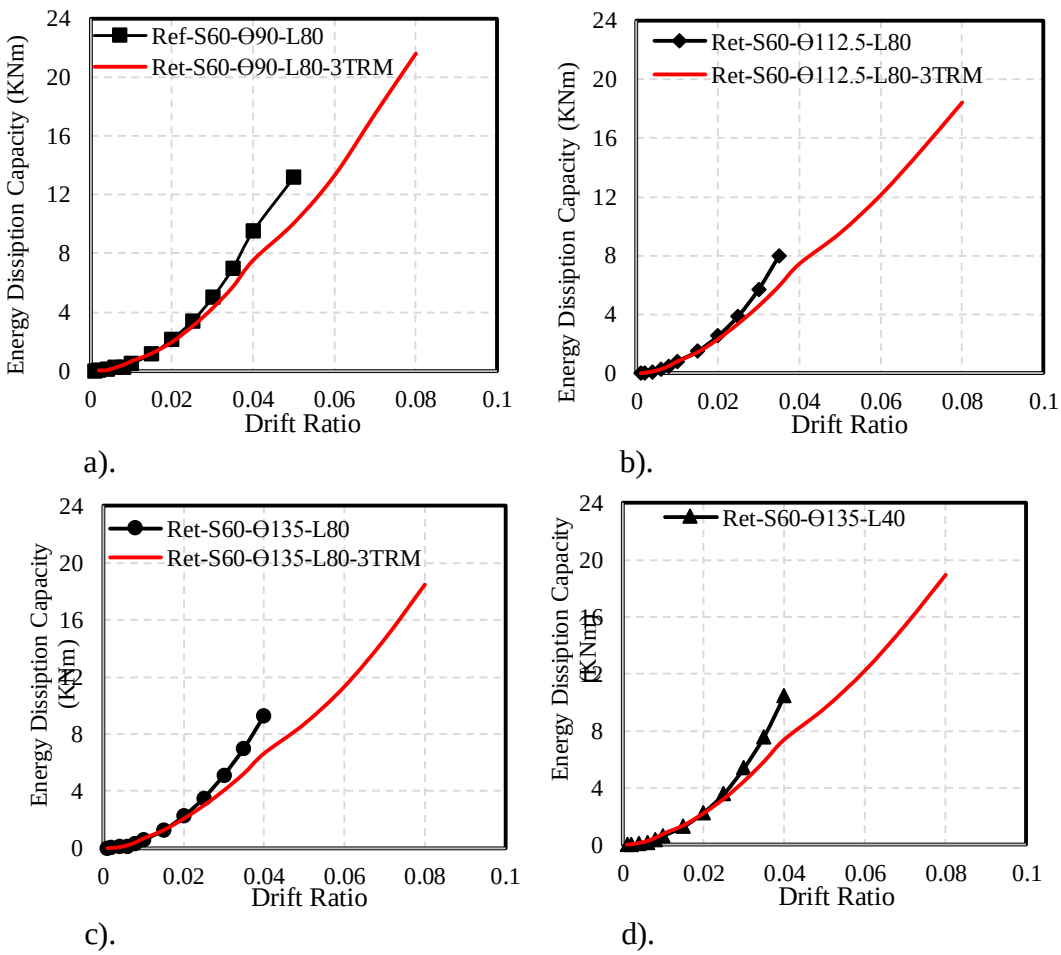

Figure 5.8 : a)Energy dissipation capacity of the Ref-S60-Θ90-L80 versus Ret-S60-Θ90-L80-3TRM. b)Energy dissipation capacity of the Ref-S60-Θ112.5-L80 versus Ret-S60-Θ112.5-L80-3TRM. c)Energy dissipation capacity of the Ref-S60-Θ135-L80 versus Ret-S60-Θ135-L80-3TRM. d)Energy dissipation capacity of the Ref-S60-Θ135-L40 versus Ret-S60-Θ135-L40-3TRM.

Confining columns with retrofitting jackets remarkably improved the seismic performance of columns, resulting in large increases in ductility and energy dissipation capacity. It should be noted that under high axial load the addition of retrofitting system resulted in significant improvement in the behavior of columns.

It was also observed that the beneficial effects measured in terms of energy dissipation capacity and ductility before the lateral load dropped by 15 %, in retrofitted columns were approximately twice as large as in reference columns.

5.4 Failure Mechanisms of Specimens

The failure mechanisms of the reference and retrofitted specimens are presented in Table 5.1. The longitudinal bars of specimens Ref-S60-Ɵ90-L80 and Ref-S60-Ɵ135-L40 buckled during the test. A large amount of concrete cover spalled off completely at the buckled region.

It is worth noting here that the development of such high axial compressive strains after bar buckling could normally have been reproduced only in concentric compression tests. The effectiveness of confinement with FRP and the newly developed textile-reinforced mortars, or TRM (Triantafillou et al. 2006), against bar buckling has been addressed to date only for the case of concentric compression. Tastani et al. (2006) investigated in a systematic way, both experimentally and analytically, the interaction between FRP jackets and embedded longitudinal compression reinforcement by testing 27 short prismatic RC columns up to failure under concentric compression. The main conclusion of that work was that the deformation capacity of FRP jacketed members is limited by bar buckling. Similar observations have been made by Bournas et al. (2007) on the basis of the experimental results of FRP- and TRM-jacketed RC prisms, in which failure of the jackets resulted from stretching both by concrete dilation and by outward bending of the longitudinal bars in the middle of the specimens. It is obvious from Table 5.1 that the bar buckling were delayed by external confinement and confinement system caused to improve the deformation capacity of the columns and residual plastic deformation were decreased in all retrofitted specimens especially in Ret-S60-Ɵ90-L80-3TRM and Ret-S60-Ɵ135-L40-3TRM.

Table 5.1 : Failure mechanisms of specimens.

Failure mechanism	Specimens							
	Ref S60-Ɵ90-L80	Ref S60-Ɵ112.5-L80	Ref S60-Ɵ135-L80	Ref S60-Ɵ135-L40	Ret S60-Ɵ90-L80-3TRM	Ret S60-Ɵ112.5-L80-3TRM	Ret S60-Ɵ135-L80-3TRM	Ret S60-Ɵ135-L40-3TRM
First Flexural Crack	0.6%	0.2%	0.4%	0.4%	0.4%	0.2%	0.2%	0.2%
Initial Flexural Crack on TRM Jacket	No Retrofitting	No Retrofitting	No Retrofitting	No Retrofitting	1.5%	1.0%	1.5%	1.5%
Yielding of Longitudinal Bar	0.8%	0.4%	0.6%	0.4%	1.5%	0.6%	1.5%	0.6%
Initial Concrete-Crushing	1.5%	1.5%	0.8%	1.5%	1.0%	1.5%	0.8%	8.0%
Spalling of Concrete Cover	3.0%	2.5%	3.0%	2.5%	4.0%	No Spalling	No Spalling	No Spalling
Buckling of Longitudinal Bar	6.0%	No Buckling	No Buckling	4.0%	No Buckling	No Buckling	No Buckling	No Buckling
Tip Residual Plastic Deformation at 2.5% Drift Ratio (Zero Lateral Load)	9.8 mm	8.5 mm	11.4 mm	11.2 mm	2.6 mm	6.8 mm	8.7 mm	3.2 mm
Maximum Applied Lateral Load (KN)	-43/42 kN (Drift 2.0 %)	-36/40 kN (Drift 2.5 %)	-39/38 kN (Drift 2.5 %)	-39/37 kN (Drift 2.0 %)	-46/47 kN (Drift 7.0 %)	-46/43 kN (Drift 7.0 %)	-47/44 kN (Drift 8.0 %)	-46/46 kN (Drift 7.0 %)
Strength Loss with Respect to Maximum Lateral Load at the End of the Test	33%	15%	18%	45%	33%	9%	6%	No Losing

It should be noted that, as it can be seen from the figures of the crack patterns (appendix A) in retrofitted specimens, when damages accumulated especially in TRM jackets, concrete crushing was occurred in earlier drift ratios and spalling in column surface were not observed except in Ret-S60-Ɵ90-L80-3TRM. All specimens photographs at the end of the test are presented in Figure 5.9.

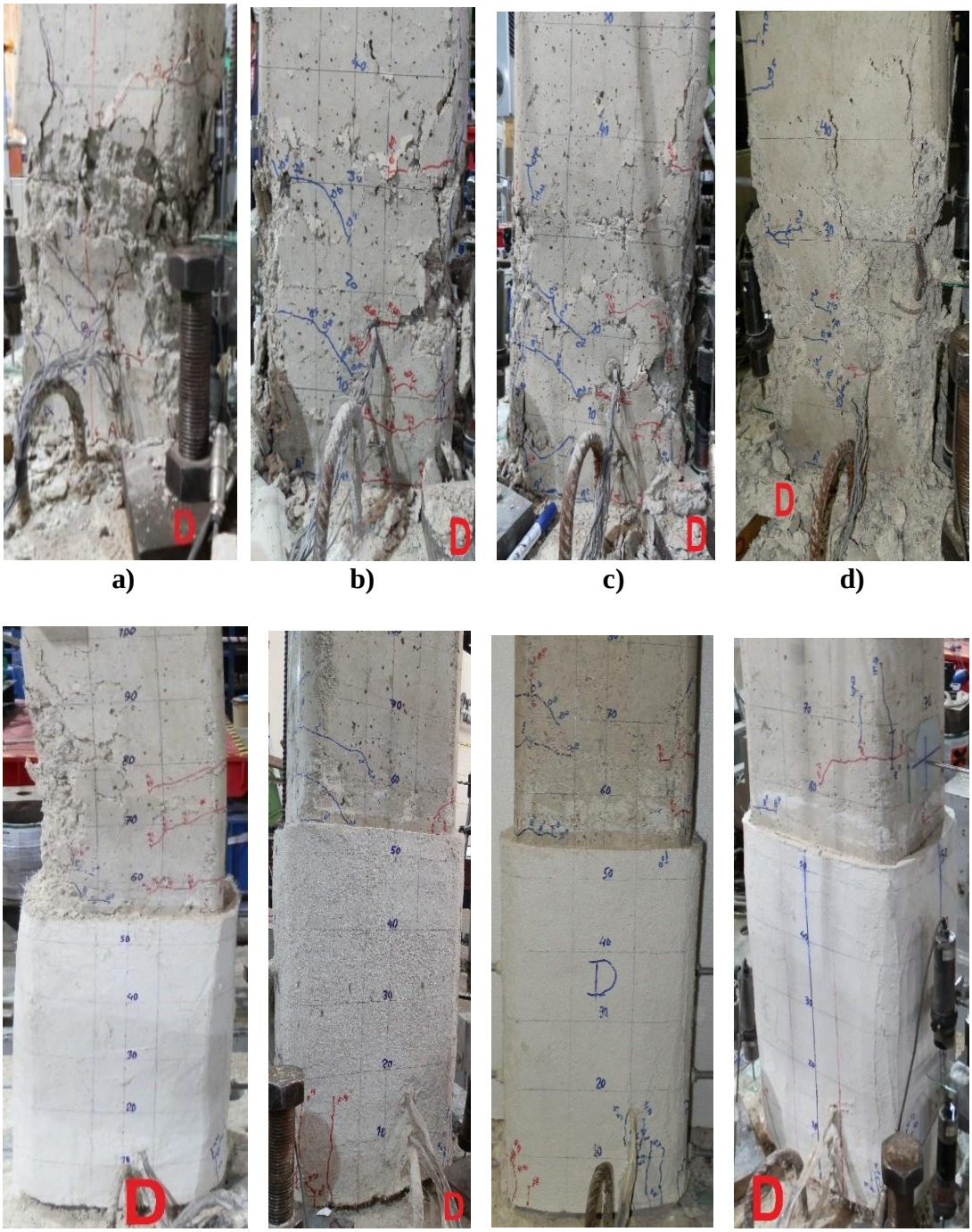

Figure 5.9 : All specimens photographs at the end of tests. a)Ref-S60-Ɵ90-L80 at the end of 6% drift ratio. b)Ref-S60-Ɵ112.5-L80 at the end of 6% drift ratio. c)Ref-S60-Ɵ135-L80 at the end of 4% drift ratio. d)Ref-S60-Ɵ135-L40 at the end of drift ratio 5%. e)Ret-S60-Ɵ90-L80-3TRM at the end of 8% drift ratio. f)Ret-S60-Ɵ112.5-L80-3TRM at the end of 8% drift ratio. g)Ret-S60-Ɵ135-L80-3TRM at the end of 8% drift ratio. h)Ret-S60-Ɵ135-L40-3TRM at the end of 8% drift ratio.

5.5 Lateral Load-Drift-Tip Displacement Relationships

Lateral Load-Drift-Displacement relationships and envelope curves for all columns are shown at the forth chapter. The points of envelope curves are the maximum load value of the every cycle at each target displacement level. Corresponding interpretations for these diagrams are pointed at the mentioned chapter out. The values of the tip displacement was taken from the data measured by the LVDT located at the same level of the actuator. It can be noted that the lateral force values was measured by actuator. Some important signs are marked on the every diagram's curve: the initial flexural and vertical cracks on column surfaces (and TRM jacketing in retrofitted specimens), the initial concrete crushing and the initial spalling of the cover concrete, yielding of the longitudinal bars and the loss of capacity (a loss in flexural capacity due to concrete spalling or ruptured longitudinal/transverse bars) and residual plastic deformation at the end of test.

5.6 Comparison of the all reference specimens:

The envelopes of lateral load-tip drift curves for all reference specimens are shown in Figure 5.10. As seen from mentioned figure, there is a little difference between the lateral loads while pulling and pushing direction. In pushing side of diagram, it is obvious that decreasing of the hook angle causes the hysteretic behavior of RC columns to show more flexure strength. It is clear that Ref-S60-Ɵ90-L80 specimen had a more ductile behavior than Ref-S60-Ɵ112.5-L80, Ref-S60-Ɵ135-L80 and Ref-S60-Ɵ135-L40 specimens before the lateral load dropped by around 15 %. Flexural strength of Ref-S60-Ɵ112.5-L80 has shown a small increment in pushing side, maybe the longitudinal bars had thicker concrete cover at the B face of column. In Ref-S60-Ɵ112.5-L80 and Ref-S60-Ɵ135-L80 specimens, tests were continued until losing around 15 % of maximum load carrying capacity, but in Ref-S60-Ɵ90-L80 and Ref-S60-Ɵ135-L40 test was stopped due to longitudinal bars buckling and large amount of cover concrete spalling. Mentioned specimens lost 33% and 45% of maximum load carrying capacity in pushing direction, respectively. By considering the behavior of Ref-S60-Ɵ135-L80 and Ref-S60-Ɵ135-L40 specimens, which had same test parameters except in hook length, it can be noted that the specimens with 80 mm of hook length had the same flexural strength and ductile behavior as same as specimen with 40 mm of hook length.

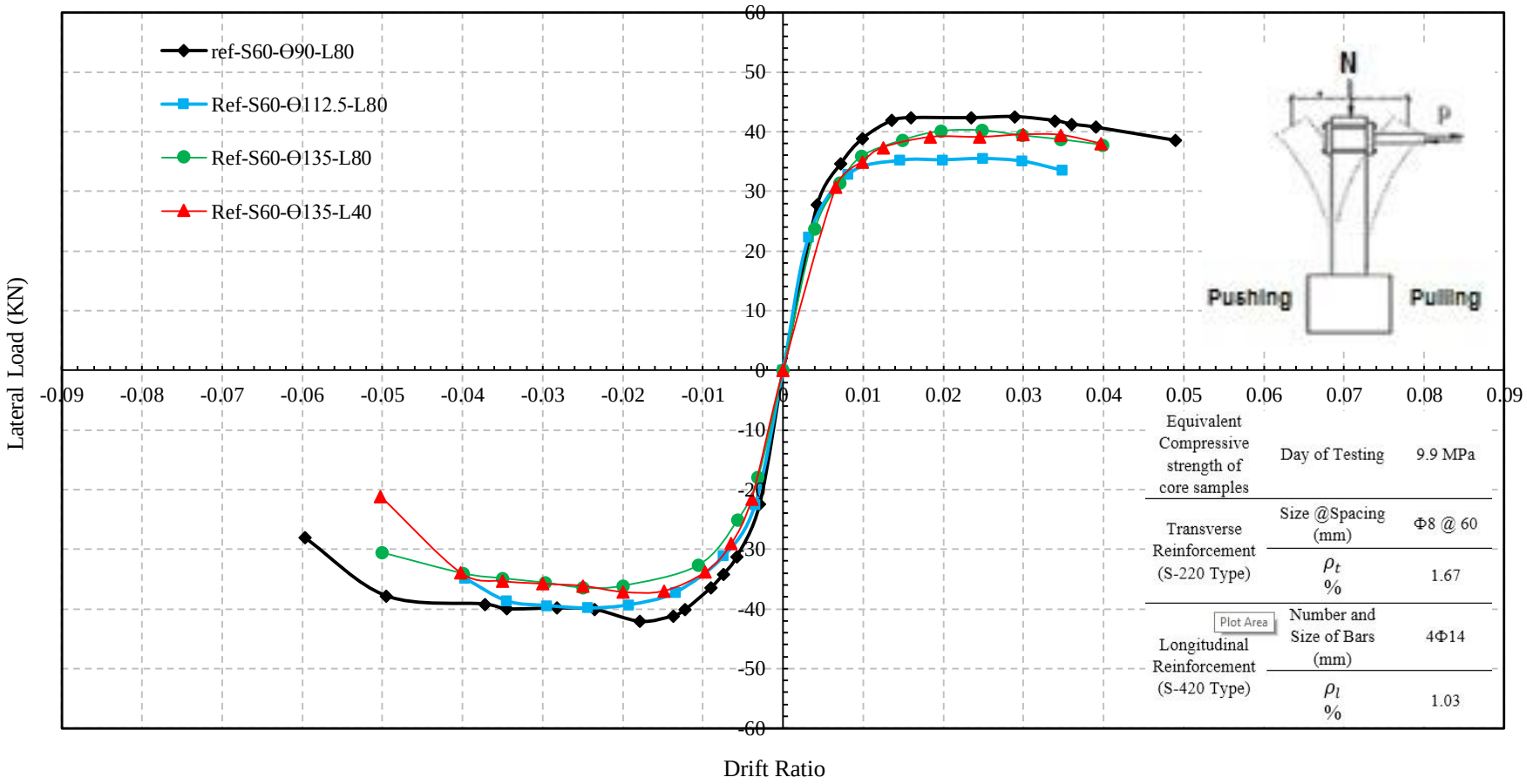

Figure 5.10 : The envelopes curves of the lateral load-drift for all reference specimens.

It is obvious from the tables of the crack patterns (appendix A), the damages were accumulated especially in 50-400 mm height of the column from top of the foundation. In all specimens, it is observed that first flexural cracks were initiated at the column-foundation interfaces approximately in 0.004 of drift ratio and the longitudinal bars were yielded before concrete crushing due to high axial load, which applied as a constant load during the test.

5.7 Comparison of the All Retrofitted Specimens:

The envelopes of lateral load-drift curves for all retrofitted specimens are shown in Figure 5.11. As seen from mentioned figure, all retrofitted specimens with different hook angle/length performed so ductile behavior and dissipated a large amount of energy, especially the poor detailed specimens with 90° hook angle (Ret-S60-Ɵ90-L80-3TRM) and 40 mm hook length (Ret-S60-Ɵ135-L40-3TRM). As an important result, it observed that variations in angle and length of hooks in retrofitted specimens had no notable effect and almost all columns showed same behavior in terms of maximum lateral deflection, flexural strength, lateral stiffness and ductility of columns. It is obvious from the figures of the crack patterns (appendix A) the damage was accumulated especially in column-foundation interface and the place, which jacketing is ended at the code of 510-750 mm from top of foundation. Along with the mentioned code in all specimens, it was possible observation of flexural cracks, which were formed due to differences in stiffness of confined and unconfined parts of columns. After ending of test, the retrofitting jacket was separated from column's body by technicians to assess penetration of cracks to under layers of jacket and column's body. This work were done so difficult because of hardness of GRC composite materials. According to the results of jacket autopsy after the tests, it was observed there was no cracks on columns body which was covered by jacketing system. There were only some cracks close to column-foundation interface on column's body. The exterior vertical cracks, which observed on the jacket surface did not deeply propagate into the mortar. Besides, no rupturing of basalt fibers were observed during the tests. Tests were ended due to use of maximum capacity of top LVDT that was measuring top displacement of column during the test. It is clear that this method of confining is acceptable for retrofitting of low strength concrete columns to improve the seismic behavior of structural elements and let the structure to have more lateral displacement with fewer damages.

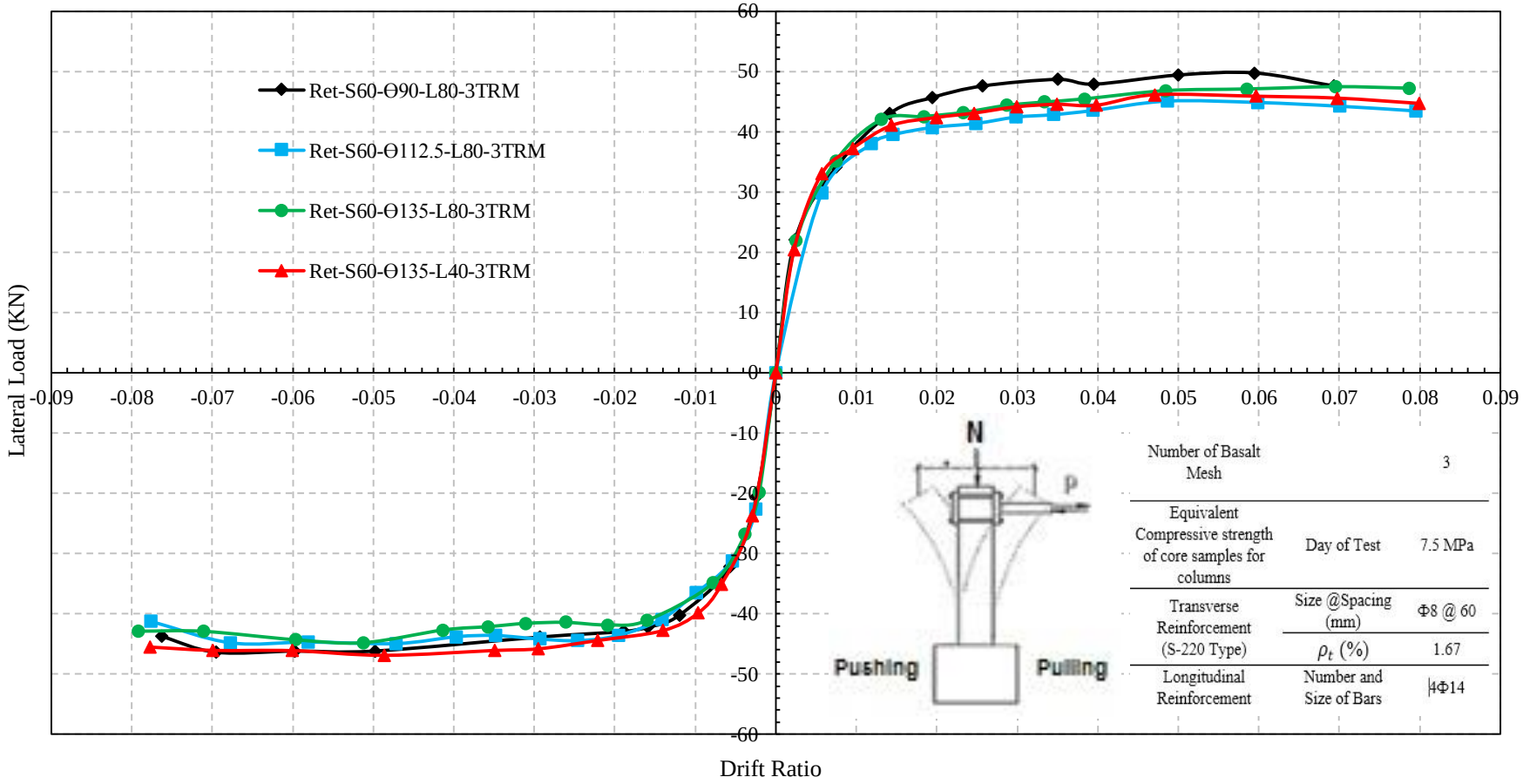

Number of Basalt Mesh		3
Equivalent Compressive strength of core samples for columns	Day of Test	7.5 MPa
Transverse Reinforcement (S-220 Type)	Size @Spacing (mm)	Φ8 @ 60
	ρ_t (%)	1.67
Longitudinal Reinforcement	Number and Size of Bars	4Φ14

Figures 5.11 : Envelopes of the lateral load-drift curves for all retrofitted specimen.

5.8 Reference Specimen versus Retrofitted Specimen

For comparing the test results of reference specimens versus retrofitted specimens, envelope curves are given in Figures 5.12 and 5.13. In these Figures, the lateral load values of the specimens were normalized by dividing the experimental lateral loads to the theoretical lateral load of specimens, which was taken from XTRACT structural engineering software. Through this normalization, the effects of low difference in concrete compressive strength of specimens was taken into account and a fair comparison was possible between the performance of the specimens.

According to the envelope curves of test results, it is obvious that the confining system, which was applied in this experimental study, had a large positive effect on flexural behavior of the low strength concrete columns.

A small stirrup spacing leads confinement system to be more efficient in RC columns. External confinement of the columns at the plastic hinge zone leaded the columns to use maximum flexural strength capacity during the large deformations.

According to the test observations, there were very little damages in retrofitted specimens. As shown in Figure 5.12 and 5.13, although a high axial load on the retrofitted columns during the tests, the proposed retrofitting technique increased the displacement ductility of sub-standard columns (the displacement ductility factor was between 6-8 for retrofitted specimens).

According to the results of all retrofitted specimens, it can be noted that BTRM jacketing causes an increment of 25 % in flexural strength. Meanwhile, the lateral stiffness of all retrofitted specimens increased a little by applying of this method. It is appeared that the increment in displacement ductility is mainly provided only by the confinement effect of basalt mesh reinforcement in absence of effect of GRC, whereas the increment in flexural strength and lateral stiffness is obtained based on the complete contribution of BTRM jacket. Furthermore, the application of mentioned strengthening method reduced tip residual plastic deformation at 2.5% of drift ratio (optional limitation for comparison of specimens at the zero lateral load) between 22-72 %. Besides, the reduced residual lateral displacement and corresponding reduced damage are probably due to elastic behavior of Glass fibers of the jacket.

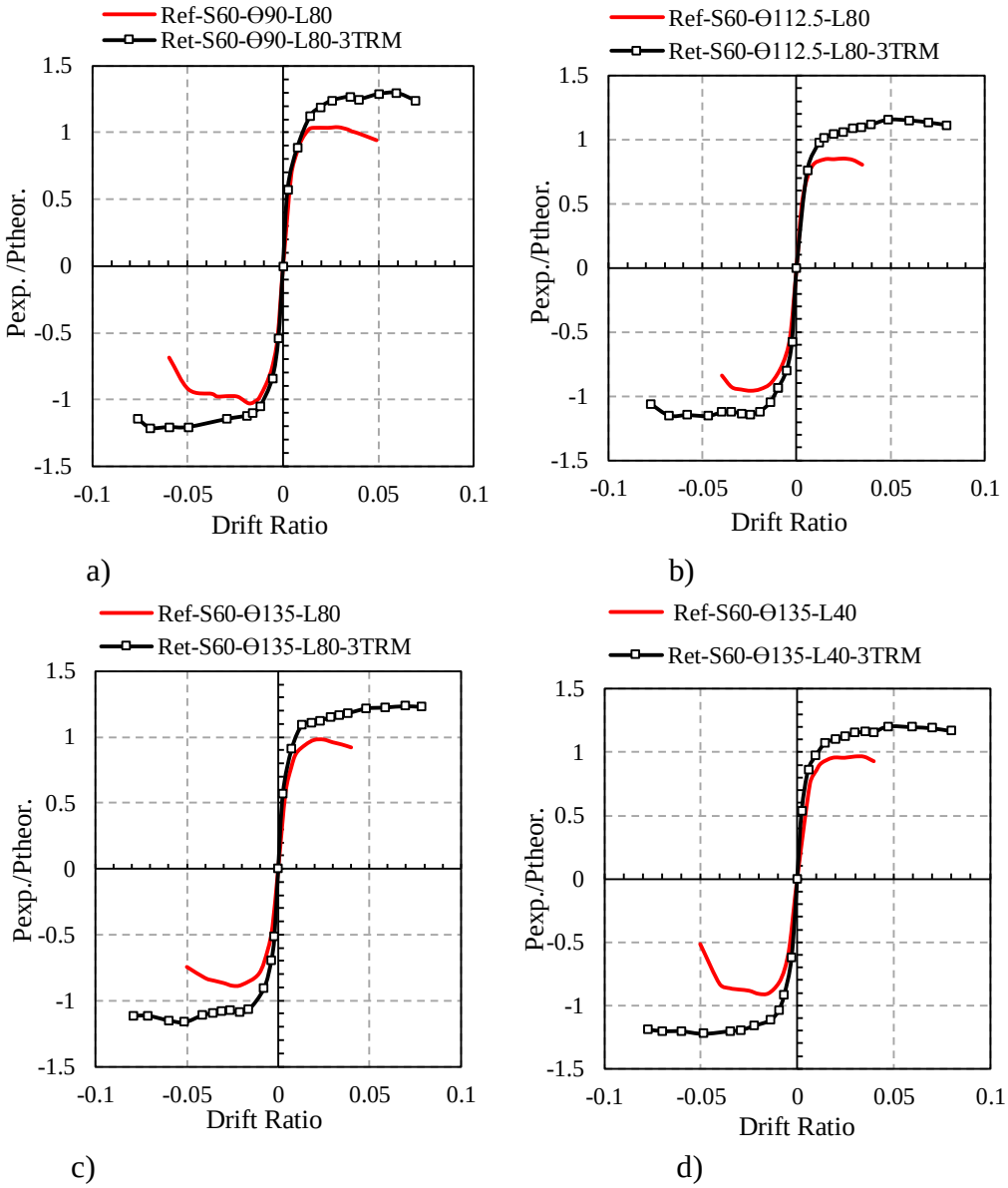

Figure 5.12 : The envelope curves of test results. a)Ref-S60-Θ90-L80 versus Ret-S60-Θ90-L80-3TRM. b)Ref-S60-Θ112.5-L80 versus Ret-S60-Θ112.5-L80-3TRM. c)Ref-S60-Θ135-L80 versus Ret-S60-Θ135-L80-3TRM. d)Ref-S60-Θ135-L40 versus Ret-S60-Θ135-L40-3TRM.

Unfortunately, due to the limited time for doing further tests for investigating of the new material's properties, it could not be assessed the contribution of basalt mesh reinforced with GRC jacketing system and the seismic performance of retrofitted columns more clearly. Then, the analytical work is under progress to assess this aim for reaching results that are more general. As illustrated in Figures 5.12.b and c, the amount of the flexural strength of the reference columns were not equal in pulling and pushing motions due to application of asymmetric axial load.

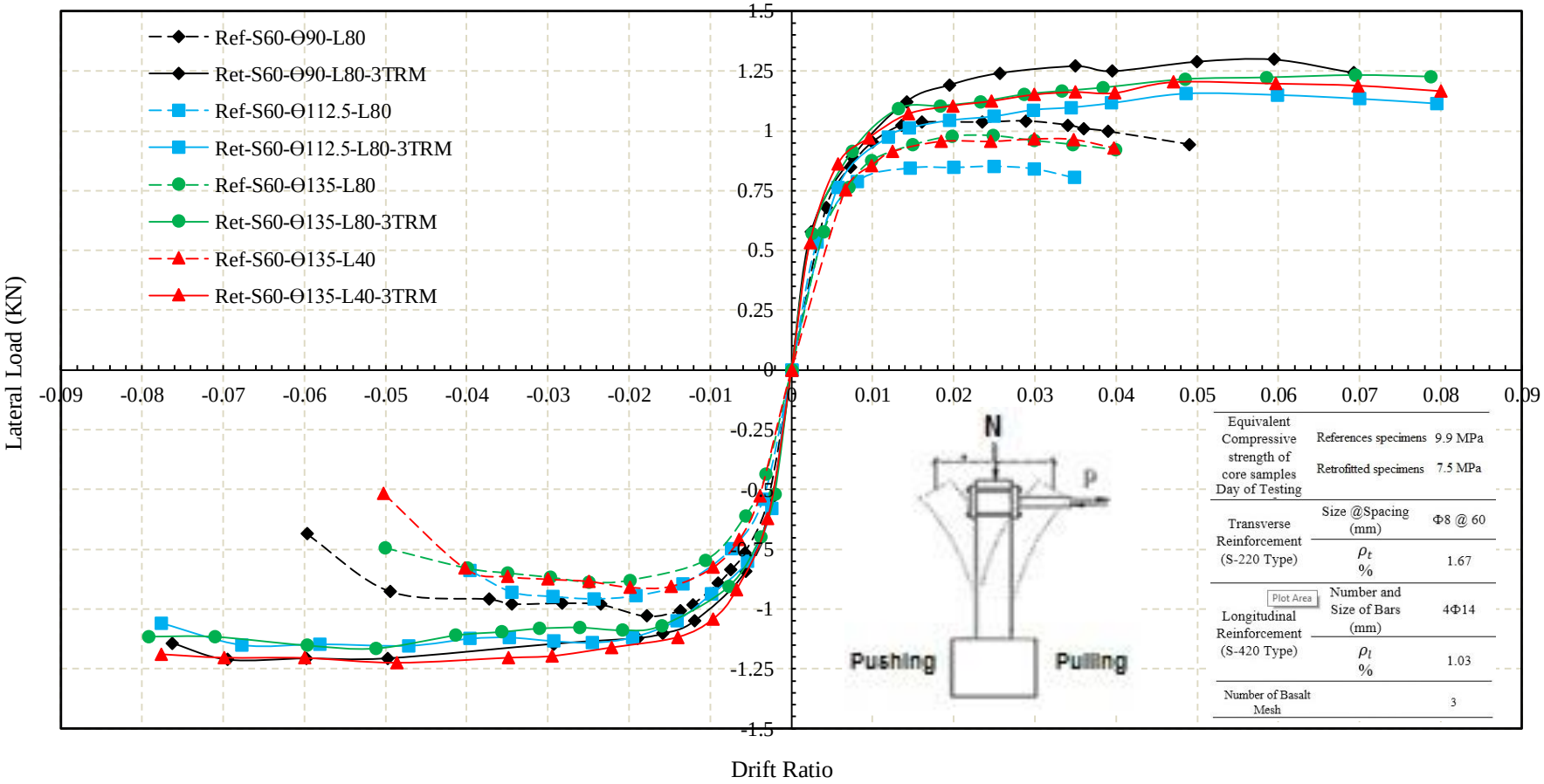

Figures 5.13 : Envelopes of the lateral load-drift curves for all reference and retrofitted specimens.

On the other hand, low quality of the concrete at the damaged section could become other reason for. During testing process of these two specimens, the load was applied 3~4 mm out of section center parallel with actuator axis. Then, during the cyclic loading, much compression force was concentrated in one side to the other side. Therefore, the compression zone reached to the maximum carrying load capacity earlier. In case of cyclic loading, it is obvious that the improvement in ductility is more efficient. Then, it is possible to change the brittle behavior of the column by new textile materials and externally confining techniques that has enormous effects on ductile behavior of low strength concrete columns.

5.9 Theoretical Results versus Experimental Test Results

For obtaining analytical lateral load-tip displacement relationships of the columns, the elastic and plastic components of the top displacement of the column ($\delta_{elastic}$ and $\delta_{plastic}$) are calculated by Eq. (5.1) and (5.4) as seen at the Figure 5.14. By using of XTRACT (structural engineering software-2007 version), the moment-curvature relationship is obtained. The moment is converted to lateral load by dividing to the effective column height. The effective column height is equal with the distance between applied lateral load at the top of foundation until the half of plastic hinge location. Plastic hinge length is assumed h/2 as proposed by Turkish Seismic Code (2007), where *h* represents the effective depth of cross-section of column in bending.

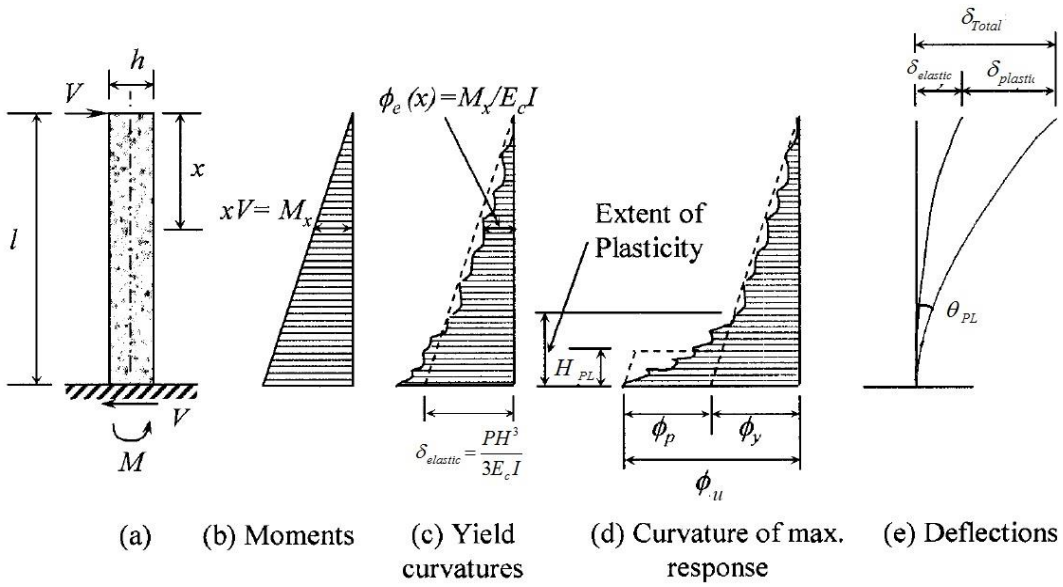

Figure 5.14 : Moment, curvature and deflection relationship for a prismatic RC cantilever (M.J.N. Priestly, F.Seible and G.M. Calvi).

$$\delta_{elastic} = \frac{PH^3}{3E_c I} \tag{5.1}$$

$$\theta_{PL} = X_{PL} . H_{PL} \tag{5.2}$$

$$\delta_{Plastic} = \theta_{PL} . H \tag{5.3}$$

$$\delta_{Total} = \delta_{elastic} + \delta_{plastic} \tag{5.4}$$

In these equations, H (mm) is the height of the column. θ_{PL} is the plastic rotation of the assumed plastic hinge. X_{PL} is the average plastic curvature assumed to be uniformly distributed over the assumed plastic hinge length, E_c (MPa) is the elasticity modulus of concrete, f_{ck} (MPa) is the characteristic compressive strength of concrete, $\delta_{elastic}$ (mm) is the elastic contribution to the total top displacement at ultimate lateral load. P (kN) is the lateral load. I (mm4) is the moment of inertia of the member, H_{PL} (mm) is the plastic hinge length of the column and $\delta_{plastic}$ is the plastic contribution to the total top displacement at ultimate lateral load (mm).

The theoretical and experimental result of lateral load-tip displacement relationships for reference specimens are compared in Figures (5.15) to (5.18).

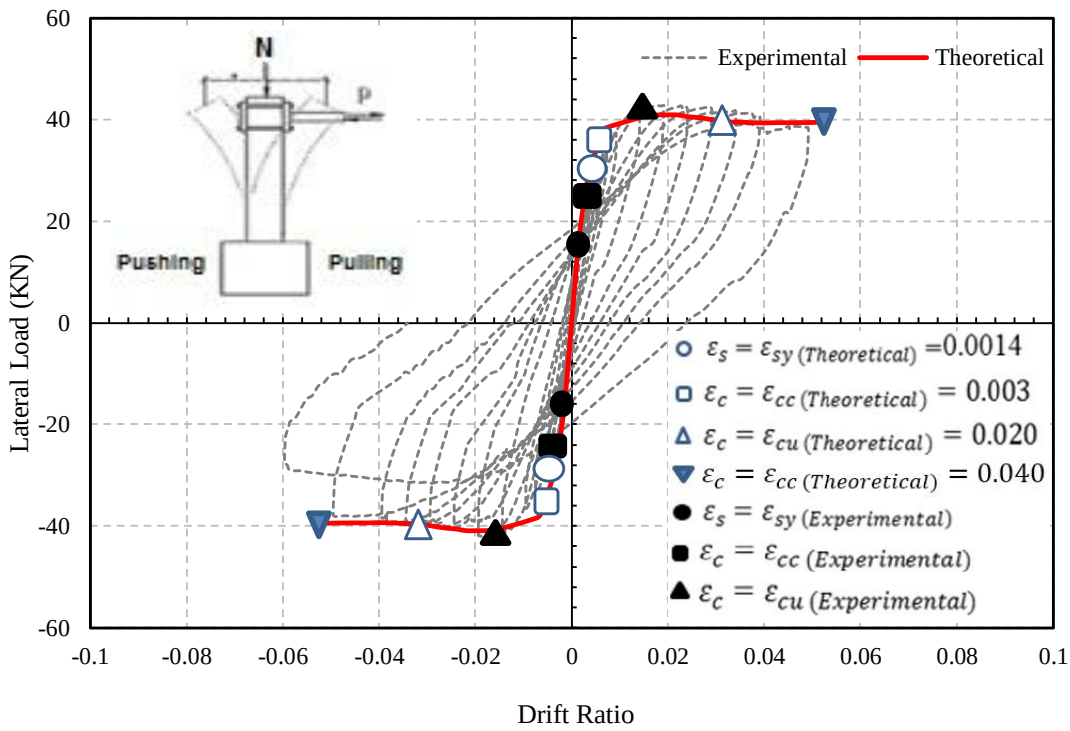

Figure 5.15 : Theoretical result versus test results Ref-S60-Θ90-L80.

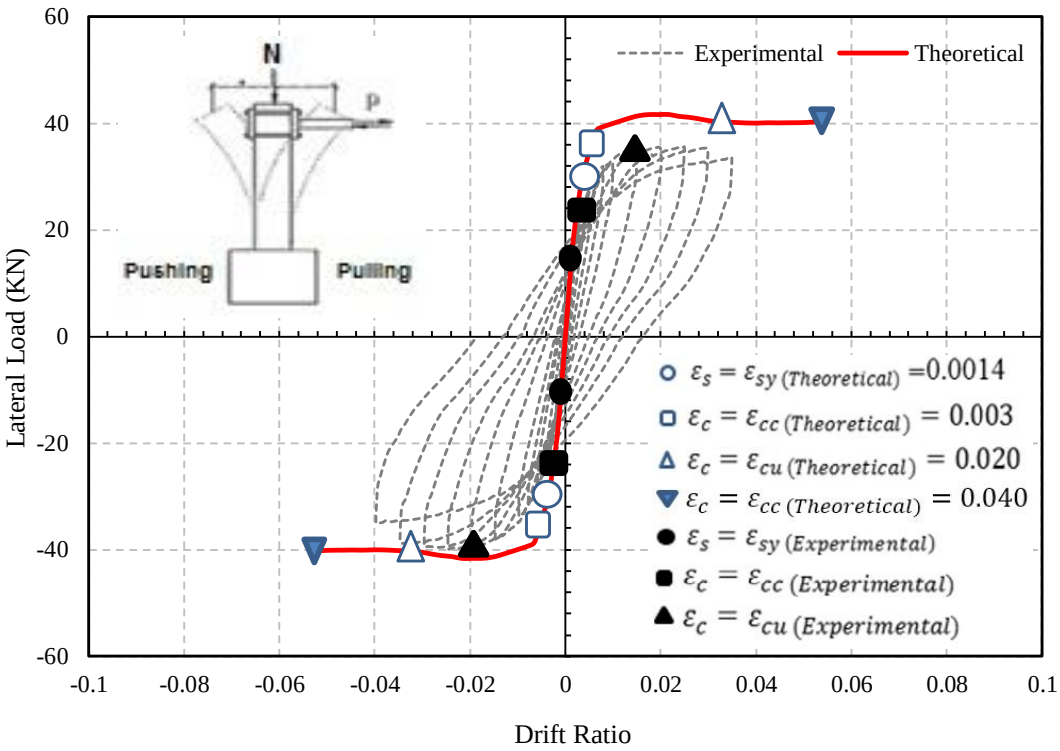

Figure 5.16 : Theoretical result versus test results Ref-S60-Θ112.5-L80.

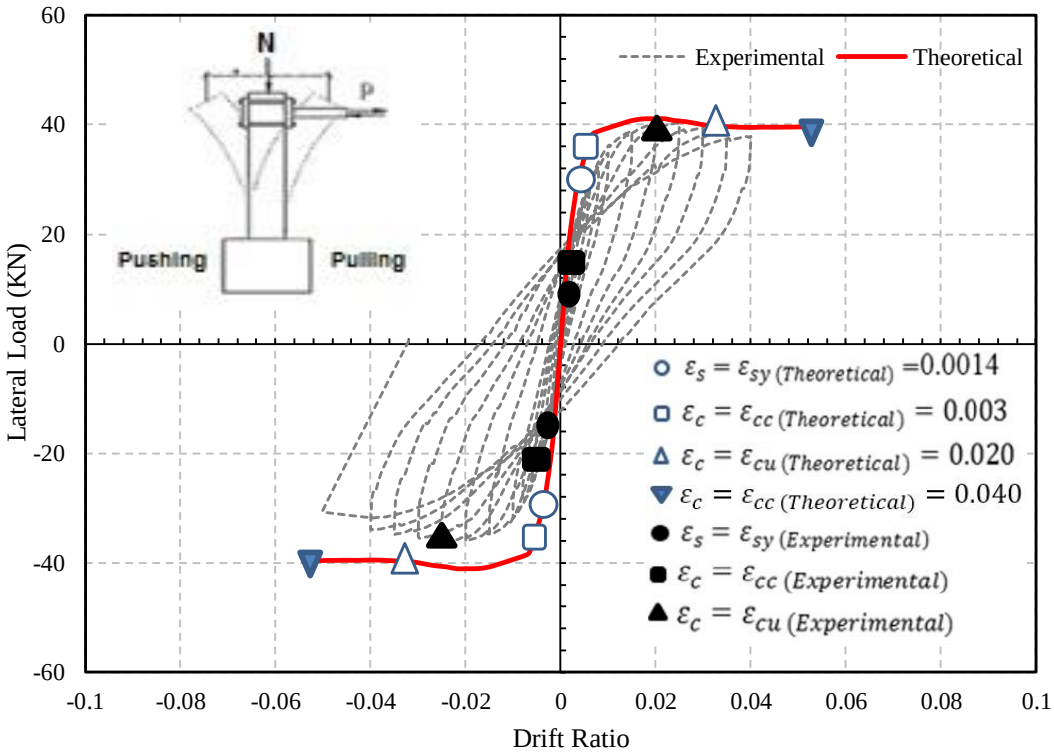

Figure 5.17 : Theoretical result versus test results Ref-S60-Θ135-L80.

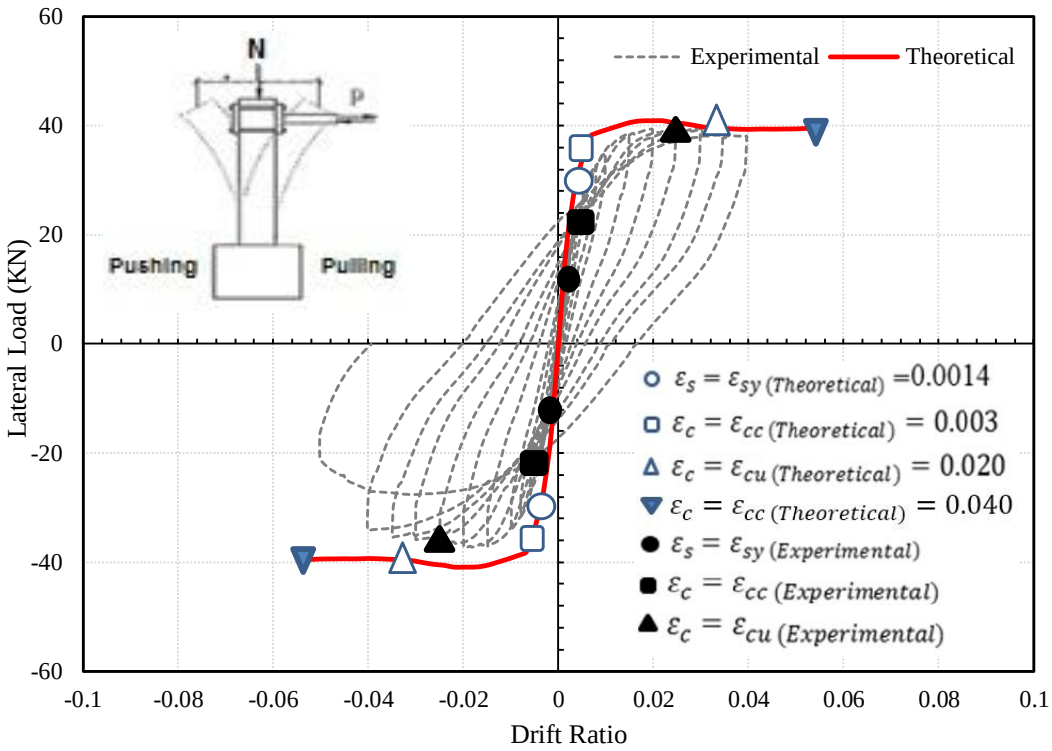

Figure 5.18 : Theoretical result versus test results Ref-S60-Θ135-L40.

As seen from Figures (5.15) to (5.18), there was a good agreement between the experimental results and predicted overall lateral force-tip displacement relationships. It is important to noted that, theoretical results should be calculated by ultimate strain of 0.02 for concrete cover, but for obtaining an idea about the behavior of specimen, the ultimate strain of concrete cover was assumed 0.04. The theoretical and experimental load displacement relationships for retrofitted specimens are compared in Figures (5.15) to (5.18).

As mentioned before, studies on the use of textiles for upgrading of concrete structures have been limited in literature and a small amount of tests have been conducted in this study to investigate the behavior of rectangular columns retrofitted with basalt mesh sprayed with GRC composites. It is clear that further tests should be carried out to determine confirmation of the GFRC effects on flexural strength of RC columns. As seen from Figures (5.19) to (5.22), the theoretical and experimental lateral force-tip displacement relationships are compared and there was a good agreement between the experimentally measured and predicted overall lateral force-displacements. It is important to noted that, in retrofitted specimens, there were no major rupture in BTRM jackets. On the other hand, all the differences between experimental and theoretical ultimate compressive strain and flexural strength comes from the effect of GFRC.

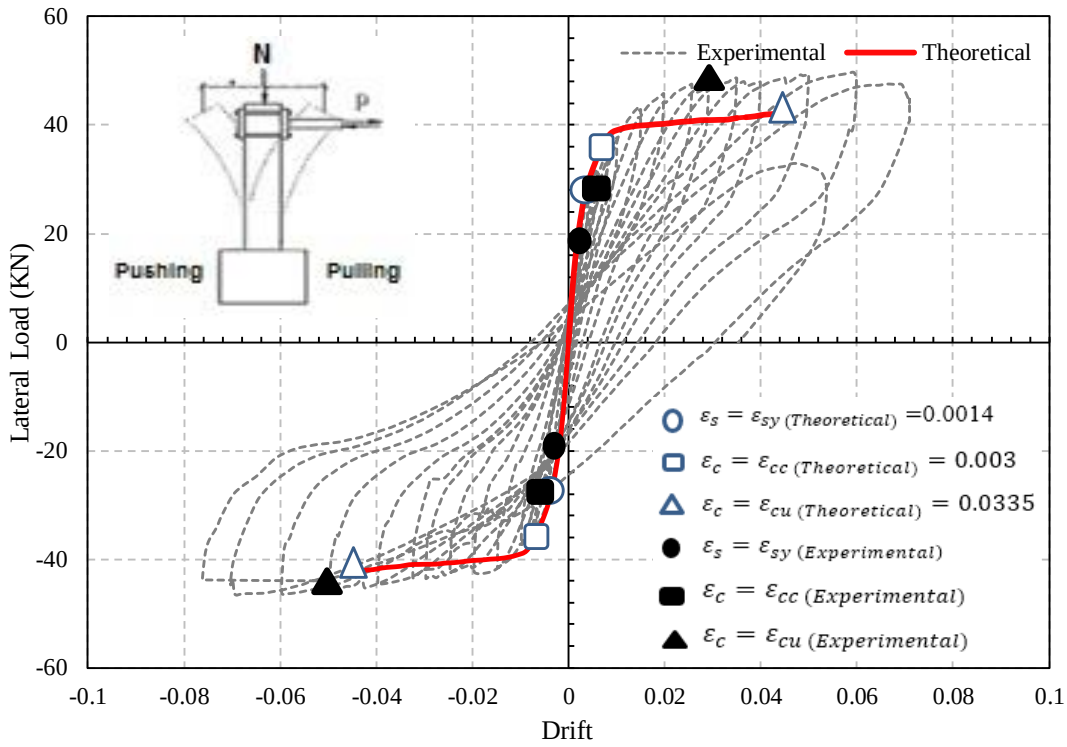

Figure 5.19 : Theoretical result and experimental result of Ret-S60-Θ90-L80-3TRM.

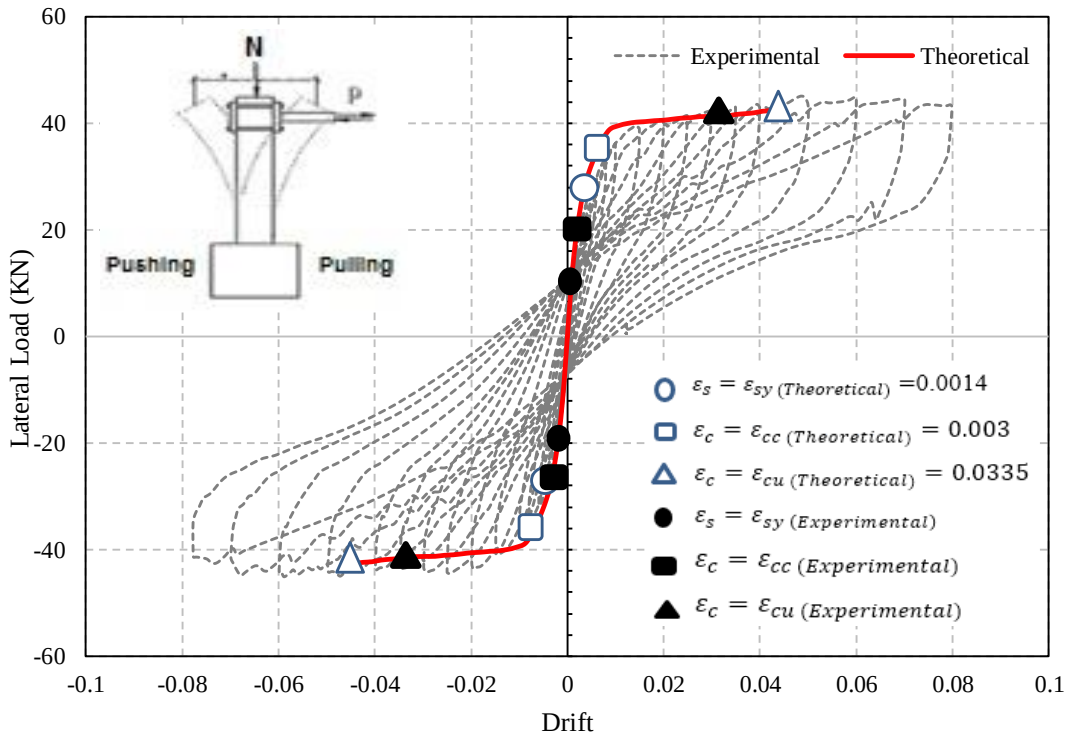

Figure 5.20 : Theoretical results and experimental results of Ret-S60-Θ112.5-L80-3TRM.

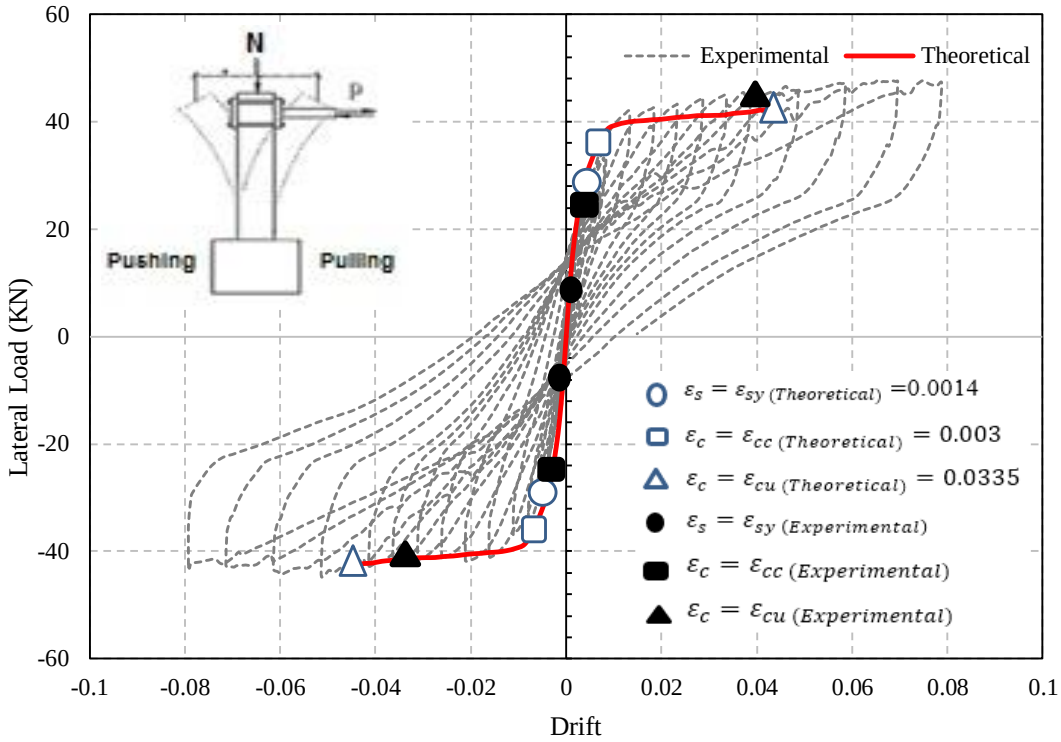

Figure 5.21: Theoretical results versus experimental results of Ret-S60-Θ135-L80-3TRM.

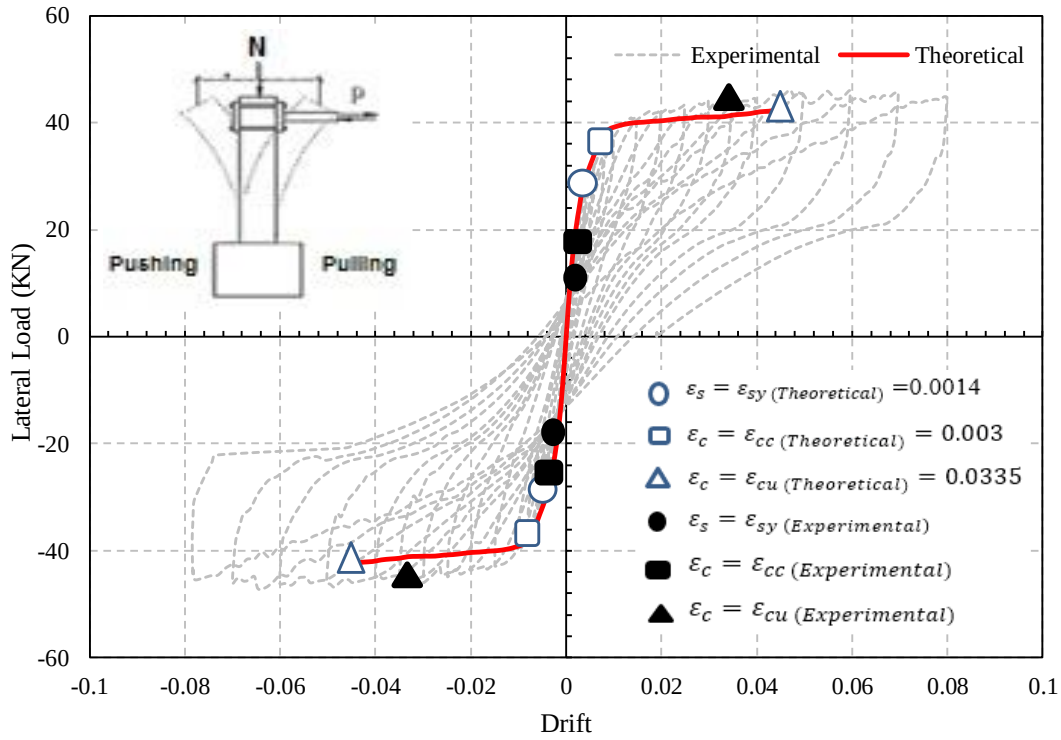

Figure 5.22 : Theoretical results versus experimental results of Ret-S60-Θ135-L40-3TRM.

Akgün (2005) studied the effect of retrofitting of the low strength concrete members with composite panels. In this study, all specimens were subjected to compression load and results showed that flexural strength were increased in all specimens but there were no significant improvement in ductility. By considering this, in our experimental study, GFRC caused to improve the flexural strength, but by increasing the strain, cracks occurred and basalt textile mesh start to carrying the lateral confinement loads up to rupture of textile meshes. In another experimental study, Yilmaz (2004), investigated the effect of retrofitting of pre-cast concrete columns with fiber-reinforced steel. All specimens were tested under constant axial load and cyclic lateral load and test results illustrated the increment of strength and ductility by additionally mounting the peace of steel in columns corners that were retrofitted by fiber-reinforced steel. By considering this, in our specimens, basalt textile reinforced GFRC were used for retrofitting and same behavior was observed during the all retrofitted specimens.

6. CONCLUSIONS AND RECOMMENDATIONS

This study investigated the effect of angle/length of hooks on seismic behavior of the externally confined and ordinary reinforced concrete columns. External confinement was applied by means of basalt mesh reinforced sprayed GRC. The research was conducted in six main phases: design and construction of specimens, design and application of seismic retrofitting, tests on determination of characteristics of retrofitting material, experimental testing and evaluation of test results and analytical considerations. The seismic performance of four ordinary and four externally confined full-scale column specimens are studied in this thesis. Specimens were tested under constant high axial load and reversed cyclic lateral loads. All specimens were constructed using low strength concrete and plain reinforcing bars. The following are the major conclusions that can be drawn from this study:

- The performances of all columns were studied through their flexural strength, deformation capacity, moment-curvature relationships of critical sections, energy dissipation, failure mechanism and strain distribution along longitudinal and transverse reinforcement bars.
- In all reference specimens, tests were continued until losing 15% of maximum load carrying capacity except Ref-S60-Ɵ90-L80 and Ref-S60-Ɵ135-L40. In these mentioned specimens, tests were stopped due to bar buckling and specimens lost 33% and 45% of maximum load carrying capacity in pushing direction, respectively.
- Interestingly and unexpectedly, the hook angle was not significantly effective on the reversed cyclic lateral performance of columns in terms of strength and ductility up to the drift ratio of 4%.
- The proposed method (basalt fiber mesh reinforced sprayed GRC jacketing) proved to be a feasible and effective alternative for seismic retrofitting of reinforced concrete columns. Through the use of proposed method for seismic

retrofit of columns, various disadvantages of using epoxy based adhesives (such as high cost, health hazards to workers, poor performance at elevated temperatures, etc.) while strengthening columns with different types of fiber products (carbon, glass, aramid, etc.) can be avoided.

- After external confinement with basalt mesh reinforced sprayed GRC, all retrofitted specimens were able to use their maximum flexural capacities. They presented a significant improvement in ductility and dissipation of energy independent of length/angle of hooks. The retrofitted columns could sustain lateral loads without a significant loss in strength up to lateral drifts of 7-8%.
- The observed responses of all retrofitted specimens were generally identical. Only minor cracking of jacket was observed during the tests and no horizontal cracks were visible on the jackets. According to the results of jacket autopsy after the tests, there was no cracks on the potential plastic hinge part of the column, which was covered by jacketing system. There were only some cracks close to column-foundation interface. The exterior vertical cracks, which were observed on the jacket surface, did not deeply propagate into the mortar. Besides, no rupturing of basalt fibers were observed during the tests.
- Another important outcome of this study is the remarkable reduction of residual displacement, deformations and damage at the end of the loading for the retrofitted specimens. Normally, when a retrofit intervention is made through external FRP jacketing, only ductility is improved with an accompanying increase in damage and residual deformations. Therefore, the proposed technique may be a retrofit option not only for prevention of collapse, but also for other performance targets such as immediate occupancy or life safety.
- Further investigation is necessary for determining characteristics of potential plastic hinges of columns retrofitted with the proposed technique.

6.1 Recommendation for Future Research

Based on research conducted in this study, there are related areas which appear to be of interest for further study. The current investigation consisted of eight full scale columns under constant high axial load and reversed cyclic loading. Therefore, a large volume of test data was produced. However, because the field of introduced retrofitting

method has little previous research conducted in the area, additional tests are recommended. Some of the recommendations for future point of research are:

- Tests of columns with different layers of basalt for retrofitting.
- Tests of columns with circular and square sections (different aspect ratios).
- Tests of columns with different percentage of glass fibers in GRC.
- Columns under concentric loading to establish the buckling length of bars between transverse reinforcement.
- Tests of columns with higher percentage of longitudinal reinforcement.
- Tests of columns with different stirrup spacing.
- Tests of columns with lap-sliced longitudinal reinforcement in the potential plastic hinge zone.
- Investigation of the environmental effects such as freeze and thaw, temperature variation and moisture.
- Development of new empirical design expression for shear resistance of concrete in GRC sprayed concrete columns.
- Development of new empirical design expression for determining of plastic hinge place in GRC sprayed concrete columns.
- Development of over-strength and ductility factors for sprayed basalt mesh reinforced GRC for seismic design.

REFERENCES

ABYYHY (1975), "Afet Bölgelerinde Yapılacak Yapılar Hakkında Yönetmelik," *Turkish Earthquake Code,* Ankara, Turkey.

Akgün D. (2005). Kompozit Panellerle Güçlendirilmiş Düşük Dayanımlı Beton Elemanlar, *MSc Thesis*, Istanbul Technical University, Istanbul, Turkey.

Bayrak, O., and Sheikh, Sh.A. (2004). Seismic Performance of High Strength Concrete ColumnsConfined with High Strength Steel, *13th World Conference on Earthquake Engineering*, Paper No 1181, Vancouver, B.C., Canada. 1-6 August.

Bournas, D. A., Triantafillou, T. C., Zygouris, K., and Stavropoulos, F. (2009). Textile-reinforced mortar versus FRP jacketing in seismic retrofitting of RC columns with continuous or lap-spliced deformed bars. Journal of Composites for Construction, Vol. 13(5), pp. 360-371.

Colajanni, P., De Domenico, F., Recupero, A., and Spinella, N. (2014). Concrete columns confined with fibre reinforced cementitious mortars: Experimentation and modelling. Construction and Building Materials, Vol. 52, pp. 375-384.

DBHBHY (2007), "Deprem Bölgelerinde Yapılacak Binalar Hakkında Yönetmelik," *Turkish Earthquake Code,* Ankara, Turkey.

Di Ludovico, M., Prota, A., Manfredi, G., and Cosenza, E. (2008). Seismic strengthening of an under-designed RC structure with FRP. Earthquake Engineering & Structural Dynamics, Vol. 37(1), pp. 141-162.

Goksu, C. (2012). Seismic behavior of RC columns with corroded plain and deformed reinforcing bars, *PhD Thesis*, Istanbul Technical University, Istanbul, Turkey.

Ilki, A., Kumbasar, N., Koç, V.(2004). "Low strength concrete members externally confined with FRP sheets." Structural Engineering and Mechanics, 18(2), 1-28.

Ilki, A., Peker, O., Karamuk, E., Demir, C., and Kumbasar, N. (2008). "FRP Retrofit of Low and Medium Strength Circular and Rectangular Reinforced Concrete Columns." Journal of Materials in Civil Engineering, ASCE, 20(2), 169-188.

Issa, M. S., Metwally I. M., Elzeiny S. M. (2011). "Structural performance of eccentrically loaded GFRP Reinforced concrete columns." International Journal of Civil and Structural Engineering, 2(1), 395-406.

Liu, J. (2013). The Seismic Behaviour of Reinforced Concrete Columns, *PhD. Thesis*, Department of Civil Engineering, University of Toronto, Toronto, Canada.

Mander, J. B., Priestley, M. J. N., Park, R. (1988), "Theoretical Stress-strain Model for Confined Concrete," *ASCE Journal of Structural Engineering*, 114 (8), 1804-1826.

Mirmiran, A., Kim, S., Mertol, H. C., Rizkalla, S., and Zia, P. (2004). Behavior of High-Strength Concrete Rectangular Columns, *Seventh International Congress on Advances in Civil Engineering*, Yildiz Technical University, Istanbul, Turkey. 11-13 October.

Mirmiran, A., and Shahawy, M. (1997). "Behavior of Concrete Columns Confined by Fiber Composites." Journal of Structural Engineering, ASCE, 123(5), 583-590.

Saribas, I. (2013). Enine Donati Detaylarindaki Yetersizliklerin Betonarme Kolonlarin Eksenel Yükler Altindaki Performansina Etkisi, *MSc Thesis*, Istanbul Technical University, Istanbul, Turkey.

Sezen H. and Miller E.Z. (2011). Experimental evaluation of axial behavior of strengthened circular reinforced-concrete columns. Journal of Bridge Engineering, Vol. 16(2), pp. 238-247.

Spoelstra MR, Monti G. (1999). FRP-confined concrete model. ASCE Journal of composites for construction ;3(3):143–50.

TS500 (1984), "Requirements for Design and Construction of Reinforced Concrete Structures,"*Turkish Standards Institute,* Ankara, Turkey.

TS500 (2000), "Requirements for Design and Construction of Reinforced Concrete Structures,"*Turkish Standards Institute,* Ankara, Turkey.

Triantafillou T.C., Papanicolaou C.G., Zissimopoulos P., and Laourdekis T. (2006). "Concrete Confinement with Textile-Reinforced Mortar Jackets." ACI Structural Journal, 103(1), 28-38.

Triantafillou T.C., and Bournas D.A.(2009). "Flexural Strengthening of Reinforced Concrete Columns with Near-Surface-Mounted FRP or Stainless Steel." ACI Structural Journal, 106(4), 495-506.

XTRACT 3.0.8, (2007), "Cross-sectional Structural Analysis of Components," TRC.

Yilmaz E. (2004). Çelık Lif Takviyeli Öndöküm Beton Paneller ile Kolon Güçlendirmesi, *MSc Thesis*, Istanbul Technical University, Istanbul, Turkey.

APPENDICES

APPENDIX A: Test Observation's Summary.

Table A.1 : Summary of the seismic behavior of the Ref-S60-Ɵ90-L80.

Drift ratio (%)	Δ (mm)	P (kN)	Max Column-Foundation crack Width	Max Column-Foundation residual crack width	Observation
0.10	±1.29	8.7/-9.2	-	-	No crack was observed
0.20	±2.58	15.4/-15.9	-	-	No crack was observed

Drift ratio (%)	Δ (mm)	P (kN)	Max Column-Foundation crack Width	Max Column-Foundation residual crack width	Observation
0.40	±5.16	24.4/-24.2	-	-	No crack was observed
0.60	±7.74	31/-31	0.2	0	Initial flexural cracks were observed in column-foundation joint 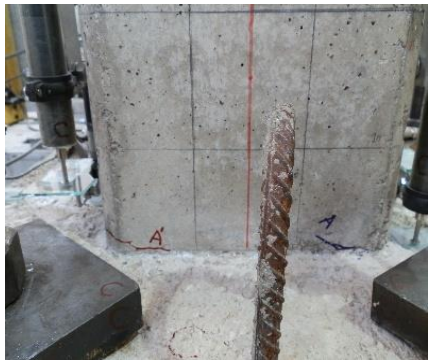

Drift ratio (%)	Δ (mm)	P (kN)	Max Column-Foundation crack Width	Max Column-Foundation residual crack width	Observation
0.80	±10.32	34/-34	0.5	0	Initial flexural cracks were observed in column surfaces and width of some previous cracks were increased
1.00	±12.9	36/-37	0.8	0	There were no new cracks, only width and length of some previous cracks were increased

Drift ratio (%)	Δ (mm)	P (kN)	Max Column-Foundation crack Width	Max Column-Foundation residual crack width	Observation
1.50	±19.35	41/-42	1.3	0.1	Width and length of some previous cracks were increased and for the first time, concrete-crushing were observed 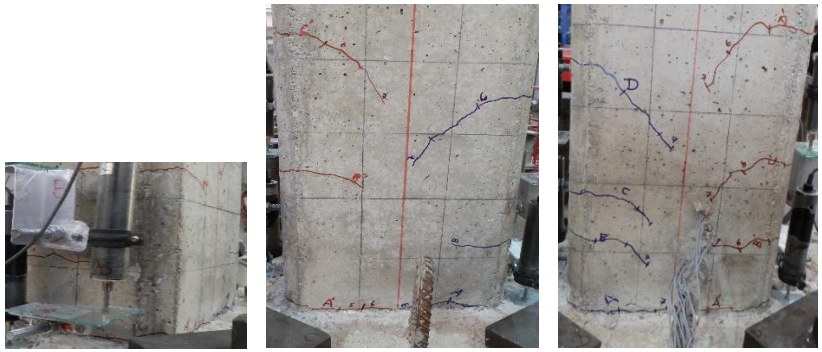
2.00	±25.8	42/-43	1.4	0.3	Width and length of the previous cracks and concrete-crushing were increased vertical cracks at the corners were observed 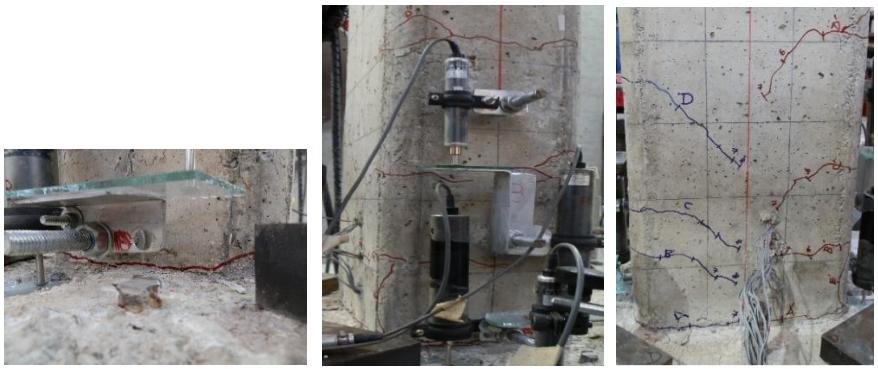

Drift ratio (%)	Δ (mm)	P (kN)	Max Column-Foundation crack Width	Max Column-Foundation residual crack width	Observation
2.50	±32.25	40/-42	1.6	0.4	Width and length of the previous cracks and concrete-crushing were increased vertical cracks at the corners were observed 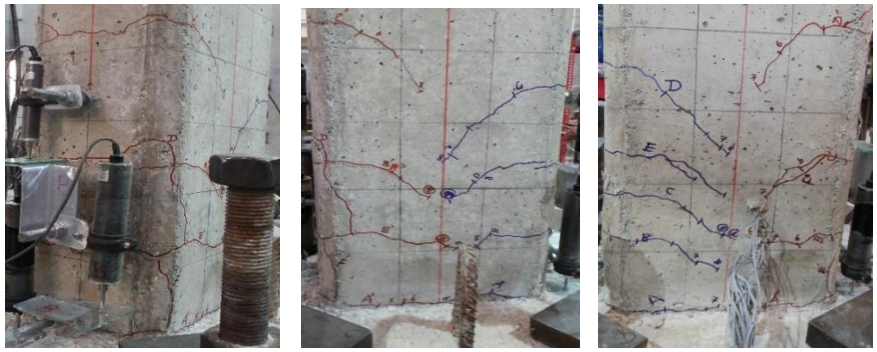
3.00	±38.7	39/-41	1.7	0.3	Width and length of some previous cracks and concrete-crushing and vertical cracks were increased. Concrete cover started to spall off at the column surfaces in compression zone

Drift ratio (%)	Δ (mm)	P (kN)	Max Column-Foundation crack Width	Max Column-Foundation residual crack width	Observation
3.50	±45.15	40/-41	Not measurable	Not measurable	Width of some previous cracks and concrete-crushing and vertical cracks were increased. Concrete cover were spalling off at the column surfaces in compression zone 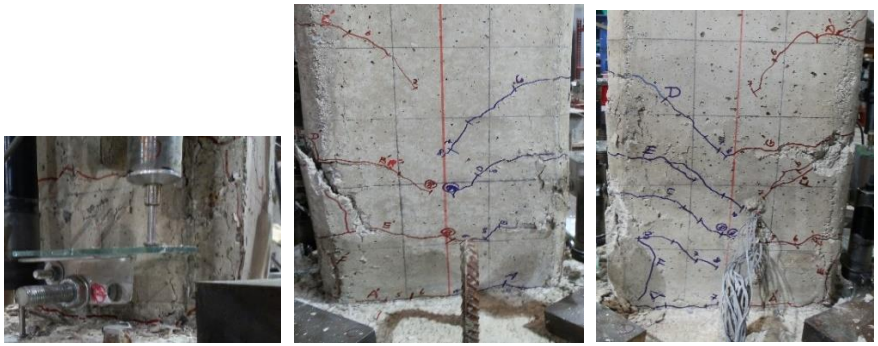
4.00	±51.6	39/-40	Not measurable	Not measurable	Significant amount of concrete cover were spalled off at plastic hinge zone Two stirrups were observed at the B-C corner

Drift ratio (%)	Δ (mm)	P (kN)	Max Column-Foundation crack Width	Max Column-Foundation residual crack width	Observation
5.00	±64.5	38/-38	Not measurable	Not measurable	Significant amount of concrete cover were spalled off at plastic hinge zone Stirrups and longitudinal bars were observed in plastic hinge zone 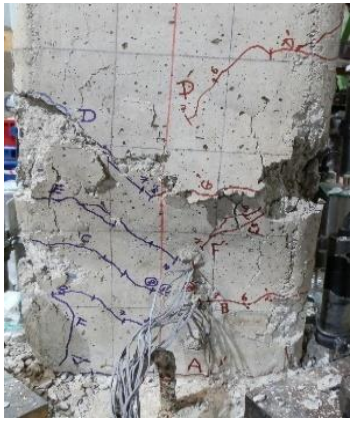 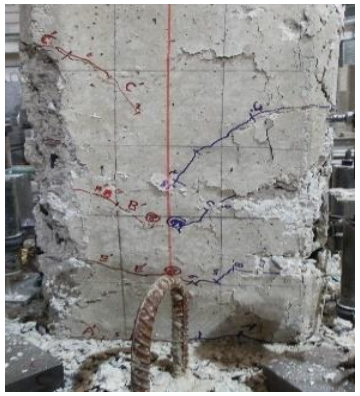 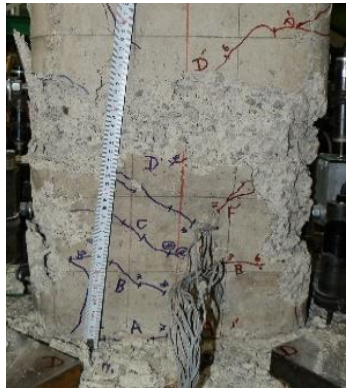

Drift ratio (%)	Δ (mm)	P (kN)	Max Column-Foundation crack Width	Max Column-Foundation residual crack width	Observation
6.00	±77.4	28	Not measurable	Not measurable	Test was ended by buckling of the longitudinal bars and losing 33% of Lateral load capacity 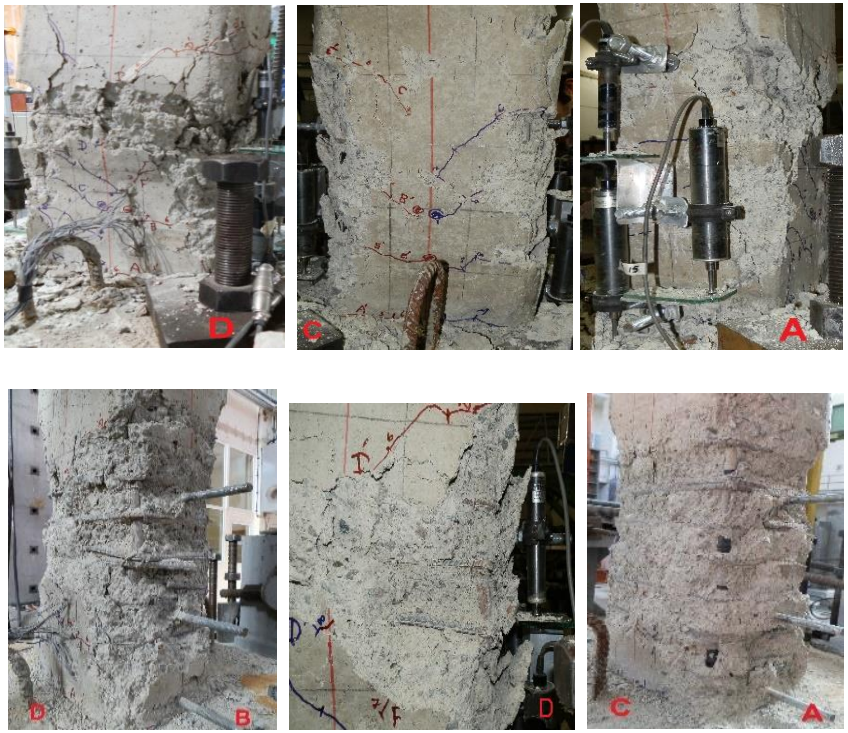

Table A.2 : Summary of the seismic behavior of the Ref-S60-Ɵ112.5-L80.

Drift ratio (%)	Δ (mm)	P (kN)	Max Column-Foundation crack width	Max Column-Foundation residual crack width	Observation
0.10	±1.269	8/-9	-	-	No crack was observed
0.20	±2.538	14 /-15	-	-	Initial flexural crack at the column-Foundation joint were observed (pulling side)

Drift ratio (%)	Δ (mm)	P (kN)	Max Column-Foundation crack width	Max Column-Foundation residual crack width	Observation
0.40	±5.076	23/-24	0.1	0	Initial flexural crack at the column-Foundation joint were observed (pushing side) width and length of some previous cracks were increased
0.60	±7.614	28/-29	0.3	0.1	Initial flexural cracks were observed in column surfaces Width and length of some previous cracks were increased 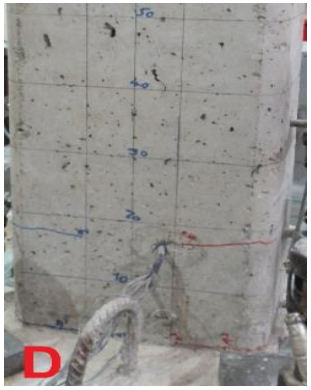

Drift ratio (%)	Δ (mm)	P (kN)	Max Column-Foundation crack width	Max Column-Foundation residual crack width	Observation
0.80	±10.152	31/-32	0.4	0.1	There were no new cracks, only width and length of some previous cracks were increased 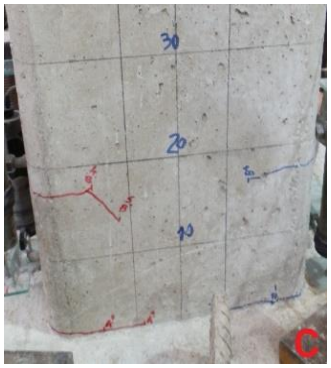 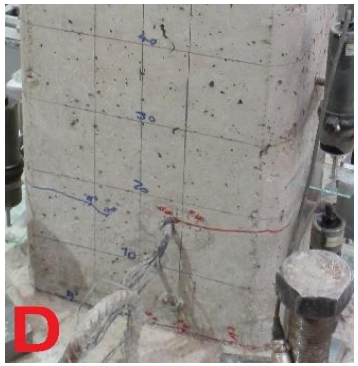
1.00	±12.69	33/-33	0.6	0.1	There were no new cracks, only width and length of some previous cracks were increased. For the first time vertical cracks were observed in column surfaces 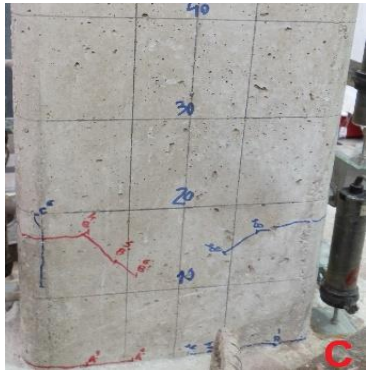

Drift ratio (%)	Δ (mm)	P (kN)	Max Column-Foundation crack width	Max Column-Foundation residual crack width	Observation
1.50	±19.035	38/-35	0.8	0.2	New flexural crack was observed in column surface and width and length of some previous cracks and concrete-crushing were increased propagation of some cracks were observed in column surface Initial vertical cracks were observed at the corners of column 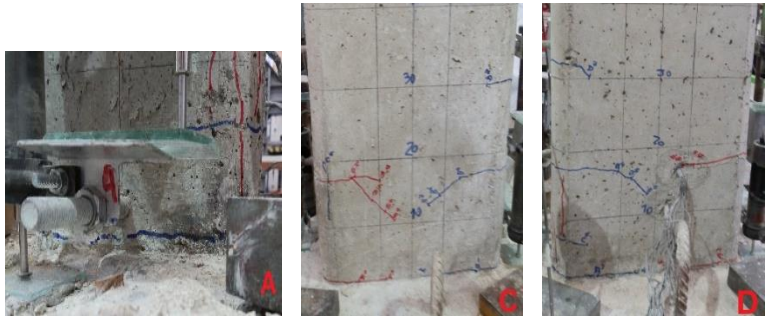
2.00	±25.38	39/-36	1	0.3	New flexural crack was observed in column surfaces width and length of some previous cracks and concrete-crushing and vertical cracks were increased

Drift ratio (%)	Δ (mm)	P (kN)	Max Column-Foundation crack width	Max Column-Foundation residual crack width	Observation
2.50	±31.725	40/-36	1	0.4	Width and length of some previous cracks and concrete-crushing were increased For the first time spalling of the concrete cover were observed
3.00	±38.07	39/-35	0.9	0.3	New flexural cracks were observed in column surface and width and length of some previous cracks and concrete-crushing were increased Concrete cover spalled off at the column surfaces in compression zone 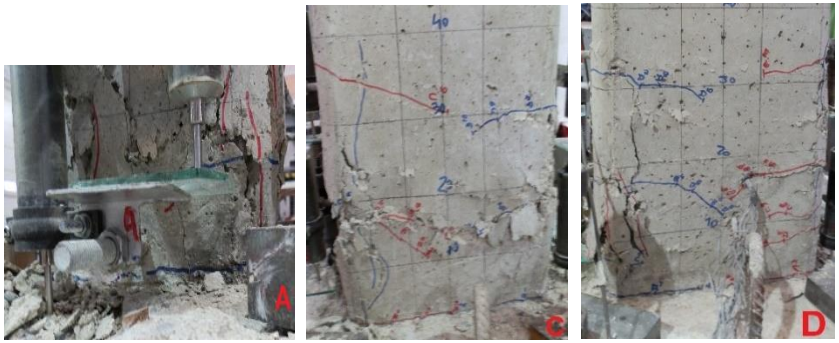

Drift ratio (%)	Δ (mm)	P (kN)	Max Column-Foundation crack width	Max Column-Foundation residual crack width	Observation
3.50	±44.415	38/-34	Not measurable	Not measurable	Significant amount of cover concrete were spalled off at the plastic hinge zone Stirrups and longitudinal bars were observed in plastic hinge zone 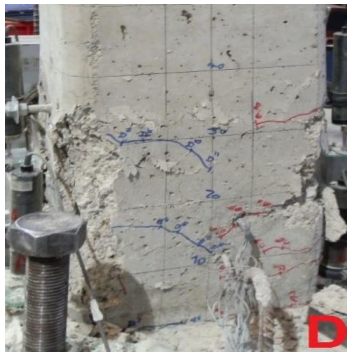

Drift ratio (%)	Δ (mm)	P (kN)	Max Column-Foundation crack width	Max Column-Foundation residual crack width	Observation
4.00	50.76	34	Not measurable	Not measurable	Test was ended by losing 15% of Lateral load capacity (Prepared for retrofitting) 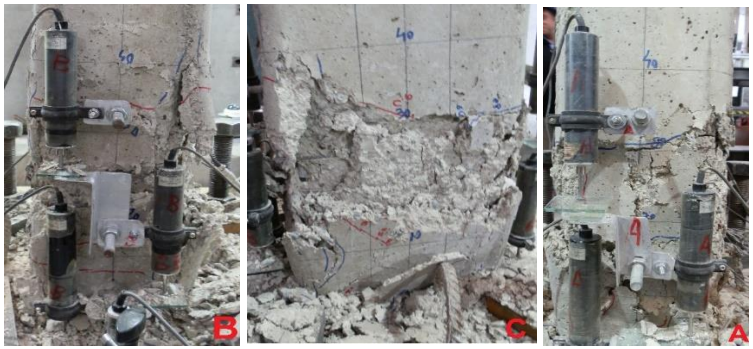

Table A.3 : Summary of the seismic behavior of the Ref-S60-Ɵ135-L80.

Drift ratio (%)	Δ (mm)	P (kN)	Max Column-Foundation crack thikness	Max Column-Foundation residual crack thikness	Observation
0.10	±1.285	7/-9	-	-	No crack was observed 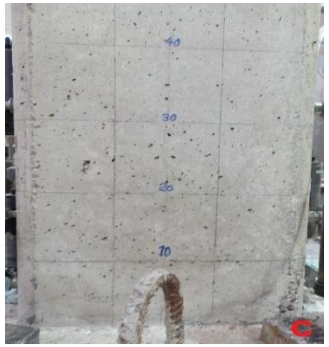 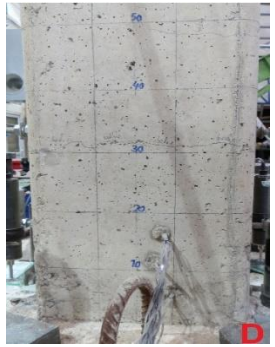
0.20	±2.57	14/-15	-	-	No crack was observed 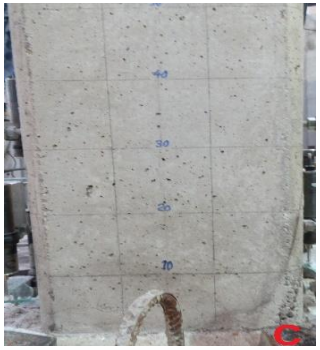

Drift ratio (%)	Δ (mm)	P (kN)	Max Column-Foundation crack thikness	Max Column-Foundation residual crack thikness	Observation
0.40	±5.14	22/-22	0.1	0	Initial flexural cracks were observed in column-foundation joint 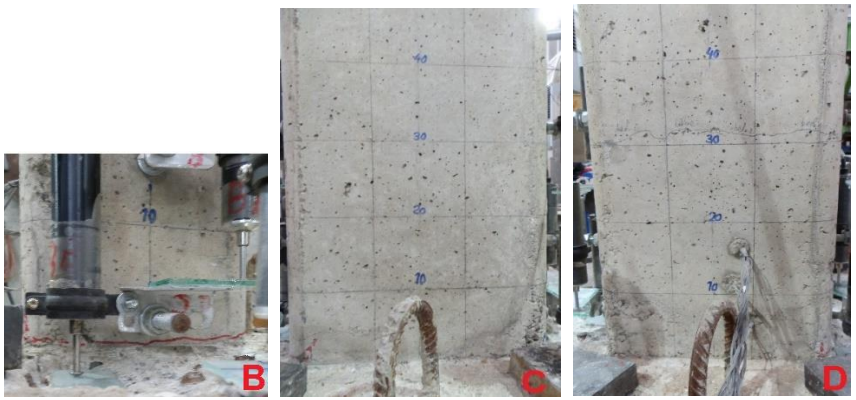
0.60	±7.71	27/-26	0.4	0	New initial flexural cracks were observed on column surfaces, width and length of the column-foundation joint cracks were increased 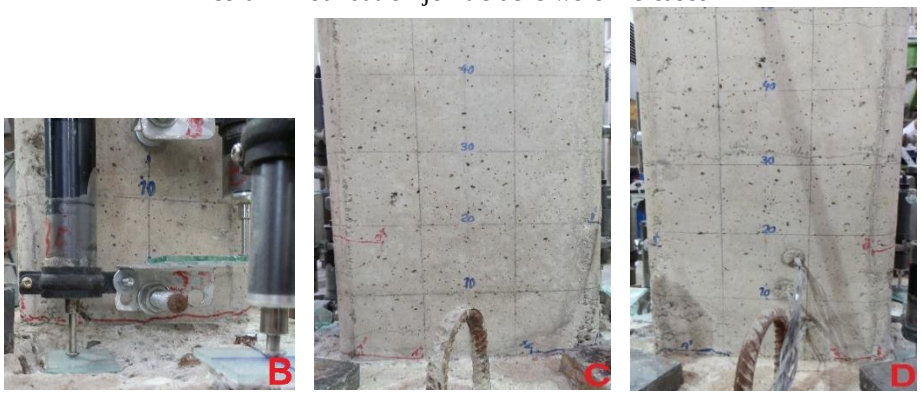

Drift ratio (%)	Δ (mm)	P (kN)	Max Column-Foundation crack thikness	Max Column-Foundation residual crack thikness	Observation
0.80	±10.28	30/-30	0.6	< 0.1	New flexural cracks were observed on column surfaces, width and length of some previous cracks were increased Initial concrete-crushing were observed on column surfaces 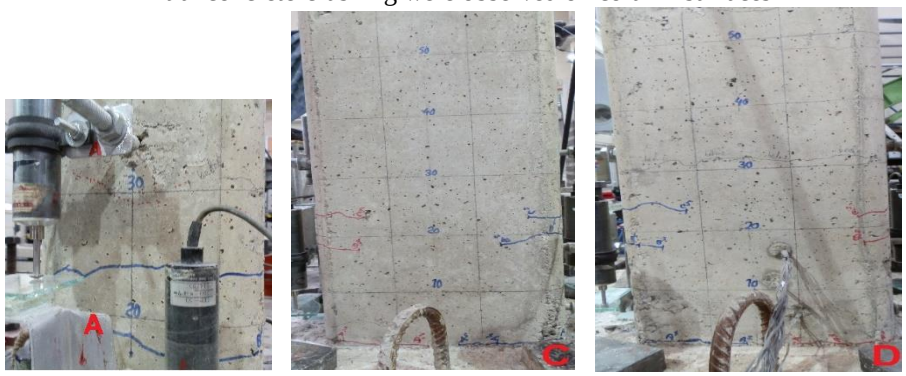
1.00	±12.85	34/-33	0.7	0.1	Concrete-crushing were increased on column surfaces a little, width and length of some previous cracks were increased 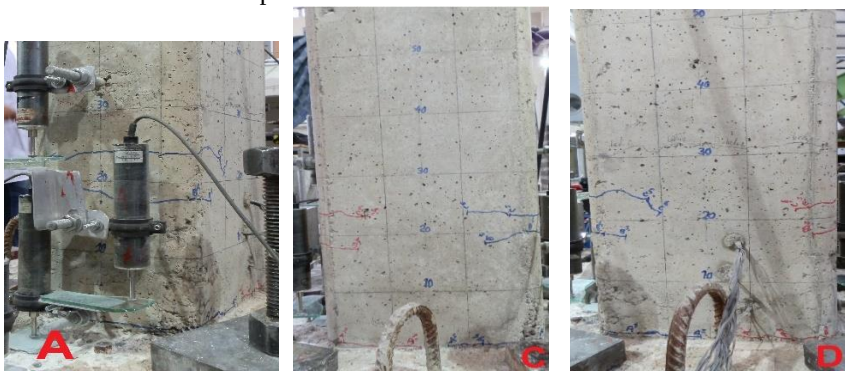

Drift ratio (%)	Δ (mm)	P (kN)	Max Column-Foundation crack thikness	Max Column-Foundation residual crack thikness	Observation
1.50	±19.28	37/-37	1.1	0.2	Initial small vertical cracks were observed on column surfaces at the corners, Width and length of some previous cracks were increased and there were some new flexural cracks 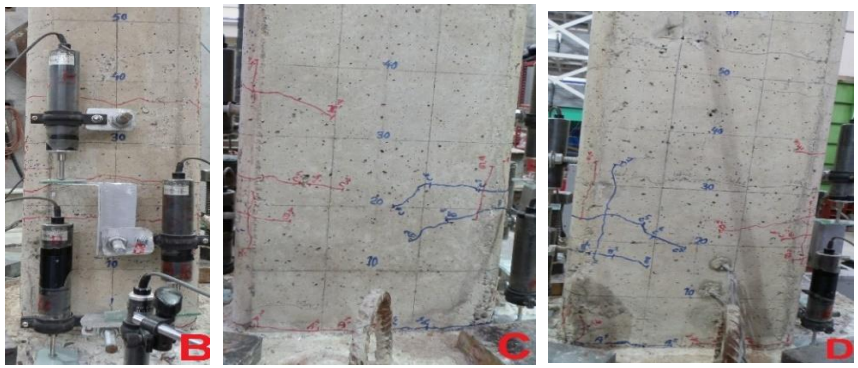
2.00	±25.7	38/-38	1.4	0.4	Concrete-crushing and small vertical cracks were increased on column surfaces, Width and length of some previous cracks were increased. New flexural crack was observed

Drift ratio (%)	Δ (mm)	P (kN)	Max Column-Foundation crack thikness	Max Column-Foundation residual crack thikness	Observation
2.50	±32.13	38/-39	1.9	0.4	There were no new cracks, only width of some previous cracks were increased. Concrete-Crushing were observed on C and D faces 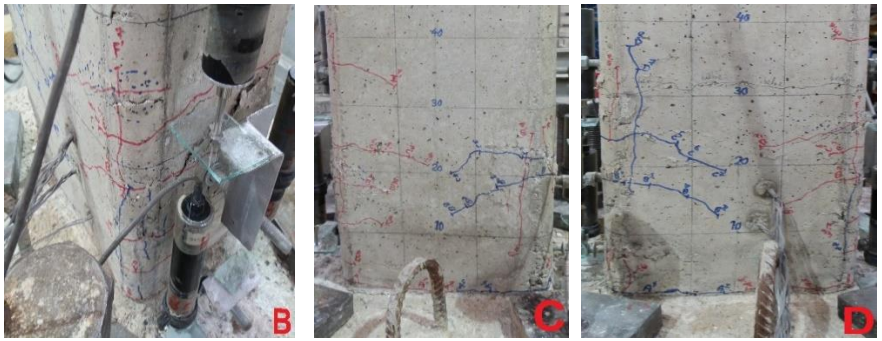
3.00	±38.55	37/-38	2	0.4	For the first time Concrete cover started to spall off at the column surfaces in compression zone There was no new flexure crack, only width and length of some previous cracks were increased 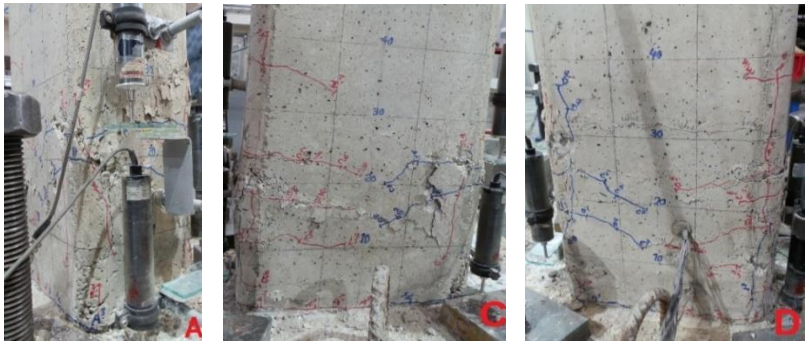

Drift ratio (%)	Δ (mm)	P (kN)	Max Column-Foundation crack thikness	Max Column-Foundation residual crack thikness	Observation
3.50	±45.98	37/-37	2.2	0.4	New flexural crack was observed and width of some previous cracks and spalling of concrete were increased
4.00	±51.4	36/-36	2.2	0.5	Width of some previous cracks and spalling of concrete were increased significantly

Drift ratio (%)	Δ (mm)	P (kN)	Max Column-Foundation crack thikness	Max Column-Foundation residual crack thikness	Observation
5.00	±64.25	32	Not measurable	Not measurable	Significently cover concrete were spalled off on column surfaces in plastic hinge zone Test was ended due to losing 18% of lateral loading capacity during loading to target displacement of 64.25 mm (drift ratio 5 %).

Table A.4 : Summary of the seismic behavior of the Ref-S60-Ɵ135-L40.

Drift ratio (%)	Δ (mm)	P (kN)	Max Column-Foundation crack thikness	Max Column-Foundation residual crack thikness	Observation
0.10	±1.29	8/-6			No crack was observed 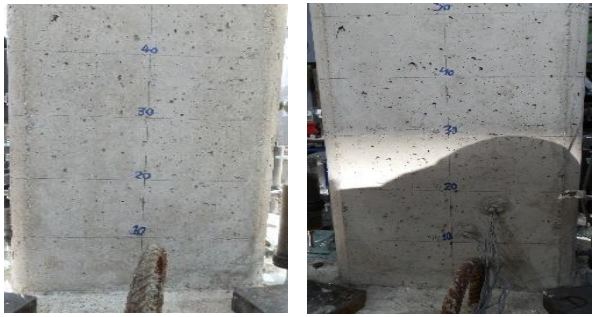
0.20	±2.58	13/-12			No crack was observed

Drift ratio (%)	Δ (mm)	P (kN)	Max Column-Foundation crack thikness	Max Column-Foundation residual crack thikness	Observation
0.40	±5.16	22/-21			Initial flexural cracks in column-foundation joint and column surfaces were observed 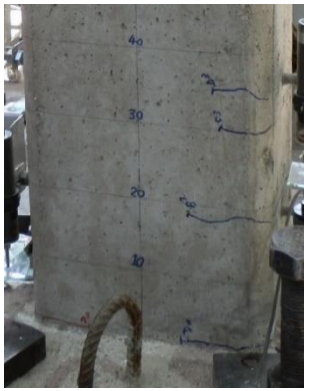
0.60	±7.74	28/-28			New flexural cracks were observed on column surfaces, width and length of some previous cracks were increased 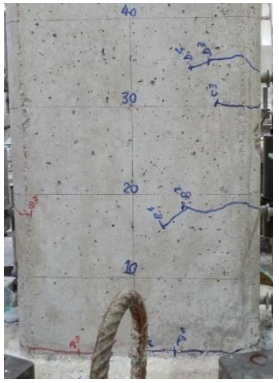

Drift ratio (%)	Δ (mm)	P (kN)	Max Column-Foundation crack thikness	Max Column-Foundation residual crack thikness	Observation
0.80	±10.32	32/-32	0.6	0.1	New flexural cracks were observed on column surfaces, width and length of some previous cracks were increased 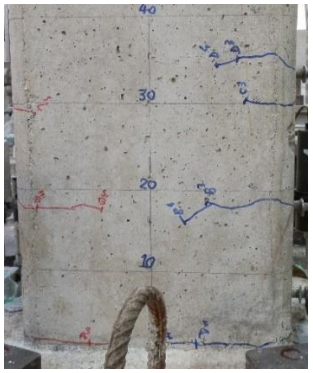 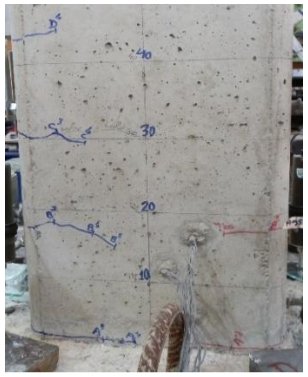
1.00	±12.9	34.4/ -34.5	0.8	0.2	New flexural cracks were observed on column surfaces, width and length of some previous cracks was increased 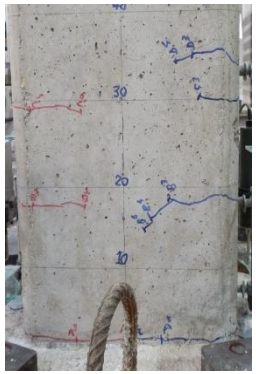 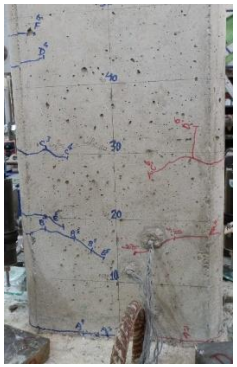

Drift ratio (%)	Δ (mm)	P (kN)	Max Column-Foundation crack thikness	Max Column-Foundation residual crack thikness	Observation
1.50	±19.35	37.4/ -37.6	1	0.2	Initial concrete-crushing and small vertical cracks were observed on column surfaces, Width and length of some previous cracks was increased 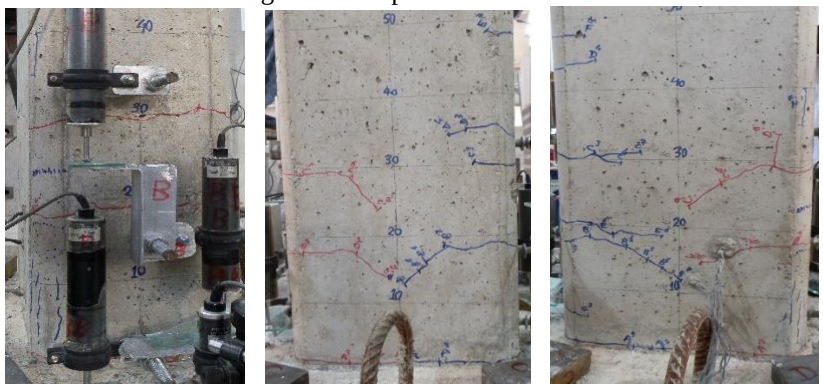
2.00	±25.8	37.6/ -39	1.1	0.3	Concrete-crushing and small vertical cracks were increased on column surfaces, Width of some previous cracks were increased 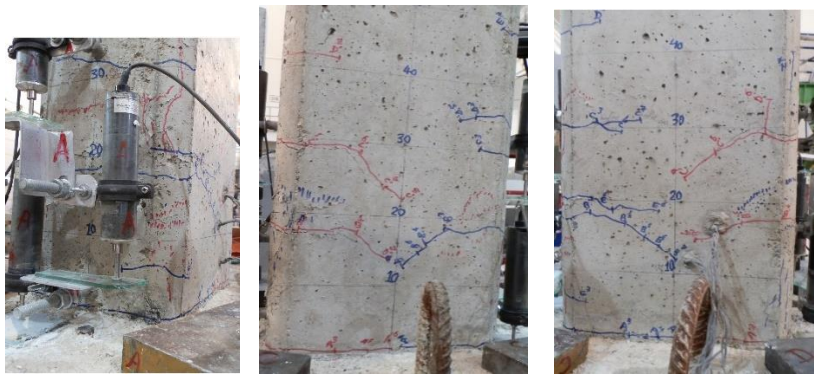

Drift ratio (%)	Δ (mm)	P (kN)	Max Column-Foundation crack thikness	Max Column-Foundation residual crack thikness	Observation
2.50	±32.25	37/-39	1.1	0.3	For the first time Concrete cover spalled off at the column surfaces in compression zone. New flexural cracks were observed on column surfaces, width and length of some previous cracks was increased.
3.00	±38.7	36/-39	1.2	0.3	Width of some previous cracks and spalling of concrete were increased longitudinal bars and stirrups were observed

Drift ratio (%)	Δ (mm)	P (kN)	Max Column-Foundation crack thikness	Max Column-Foundation residual crack thikness	Observation
3.50	±45.15	36/-39	1	0.3	Significent part of concrete cover were spalled off at column surface in plastic hinge zone
4.00	±51.6	34/ -37.5	1	0.2	Initial buckling were observed in longitudinal bars at plastic hinge zone

Drift ratio (%)	Δ (mm)	P (kN)	Max Column-Foundation crack thikness	Max Column-Foundation residual crack thikness	Observation
5.00	±64.5	21.5			Test was ended due to buckling of longitudinal bars in compression zone and losing 43% of lateral loading capacity during loading to target displacement of 64.5 mm (drift ratio 5 %).

Table A.5 : Summary of the seismic behavior of the Ret-S60-Ɵ90-L80-3TRM.

Drift ratio (%)	**Δ** (mm)	**P** (kN)	**Max Column-Foundation crack width**	**Max Column-Foundation residual crack width**	**Observation**
0.10	±1.293	10/-12	-	-	No crack was observed
0.20	±2.586	18/-19	-	-	No crack was observed

Drift ratio (%)	Δ (mm)	P (kN)	Max Column-Foundation crack width	Max Column-Foundation residual crack width	Observation
0.40	±5.172	27/-27	0.3	0	Initial flexural cracks in column-foundation joint were observed
0.60	±7.758	35/-31	0.7	0	Initial flexural cracks on column surfaces were observed width and length of the previous crack in column-foundation joint was increased 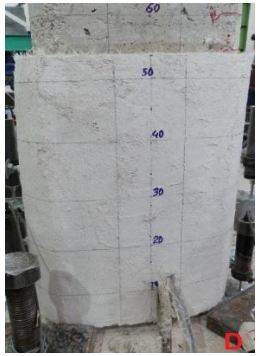

Drift ratio (%)	Δ (mm)	P (kN)	Max Column-Foundation crack width	Max Column-Foundation residual crack width	Observation
0.80	±10.344	35/-33	1	0	New flexural cracks on column surfaces were observed Width and length of previous crack were increased 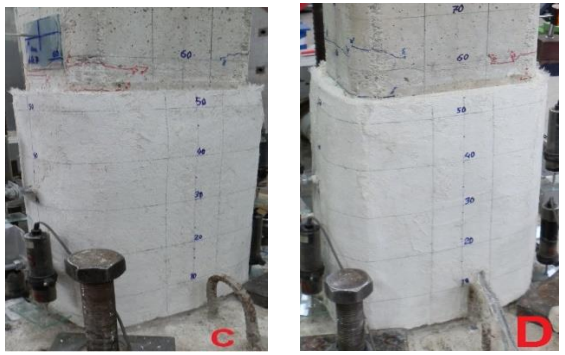
1.00	±12.9	40/-37	1.3	0.2	New flexural cracks were observed in column surfaces and width and length of some previous cracks were increased and for the first time vertical cracks and concrete-crushing were observed in column corners at compression zone

Drift ratio (%)	Δ (mm)	P (kN)	Max Column-Foundation crack width	Max Column-Foundation residual crack width	Observation
1.50	±19.395	42/-43	2.3	0.4	New flexural crack was observed and width and length of some previous cracks were increased Initial vertical crack were observed on TRM jacket 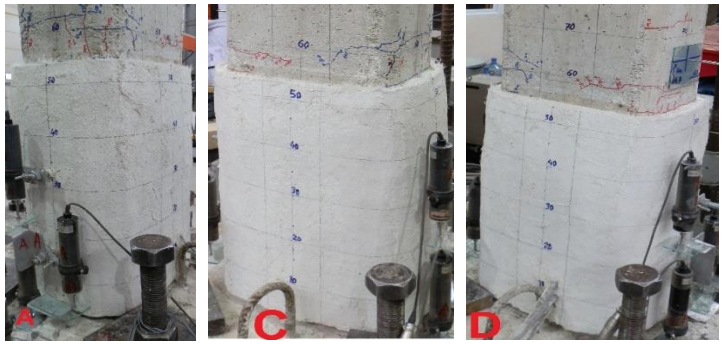
2.00	±25.86	43/-45	3	0.5	Initial vertical crack was observed on TRM jacket and width and length of some previous cracks and concrete crushing were increased 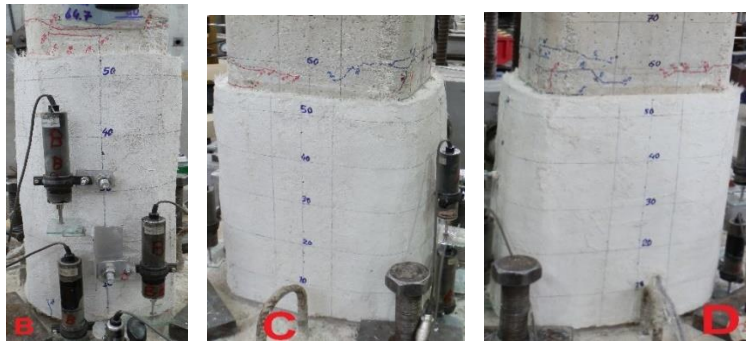

Drift ratio (%)	Δ (mm)	P (kN)	Max Column-Foundation crack width	Max Column-Foundation residual crack width	Observation
2.50	±32.325	43/-47	4	0.4	New vertical cracks were observed in column surfaces and width and length of some previous cracks and concrete crushing were increased. 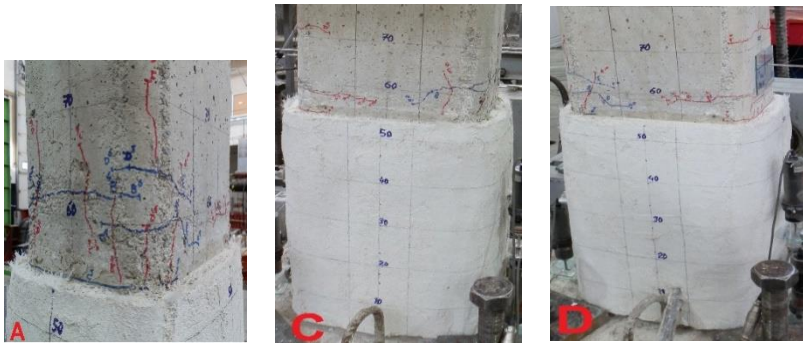
3.00	±38.79	44/-46	5	0.4	There were no new cracks on column surfaces, only width and length of some previous cracks and concrete-crushing were increased New vertical crack was observed on TRM jacket 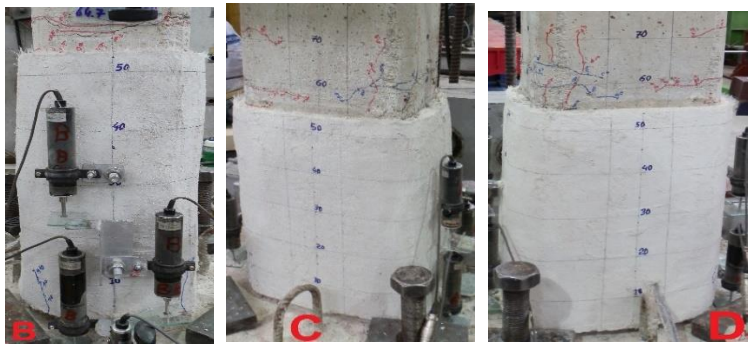

Drift ratio (%)	Δ (mm)	P (kN)	Max Column-Foundation crack width	Max Column-Foundation residual crack width	Observation
3.50	±45.255	44/-48	6	1	There were no new cracks, only width and length of some previous cracks were increased 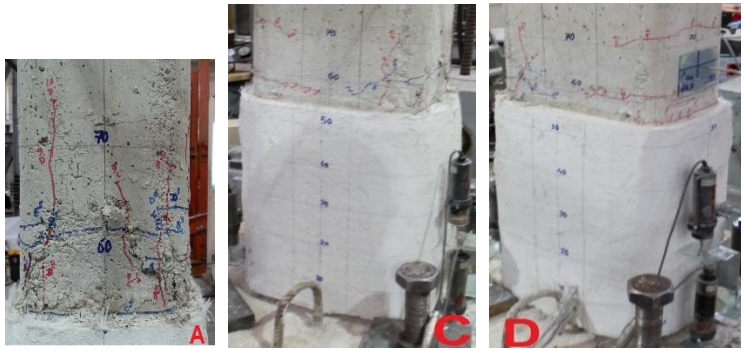
4.00	±51.72	45/-47	10	0.6	There were no new cracks, only width of some previous cracks and concrete crushing were increased For the first time spalling of the concrete were observed in column surface 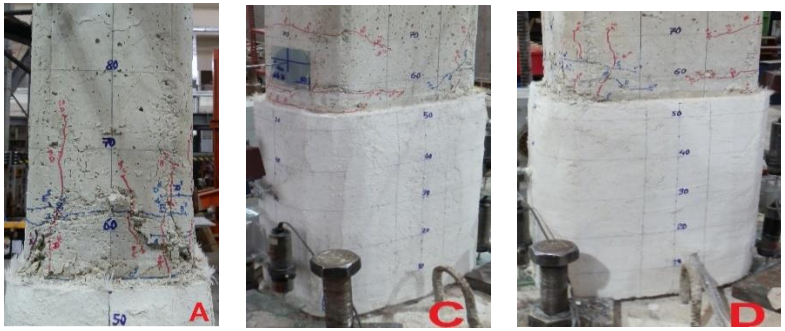

Drift ratio (%)	Δ (mm)	P (kN)	Max Column-Foundation crack width	Max Column-Foundation residual crack width	Observation
5.00	±64.65	46/-48	13	1	New vertical cracks were observed on TRM jacket width and length of some previous cracks and concrete-crushing were increased 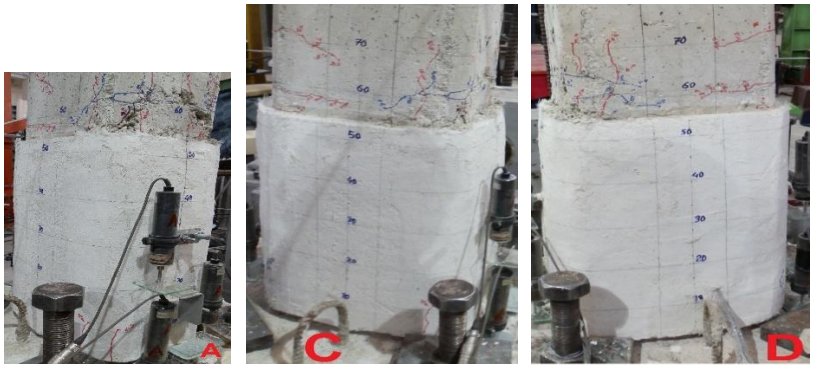
6.00	±77.58	47/-48	18	1.3	New vertical cracks were observed on TRM jacket width and length of some previous cracks and concrete-crushing were increased 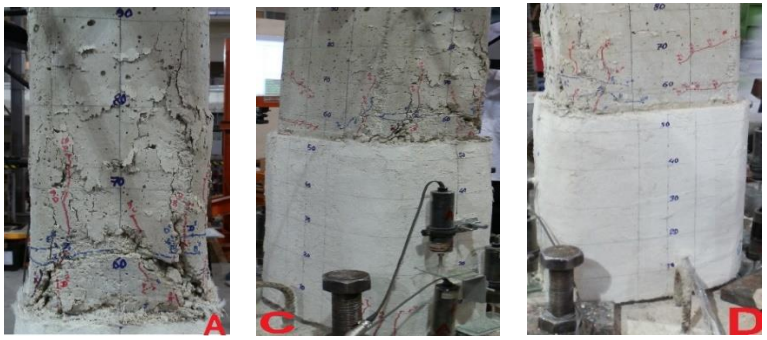

Drift ratio (%)	Δ (mm)	P (kN)	Max Column-Foundation crack width	Max Column-Foundation residual crack width	Observation
7.00	±90.51	47/-46	20	4	New flexure crack was observed in column surface width and length of some previous cracks and concrete-crushing and spalling were increased in pulling direction 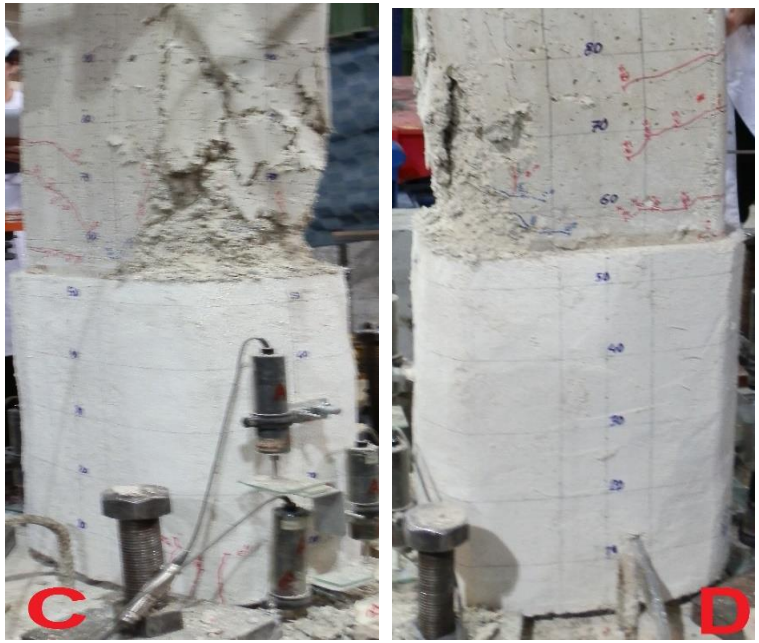

Drift ratio (%)	Δ (mm)	P (kN)	Max Column-Foundation crack width	Max Column-Foundation residual crack width	Observation
8.00	±103.44	47/-32	30	4	There were no new cracks, only width of column-foundation joint cracks were increased Test was ended due to 33% losing lateral load capacity during loading to target drift ratio -8 %. Stirrups and longitudinal bars were observed at face A.

Table A.6 : Summary of the seismic behavior of the Ret-S60-Ɵ112.5-L80-3TRM.

Drift ratio (%)	Δ (mm)	P (kN)	Max Column-Foundation crack width	Max Column-Foundation residual crack width	Observation
0.10	±1.283	10/-12	-	-	No crack was observed 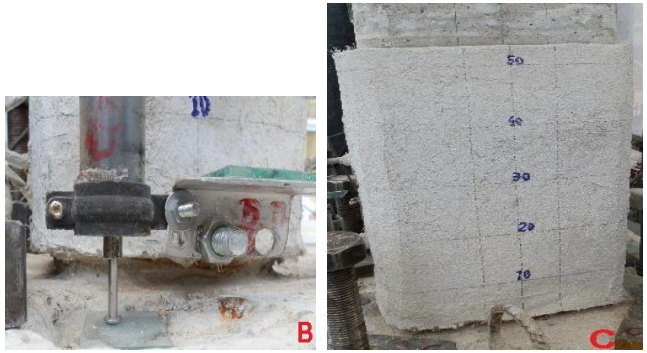
0.20	±2.566	17/-19	< 0.1	0	Initial flexural crack in column-foundation joint was observed (only in face A)

Drift ratio (%)	Δ (mm)	P (kN)	Max Column-Foundation crack width	Max Column-Foundation residual crack width	Observation
0.40	±5.132	26/-26	0.3	0	Initial flexural cracks were observed in column-foundation joint (only in face B) width and length of the previous crack in column-foundation joint was increased
0.60	±7.698	30/-31	0.6	0	Initial flexural cracks on column surfaces were observed width and length of the previous cracks were increased

Drift ratio (%)	Δ (mm)	P (kN)	Max Column-Foundation crack width	Max Column-Foundation residual crack width	Observation
0.80	±10.264	32/-34	1	0	New flexural cracks were observed on column surfaces width and length of some previous cracks were increased 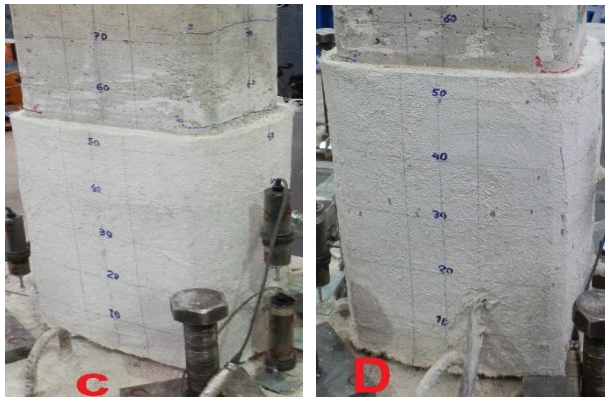
1.00	±12.83	35/-38	1.4	0.2	New flexural cracks were observed in column surfaces and on TRM jacket and width and length of some previous cracks were increased Initial concrete- were observed at compression zone 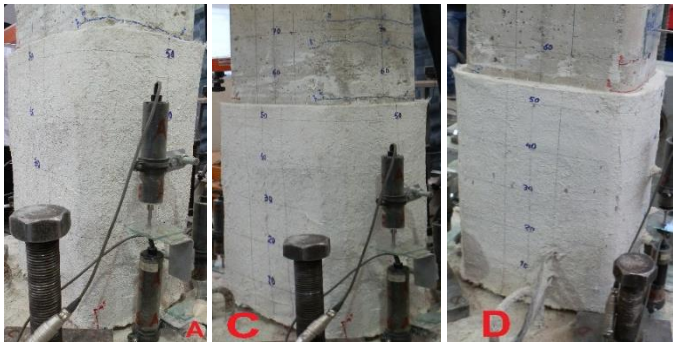

Drift ratio (%)	Δ (mm)	P (kN)	Max Column-Foundation crack width	Max Column-Foundation residual crack width	Observation
1.50	±19.245	40/-41	2	Not measurable	New flexural crack were observed in column surfaces and width and length of some previous cracks were increased and Initial concrete-crushing were observed 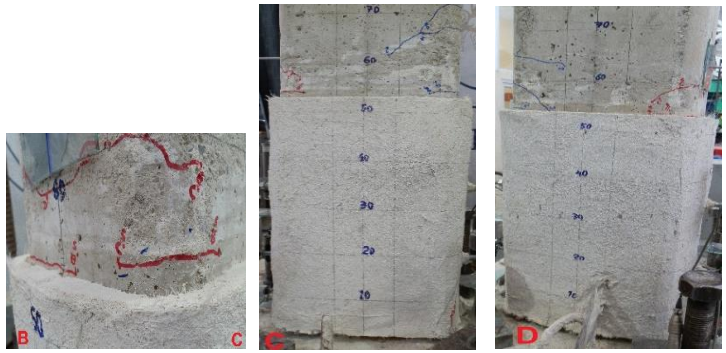
2.00	±25.66	43/-42	3	0.6	Initial vertical crack was observed in column surface and width and length of some previous cracks and concrete crushing were increased 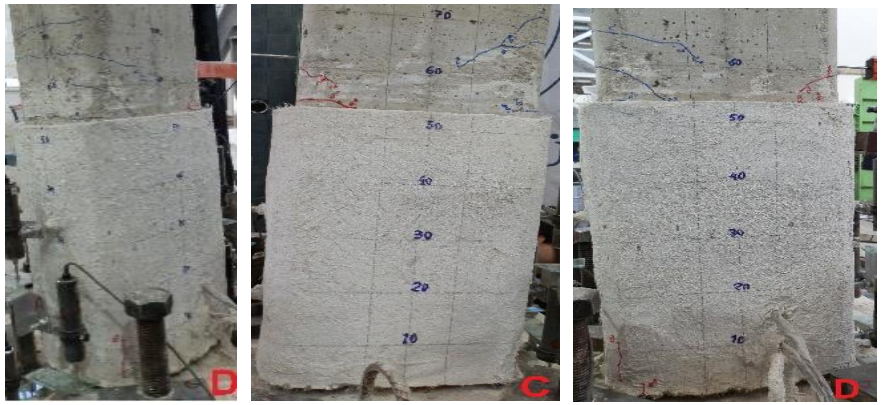

Drift ratio (%)	Δ (mm)	P (kN)	Max Column-Foundation crack width	Max Column-Foundation residual crack width	Observation
2.50	±32.075	43/-43	4	Not measurable	There was no new flexural crack, only width and length of some previous cracks were increased and New vertical crack were observed on TRM jacket 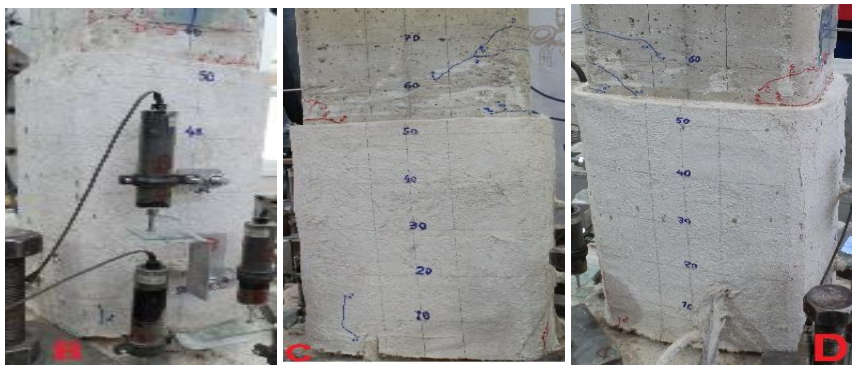
3.00	±38.49	43/-44	4	Not measurable	There was no new flexural crack, only width and length of some previous cracks were increased and New vertical crack were observed on TRM jacket 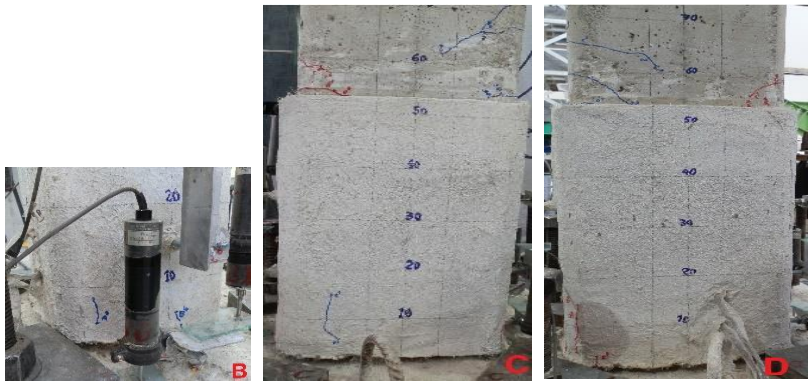

Drift ratio (%)	Δ (mm)	P (kN)	Max Column-Foundation crack width	Max Column-Foundation residual crack width	Observation
3.50	±45.905	43/-44	4	Not measurable	There was no new crack, only width and length of some previous cracks and concrete crushing were increased 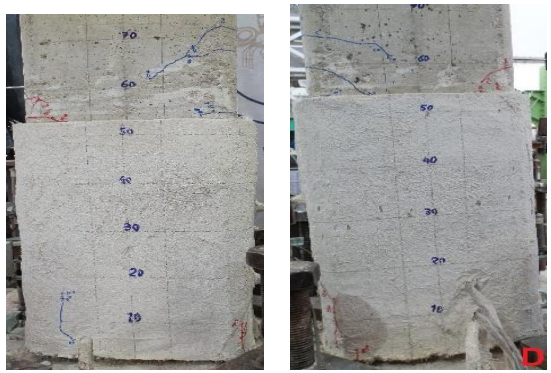
4.00	±51.32	42/-44	4	1	New vertical crack was observed on TRM jacket and concrete crushing were increased

Drift ratio (%)	Δ (mm)	P (kN)	Max Column-Foundation crack width	Max Column-Foundation residual crack width	Observation
5.00	±64.15	42/-44	5	Not measurable	There were no new flexural cracks, only width of some previous cracks and concrete crushing were increased,New vertical crack was observed on TRM jacket 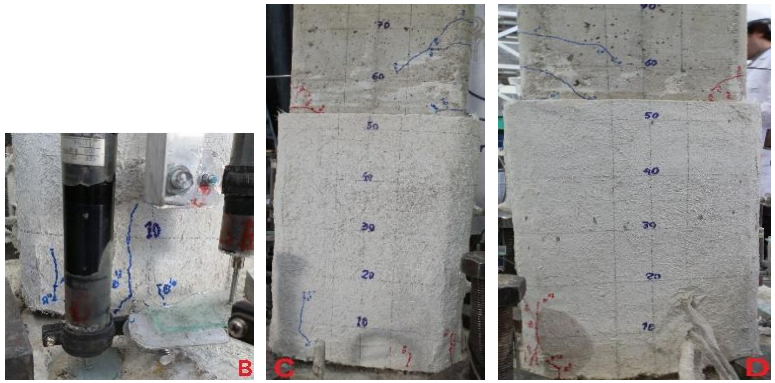
6.00	±76.98	43/-45	5	Not measurable	New vertical cracks were observed on TRM jacket width of some previous cracks were increased 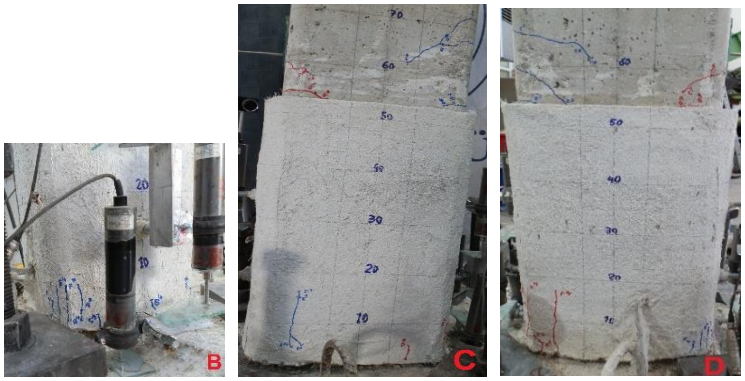

Drift ratio (%)	Δ (mm)	P (kN)	Max Column-Foundation crack width	Max Column-Foundation residual crack width	Observation
7.00	±89.81	43/-46	5	Not measurable	New flexural cracks were observed on TRM jacket- Some rupturing sounds come from TRM jacket and width of some previous cracks and concrete-crushing were increased 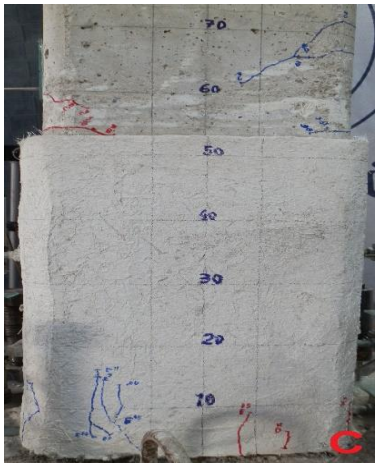 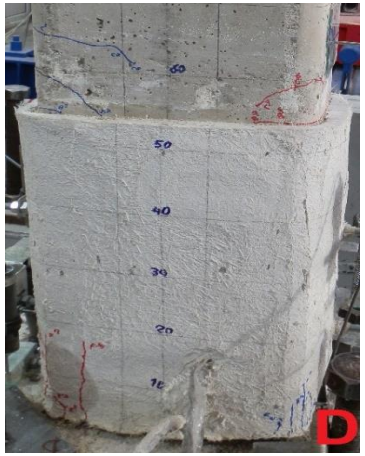 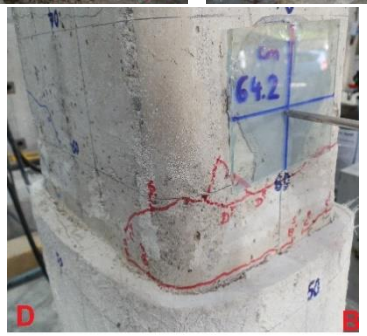

Drift ratio (%)	Δ (mm)	P (kN)	Max Column-Foundation crack width	Max Column-Foundation residual crack width	Observation
8.00	±102.264	42/44	4	Not measurable	New vertical crack was observed on TRM jacket 9% losing of lateral load, after loading to target displacement of -103.64 mm (drift ratio -8%) test was finished. Test was ended due to use maximum capacity of top LVDT which was measured top displacement of column. 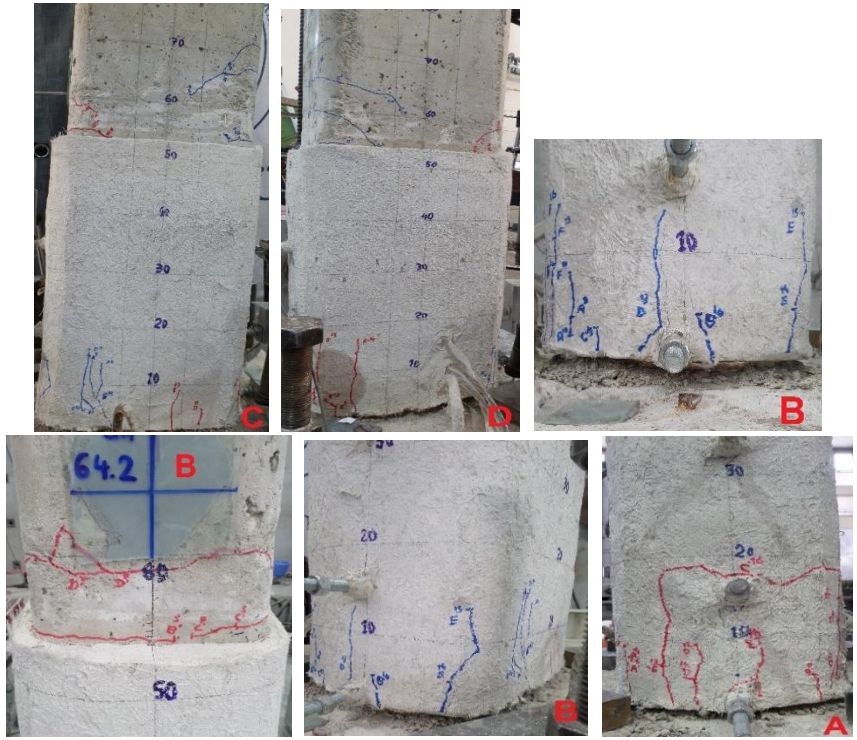

Table A.7 : Summary of the seismic behavior of the Ret-S60-Ɵ135-L80-3TRM.

Drift ratio (%)	**Δ (mm)**	**P (kN)**	**Max Column-Foundation crack width**	**Max Column-Foundation residual crack width**	**RObservation**
0.10	±1.286	7/-10	-	-	No crack was observed
0.20	±2.572	14/-16			Initial flexural cracks in column-foundation joint were observed 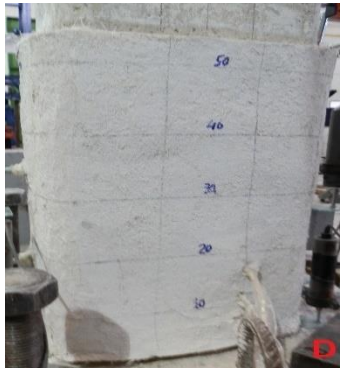

Drift ratio (%)	Δ (mm)	P (kN)	Max Column-Foundation crack width	Max Column-Foundation residual crack width	Observation
0.40	±5.144	25/-25			Initial flexural crack was observed in column surfaces width and length of previous crack in column-foundation joint was increased
0.60	±7.716	31/-30			New flexural cracks on column surfaces were observed width and length of some previous cracks were increased

Drift ratio (%)	Δ (mm)	P (kN)	Max Column-Foundation crack width	Max Column-Foundation residual crack width	Observation
0.80	±10.288	35/-32			Initial concrete-crushing were observed on column surfaces Width and length of some previous cracks were increased
1.00	±12.86	37/-36			New flexural cracks were observed in column surfaces and width and length of some previous cracks were increased and concrete-crushing were increased at compression zone

Drift ratio (%)	Δ (mm)	P (kN)	Max Column-Foundation crack width	Max Column-Foundation residual crack width	Observation
1.50	±19.29	41/-41			There was no new flexural crack, only width and length of some previous cracks were increased Initial vertical crack was observed on TRM jacket
2.00	±25.72	42/-42			Initial vertical cracks were observed in column surface and on TRM jacket Width and length of some previous cracks and concrete crushing were 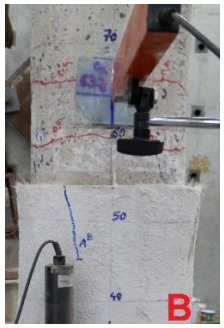

Drift ratio (%)	Δ (mm)	P (kN)	Max Column-Foundation crack width	Max Column-Foundation residual crack width	Observation
2.50	±32.15	42/-43			New vertical cracks were observed in column surface and on TRM jacket Width and length of some previous cracks were increased
3.00	±38.58	42/-44			New flexural cracks were observed in column surfaces New vertical crack was observed on TRM jacket Width and length of some previous cracks and concrete-crushing were increased

Drift ratio (%)	Δ (mm)	P (kN)	Max Column-Foundation crack width	Max Column-Foundation residual crack width	Observation
3.50	±45.01	42/-44			New vertical cracks were observed in column surfaces and on TRM jacket Width and length of some previous cracks, vertical cracks and were increased
4.00	±51.44	43/-45			There were no new cracks, only width of some previous cracks, vertical cracks and concrete crushing were increased

Drift ratio (%)	Δ (mm)	P (kN)	Max Column-Foundation crack width	Max Column-Foundation residual crack width	Observation
5.00	±64.3	45/-45			New vertical cracks were observed on TRM jacket Width of some previous cracks and concrete crushing were increased
6.00	±77.16	44/-47			New vertical cracks were observed on TRM jacket width and length of some previous cracks and concrete-crushing were increased

Drift ratio (%)	Δ (mm)	P (kN)	Max Column-Foundation crack width	Max Column-Foundation residual crack width	Observation
7.00	±90.02	43/-47			New flexural crack was observed on TRM jacket width and length of some previous cracks and concrete-crushing were increased 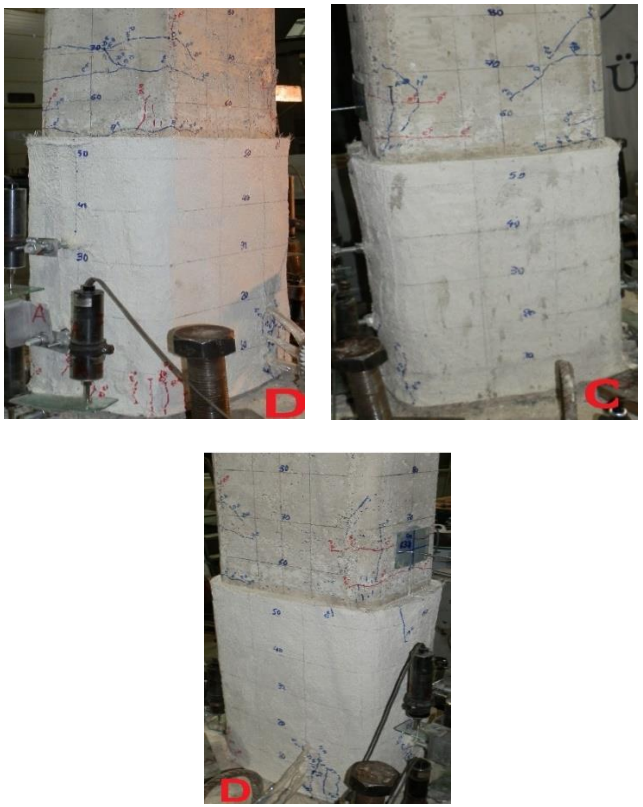

Drift ratio (%)	Δ (mm)	P (kN)	Max Column-Foundation crack width	Max Column-Foundation residual crack width	Observation
8.00	±102.08	44/47			New flexural cracks were observed in column surfaces. Width of column-foundation joint crack and concrete-crushing were increased Test was ended due to losing lateral load capacity during loading to target drift ratio -8 %. 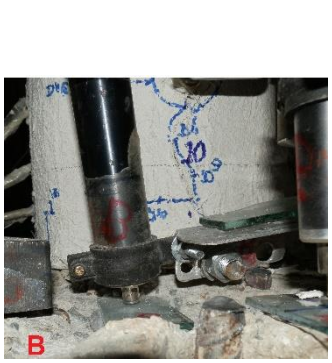 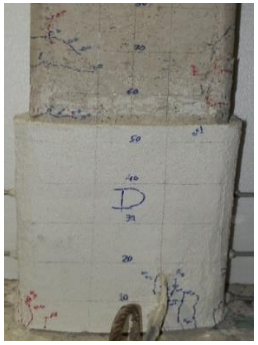 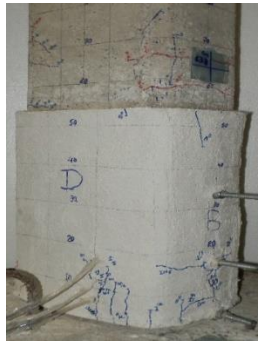

Table A.8 : Summary of the seismic behavior of Ret-S60-Ɵ135-L40-3TRM.

Drift ratio (%)	**Δ** (mm)	**P** (kN)	**Max Column-Foundation crack width**	**Max Column-Foundation residual crack width**	**Observation**
0.10	±1.29	12/-10	-	-	No crack was observed
0.20	±2.58	19/-17	0.1	0	Initial flexural crack in column-foundation joint (only in B-Face) were observed

Drift ratio (%)	Δ (mm)	P (kN)	Max Column-Foundation crack width	Max Column-Foundation residual crack width	Observation
0.40	±5.16	27/-26	0.4	0	width and length of the previous crack in column-foundation joint were increased 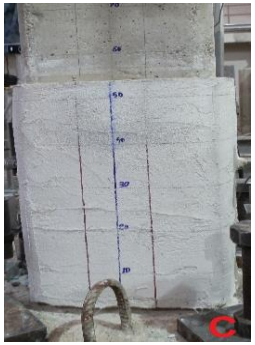
0.60	±7.74	33/-32	0.7	0	There were no new cracks, only width and length of previous crack were increased 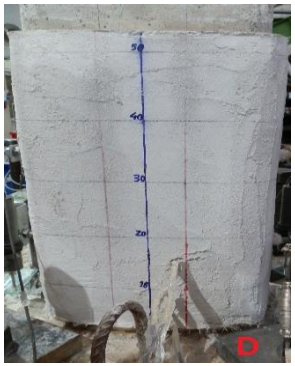

Drift ratio (%)	Δ (mm)	P (kN)	Max Column-Foundation crack width	Max Column-Foundation residual crack width	Observation
0.80	±10.32	37/-36	1	0	Initial flexural cracks were observed in column surfaces and width and length of previous cracks were increased and for the first time Concrete crushing were observed at the column surfaces in compression zone
1.00	±12.9	40/-37	1.2	0.4	New flexural cracks were observed in column surfaces and width and length of some previous cracks were increased 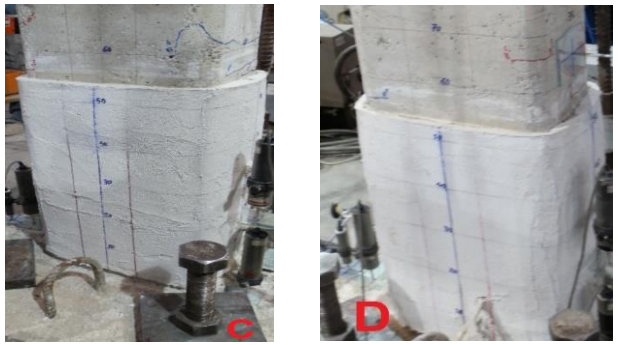

Drift ratio (%)	Δ (mm)	P (kN)	Max Column-Foundation crack width	Max Column-Foundation residual crack width	Observation
1.50	±19.35	43/-41	1.6	0.3	New flexural cracks were observed in column surfaces and width and length of some previous cracks were increased Initial vertical crack were observed on TRM jacket 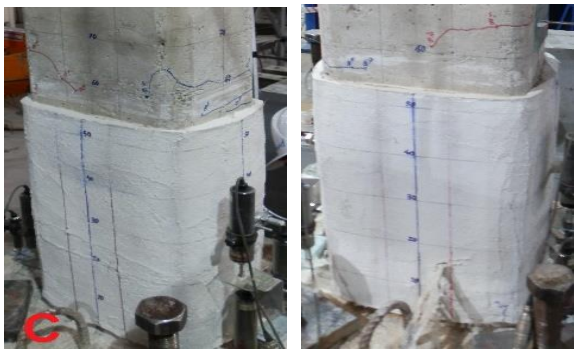
2.00	±25.8	44/-42	2.5	Not measurable	Initial vertical crack was observed on column surface and width and length of some previous cracks and concrete crushing were increased 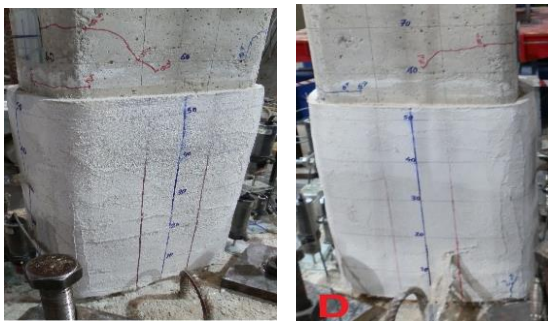

Drift ratio (%)	Δ (mm)	P (kN)	Max Column-Foundation crack width	Max Column-Foundation residual crack width	Observation
2.50	±32.25	45/-43	3.2	0.6	New small vertical cracks and were observed on column surfaces width and length of some previous cracks and concrete crushing were increased new New vertical cracks on TRM were observed 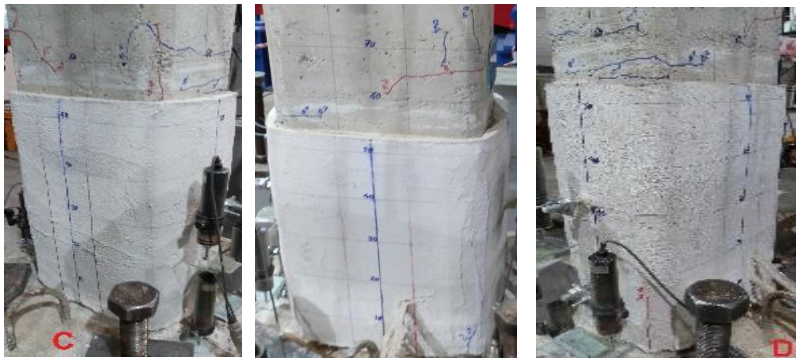
3.00	±38.7	46/-44	4	1	There were no new cracks on column surfaces, only width of some previous cracks were increased New vertical cracks were observed on TRM jacket

Drift ratio (%)	Δ (mm)	P (kN)	Max Column-Foundation crack width	Max Column-Foundation residual crack width	Observation
3.50	±45.15	46/-45	5	0.5	New vertical crack and concrete-crushing were observed at the corner of column New vertical crack on the TRM was observed and length of some previous cracks were increased 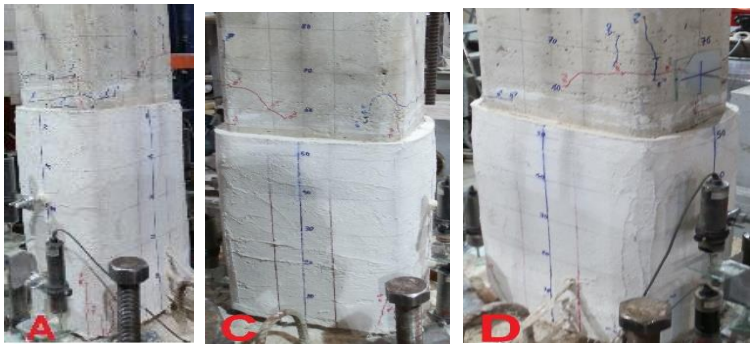
4.00	±51.6	45/-44	7	0.8	New vertical cracks were observed in column surfaces and width of some previous cracks and concrete crushing were increased

Drift ratio (%)	Δ (mm)	P (kN)	Max Column-Foundation crack width	Max Column-Foundation residual crack width	Observation
5.00	±64.5	46/-45	10	1.2	New vertical cracks were observed on TRM jacket width and length of some previous cracks were increased 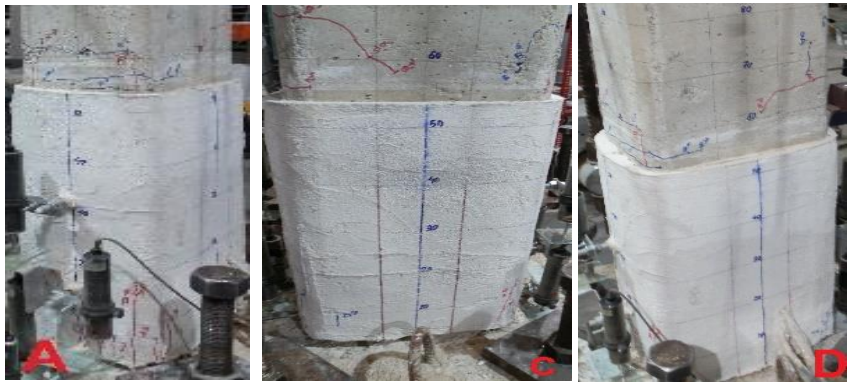
6.00	±77.4	46/-46	13	3	New flexure crack was observed on TRM jacket and width of column-foundation joint crack were increased 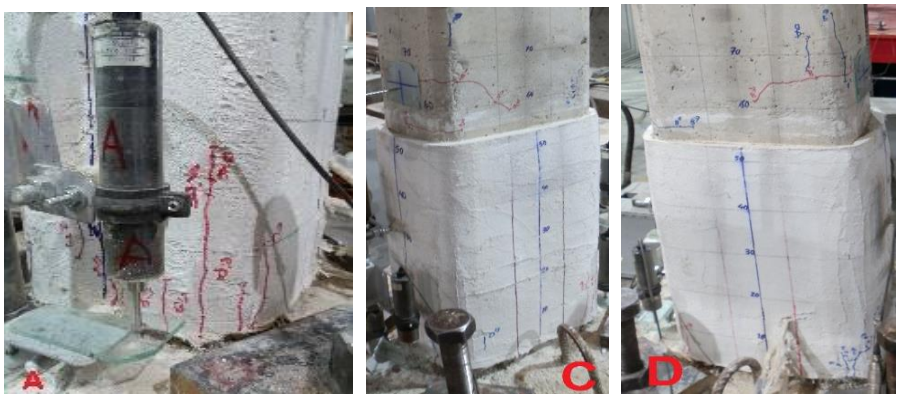

Drift ratio (%)	Δ (mm)	P (kN)	Max Column-Foundation crack width	Max Column-Foundation residual crack width	Observation
7.00	±90.3	46/-46	10	Not measurable	There were no new cracks, only width of column-foundation joint crack were increased 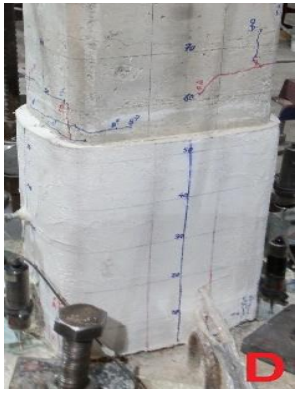

Drift ratio (%)	Δ (mm)	P (kN)	Max Column-Foundation crack width	Max Column-Foundation residual crack width	Observation
8.00	±103.2	45/-45	15	Not measurable	There were no new cracks, only width of column-foundation joint cracks were increased Test was ended due to use maximum capacity of top LVDT which was measured top displacement of column and without losing any lateral load, after loading to target displacement of -103.2 mm (drift ratio -8%) test was finished.

APPENDIX B: Technical Drawings of Specimens.

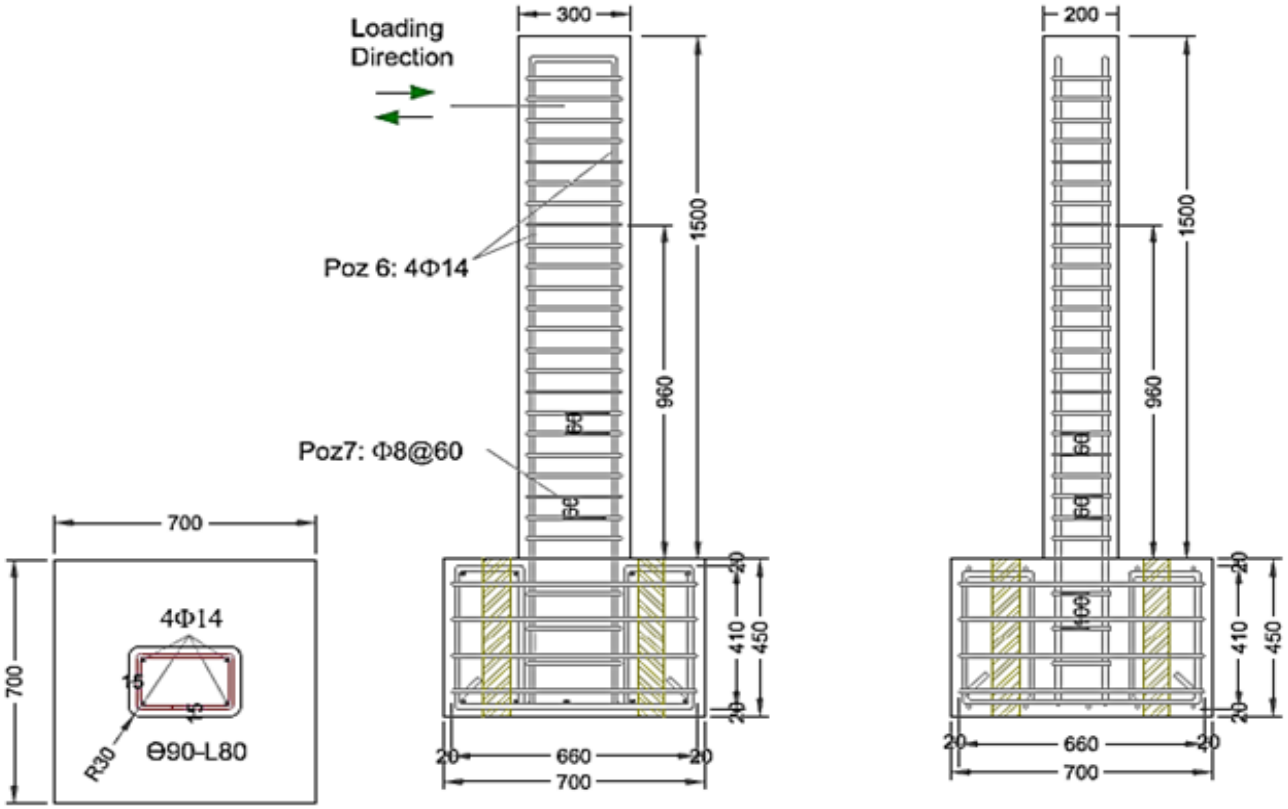

Figure B.1: Specimen detail for Ref-S60-Θ90-L80.

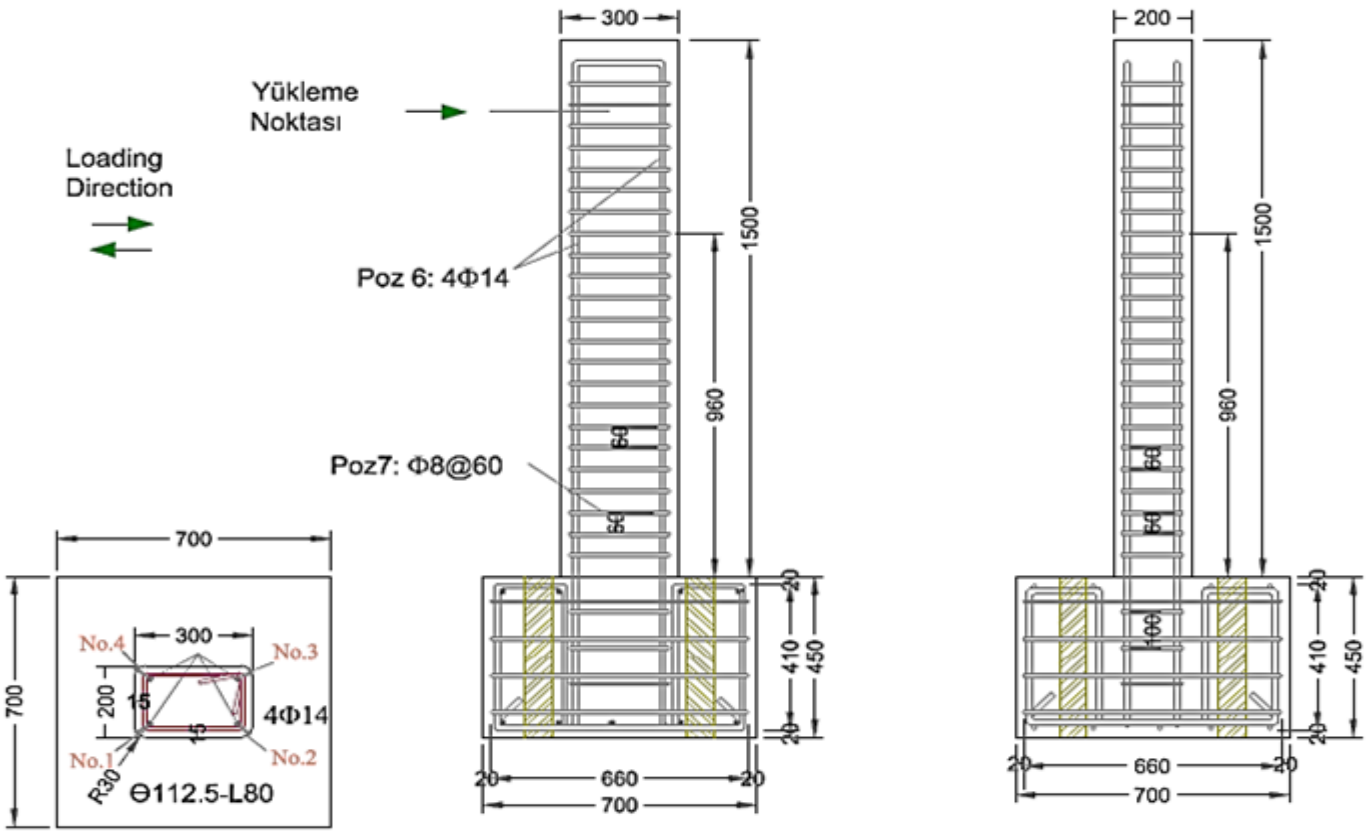

Figure B.2 : Specimen detail for Ref-S60-Θ112.5-L80.

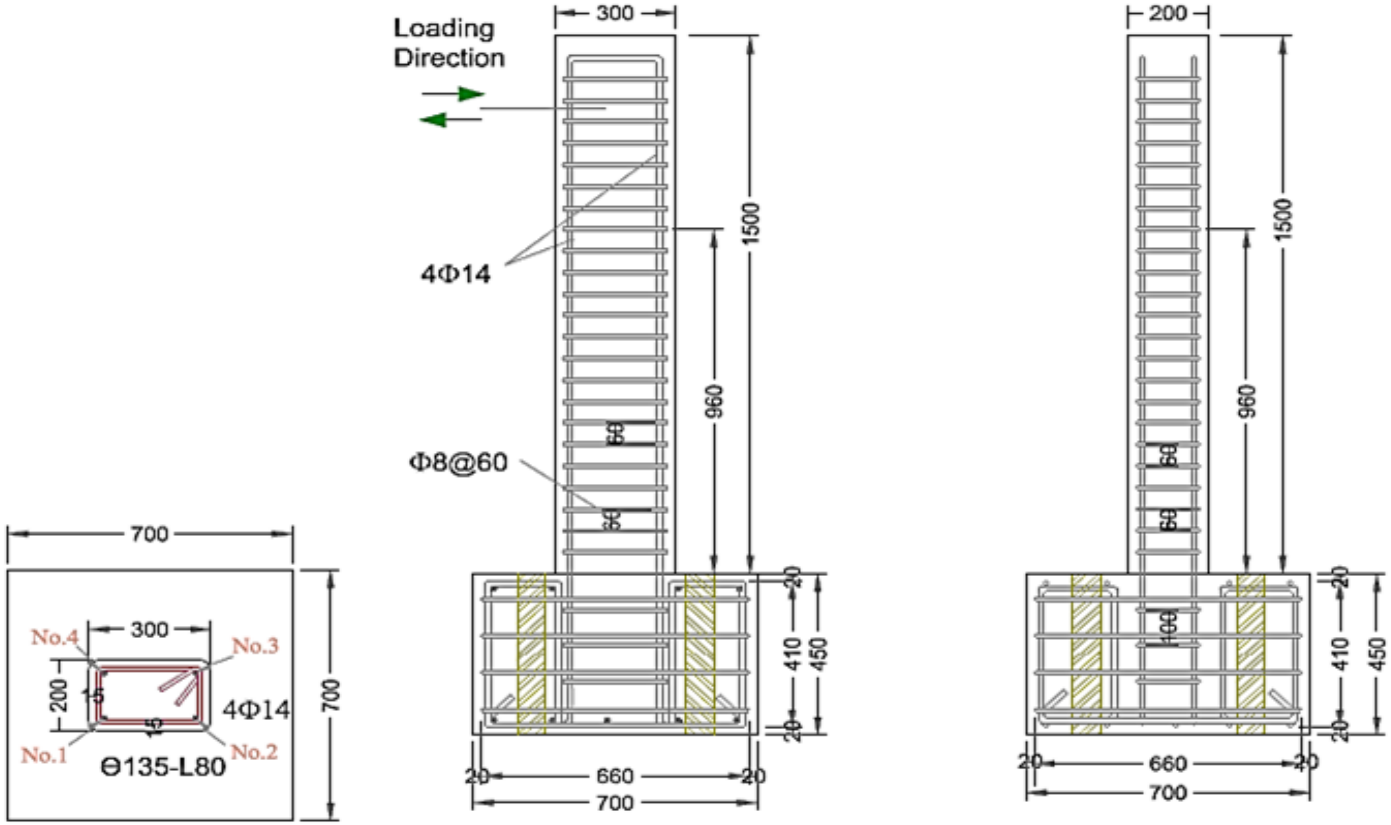

Figure B.3 : Specimen detail for Ref-S60-Θ135-L80.

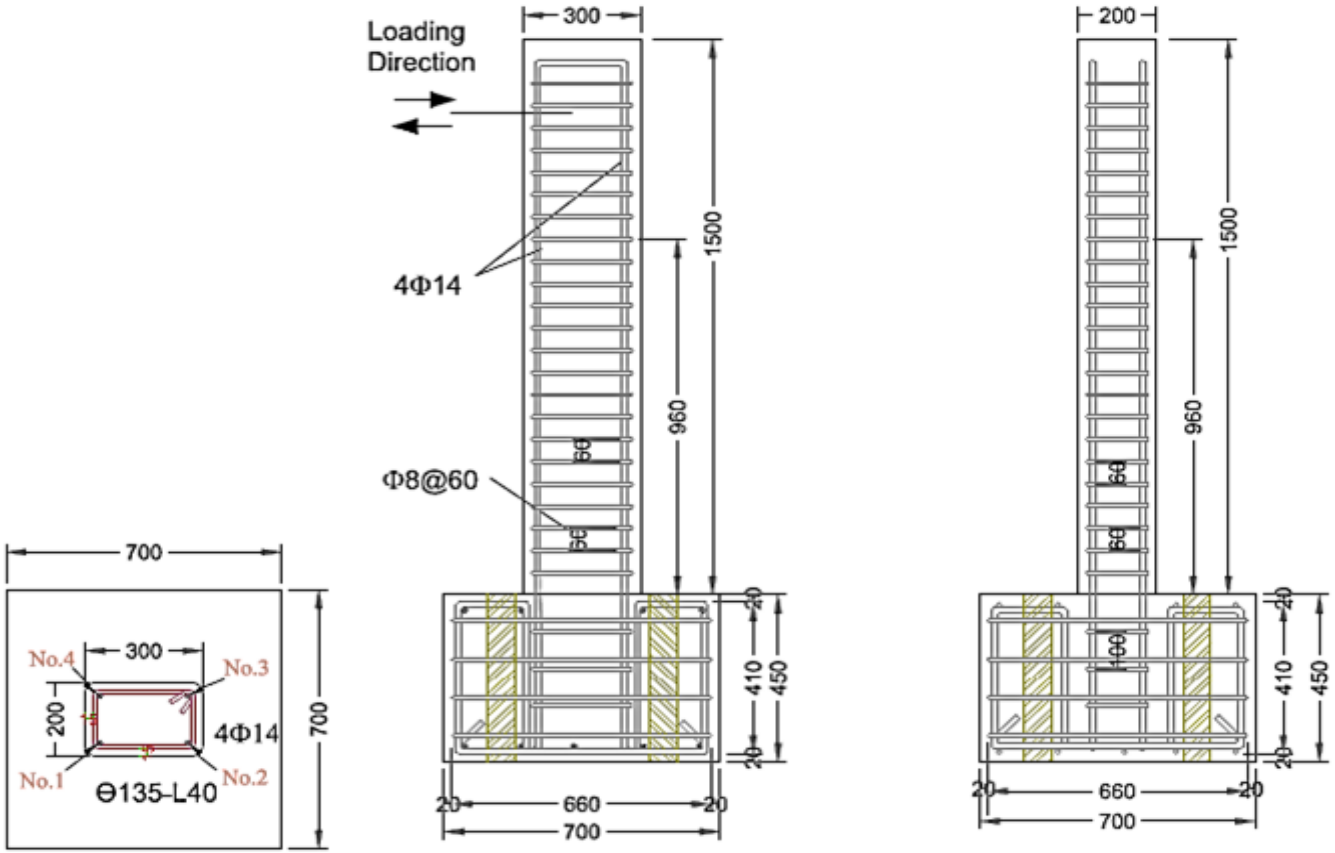

Figure B.4: Specimen detail for Ref-S60-Θ135-L40.

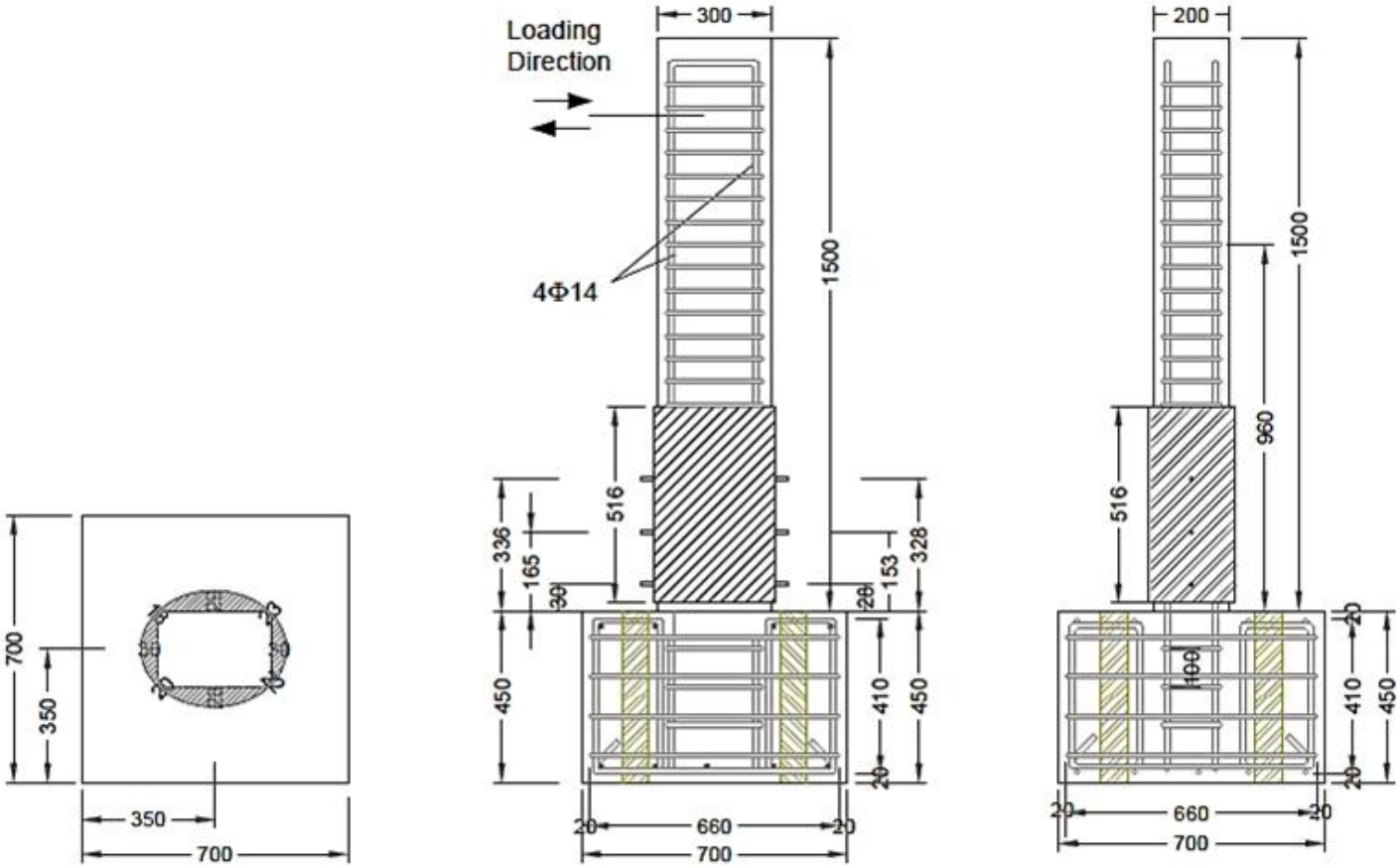

Figure B.5: Specimen detail for Ret-S60-Ɵ90-L80-3TRM.

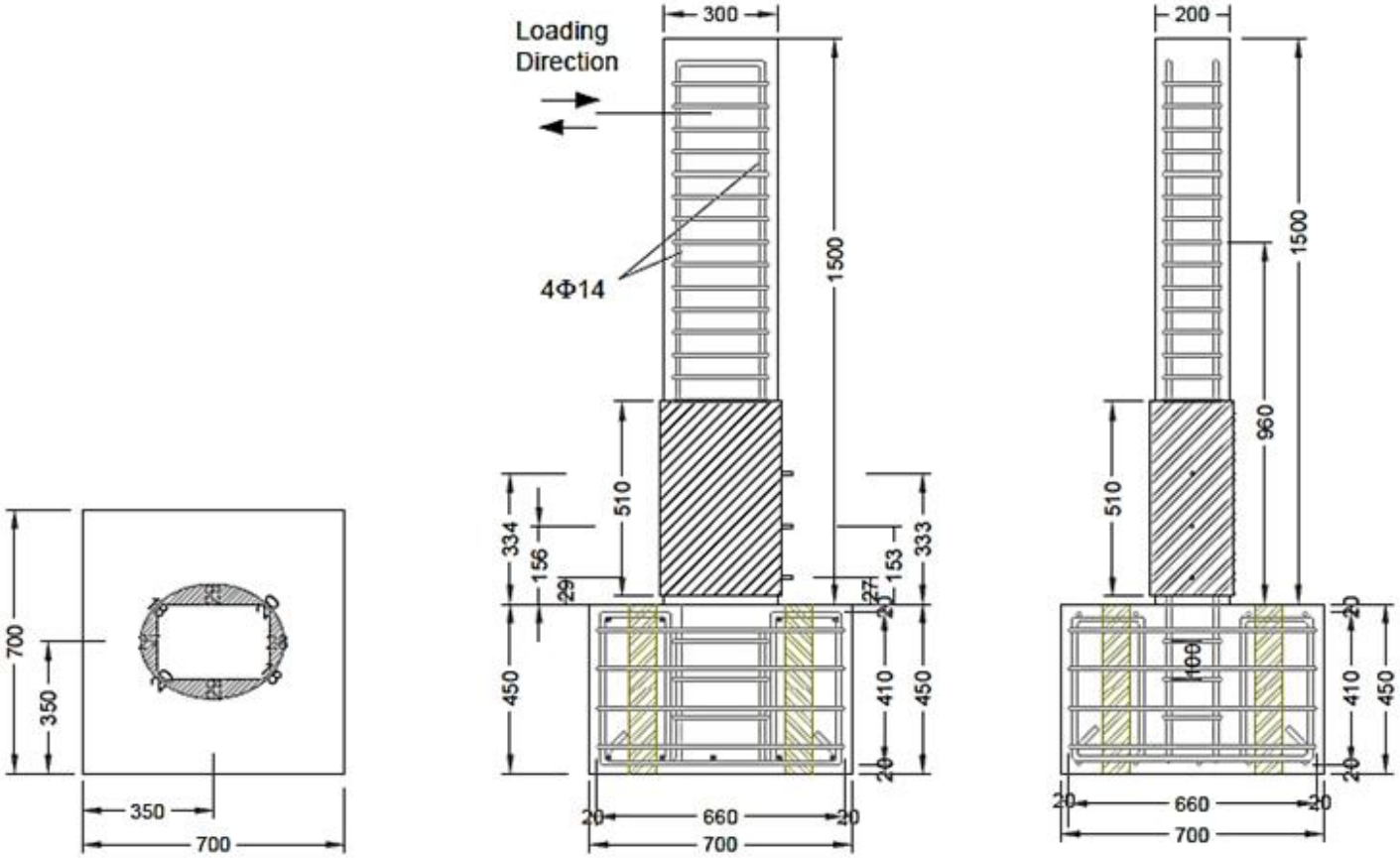

Figure B.6: Specimen detail for Ret-S60-Θ112.5-L80-3TRM.

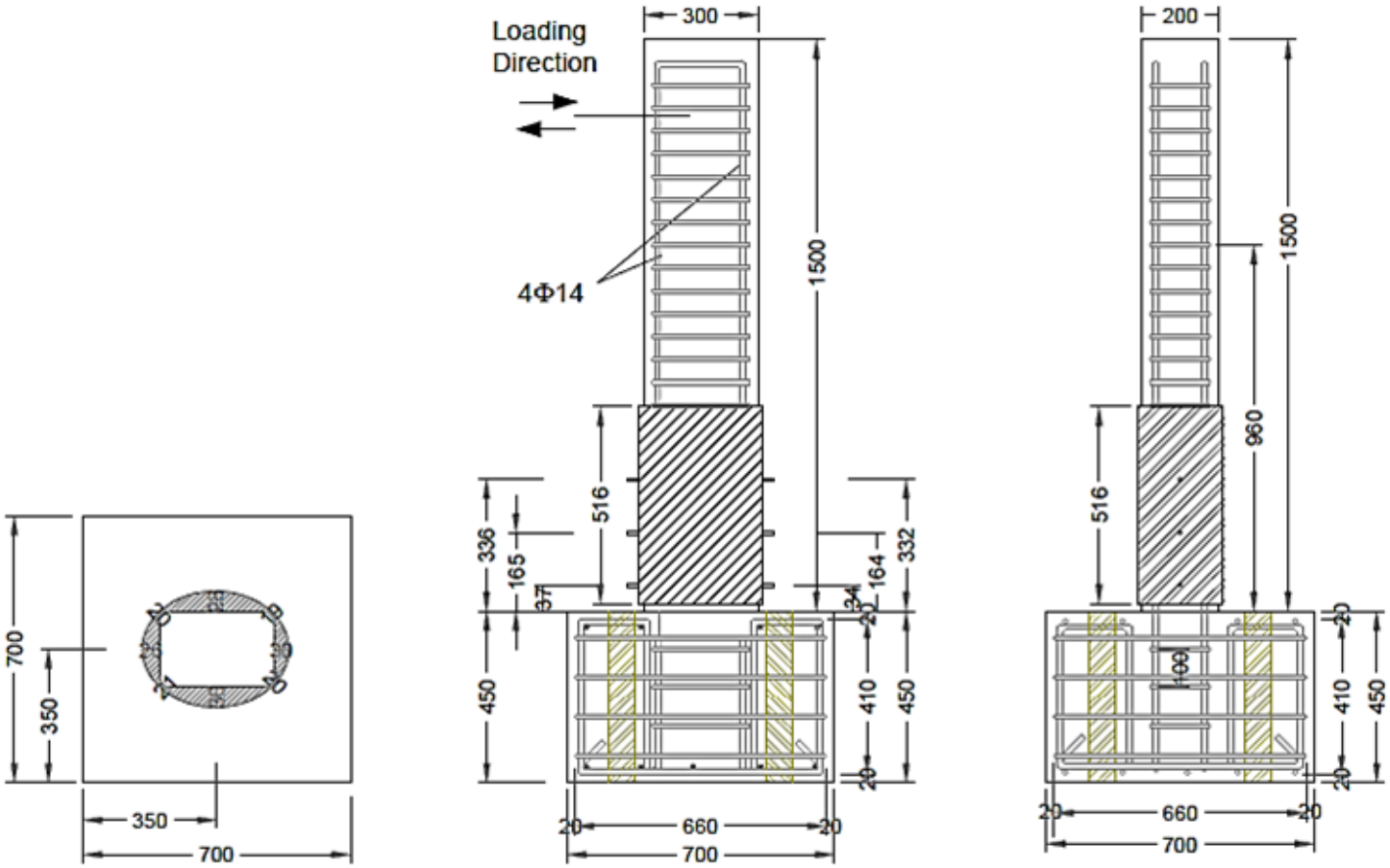

Figure B.7 : Specimen detail for Ret-S60-Θ135-L80-3T.

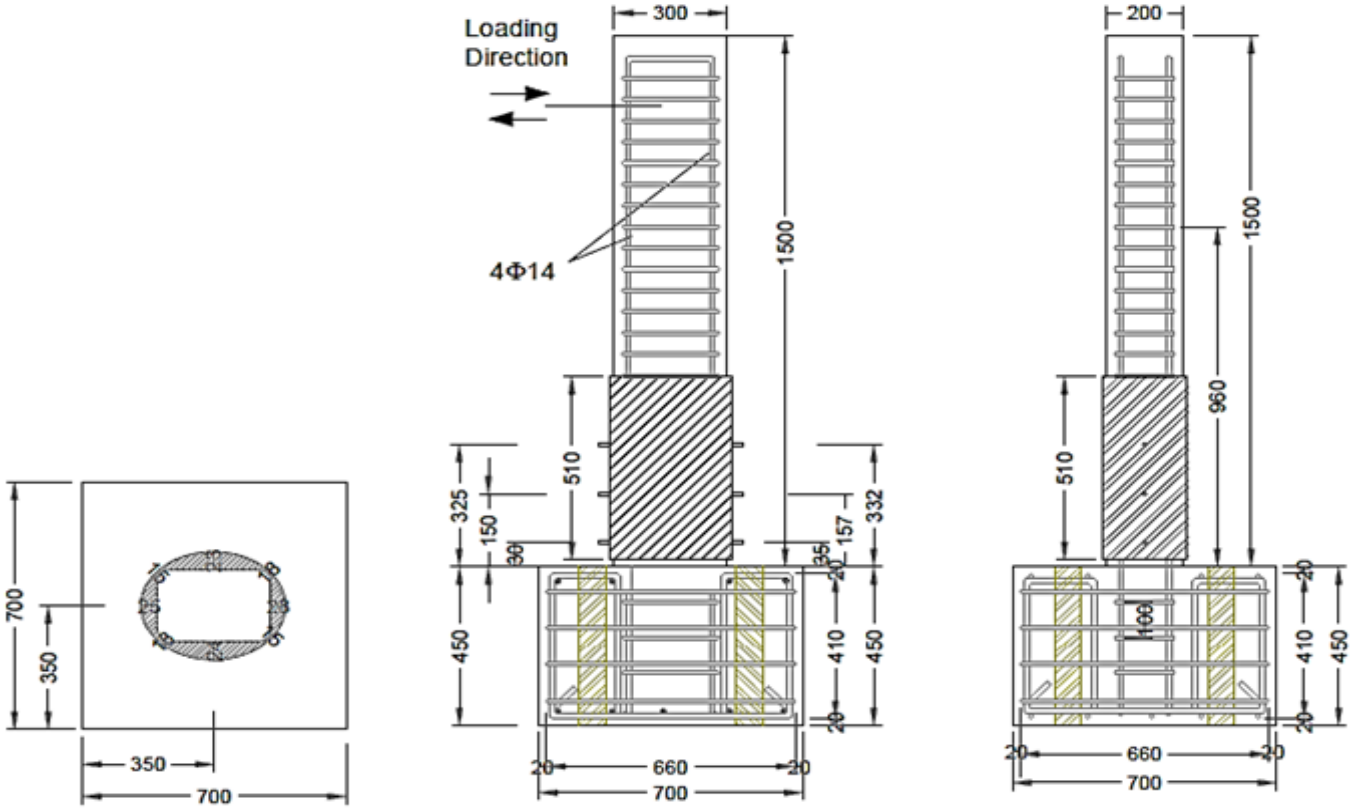

Figure B.8 : Specimen detail for Ret-S60-Θ135-L40-3TRM.

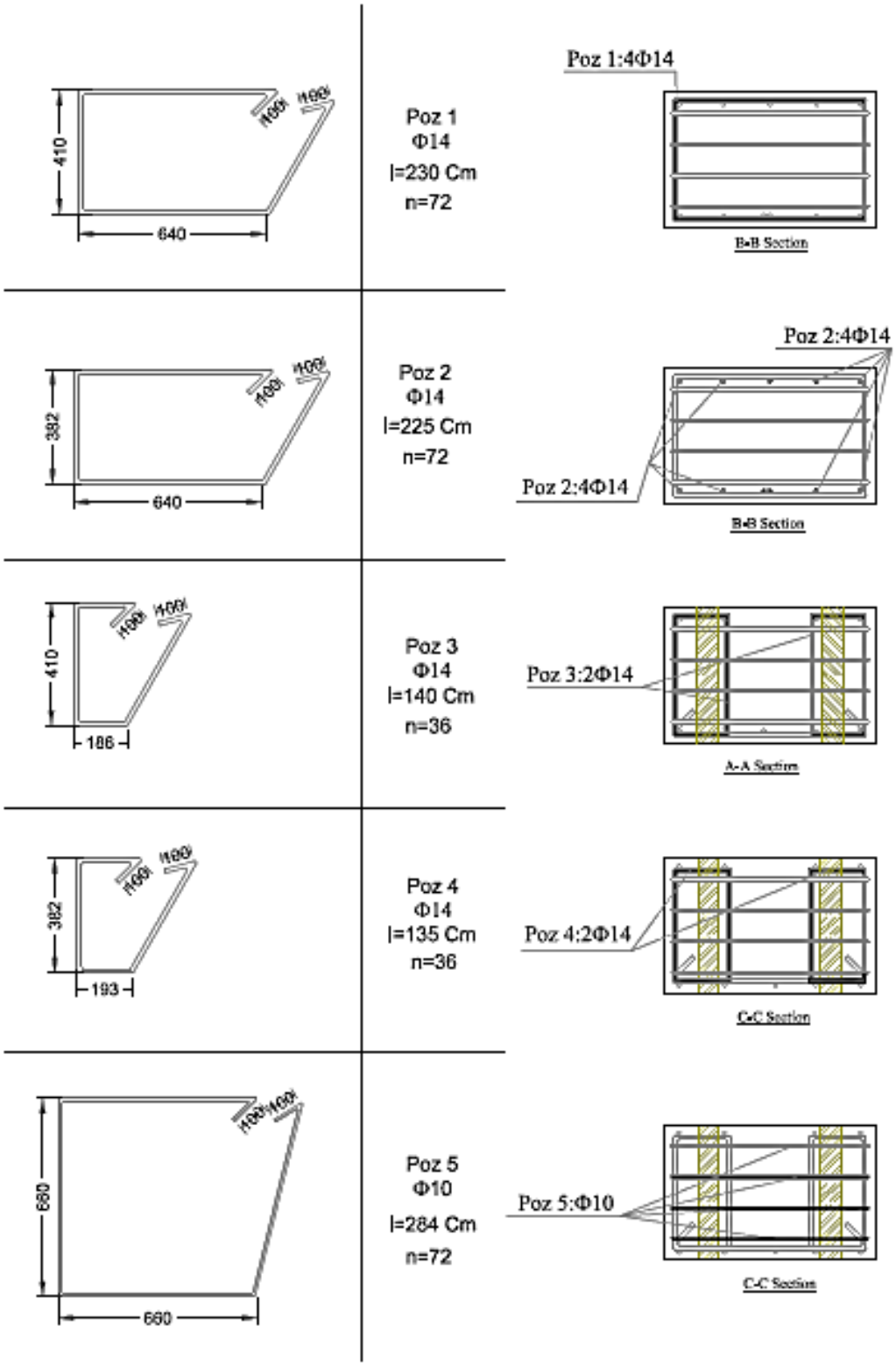

Figure B.9 : The arrangement of reinforcement and assembly of cages.

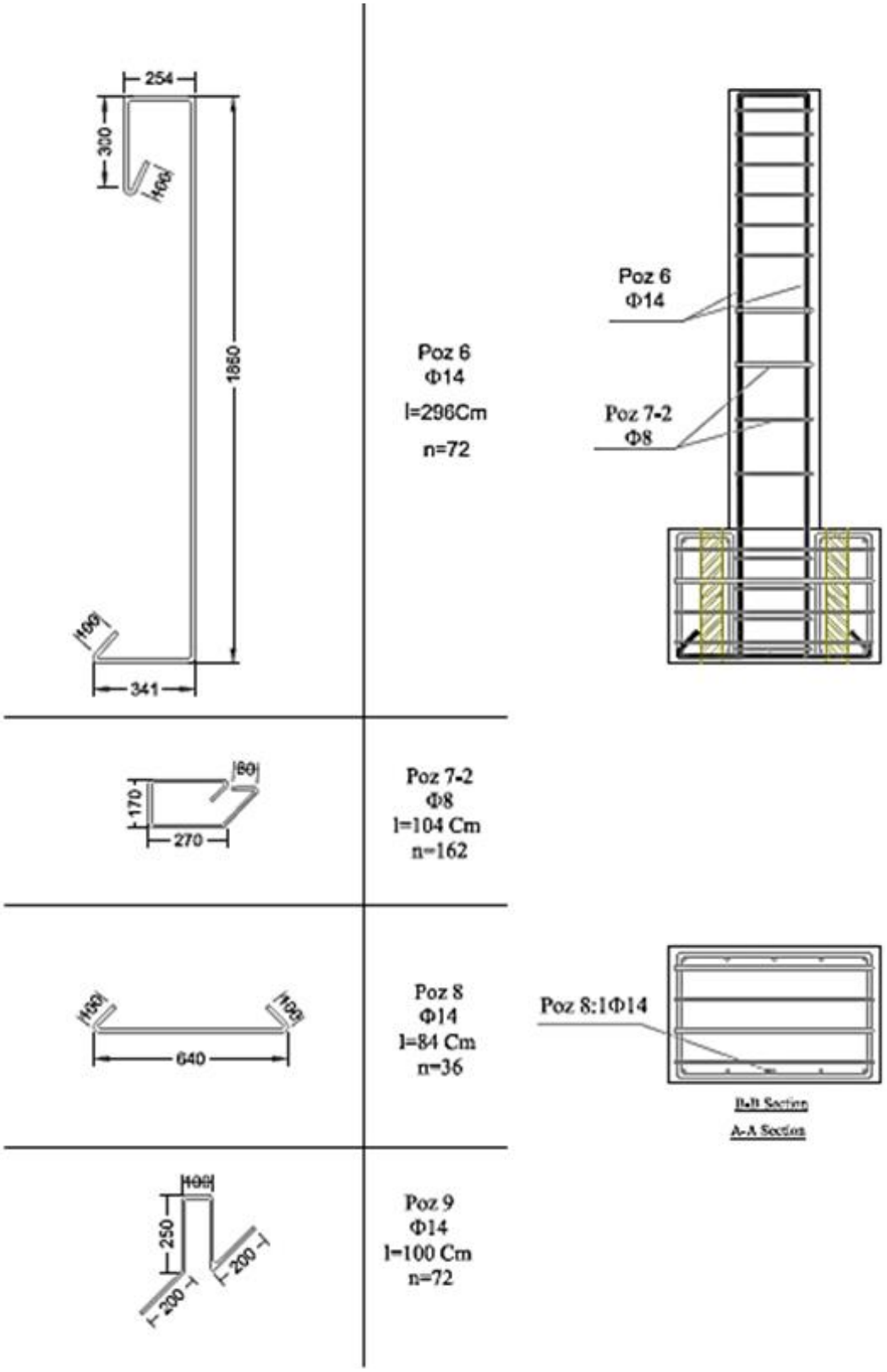

Figure B.10 : The arrangement of reinforcement and assembly of cages.

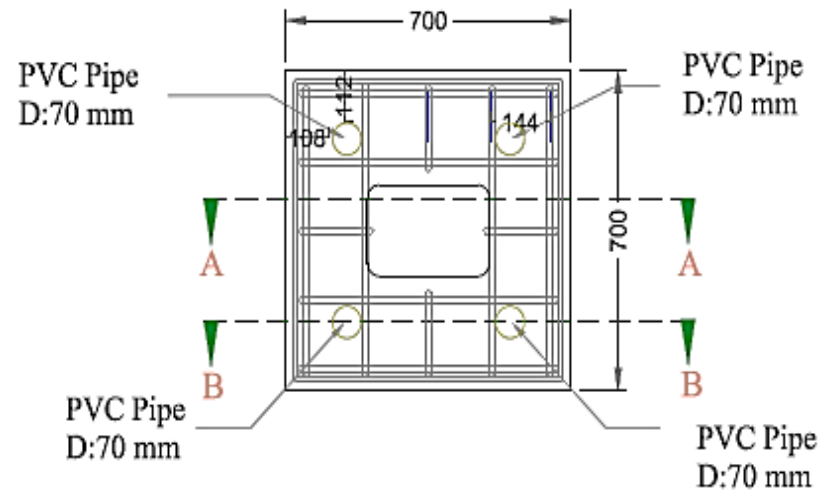

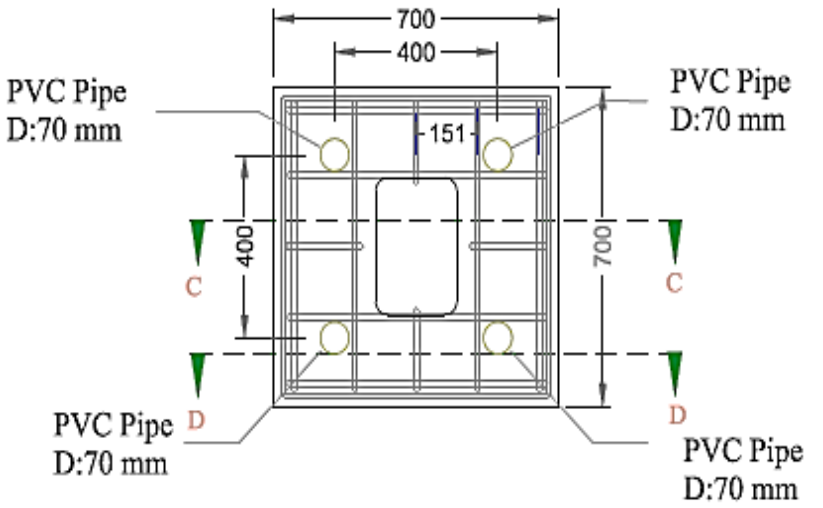

Figure B.11 : The arrangement of reinforcement and assembly of cages.

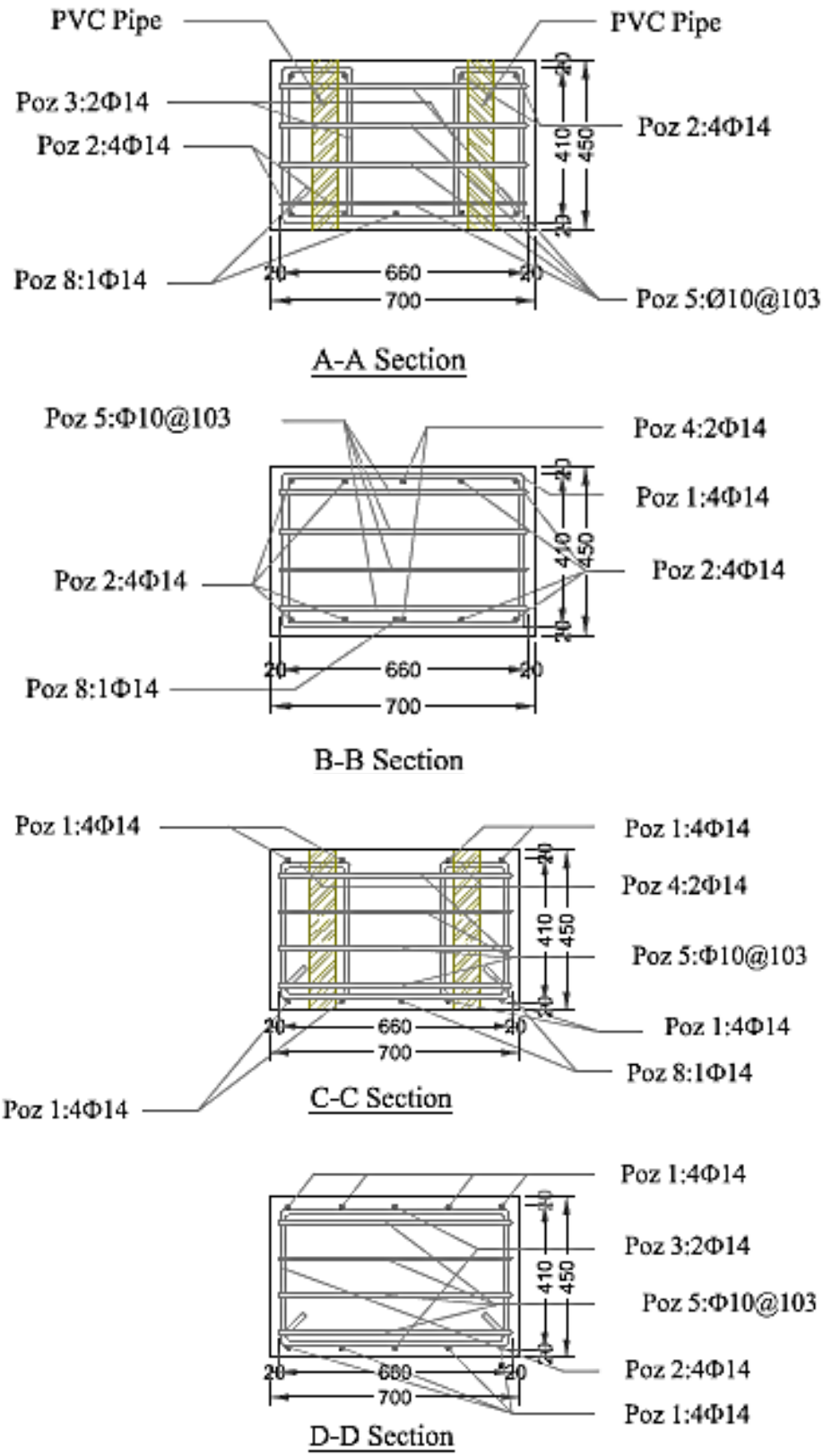

Figure B.12 : The arrangement of reinforcement and assembly of cages.

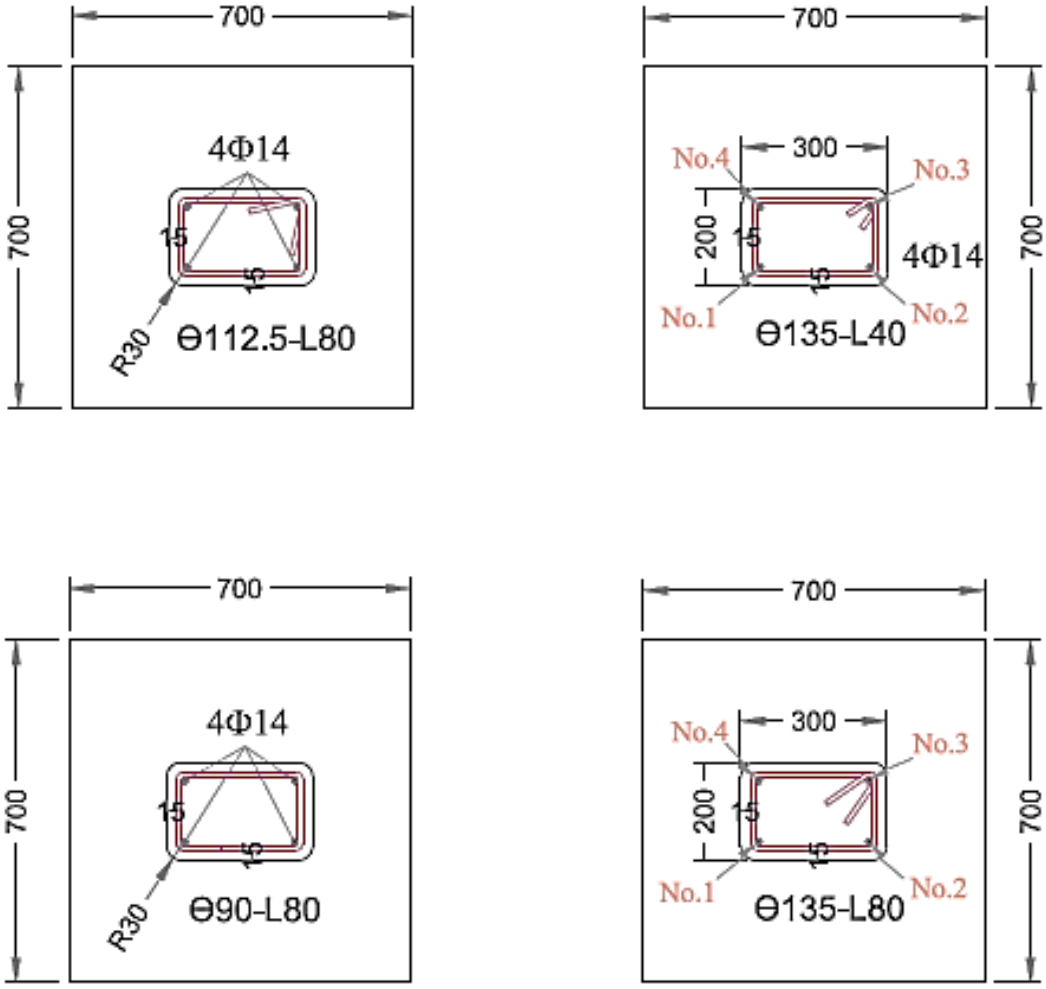

Figure B.13 : Specimens hook details.

APPENDIX C: The effectiveness of the jacket in reducing the strains in the longitudinal bars is shown in Fig. C.1 through C.4.

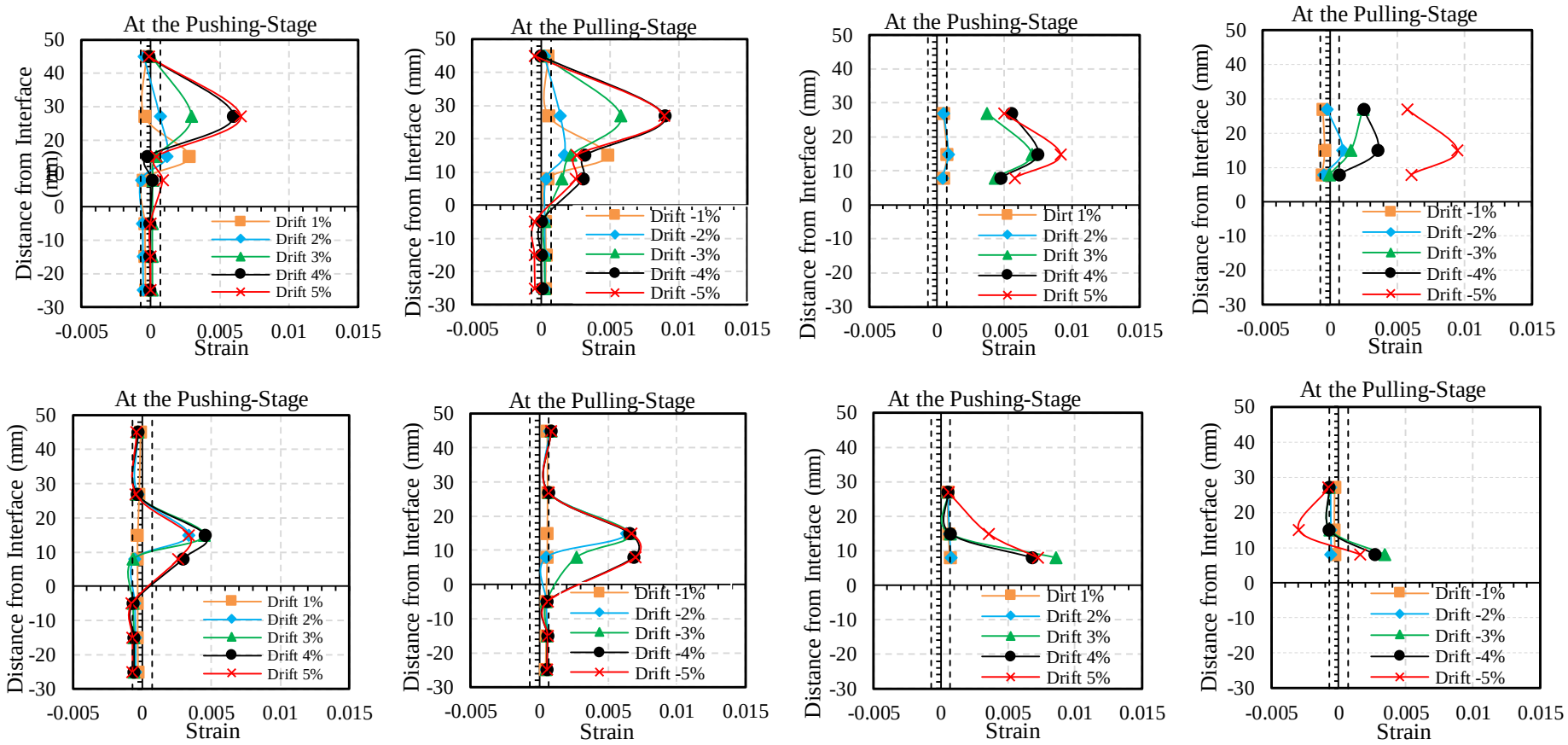

Figure C.1: The strain distribution in the longitudinal reinforcing bars of specimen Ref-S60-Θ90-L80 and Ret-S60-Θ90-L80-3TRM. a)Bar which has 7 strain-gages at the pushing. b)Bar which has 7 strain-gages at the pulling. c)Bar which has 3 strain-gages at the pushing. d)Bar which has 3 strain-gages at the pulling. e)Bar which has 7 strain-gages at the pushing. f)Bar which has 7 strain-gages at the pulling. g)Bar which has 7 strain-gages at the pushing. h)Bar which has 7 strain-gages at the pulling.

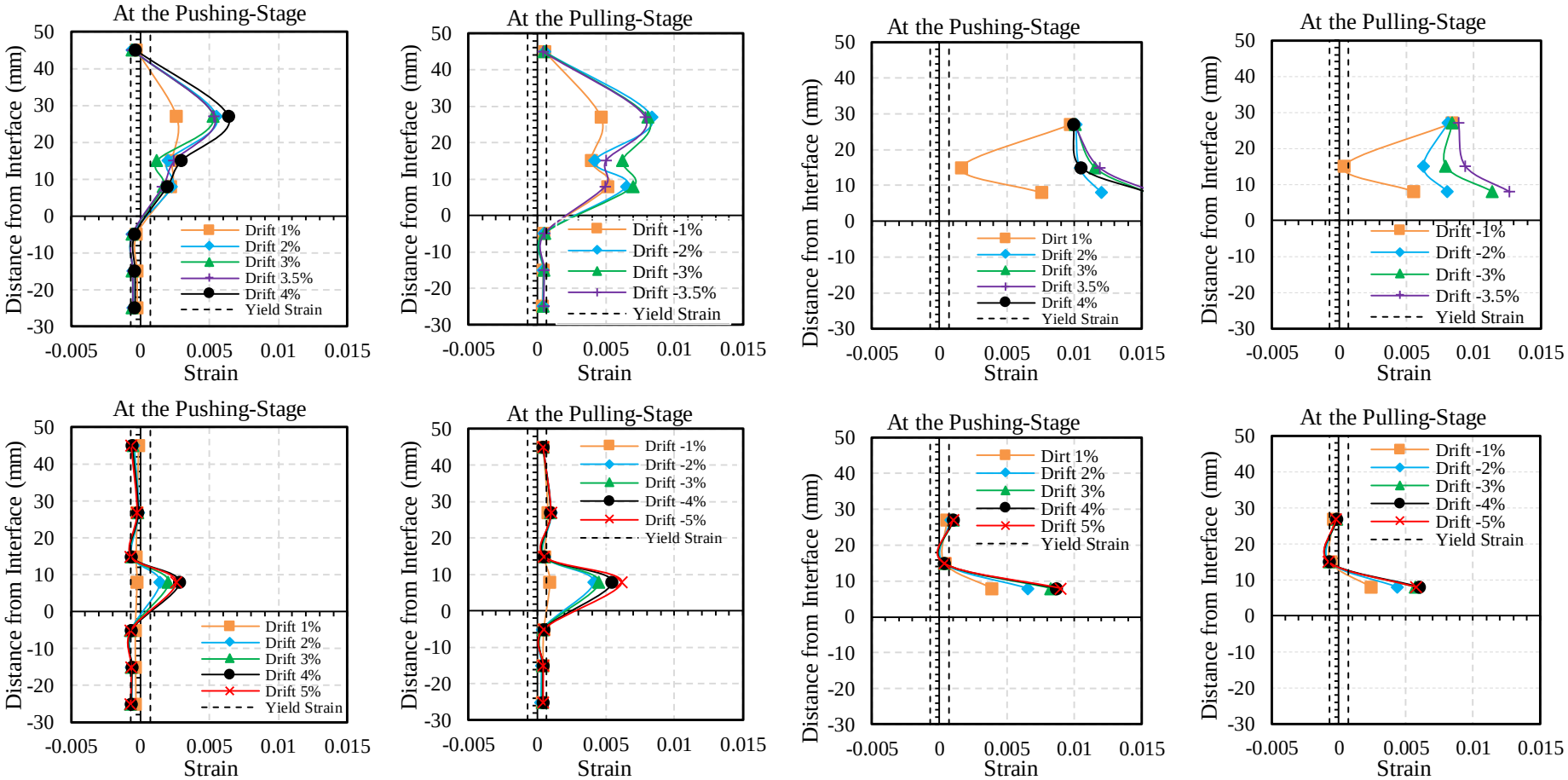

Figure C.2 : The strain distribution in the longitudinal reinforcing bars of specimen Ref-S60-Ɵ112.5-L80 and Ret-S60-Ɵ112.5-L80-3TRM. a)Bar which has 7 strain-gages at the pushing. b)Bar which has 7 strain-gages at the pulling. c)Bar which has 3 strain-gages at the pushing. d)Bar which has 3 strain-gages at the pulling. e)Bar which has 7 strain-gages at the pushing. f)Bar which has 7 strain-gages at the pulling. g)Bar which has 7 strain-gages at the pushing. h)Bar which has 7 strain-gages at the pulling.

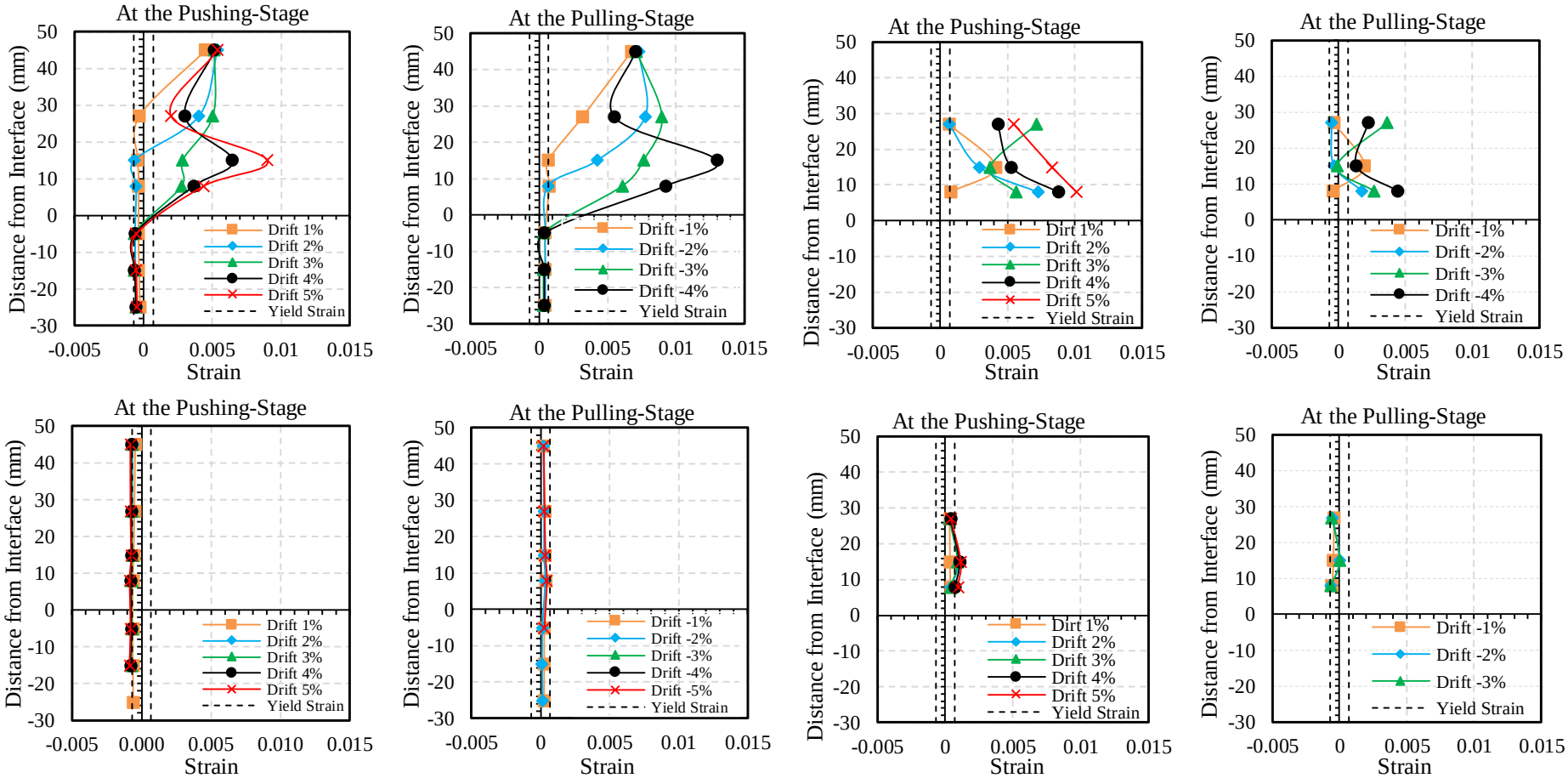

Figure C.3: The strain distribution in the longitudinal reinforcing bars of specimen Ref-S60-Θ135-L80 and Ret-S60-Θ135-L80-3TRM a) Bar which has 7 strain-gages at the pushing b) Bar which has 7 strain-gages at the pulling c) Bar which has 3 strain-gages at the pushing d) Bar which has 3 strain-gages at the pulling e) Bar which has 7 strain-gages at the pushing f) Bar which has 7 strain-gages at the pulling g) Bar which has 7 strain-gages at the pushing h) Bar which has 7 strain-gages at the pulling.

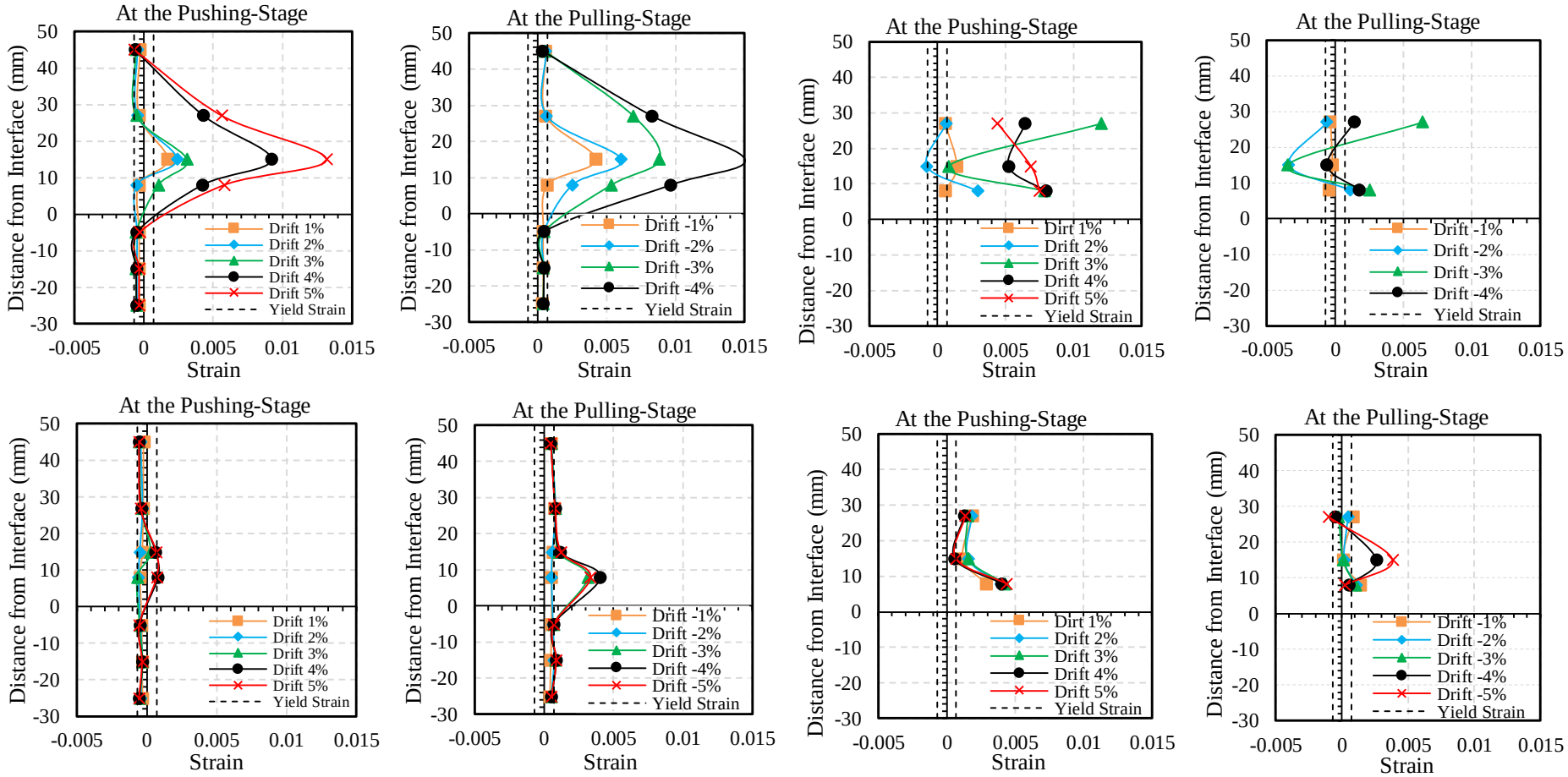

Figure C.4: The strain distribution in the longitudinal reinforcing bars of specimen Ref-S60-Θ135-L40 and Ret-S60-Θ135-L40-3TRM a) Bar which has 7 strain-gages at the pushing b) Bar which has 7 strain-gages at the pulling c) Bar which has 3 strain-gages at the pushing d) Bar which has 3 strain-gages at the pulling e) Bar which has 7 strain-gages at the pushing f) Bar which has 7 strain-gages at the pulling g) Bar which has 7 strain-gages at the pushing h) Bar which has 7 strain-gages at the pulling.

Curriculum Vitae:

Name:	**Saeid**
Surname:	**HAJIHOSSEINLOU**
Place and Date of Birth:	**Azerbaijan Gharbi- Iran, 1984**
E-Mail address:	saeid.hh.civil@gmail.com
	hajihosseinlou@itu.edu.tr

International conference papers:

Comert, M., Hajihosseinlou, S., Nasrinpour, A., Ates, A. O., Demir, C., Marasli, M., and Ilki, A. (2014). Seismic retrofit of sub-standard RC columns through basalt mesh reinforced sprayed GFRC jacketing, *Second FRC International Workshop (1ST ACI–FIB Joint Workshop), Fibre Reinforced Concrete: From Design to Structural Applications*, University of Polytechnique Montreal, Montreal, Canada. 24-25 July.